EXPERIMENTAL AND NUMERICAL INVESTIGATION OF FIRE BEHAVIOUR IN POLYURETHANE FOAMS

A Thesis Submitted to the

College of Graduate and Postdoctoral Studies

In Partial Fulfilment of the Requirements

For the Degree of Master of Science

In the Department of Mechanical Engineering

University of Saskatchewan

Saskatoon

By

OBIORA UGO-OKEKE

PERMISSION TO USE

In presenting this dissertation in partial fulfilment of the requirements for a Postgraduate degree from the University of Saskatchewan, I agree that the Libraries of this University may make it freely available for inspection. I further agree that permission for copying of this dissertation in any manner, in whole or in part, for scholarly purposes may be granted by the professor who supervised my dissertation work or, in their absence, by the Head of the Department or the Dean of the College in which my thesis work was done. It is understood that any copying or publication or use of this thesis/dissertation or parts thereof for financial gain shall not be allowed without my written permission. It is also understood that due recognition shall be given to me and to the University of Saskatchewan in any scholarly use which may be made of any material in my dissertation.

Requests for permission to copy or to make other uses of materials in this dissertation in whole or part should be addressed to:

Head of the Department of Mechanical Engineering
University of Saskatchewan
57 Campus Dr.
Saskatoon, Saskatchewan S7N 5A9
Canada

OR

Dean
College of Graduate and Postdoctoral Studies
University of Saskatchewan
Room 116 Thorvaldson Building, 110 Science Place
Saskatoon, Saskatchewan S7N 5C9
Canada

DISCLAIMER

The names of certain commercial products were exclusively used to meet the dissertation and/or exhibition requirements for the degree of Master of Science at the University of Saskatchewan. Reference in this dissertation to any specific commercial products, process, or service by trade name, trademark, manufacturer, or otherwise, does not constitute or imply its endorsement, recommendation, or favouring by the University of Saskatchewan. The views and opinions of the author expressed herein do not state or reflect those of the University of Saskatchewan and shall not be used for advertising or product endorsement purposes.

ABSTRACT

Due to the complex and varying nature of a flame and its products, the scaling of fire behaviour has been a challenge in the area of fire science. The use of small-scale test data to interpret full-scale fire behaviour is an area of ongoing research with potential savings for manufacturers required by code to test products for large-scale fire behaviour. Polyurethane foam was selected as the sample material for the research due to its widespread application in home and office furniture and its potential to act as a fuel source in fires due to a high hydrocarbon content. The heart of the problem lies with predicting how much heat is released by the fire and the rate at which flame spreads across the material. This research builds on previous University of Saskatchewan research and seeks to provide a method to predict full-scale flame spread across a material. Additionally, methodologies such as the Combustion Behavior of Upholstered Furniture (CBUF) Model applied for full-scale heat release rate (HRR) predictions and Alpert's correlation employed in predicting compartment temperatures are also evaluated.

Small-scale cone calorimeter tests which serve as input to the CBUF model were conducted for foam thickness of 2.5, 7.5 and 10 cm at incident heat fluxes of 5, 10, 15, 20, 35 and 50 kW/m^2. Separate small-scale tests were conducted on foams instrumented with thermocouples to measure temperatures on the surface and at depth. A numerical model was proposed to predict the surface temperatures and estimate the time to ignition of the small-scale foam specimens. Full-scale compartment fire tests were conducted for centre and edge ignition at the University of Waterloo Live Fire Facility. Compartment temperatures and flame areas were measured. A model was developed to predict flame spread based on the data collected from previous University of Saskatchewan furniture calorimeter test.

The results of the flame spread model showed promise in predicting the area spread rates. The model, however, did not capture some of the edge effects that occurred due to the flame reaching the foam boundaries. The area spread model was used within the CBUF model which satisfactorily predicted the full-scale HRR. The HRR predictions were then applied to a modified version of Alpert's correlation which predicted ceiling jet temperatures accounting for the spread of flame. Predictions of ceiling jet temperatures made using Alpert's correlation was improved by considering flame spread.

ACKNOWLEDGEMENTS

My foremost gratitude is to the most high God who has seen me through the highs and lows of my program and in whom I have always found my resting place. I would like to thank my Supervisor Professor David Torvi, who's continued guidance and financial support has been instrumental in completing my research. I also acknowledge the assistance of the members of my supervisory committee, Professor C.J. Simonson and Professor D.J. Bergstrom who have reviewed my work.

I would like to appreciate the members of the Department of Mechanical Engineering Thermo/Fluids research group. The small/full-scale cone calorimeter data collected by Luke Robson combined with his implementation of the CBUF model formed the foundation for my research. Hayden Reitenbach, Shawn Reinick, Melanie Fauchoux, your continual technical advice is much appreciated. Cathleen Lupien's work on the development of the MATLAB code used to obtain temperatures form infrared measurements is acknowledged. Also, I appreciate the input from Professor E.J. Weckman and the University of Waterloo fire research group.

A big thanks to my family and friends for their constant support. My mum, Nkiru who's two Master's degrees has been inspirational in letting me know that I can do it if I believe. I also appreciate my support system Barbara who was there encouraging me through all the sleepless nights. My dad (Joseph), Ada, Kosy, Izu, Henry, you guys are the best family anyone can ask for.

Finally, financial support from Natural Science and Engineering Research Council of Canada (NSERC), Department of Mechanical Engineering, and College of Graduate and Postdoctoral Studies at the University of Saskatchewan is appreciated.

TABLE OF CONTENTS

LIST OF TABLES

LIST OF FIGURES

LIST OF SYMBOLS

English Letters

A	surface area (m^2)
c_p	specific heat (J/kg°C)
E	heat release per unit volume of oxygen consumed, 17,200 (kJ/m^3)
f	view factor
g	acceleration due to gravity (m/s^2)
G	thermal energy generation rate per unit volume (W/m^3).
h	convective heat transfer coefficient (W/m^2K)
k	thermal conductivity (W/m°C), factor that accounts for the location of the fire
$\dot{m}''$	mass burning rate per unit area (kg/m^2s)
Nu	Nusselt number
Q	heat release rate (kW)
q	heat release rate density from cone the calorimeter (kW/m^2)
r	radial distance (m)
Ra_L	Rayleigh number
Re	Reynolds number
T	temperature (°C)
t	time (s)
x, y, z	distances in the various coordinates (m)
ΔH_c	heat of combustion of the volatiles (kJ/kg)

Greek Letters

α	fire growth coefficient depending on fuel type (kW/s^2)
β	empirical coefficient of flame spread (s^{-2})
ε	emissivity
ρ	density (kg/m^3)
σ	Stephan-Boltzmann constant (W/m^2K^4)

LIST OF ABBREVATIONS AND ACRONYMS

ASTM	American Society for Testing and Materials
C	Centre Ignition
CBUF	Combustion Behavior of Upholstered Furniture
CFD	Computational Fluid Dynamics
CFR	Code of Federal Regulation
CGSB	Canada General Standards Board
E	Edge Ignition
HRR	Heat Release Rate
IR	Infrared
NBS	National Bureau of Standards
NFPA	National Fire Protection Association
TDI	Toluene Diisocyanate
TGA	Thermogravimetric Analysis
THR	Total Heat Release
UofS	University of Saskatchewan

1. INTRODUCTION

Fire safety is one of the critical issues faced by society today. The increased use of combustible materials in residential and commercial environments has amplified the risk factors associated with fire incidents. In a study conducted by Statistics Canada from 2005 to 2014, a total of 439,256 fire incidents were reported in Canada to the National Fire Incident Database (NFID) with structural fires (primarily buildings) accounting for 56% of the reported fire incidents (Statistics Canada, 2017). In addition, 1,733 fire-related deaths were recorded over this period and 87% of the deaths were due to structural fires (Statistics Canada, 2017). Fires in homes represented a majority of the structural fire deaths, ranging from 87% in 2009 to 95% in 2008 and 2010 (Statistics Canada, 2017). The study further noted that the leading reason for deaths in structural fires where evacuation did not occur was that victims were trapped by spreading fire or smoke (Statistics Canada, 2017). These alarming statistics highlight the dangers of residential fires and the effects of flame spread on the chances of survival in fire incidents.

In order to mitigate fire risk, a variety of methods may be applied. Experimental fire testing and computational fire modelling are two of the major approaches used to obtain information for fire protection system design. In recent times, as the accuracy and processing speed of computers has increased, predicting fire behaviour from a computational standpoint has become of interest to a variety of industries. Computational fire modelling offers an alternative to repeating experiments. Engineering fire modelling tools such as the National Institute of Standards and Technology's (NIST) Fire Dynamics Simulator (McGrattan, et al., 2013), and ANSYS Fluent (ANSYS, 2013) are sometimes used in fire protection system design. Other relatively simplistic empirical correlations, which predict fire behaviour based on the heat release rate of the fire and geometry of the room, may also be used (Drysdale, 2011). To correctly predict fire behaviour, the factors that play a role in the fire dynamics must be accounted for.

While there are many benefits of computational fire modelling, the inputs to the models are still supplied from experimental measurements. Final validation of the models can also be

done by comparison with experimental results. Depending on the type of information required, experiments are often carried out to applicable standards, or these standards can be modified to simulate the appropriate fire scenario. These experiments are usually categorised as small-scale or full-scale fire tests, which are discussed in detail in later sections. This research will comprise of small-scale experimental testing, focusing on a computational approach to predict flame spread occurring in full-scale tests, as well as methodology to predict full-scale fire rate of energy release and temperatures in a fire compartment. Final validation is done using results from previous University of Saskatchewan and University of Waterloo fire research (Fulton et. al., 2016, Robson, 2014, Ezinwa, 2009, Threlfall, 2005).

When a material is ignited, the flame spreads from the point of ignition to other areas of the material. The manner and rate at which flame spreads across the material are influenced by factors such as the external airflow, fuel type, material composition, structure and ignition location. The spread of the flame affects the growth of the fire as well as the interaction of the fire with other materials within the space. This constitutes a challenge in the design of fire protection systems. In residential buildings where furnishings are in close proximity to each other, the danger of flame spread is further magnified (National Fire Protection Association, 2005b).

Furnishings such as chairs and mattresses are normally made with some form of cushioning material for increased comfort. In older furnishings, the cushioning materials were made using natural fibres (cotton, wool and horsehair). In recent times, cushioning materials have transitioned to synthetic materials (usually polyurethane). The application of more synthetic material in various household furnishing, as well as the increased number of items within a space, has greatly increased room fire potential with faster flame propagation rates. These effects were demonstrated in experiments conducted by Underwriters Laboratories (Kerber, 2012). Fire behaviour in rooms containing modern furnishings was compared to rooms containing legacy furnishings. Regardless of the fact that both room types had similar fuel loads (19 kg/m^2 and 22.9 kg/m^2), the heat release rate curves and time to peak heat release rates were significantly different. The modern room achieved its peak heat release rate (7.5 MW) after approximately eight minutes, while the legacy room peaked (6 MW) after 30 minutes. The transition to flashover (spontaneous combustion of all items within the same space as discussed in

Section 1.2.2) was observed at approximately five minutes for the modern room, while flashover was seen to occur after 34 minutes in the legacy room. The rate at which the modern room achieved its peak heat release rate indicates that there is reduced time for occupants to safely evacuate a modern house in event of a fire. Information such as this is crucial for fire protection system design and therefore, the flame spread predictions for this research will be made based on synthetic material properties (polyurethane).

In another fire statistics report put together by the National Fire Protection Association, from 2005 to 2009 local fire departments responded to an average of 10,260 home fires per year that started with mattresses and beddings, leading to 371 civilian deaths, 1,340 civilian injuries and $382 million in direct property damage annually (Evarts, 2011). This data has strongly motivated this research, which will focus on predictions of mattress fire behaviour. Simulations of mattress fires will allow for simplifications to be made since the geometry of a bed can be treated as rectangular with flame spread occurring primarily over the horizontal surface. This represents less complexity when compared to other types of furnishing, as vertical flame spread can be neglected while still suitably capturing the general behaviour of mattress fires. The subsequent sections of this introductory chapter will discuss the properties of polyurethane and briefly review various fire test methods. Fire scaling and flame spread will also be discussed and previous University of Saskatchewan research on computational fire models related to mattresses are highlighted.

1.1 POLYURETHANE FOAM

Polyurethane foam is a thermoplastic made up of carbon-based organic compounds. Products manufactured using flexible polyurethane foam have found widespread application in a variety of industries. Its versatility can be seen in the annual production of over 1.3 billion pounds of foam every year (Polyurethane Foam Association, 2016a). One major area of application is in the production of mattresses and cushioning for upholstered furniture. Its ability to provide support, comfort and durability makes it a popular material for use in cushioning. Polyurethane foam is easily manufactured, relatively inexpensive and can be cut into a variety of shapes and sizes. The raw materials for processing are also readily available (Polyurethane Foam Association, 2016b).

1.1.1 Combustion of Polyurethane

Polyurethanes are formed by reacting polyol with an isocyanate (Witkowski, Stec, & Hull, 2016). The chemical structure is shown in Figure 1-1. The base compounds of polyurethane foam are derived from crude oil thus, it is easily ignited and highly flammable. There is an increased surface area for burning due to the open cells within the foam. This also provides easy access for oxygen during fires. A large amount of heat energy is also evolved during foam fires, which may quickly lead to an uncontrolled fire condition if proper measures are not put in place.

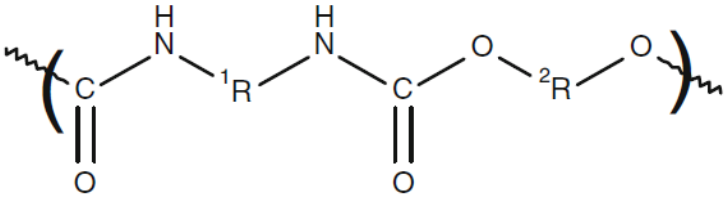

Figure 1-1: Structure of Polyurethane (Used with Permission. Witkowski, Stec, & Hull, 2016)

The combustion of polyurethane foam is an exothermic process. The foam may experience two types of combustion, smouldering or flaming combustion (Witkowski, Stec, & Hull, 2016). This is dependent on factors such as the level of heat flux exposure, the type of ignition source and the availability of oxygen. For combustion to ensue, thermal decomposition of the polyurethane foam, which involves the formation of molten products followed by gaseous species (volatiles), must occur (Drysdale, 2011). This process is called pyrolysis. The volatiles are composed of a mix of pyrolysis products which breakdown at the critical temperature of polyurethane. The material must reach this critical temperature since sufficient thermal energy must be added to the material to overcome the bonding forces at the surface of the condensed fuel (Kashiwagi, 1994). The process of formation of volatiles is shown in Figure 1-2. The rate of decomposition is also boosted by an increased presence of oxygen (Kashiwagi & Ohlemiller, 1982)

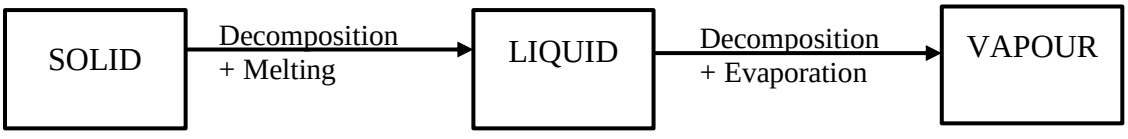

Figure 1-2: Thermal Decomposition of Polyurethane Foam (Used with Permission. Drysdale, 2011)

Smouldering is a flameless combustion process occurring by the reaction of atmospheric oxygen with a porous combustible solid (Witkowski, Stec, & Hull, 2016). Since polyurethane foam is a porous material, a reaction zone moves through the foam, releasing gaseous volatiles and high-temperature liquid which condenses to form an aerosol smoke as it mixes with cool air (Drysdale, 2011). This flameless combustion is characterised by material charring and the production of toxic fumes (Ohlemiller, 1985). Char and tar formation in polyurethane foam have been shown to impede the development of smouldering combustion due to the insulating capabilities of the material (Drysdale, 2011). Smouldering combustion of polyurethane foam typically occurs at significantly lower heat flux exposures (7 kW/m^2 – 13 kW/m^2) when compared to flaming ignition (Hadden, Alkatib, Rein, & Torero, 2014). The temperatures and spread rates are in the range of 300℃ to 400℃ and 0.05 mm/s to 0.5 mm/s respectively (Hadden, Alkatib, Rein, & Torero, 2014).

There is still a possibility that some material may transition from smouldering to flaming combustion. This complex phenomenon occurs due to the material reaching its auto-ignition temperature in the vapour phase during smouldering combustion. Various researchers have investigated this phenomenon (Putzeys, Fernandez-Pello, Rein, & Urban, 2008, Hadden, Alkatib, Rein, & Torero, 2014). Drysdale (2011) also discusses smouldering combustion and the factors affecting the propagation of smouldering.

In flaming combustion, visible flames occur as heat is released from the material. The flame radiates and heats other areas of the material causing the fire to spread even further. For flaming combustion to occur, the fuel must be transformed to its molecular form in the vapour phase (pyrolysis), where rapid reaction with atmospheric oxygen ensues, (Witkowski, Stec, & Hull, 2016) and reach its ignition temperature. One common approach that is used for estimating ignition times for building materials and other materials such as polyurethane foam is to treat these as a semi-infinite solid (see Section 2.6). If this approach is used, thermal inertia ($k\rho c$), which is a product of the material thermal conductivity (k), density (ρ) and specific heat (c), determines the rate at which a material reaches its ignition temperature. The density of polyurethane foam is low, which results in rapid surface temperature rise allowing the foam to reach ignition temperature quickly. The ratio of the volatiles from the decomposition of the foam

to the oxygen supplied must be within a range of values to sustain flame propagation (Drysdale, 2011). A summary of the macro scale burning process is given in Table 1-1.

Table 1-1: Macro Scale Burning Process of Polyurethane Foam (Witkowski, Stec, & Hull, 2016)

Stage 1	Heating	Exposure to the critical heat flux causing a temperature rise which is dependent on the thermal inertia ($k\rho c$) of polyurethane foam
Stage 2	Pyrolysis	The heat flux causes decomposition of the polyurethane foam leading to formation of char and combustible gases.
Stage 3	Ignition	Volatile gases react with oxygen. At the appropriate air/fuel ratio range, ignition will occur. The rate of reaction increases and produces products of combustion.
Stage 4	Flame spread	The flame, which is a result of ignition, becomes a radiant source of heat leading to pyrolysis of adjacent surface and subsequent ignition.
Stage 5	Fire development	As flame spreads, depending on the room geometry, entrainment of oxygen may decrease leading to products of incomplete combustion (soot) which increase the radiative component of heat transfer.

Since polyurethane fires generate a large amount of heat, they have the ability to radiate and ignite surrounding combustible items. In addition, once ignited, polyurethane melts and flows, which may cause surrounding items to become involved in the fire due to direct flame impingement. In foam fires with a limited amount of oxygen (under-ventilated conditions), polyurethanes produce significant quantities of hydrogen cyanide (Levin, Paabo, Gurman, & Harris, 1987). Toxic gases have been shown to be responsible for a majority of fire deaths (Purser, 2010). Furthermore, visibility is lowered due to the production of a dense smoke cloud. This reduces the chances of escape and increases the fire risks associated with polyurethane foam fires. Figure 1-3 shows an example of the smoke produced by a room fire during a live-fire demonstration.

Figure 1-3: Smoke Production in a Room Fire

Various steps have been taken to mitigate the hazards from a polyurethane foam fire. One method applied in the manufacturing stage is the use of fire retardants. Fire retardants are chemicals added to the foam that affect the efficiency of combustion by altering either the heat of combustion or the heat of gasification. Some retardants affect both factors simultaneously (Drysdale, 2011). One or more stages in the burning process mentioned in Table 1-1 are disrupted by the flame-retardants (Hilado, 1968). The retardant may slow down the rate of temperature rise in stage one or support the formation of char and non-combustible gases in stage two. In stage three, the rate of production of combustible gases may be slowed down to prevent ignition of the foam by altering the air/fuel ratio. Stage 4 and 5 are dependent on stage 1 to 3 and thus, the fire retardant should have sufficiently slowed down the rate of combustion preventing large fire development (Hilado, 1968). Another strategy applied to mitigate polyurethane fire hazards is the use of barrier fabrics, which shield the foam from the flame (Chivas, Guillaume, Sainrat, & Barbosa, 2009).

Test standards are used to assess the fire behaviour of polyurethane foam. These standards are a set of experimental tests, which are developed by standards organisations and government agencies. The standards dictate strict criteria for combustibility of polyurethane foam. Flammability tests that evaluate factors such as time to ignition, heat release rate, the total energy released and smoke production are aimed at limiting the hazards associated with polyurethane fires. The following section highlights some of the various standards applicable to mattress testing and gives a background on the parameters measured to understand the behaviour of a polyurethane foam fire.

1.2 FIRE TESTING

With evolutions in the material manufacturing process, fire testing has become increasingly important to identify the fire risks associated with any material. Organizations such as the American Society for Testing and Materials (ASTM), International Organization for Standardization (ISO) and Underwriters Laboratory of Canada (ULC) develop standards to which fire tests are conducted. The heat release rate (HRR) of materials has been adjudged one of the most critical parameters in controlling a fire's behaviour (Lawson, 2012).

The heat release rate is a measure of the exothermal energy evolved from the combustion of a material. It is a combination of the radiative, convective and conductive heat given off to the surroundings by the combustible material. Therefore, the heat release rate is also used as a means to rank the propensity of materials to burn. While different materials may burn at similar temperatures, the rate at which energy is released can vary significantly. The total amount of energy released, and the peak energy released are a function of the chemical composition and structure of the materials. Conventional fire testing equipment is designed to measure the heat release rate (typically using oxygen consumption calorimetry) and other parameters such as ignitability, mass loss and smoke production. Fire testing is generally categorised as three types; small-scale fire tests, full-scale fire tests and field fire tests. A selection of test type is dependent on the type of information required, as well as the condition to be simulated and in some cases, the availability of test facilities.

1.2.1 Heat Release Rate and Oxygen Consumption Calorimetry

Having established the importance of heat release rate measurements, various methods have been used to determine the rate of energy release. Theoretically, the heat release rate is calculated as:

$$Q = X\dot{m}'' A_f \Delta H_c \tag{1.1}$$

Where Q is the heat release rate (kW),

X is a factor to account for incomplete combustion (< 1.0),

$\dot{m}''$ is the mass burning rate per unit area (kg/m^{2}s),

A_f is the fuel surface area (m^2), and

ΔH_c is the heat of combustion of the volatiles (kJ/kg).

However, the use of this method results in some uncertainties. The heat of combustion of a material is not a constant property and its value changes as the material burns (Babrauskas, Heat Release Rates, 2016a). In addition, the heat of combustion that is measured in a bomb calorimeter in 100% oxygen may be misleading, as it is not evaluated under a realistic fire scenario. It is also the maximum amount of heat that can be released (Janssens, 2016). Determining the heat release rate with this method may lead to an overestimation. Therefore, the factor *X* which accounts for incomplete combustion is used to estimate heat release rate. There are however challenges in determining *X*.

Oxygen consumption calorimetry is the most popular modern-day experimental technique used for the measurement of heat release rate. In 1917, researchers found that for complete consumption a nearly constant amount of heat is released per unit mass of oxygen consumed (Janssens, 2016). This principle, known as the Thornton rule, is foundational for oxygen consumption calorimetry. Thus, in order to measure the net heat release rate, it is sufficient to measure the oxygen consumed. A constant *E* which represents the heat released per unit mass of oxygen consumed for every material was approximated as 13.1 MJ/kg. This value is accurate to ± 5% for most organic fuels (Janssens, 2016), however, more accurate values of *E* for cases in which the burning material is well known may be obtained from the literature. Oxygen consumption calorimetry was later refined to include carbon dioxide (CO_2) and carbon monoxide (CO) measurements to account for the effects of incomplete combustion (Steckler, 2001). Based on ASTM E1590 (ASTM, 2017c), the equations for heat release rate using oxygen consumption calorimetry when oxygen and carbon dioxide concentrations are known are given as:

$$Q = EVO_2^i \left(\frac{\varphi}{\varphi(\alpha_c - 1) + 1} \right) \tag{1.2}$$

where Q is the heat release rate (kW),

E is heat release per unit volume of oxygen consumed, 17,200 (kJ/m^3),

α_c is the combustion expansion factor (approximated as 1.105),

O_2^i is the initial reading of the oxygen analyzer (mole fraction), and

φ, the oxygen depletion factor is given as equation (1.3) when only oxygen is considered, or (1.4) when considering both oxygen and carbon dioxide.

$$\varphi = \frac{O_2^i - O_2}{O_2^i(1 - O_2)} \tag{1.3}$$

$$\varphi = \frac{O_2^i(1 - CO_2) - O_2\left(1 - CO_2^i\right)}{O_2^i(1 - CO_2 - O_2)} \tag{1.4}$$

where O_2 is the oxygen analyzer reading at the time of interest (mole fraction),

CO_2^i is the initial reading of the carbon dioxide analyzer (mole fraction),

CO_2 is the carbon dioxide analyzer reading at time of interest (mole fraction) and

V is the volumetric flow rate through the exhaust duct, given as equation (1.5) corrected to 25ºC (m^3/s).

$$V = \frac{26.54}{\rho_{298}} \frac{A\ k}{f(Re)} \sqrt{\frac{\Delta P}{T}} = 2.69k \sqrt{\frac{\Delta P}{T}} \tag{1.5}$$

Where ρ_{298} is the density of air at 25ºC, 1.18 (kg/m^3),

A is the cross-sectional area of the exhaust duct (m^2),

k is the duct calibration factor ($m^2/s^{3/2}N^{1/2}$),

$f(Re)$ is the Reynolds number correction for the bidirectional probe (Pa),

ΔP is the pressure difference recorded by the bidirectional probe (Pa), and

T is the temperature of the gases in the exhaust duct (K).

1.2.2 Full-Scale Tests

Full-scale testing involves experiments carried out on materials in their end-use configuration. The testing conditions simulate controlled fire scenarios. Standards like the CAN/ULC-S137 in Canada (Underwriters Laboratories of Canada, 2017) and 16 CFR Part 1633 in the United States of America (U.S. Consumer Product Safety Commission, 2011) are full-scale tests that have been adopted to regulate mattresses. These tests aim to reduce the possibility

of room flashover by only allowing the production of mattresses with slower rates of fire growth. Figure 1-4 shows the typical fire growth curve. In room fires where the heat release rate exceeds 1000 kW, the room typically experiences flashover conditions depending on the size of the room and other factors. According to ASTM, Flashover is considered to have occurred when the test room reaches any two of the following conditions (ASTM, 2017d);

- Heat release rate exceeds 1 MW,
- Heat flux at the floor exceeds 20 kW/m^2,
- Average upper layer temperature exceeds 600°C,
- Flames propagate through the doorway, and/or
- Autoignition of paper on the floor.

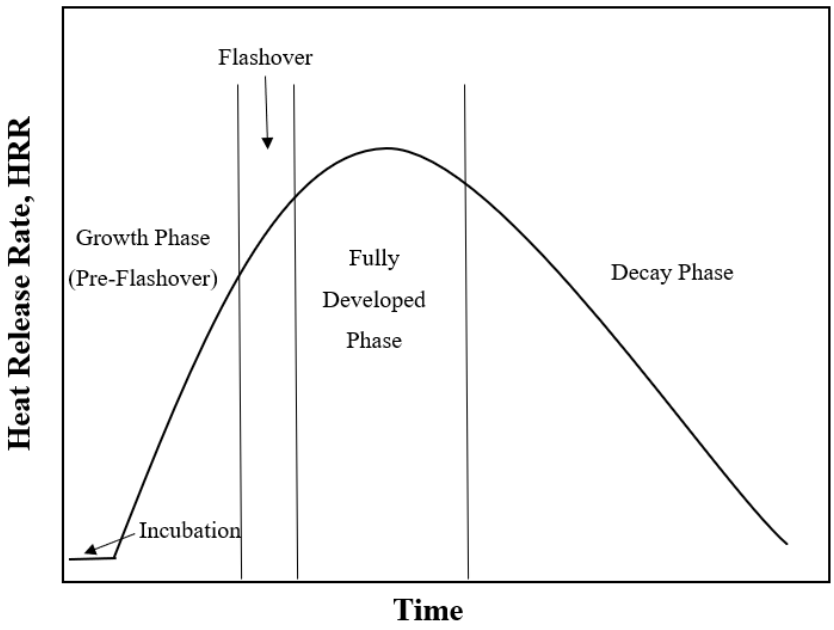

Figure 1-4: Fire Growth Curve (Drysdale, 2011)

The aforementioned full-scale tests are open flame mattress tests that investigate the rate of temperature rise of the mattress. 16 CFR Part 1633 (U.S. Consumer Product Safety Commission, 2011) requires that the material does not exceed a peak heat release rate of 200 kW at any time within the 30 minute test period and the total heat release rate does not exceed 15 MJ for the first 10 minutes of the test. A propane burner is specified as the ignition source and the

mattress is ignited on the top and side of the specimen. This exposure simulates pre-ignition from an external flaming source, which is typical in actual mattress fires.

These tests, however, have some limitations. The use of propane burners simulates only high heat flux exposures for piloted ignition. Information on lower heat fluxes and non-piloted ignition cannot be obtained from this test method. The standard does not assess directly the contribution of the mattress to a developing fire within a compartment. Thus, if there are other combustibles within the space, there is a tendency that actual room fire conditions may exceed design conditions. ASTM E1590 (ASTM, 2017c), which is a method to determine the burning behaviour of mattresses and mattress foundations in public occupancies and CFR 1632 (U.S. Consumer Product Safety Commission, 2014), which is established to determine the smouldering ignition resistance of mattress and mattress padding when exposed to a smouldering ignition source are other full-scale tests. Because testing involves full-sized specimens, tests are very expensive, and few specialized facilities are able to carry out the experiments.

The furniture calorimeter is often used to measure the heat release rate of materials in full-scale testing. Items such as upholstered furniture and mattress are currently tested in full-scale since small-scale testing of individual components (fabrics, foam, and springs) may not give an accurate representation of the fire behaviour of the complete item. The furniture calorimeter shown in Figure 1-5 consists of a load cell (weighing platform) placed under a standard fume hood. When the material to be tested is ignited and allowed to burn under open-air conditions, the gases from combustion are collected through the fume hood and oxygen consumption, flowrate, and smoke production and density are measured in the exhaust duct. The process of oxygen consumption calorimetry (equation 1.2) is used to determine the material rate of heat release (Janssens, 2016). Some examples of standards developed to regulate full-scale testing of mattress and chairs are ASTM E1590 (ASTM, 2017c) and 16 CFR 1633 (U.S. Consumer Product Safety Commission, 2011).

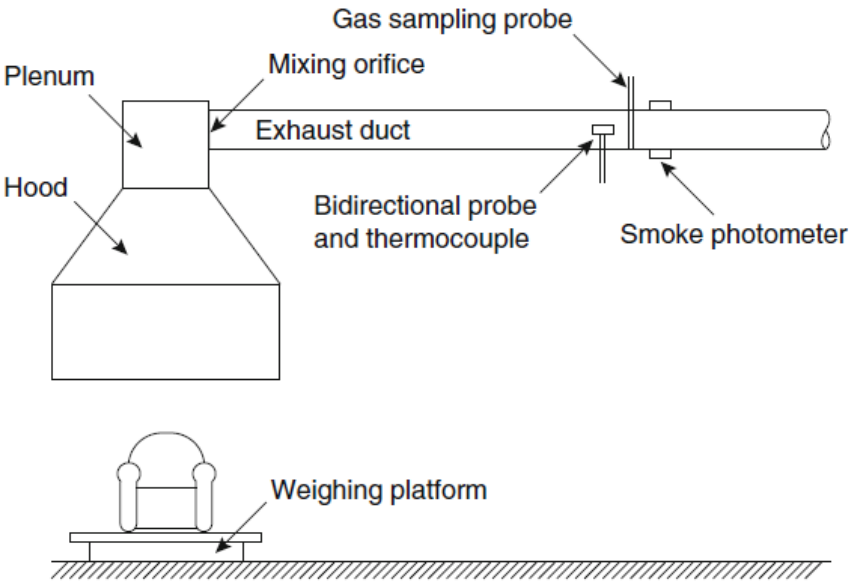

Figure 1-5: Schematic View of the Furniture Calorimeter (Used with Permission. Janssens, 2016)

Room fire tests are full-scale tests used to evaluate the fire performance of materials in a compartment under specific fire scenarios. The contribution of the wall and ceiling linings to fire growth is observed. Heat release rate and room temperatures are among the parameters that are measured. It is important to note that some mattress room test standards also give an option for testing to be carried out in a furniture calorimeter. ISO 9705 (ISO, 2016b) and ASTM E2257 (ASTM, 2017d) are two common standards for room fire tests. The fire test is carried out in a 2.4 m wide by 3.6 m long by 2.4 m high room with a doorway (ventilation opening) of 0.8 m by 2 m. The room is naturally ventilated, and the exhaust gases are collected through a fume hood similar in operation to the furniture calorimeter as shown in Figure 1-6.

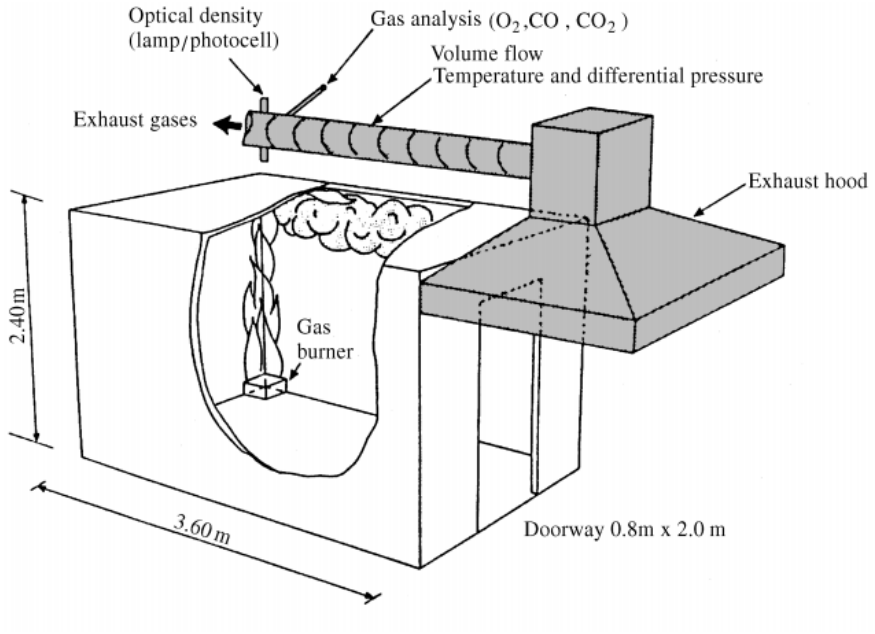

Figure 1-6: The ISO 9705 Room Fire Test (Used with Permission. Drysdale, 2011)

The CAN/ULC-S137 is another room fire test standard similar to the ISO 9705 albeit with a few differences. The room dimensions of the CAN/ULC-S137 test room measures 3.6 m wide by 3.05 m long by 2.4 m high with a doorway located at one end of the room width measuring 0.8 m by 2 m. This difference may lead to variations in flame propagation and smoke movement. The information obtained from room fire tests is used to evaluate the conditions in the room as well as determine the potential of the fire to spread beyond the room by evaluating the time for the room to flashover. The test is stopped once flashover occurs or after a specified duration.

1.2.3 Small-Scale Tests

The cone calorimeter is a similar apparatus to the furniture calorimeter although, much smaller with the addition of a conical radiant heating panel (cone heater). Fire behaviour of smaller sized specimens can be studied using the cone calorimeter. Similar to the furniture calorimeter, heat release rate, smoke production, heat of combustion and mass loss rate are measured. A schematic view of the cone calorimeter is shown in Figure 1-7.

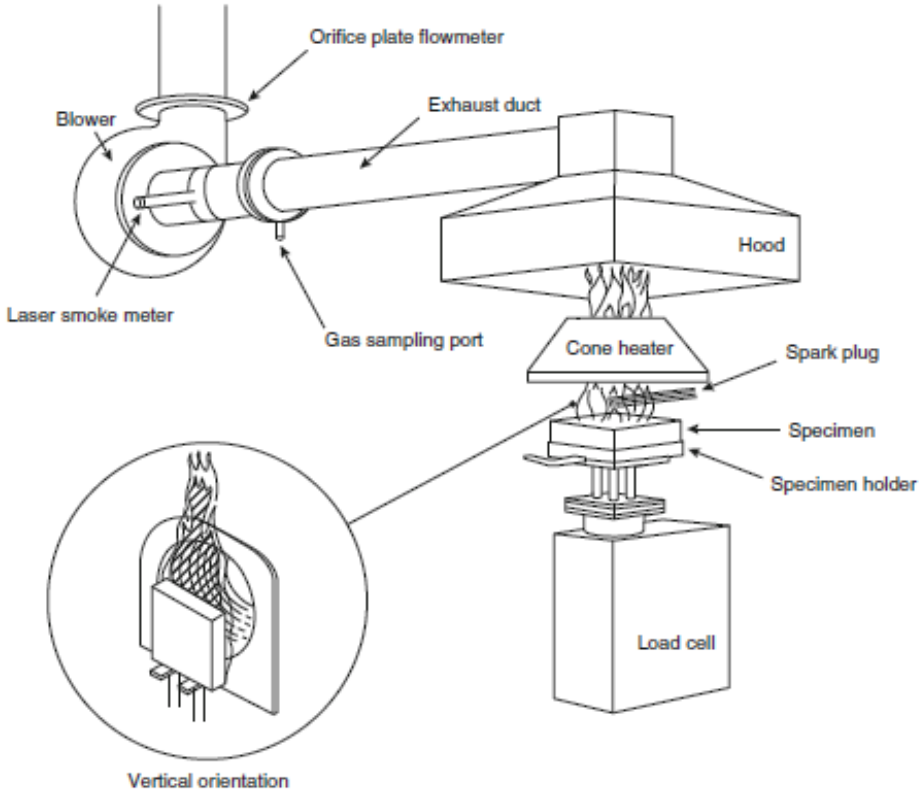

Figure 1-7: Schematic View of the Cone Calorimeter (Used with Permission. Janssens, 2016)

ASTM E1354 (ASTM, 2017b), NFPA 271 (National Fire Protection Association, 2004a) and ISO 5660 (ISO, 2015a) are standards for cone calorimeter operation. The equipment is made up of an electric cone heater which delivers heat fluxes up to 100 kW/m^2 based on its temperature. Specimens with dimensions of 10 cm by 10 cm are tested by placing them on a load cell located under the cone heater. The orientation of the cone heater may be adjusted from horizontal to vertical depending on the type of material being tested. Due to the radiant heating of the material, pyrolysis occurs and the products are ignited using a spark igniter located at the top of the specimen. The load cell measures the mass loss rate while the gas analyzers measures the concentration of oxygen, carbon dioxide and carbon monoxide. The cone heater is calibrated using a Schmidt-Boelter heat flux gauge to ensure proper heat flux exposures. The gas analyzer is calibrated using gas samples of nitrogen, and carbon dioxide and carbon monoxide with known concentrations and flowrates.

Small-scale testing addresses some of the challenges associated with full-scale tests. Small-scale tests involve burning a component of the actual sized material. This is a cost-

effective approach and the tests have the ability to offer insight on the micro-scale burning behaviour of the material. However, some realism is lost, as these tests do not completely represent the full-scale burning behaviour. ASTM E1354 is the test standard for measuring heat and smoke release rate using the cone calorimeter (ASTM, 2017b). The standard is similar to ISO 5660 (ISO, 2015a). ASTM E1474 is used to determine the fire behaviour of reduced size mattress specimens (ASTM, 2017g).

There are other small-scale test standards that are applicable to mattresses. CAN/CGSB-4.2 No./N° 27.7-2013 (Standards Council of Canada, 2013) involves the use of a cigarette as an ignition source. ASTM E906 (ASTM, 2017f) is used to measure the changes in temperature and optical density of the gases evolved from materials that are exposed to a radiant heat source. From the test data, the heat release rate and visible smoke are calculated. ASTM D 3675 is used to measure the heat evolved from materials that are difficult to ignite, by exposing the top of the specimen to a radiant heat source. A heat flux of about 12 kW/m^2 (radiant output equaling intensity of a blackbody at 670 ± 4°C) is incident on the test specimen. This standard finds application in fabrics, insulation and cushioning materials for high-temperature industrial use (ASTM, 2017a).

1.2.4 Field Fire Tests

Field fire testing involves testing of materials in their end-use conditions. Increased realism is one of the main advantages of this type of test. Test conditions are not typically controlled; as such ambient temperature, wind speed and direction, humidity and other factors are dependent on the weather conditions at the time of testing. Testing of various materials is often done in remote locations to reduce the fire risk to adjacent structures or people, hence equipment is usually set-up and calibrated in labs before transportation to the experiment sites. Regardless of the large uncertainties associated with field tests, they are an essential tool to understand real-life fire behaviour of materials. Parameters such as temperature, heat flux, and smoke production can be monitored while looking at the interaction of a specimen with adjacent materials within the space. These tests also offer opportunities for collaboration with various research group and the fire service and contribute greatly to information used to develop environmental and safety regulations.

Some notable field fire tests include the St. Lawrence burns conducted by the National Research Council in 1958 (Stephenson, 1959). This test investigated the intensity of radiation emitted from burning buildings. The results of these test carried out in abandoned buildings in Ontario were instrumental in determining the minimum separation distance for buildings stipulated by the National Building Code of Canada. The Kemano fire tests, also conducted by the National Research Council, examined smoke detector responses in compartment fires. Compartment temperatures, gas concentrations and egress routes were also studied (Su, 2002).

1.3 FIRE SCALING

Fire scaling involves using small-scale test data to predict full-scale fire behaviour. Full-scale heat release rate data is typically used in fire modelling. However, due to limited test centres and the high cost of testing in full-scale experiments, it has become desirable for manufacturers, researcher, regulators and others to use small-scale data to model material fire performance. The challenge with small-scale data is the fact that the information obtained is not able to fully describe the real-life fire behaviour of the material. Researchers have attempted to predict the full-scale burning behaviour by creating pyrolysis models (Babrauskas, 2016). The idea behind this approach is that the burning of the material is driven by the rate of pyrolysis. For a material to burn, it is required to off-gas, hence, a direct relationship exists between the rate at which the material decomposes and the rate of burning. This brief explanation does not fully describe the complexities of the pyrolysis process. The material may undergo various physical and chemical changes during this process. Changes in density, porosity, oxygen entrainment within the combustible material will lead to various difficulties and uncertainties in modelling the burning process.

Various researchers have implemented fire models for mattresses using either a pyrolysis model or solving the Naiver-Stokes equations (using the finite element or finite volume method) for fluid transport. (Prasad, et al., 2009) (Butler, 2009) (Saber, Kashef, Bwalya, & Lougheed, 2010). Notwithstanding the models' ability to predict full-scale fire behaviour, a large number of input data was required, and the models were computationally tasking.

Another significant contribution to mattress fire scaling involves the development of three fire models referred to as model I, II and III by the European Combustion Behaviour of Upholstered Furniture (CBUF) research program (Sundstrom, 1996). The three models attempt

to predict the fire behaviour of mattresses and upholstered furniture based on cone calorimeter tests of representative specimens of the actual furniture. Model I involved the use of statistically correlated factors to predict the peak heat release rate, time to peak heat release rate and time to which room conditions are considered untenable. The application of the model was limited to upholstered chairs.

The development of Model II was based on the concept that only ignited portions in a room fire will contribute to the overall heat release rate. Cone calorimeter data was used to model the heat release rate under the assumption that the ignited material will contribute the same heat release rate to the room as its heat release curve in the cone calorimeter test. The general idea was developed as an extension of flame spread models for wall and ceiling linings (Cleary, Ohlemiller, & Villa, 1992). The full-scale heat release rate is obtained as a convolution product of the cone calorimeter data and the burning area. It is expressed mathematically as (Sundstrom, 1996):

$$Q(t) = \int_0^t q''(t-\tau) A_f(\tau) d\tau \qquad (1.6)$$

Where; $Q(t)$ is the predicted full-scale heat release rate of the mattress (kW)

$q''(t-\tau)$ is the heat release rate density from the cone calorimeter (kW/m^2),

$A_f(\tau)$ is the area burning rate (m^2/s),

τ is a dummy variable (s).

In order to estimate the area burning rate, an effective area was determined by the deconvolution of the full-scale heat release rate curve to match the cone calorimeter heat release rate curve. The CBUF research program applied this method to 20 different types of armchairs. Once the deconvolution was carried out for a certain furniture geometry, a determination of the heat release rate was done for different materials with similar geometry. The results of the model showed reasonable agreement to experimental data for similar geometries. The authors noted that more study would be required to develop burning rates for other geometries.

Model III was developed more specifically to mattresses. It bore close similarities to Model II as it predicted full-scale heat release rate using cone calorimeter data. The model was

based on thermal fire spread theory of upward and concurrent flame spread (Baroudi & Kokkala, 1992). The flame from the mattress was modelled as a cylinder. The simplification allows for the calculation of radiative heating of the unburnt foam. Once the flame spread rate is found, the full-scale heat release rate was obtained similar to Model II by applying the convolution method. Model III was used to determine the heat release rate of various mattresses and showed good agreement with experimental results (Sundstrom, 1996).

1.4 FLAME SPREAD

The growth of fire is influenced by the spread of flame. The faster the flame spread the greater the propensity of the material to burn. As flame spread is highly dependent on the heat transfer between the flame front and the unburnt material, the rate of flame spread over a semi-infinite solid is inversely proportional to the material's thermal inertia (Drysdale, 2011). Factors such as chemical, physical and environmental conditions affect the rate of flame spread. Flame spread is covered in depth in subsequent chapters. With regards to determining flame spread as an input to the CBUF models, previous University of Saskatchewan research has adopted various experimental and computational methods for flame spread determination highlighted in the next section.

1.5 PREVIOUS UNIVERSITY OF SASKATCHEWAN RESEARCH

Mattress fire research at the University of Saskatchewan has involved a variety of small-scale, full-scale and field fire tests. These tests are often accompanied by numerical fire modelling as research attempts to bridge the gap between small and full-scale fire test results. One of the first field fire tests involving the University of Saskatchewan was conducted in collaboration with the University of Alberta (Dale, Ackerman, Torvi, Threlfall, & Thorpe, 2004, Threlfall, Torvi, & Thorpe, 2004). Temperature and heat flux measurements for three individual room fires followed by a whole house fire was acquired from the experiments conducted in Edmonton in July, 2003. Peak heat fluxes of 50 kW/m^2 were measured for the individual rooms while a heat flux of approximately 15 kW/m^2 was measured at a distance of four metres from the exterior wall of the building. Individual room temperatures rose to 600℃.

Another set of field fire tests were conducted in Edmonton in September, 2004 (Threlfall & Torvi, 2005). Temperatures and heat fluxes from three mattress fires were examined. Two mattresses were made of polyurethane foam and the other was made of fibre and rayon. The wall

and ceiling temperature distributions were measured. The polyurethane foam experienced flaming combustion while the fibre and rayon mattress only smouldered. Threlfall and Torvi compared the room temperature data with temperatures predicted using Alpert's correlation (Threlfall & Torvi, 2006).

Alpert (1972), in his study of the behaviour of fire plumes near the ceiling of a room, developed a correlation which predicts the ceiling temperature rise as a function of the convective heat release rate, the height of the compartment, the radial distance along the ceiling from the centre of the plume and a factor (k) that accounts for the location of the fire relative to its position with the walls of the room. Alpert's two ceiling jet equations are given as (Drysdale, 2011):

$$T_{max} - T_{amb} = 5.38\frac{(\frac{k\mathrm{Q}}{r})^{\frac{2}{3}}}{H} \qquad [r > 0.18H] \tag{1.7}$$

$$T_{max} - T_{amb} = 16.9\frac{(k\mathrm{Q})^{\frac{2}{3}}}{H^{\frac{5}{3}}} \qquad [r \leq 0.18H] \tag{1.8}$$

Where Q is the convective heat release rate (kW),

H is the height of the compartment (m),

r is the radial distance along the ceiling from the centre of the plume (m), and

k is a factor that accounts for the location of the fire.

The major shortfall of Alpert's correlation is its inability to account for flame spread in a room. It assumes the fire is at a fixed location and is stationary (i.e., r in the above equations does not change with time). This may not be the case in a real-life room fire. It is more likely that flame will spread across a large burning surface and other materials in the room. Alpert's correlation requires heat release rate inputs which were not measured during the experiments. Instead, an idealized curve was used to model the rate of energy release. The model was a t-squared fire model expressed mathematically as (Drysdale, 2011);

$$Q = \alpha(t - t_0)^2 \tag{1.9}$$

Where Q is the heat release rate in kilowatts (kW),

α is a fire growth coefficient depending on fuel type (kW/s^2),

t is the time (s), and

t_0 is the incubation time in seconds (The incubation time accounts for the time taken to sufficiently heat up the material for combustion. Figure 1-4).

This model is a parabolic fire growth curve in which the fire growth coefficient (α) defines the rate of flame propagation. α is dependent on the fuel type, and often a design fire is described as slow (0.00278 kW/s^2), medium (0.01111 kW/s^2), fast (0.04444 kW/s^2) or ultra-fast (0.17778 kW/s^2). Hurd et al. (2007) applied a different method for determining the heat release rate. An assumption was made that the product of the time-dependent fire area ($A_f(t)$), obtained from full-scale test photographs and video records, and the average heat release rate density ($\ddot{q}$) measured in the cone calorimeter could predict the full-scale heat release rate ($Q(t)$) of the mattress (Hurd, Torvi, Weckman, & Enninful, 2007). This is mathematically expressed as;

$$Q(t) = A_f(t)\ddot{q} \tag{1.10}$$

The predicted heat release rates were compared to experimental data; one example is shown in Figure 1-8. Both models were able to reasonably predict the fire growth in these experiments. The t-squared fire does a better job predicting the growth phase of the fire, but is unable to predict the fire decay (Figure 1-4) as this is not accounted for in the equation. The flame spread model over predicted the growth phase which was attributed to the use of an average heat release rate density rather than a time-dependent value. In reality, during the earlier stages, the fire will not be fully developed (steady burning, Figure 1-4) and hence heat release rates will be much lower. The flame spread model is, however, able to better predict the decay phase of the fire.

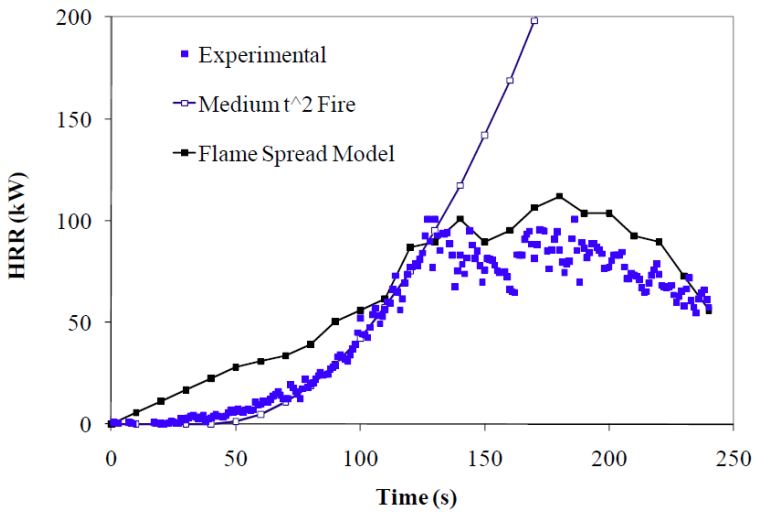

Figure 1-8: Heat Release Rates Comparisons (Hurd et al., 2007)

Previous University of Saskatchewan research on the use of the CBUF models for mattress fire scaling can be summarised as shown in Figure 1-9. Heat release rate density data obtained from the University of Saskatchewan cone calorimeter tests are combined with flame spread rates obtained via different methods. The output heat release rate from the CBUF model (equation 1.6) is compared to full-scale heat release rates measured at the University of Waterloo fire testing laboratory.

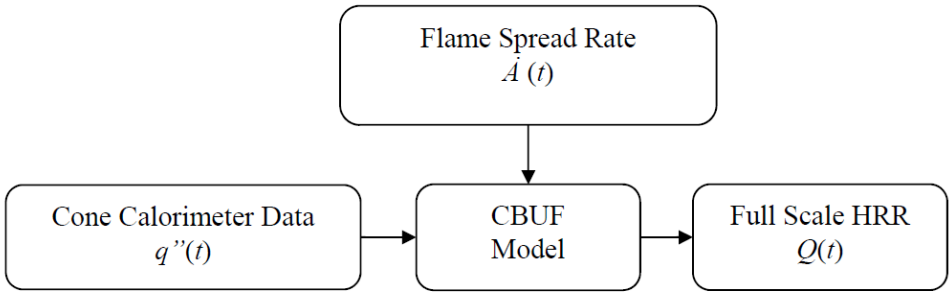

Figure 1-9: Fire Scaling Flowchart (Robson, 2014)

Ezinwa et al (2009) used the CBUF model to estimate the heat release rate of polyurethane foam. The model takes into account the changing area of the foam with time as the material burns. The area spread was determined by drawing gridlines on the mattress for the full-scale burns and using video and infrared records to manually determine the area of the foam on

fire at any point in time Ezinwa (2009). The model showed good agreement with experimental data but required full-scale flame spread data to determine the heat release rate.

Robson et al (2010) examined the effects of foam thickness and ignition location on flame spread and heat release rate predictions using the convolution model. The model did a better job of predicting the heat release rate for edge ignition when compared with centre ignition. Similar to Ezinwa (2009), the flame spread model used by Robson (2014) was obtained using infrared images from the full-scale tests but Robson (2014) applied binary image transformation based on the assumption that the flame front is located at any point that measures 300℃ on the mattress. This allowed the time-dependent flame area to be determined automatically. Contour lines, as seen in Figure 1-10, were generated which showed the movement of the flame front, which appeared to be influenced by the direction of airflow under the exhaust hood.

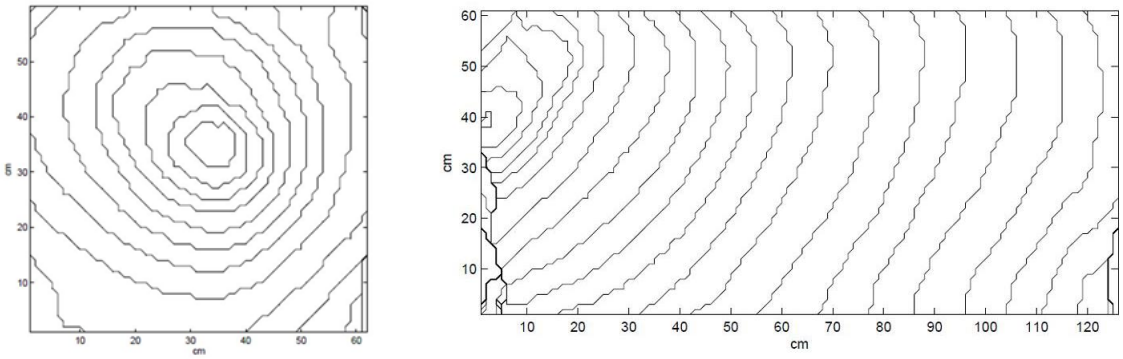

Figure 1-10: Flame Spread Contours: Center Ignition - Left, Edge Ignition – Right (Robson, 2014)

Figure 1-11 shows an example of Robson's (2014) results. The CBUF model does a good job of predicting the fire growth phase (A), the peak heat release rate (B) and the fire decay phase (C). The results showed generally good repeatability over a range of mattress thicknesses, but predictions were better for the thinner foams when compared to the thicker foams.

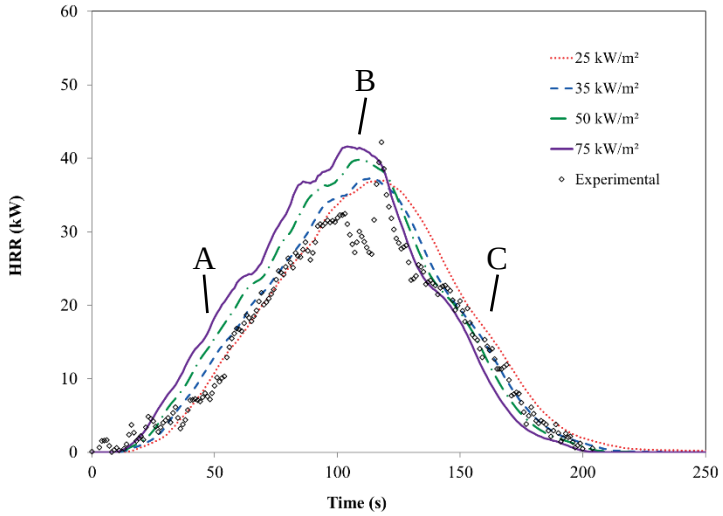

Figure 1-11: Comparison of Heat Release Rate Results: A – Growth Phase, B – Peak HRR, C – Decay Phase. (Robson, 2014)

Finally, because both models require flame spread input from a full-scale test, this approach did not allow the CBUF model to operate as a fully predictive model. The use of the convolution model in combination with an independent flame spread model would enable the prediction of full-scale fire behaviour using solely small-scale data.

1.6 SCOPE AND OBJECTIVES OF RESEARCH

The main goal of this research is to improve methods for scaling small-scale fire test data to predict full-scale fire behaviour. The focus of this work will be on polyurethane foams which have been shown to be a major contributor to residential fires. To achieve this goal, the University of Saskatchewan, in collaboration with the University of Waterloo fire research group, carried out a series of polyurethane foam fire tests in a shipping container at the University of Waterloo Live Fire Facility in 2014. Temperatures and heat fluxes were measured, and infrared and live video, and still images were taken.

This research will attempt to predict the heat release rate of the room using the CBUF model, and then predict temperatures in the shipping container using Alpert's correlation. The information gathered from the full-scale and small-scale tests will be used to develop a mathematical flame spread model of the foam. The flame spread model takes advantage of experimental data to predict time-dependent flame spread areas. The specific objectives of the research are:

1. To conduct further cone calorimeter tests on foam samples which will be used to determine the critical heat flux of polyurethane foams. The focus of testing will be on the exposure of the foams to lower heat flux levels. The new test data will supplement the cone calorimeter data obtained by Robson (2014).
2. To collect small-scale infrared and thermocouple temperature measurements using the cone calorimeter for different heat fluxes. This data will be essential in understanding the foam heat transfer and allow for investigation on the influence of heat flux on foam burning characteristics.
3. To develop small-scale heat transfer models of polyurethane foam for cone calorimeter tests. The models will be focused on predicting temperature rise pre foam ignition.
4. To develop a time-dependent flame spread model for polyurethane foam. The model will be based on analysis of cone calorimeter test data. The model will account for centre and edge ignition.
5. To incorporate the time-dependent flame spread model into existing fire protection engineering correlations. Predictions from models such as CBUF model (for full-scale heat release rate predictions) and Alpert's correlation (for temperature predictions) will be compared to University of Waterloo furniture calorimeter and shipping container fire test data for model validation.

To achieve these objectives, small-scale cone calorimeter tests were conducted using 5, 7.5 and 10 cm thick foams exposed to 5 kW/m^2, 10 kW/m^2, 15 kW/m^2, 20 kW/m^2, 35 kW/m^2 and 50 kW/m^2. Data from previous small-scale and full-scale polyurethane foam tests were analysed to inform modelling decisions. Chapter 1 of this thesis gives a general introduction on topics considered critical to understanding fire testing, modelling and scaling. Chapter 2 details the methodology and results obtained from small-scale cone calorimeter tests of polyurethane specimen carried out at the University of Saskatchewan fire laboratory. Thermocouple and infrared temperatures measurements collected during small-scale tests are reported. Chapter 3 discusses the full-scale foam test performed at the University of Waterloo shipping container facility. This chapter also reports temperature measurements obtained in the space during testing. Chapter 4 provides an approach to small-scale fire modelling. The focus of the model was on the

solid phase heat transfer process prior to ignition of the foam specimen. Chapter 5 describes the scaling of fire test results and compares predictions of shipping compartment temperatures with measured values. Conclusions and recommendations for future work are provided in Chapter 6.

2 SMALL-SCALE EXPERIMENTS

As mentioned in the introductory chapter, the over-arching goal of this research is to improve the understanding of fire scaling. This chapter details the small-scale (cone calorimeter) experimental procedure, apparatus and materials as well as the results obtained. Small-scale polyurethane foam testing carried out in the cone calorimeter was required for full-scale fire behaviour predictions. The data obtained supplemented data from prior University of Saskatchewan small-scale tests (Robson, 2014).

2.1 CONE CALORIMETER TEST SPECIMEN

The polyurethane foams used in the cone calorimeter experiments were specimens taken from the same pieces of foam used by previous University of Saskatchewan fire group researchers (from 2008 – 2011). The majority of the foams in this study were also used by Robson in his research (Robson, 2014). Robson reported that the foams were purchased from outlets of a Canadian retail chain in Saskatoon or Waterloo. Robson found no details about the specific chemical compositions of the foams but stated that the foams were less dense than foams typically found in furniture and did not appear to contain fire retardants. This was confirmed by the author as small-scale tests showed that the foams were easily ignited under sufficient heat flux exposures. Fires in small-scale tests also propagated quickly consuming the entire test specimen. The other foam specimens were used by Ezinwa (2008). It is important to note that there were variations in foam properties from specimen to specimen due to the differences in time of purchase and foam conditions during storage.

2.2 CONE CALORIMETER TESTING

As discussed in Section 1.2.3, small-scale tests were carried out in accordance with ASTM E1474 (ASTM, 2017g). The small-scale test apparatus used in this research was the University of Saskatchewan's Fire Testing Technology (FTT, East Grinstead) Dual Cone Calorimeter, located in the Thermo-Fluids Laboratory in the Engineering Building at the

University of Saskatchewan. Figure 2-1 shows a photograph of the cone calorimeter apparatus. Valuable information such as the heat release rate, mass loss rate, effective heat of combustion, ignition time and extinction time can be measured using this device.

Figure 2-1: University of Saskatchewan Cone Calorimeter

The cone calorimeter can be categorised into three functional parts: the cone heater, the cone tower and the gas analyzer tower. The cone heater is a conical shaped electric heating element which delivers the required heat flux exposure for testing (0 – 100 kW/m^2). The cone heater element is maintained at a predetermined temperature corresponding to the heat flux required. Studies conducted by prior University of Saskatchewan researchers show that the cone heater delivers a relatively uniform heat flux exposure. Heat flux measured at the outer edges of the 10 cm by 10 cm test specimen is expected to be approximately 90% of the heat flux measured at the middle of the test specimen (Rezazadeh, 2014). The University of Saskatchewan cone heater is designed with an air-cooled shutter to prevent significant heating of the test specimen before the start of the heat flux exposure. When the air-cooled shutter is opened, it engages the igniter and when closed, it locks out the spark igniter. This process signals the start

and end of the test. The exhaust ducting is mounted on the cone tower, which also contains the cone temperature and exhaust controls as well as a load cell for measuring the mass of specimens. The Servomex Xentra 4100 gas analyzer (Servomex Company Inc., Boston) is contained in the gas analyzer tower and measures the concentration of exhaust gases (oxygen, carbon dioxide, and carbon monoxide). The plumbing required to pump, cool and dry the exhaust gases is also contained in the gas analyzer tower.

Data acquisition is carried out using an internal and external Agilent 34970A data acquisition systems (Hewlett Packard, Santa Clara). The data from the cone calorimeter is finally collected for post-processing on the computer by means of the ConeCalc 5 software program (also supplied by FTT), which provides the user interface.

2.3 CONE CALORIMETER SPECIMEN PREPARATION

In this research, three thicknesses of polyurethane foam were selected for the cone calorimeter tests: 5 cm (2 in), 7.5 cm (3 in) and 10 cm (4 in). The test specimens were cut using a knife so that their exposed surface area was 10 cm by 10 cm (see Figure 2-2) in accordance with ASTM E1474 test standard (ASTM, 2017g).

Figure 2-2: Foam Test Specimen

The pre-conditioned specimens were weighed using the Voyager® Pro balance (Ohaus, Pine Brook). Specimen information is given in Table 2-1. The naming convention used in the

cone calorimeter tests is: thickness (inches) – heat flux – test number (i.e. 4-5-1 will represent a foam 4 inches (101.6 mm) thick exposed to a 5 kW/m^2 heat flux which was the first test in this series). The average mass reported was determined over the individual tests in the series. The standard deviation (σ) of the measured mass was calculated to be less than one gram (1 g) for all the test series. The variations in mass can be mainly attributed to the uncertainties in cutting the foam specimens to test sizes. The past University of Saskatchewan test procedure (Robson, 2014) was used; only the bottom 1 cm of the test specimen was wrapped in aluminium foil (see Figure 2-4), in order to contain the molten foam. This procedure differs slightly from the ASTM E1474 standard, which suggests the entire outer surface of the foam be wrapped with the aluminium foil to prevent heat losses (ASTM, 2017g).

Table 2-1: Test Specimen Information

Test Series	Mass (g)		Thickness (cm)	Density (g/cm^3)
	Average	σ		
4-5	15.87	0.18	10	0.016
4-10	16.19	0.80	10	0.016
4-15	15.86	0.45	10	0.016
4-35	16.24	0.14	10	0.016
3-5	12.33	0.66	7.5	0.016
3-10	11.78	0.62	7.5	0.016
3-15	12.67	0.84	7.5	0.017
3-35	12.92	0.25	7.5	0.017
2-5	8.27	0.36	5	0.017
2-10	8.51	0.34	5	0.017
2-15	8.51	0.46	5	0.017
2-20	8.35	0.08	5	0.017
2-35	7.99	0.31	5	0.016
2-50	8.16	0.21	5	0.016

The specimens were conditioned using an aqueous solution of magnesium chloride with a density of 1.27 g/cm^3. The solution was placed at the bottom of a container to maintain a relative humidity of 50% ± 5% inside the container (ASTM, 2017g). The temperature inside the container was maintained at 22℃ ± 5℃ by the building air handling system. As shown in Figure 2-3, the conditioning chamber was constructed using a camping cooler with wire racks mounted for specimen storage. The specimens were placed inside the cooler and conditioned for

at least 24 hours. The temperature and relative humidity inside the cooler were monitored using a CON4095 High Accuracy Thermo-Hygrometer (Fisher Scientific, Ottawa).

Figure 2-3: Foam Test Specimen Conditioning Cooler

The laboratory temperature was controlled centrally by the building air handling system and the value varied between 22℃ to 27℃ during the test period. The building did not provide humidity control and hence relative humidity in the laboratory varied from 22 to 36%. After conditioning for 24 hours, the specimen was removed from the cooler and placed on the load cell of the cone calorimeter for testing. This briefly exposed the test specimen to the ambient room conditions before the actual test start time. Because the relative humidity of the space was significantly lower than the relative humidity of the conditioned specimen, the specimen will tend to lose moisture to the surroundings. This effect was accounted for by reducing the time between when the specimen was removed from the conditioning cooler and when it was tested to less than five minutes.

2.4 EXPERIMENTAL PROCEDURE

The cone calorimeter experiments were designed to measure parameters of interest to this research. The ignition times of the polyurethane foams for varying heat flux exposures, the

effective heat of combustion of the foam specimens, the heat release rate density of the foams and the internal foam temperatures were measured. Infrared and digital photographs and videos were also recorded.

Before testing, calibration of the cone calorimeter was required. The gas analyzer system was calibrated using atmospheric oxygen to produce a voltage corresponding to 21% oxygen and was zeroed by supplying nitrogen gas from the cylinder shown in Figure 2-1. Carbon dioxide and carbon monoxide voltages were spanned using known concentrations delivered from the gas cylinders (Figure 2-1). The heat release rate measurement was calibrated using a 5 kW methane gas burner at an airflow rate of 24 L/min. A calibration factor was obtained and used to determine heat release rates measured over the course of testing. For the various heat flux exposures, the cone heater element was calibrated using a Schmidt-Boelter heat flux gauge positioned at 2.5 cm away from the centre of the cone heater element.

A minimum of three tests were conducted for each foam thickness at heat flux exposures of 5 kW/m^2, 10 kW/m^2, 15 kW/m^2, 20 kW/m^2, 35 kW/m^2 and 50 kW/m^2. The lower heat fluxes (5 kW/m^2 - 20 kW/m^2) were selected to investigate combustion behaviour at lower heat intensities, while the higher heat flux exposures were selected to carry out repeatability studies as data was available from previous research (Robson, 2014). The specimens were placed horizontally on the load cell at a distance of 2.5 cm from the cone heater. The shutter was opened to signal the start of the test. This engaged the spark igniter located above the surface of the test specimen. The spark igniter provides a source of a pilot for ignition of the specimen as a result of the gases evolved from pyrolysis due to heat flux exposure. Once flaming ignition was sustained, the spark igniter was moved to avoid continuous contact with the flames. Figure 2-4 shows photographs of the cone calorimeter test.

Figure 2-4: Cone Calorimeter Heat Release Rate Density Test

The test measurements were recorded at one-second (1 s) intervals by the data acquisition system. Video records of each heat flux exposure were obtained using a Canon Vixia HF R500 video camera. A total of 42 tests were carried out for the polyurethane foam specimens. Each specimen was allowed to completely burn, and the end of the test is indicated by the extinction of visible flames.

To investigate transient heat transfer in the polyurethane foams during small-scale experiments, internal foam temperatures of the 10 cm specimens were measured by instrumenting the foam with five 24-gauge type K thermocouples. The first thermocouple was placed on the top surface of the foam, which provided an indication of the beginning of the heat flux exposure. As shown in Figure 2-5, the other thermocouples were placed two-centimetres apart (2 cm) in holes drilled five-centimetre (5 cm) to the centre of the foam using a pilot hole and screwdriver. The holes secured the thermocouples in place while ensuring that the temperatures obtained from the thermocouples are representative of the internal foam temperature. A FLIR E60 infrared camera (FLIR Systems, Burlington, ON) was also used to obtain infrared videos of the test. The 10 cm specimens were exposed to 5 kW/m^2, 10 kW/m^2, 20 kW/m^2 and 35 kW/m^2 heat fluxes. A minimum of three tests with thermocouples were carried out for each heat flux exposure. After the thermocouples were placed in the foams, the test specimens were conditioned as discussed previously. The voltage readings from the thermocouples were collected by the Agilent 34970A data acquisition system (Hewlett Packard, Santa Clara) at a sample rate of five readings per second and converted to temperature readings for processing.

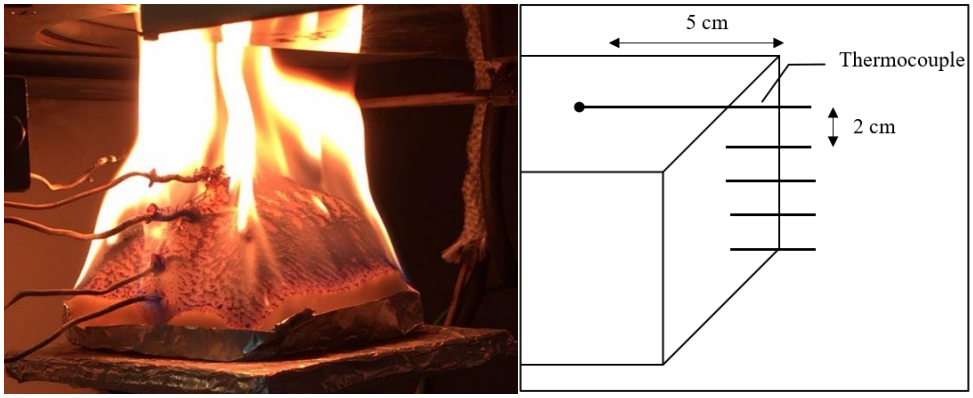

Figure 2-5: Temperature Measurement Test Showing Thermocouple Locations

2.5 HEAT RELEASE RATE DENSITY MEASUREMENTS

This section discusses the results from the cone calorimeter tests. The test results will be described using the nomenclature given in section 2.3. The parameters reported are the peak HRR density, the mean HRR density and the total heat released. These parameters were determined by the cone calorimeter based on oxygen consumption calorimetry (Section 1.2.1). The peak HRR density is the maximum heat release rate density measured over the test duration. The mean HRR density shows the average heat release rate over the test period, from ignition due to the exposure of the foam to the incident heat flux, until material burnout (flameout). The total heat released is the area under the heat release rate curve. It is the total energy released from the combustion of the foam specimen. This section also provides representative plots of the HRR density curves for the various foam thickness. The HRR density curves were normalized to time equals zero (t = 0 s) when the ignition of the foam occurs. Table 2-2 gives the average results for the various parameters measured for the 10 cm thick polyurethane foam for the range of heat flux exposures.

Table 2-2: Cone Calorimeter Test Results (10 cm Thickness)

Test Series	**Peak HRR Density (kW/m^2)**		**Mean HRR Density (kW/m^2)**		**Total Heat Release (MJ/m^2)**	
	Average	**σ**	**Average**	**σ**	**Average**	**σ**
4-5	302.2	26.5	152.4	11.6	39.2	1.6
4-10	332.9	28.1	173.2	7.3	40.0	0.8
4-15	332.0	10.7	173.2	13.5	39.4	1.4
4-35	406.4	35.0	264.1	44.8	39.2	1.3

Over the range of heat flux exposures measured for the 10 cm thick foams, the total heat released is seen to be reasonably consistent (39 MJ/m^2 average) with a maximum standard deviation of 1.6 MJ/m^2 (approximately 4% of the measured values). The highest peak HRR density measured for the 10 cm specimen was 406.4 kW/m^2 for the 35 KW/m^2 heat flux exposure, while the lowest peak measured was 302.2 kW/m^2 for the 5 kW/m^2 heat flux exposure. As shown in Figure 2-6, the peak HRR density is thus seen to be influenced by the incident heat flux. Deviations of approximately 8% of the measured values were calculated in the peak HRR density.

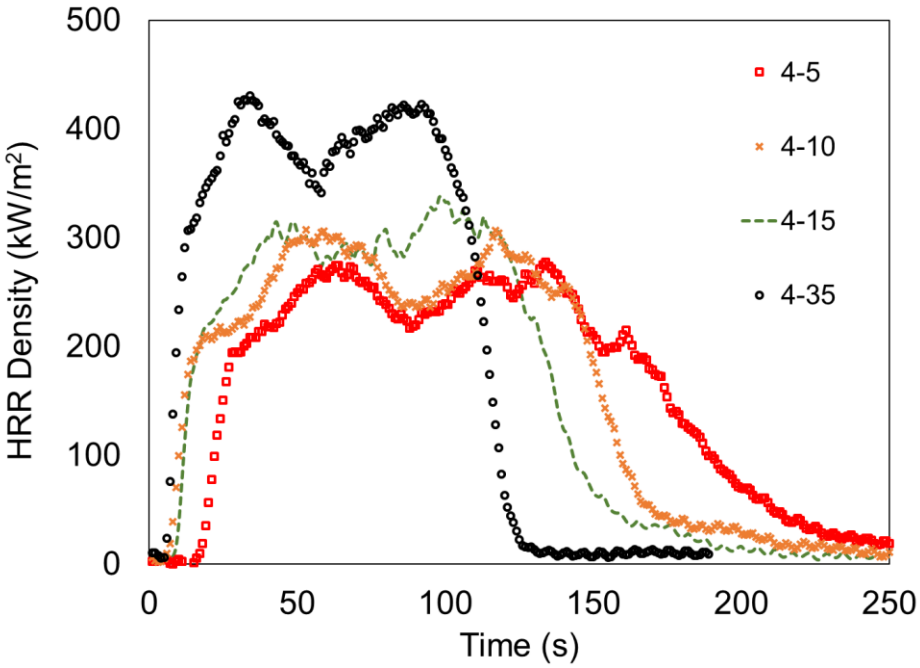

Figure 2-6: HRR Density Curves for the 10 cm Thick Specimen exposed to 5 kW/m^2, 10 kW/m^2, 15 kW/m^{2}and 35 kW/m^2 Heat Flux Exposures

The effect of the incident heat flux on the peak HRR density was also observed by Robson (Robson, 2014). For a range of heat fluxes incident on polyurethane foam with varying thicknesses, the peak HRR density increased with increase in incident heat flux. It was also noted that the general shape of the HRR density curves showed two peaks and was consistent for all the heat fluxes tested for the 10 cm foam specimen. For comparisons of HRR density measurements across foam tests of different sizes, a good approach is to normalize the total heat released with the mass of the specimen. This allows for comparable values as it is expected that

the measured variables should be the same across similar material types (Robson, Torvi, Obach, & Weckman, 2014).

A similar trend to the 10 cm thick foam was seen to occur in the 7.5 cm and 5 cm thick foams. The total heat released measured was relatively constant for similar foam thickness and was independent of the heat flux exposures (Table 2-3 and Table 2-4). However, as foam thickness reduces, variations in the shape of the HRR curve occurs for different heat flux exposures. For the 5.0 cm specimen, the peaks are harder to distinguish at the 5 kW/m^2 heat flux level. This behaviour is attributed to less pools forming from the molten foam at lower heat fluxes as the entirety of the foam is sufficiently heated to ignition temperature. The standard deviations in the parameters obtained over a given test series were fairly small. Figure 2-7 and Figure 2-8 further illustrate the effects of the heat flux exposure on the peak HRR density. The peak HRR density is seen again to increase with an increase in the incident heat flux. For the 5 cm thick foam, additional tests for heat flux exposures of 20 kW/m^2 and 50 kW/m^2 were conducted. The tests supplemented data collected by Robson in 2011 for small-scale polyurethane foam fire behaviour (Robson, 2014).

Table 2-3: Cone Calorimeter Test Results (7.5 cm Thickness)

Test Series	**Peak HRR Density (kW/m^2)**		**Mean HRR Density (kW/m^2)**		**Total Heat Release (MJ/m^2)**	
	Average	**σ**	**Average**	**σ**	**Average**	**σ**
3-5	325.2	49.6	171.6	11.7	31.4	1.1
3-10	352.2	37.7	211.8	23.9	30.5	1.1
3-15	377.0	51.4	180.3	16.4	31.3	2.3
3-35	520.4	43.7	311.8	22.0	33.4	0.3

Table 2-4: Cone Calorimeter Test Results (5 cm Thickness)

Test Series	**Peak HRR Density (kW/m^2)**		**Mean HRR Density (kW/m^2)**		**Total Heat Release (MJ/m^2)**	
	Average	**σ**	**Average**	**σ**	**Average**	**σ**
2-5	281.9	11.1	136.5	16.8	20.9	0.6
2-10	340.2	59.6	145.5	31.3	21.2	0.6
2-15	400.5	23.6	158.8	34.9	21.2	1.5
2-20	411.8	15.8	248.0	5.1	21.7	0.1
2-35	544.1	37.1	258.4	7.6	20.2	0.7
2-50	694.7	49.8	311.0	4.4	20.5	0.1

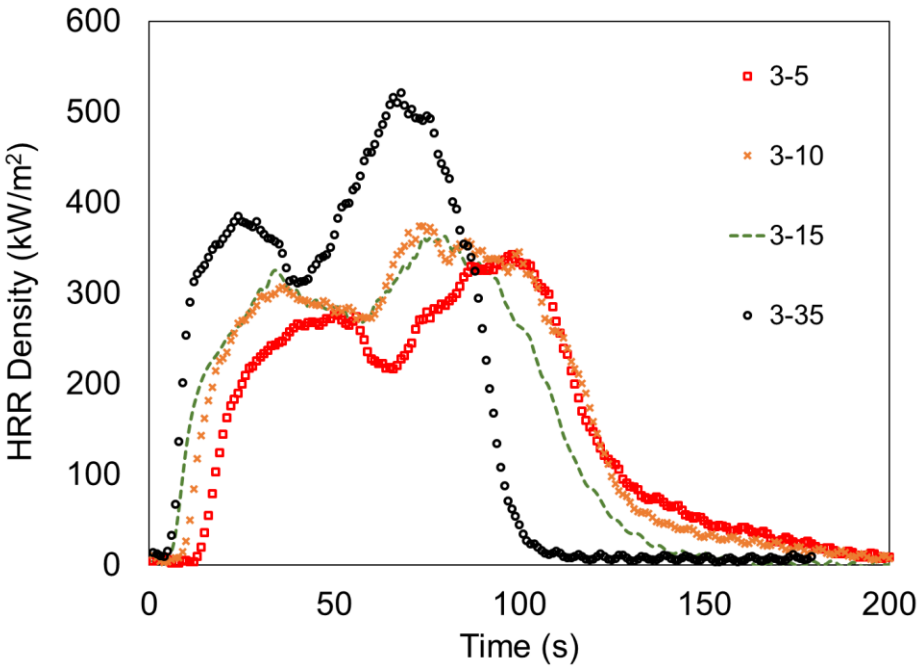

Figure 2-7: HRR Density Curve for the 7.5 cm Thick Specimen exposed to 5 kW/m^2, 10 kW/m^2, 15 kW/m^{2}and 35 kW/m^2 Heat Flux Exposures

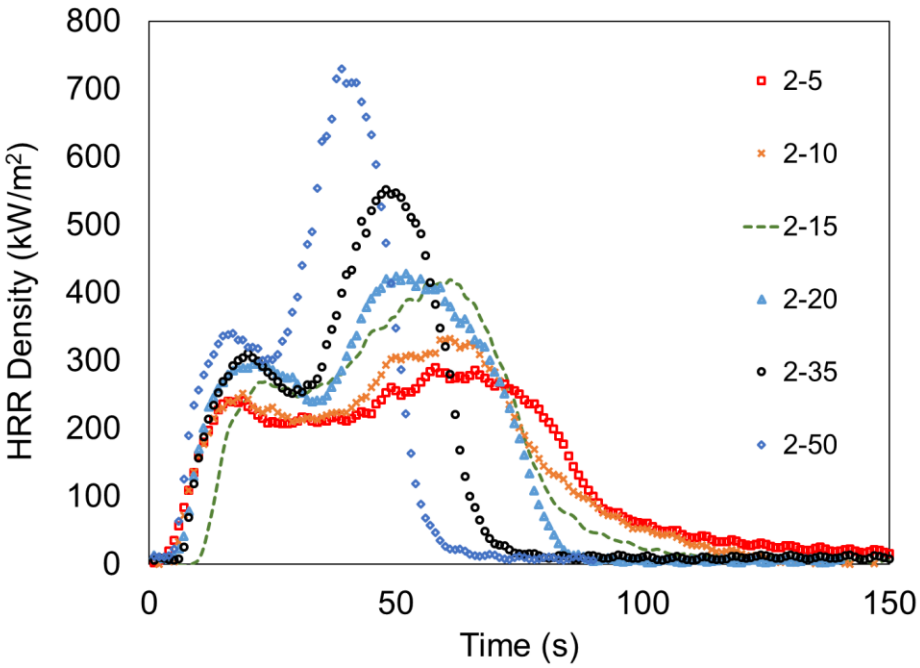

Figure 2-8: HRR Density Curve for the 5 cm Thick Specimen exposed to 5 kW/m^2, 10 kW/m^2, 15 kW/m^2, 20 kW/m^2, 35 kW/m^2 and 50 kW/m^2 Heat Flux Exposures

As mentioned earlier, another component of the experimental research was to supplement previous University of Saskatchewan small-scale fire research with additional cone calorimeter data. This will help enhance the understanding of fire behaviour of polyurethane foam. Table 2-5 gives a summary of information gathered from prior testing done by Robson in 2011. 2.5 cm (1 in) thick specimens were tested in addition to the 5 cm (2 in), 7.5 cm (3 in) and 10 cm (4 in) specimens. The specimens were tested with heat fluxes of 25 kW/m^2, 35 kW/m^2, 50 kW/m^2 and 75 kW/m^2 (Robson, 2014).

The peak HRR density, the mean HRR density and the total heat released measured in the test are reported. Similar to the cone calorimeter tests carried out in this study, there was consistency in the total heat released while greater deviations occurred in the peak HRR density and mean HRR density measurements. A discussion about the repeatability of the cone calorimeter measurements is given in the next section.

Table 2-5: Small-Scale Polyurethane Test Summary (Robson, 2014)

Test Series	**Peak HRR Density (kW/m²)**		**Mean HRR Density (kW/m²)**		**Total Heat Release (MJ/m²)**	
	Average	**σ**	**Average**	**σ**	**Average**	**σ**
1-25	428	34.4	241	7.2	10.5	0.19
1-35	556	29.6	225	11.8	10.4	0.07
1-50	749	63.5	322	72.8	11.1	0.28
1-75	950	57.4	370	25.6	11.3	0.39
2-25	419	13.8	245	12.5	19.6	0.31
2-35	472	19.5	251	2.1	19.5	0.09
2-50	670	17.9	382	14.6	19.7	0.4
2-75	989	26.6	505	13.3	21	0.24
3-25	424	21.4	260	10.2	31.3	0.55
3-35	504	20.6	274	14.1	30.5	1.09
3-50	603	9.9	367	13.9	30.6	1.22
3-75	919	16.4	520	4.8	31.5	0.03
4-25	373	4.8	246	7.9	38.9	0.37
4-35	420	19.5	273	1.6	38	0.63
4-50	503	52.8	347	14.9	37.6	0.88
4-75	723	33	449	50.5	39.6	0.18

2.5.1 Repeatability of the Cone Calorimeter Measurements

This section focuses on the repeatability of the cone calorimeter tests done in this study (2018). Results obtained in 2018 were compared to the Robson's test results. To combine the past and recent data for analysis, it was necessary to limit errors by confirming that heat release rate density measurements are comparable for the same foam thicknesses. The peak HRR density, the mean HRR density and the total heat released were compared in Table 2-6, Table 2-7 and Table 2-8 respectively. A comparison of HRR density curves is shown in Figure 2-9.

The comparison of the Robson's and the 2018 polyurethane foam test series was done for the 35 kW/m^2 heat flux exposure. In general, test results show good agreement albeit with small differences. The standard deviation calculated in the 2018 test series were higher than Robson's. Factors such as variations in foam type, ageing and storage conditions of the foams used for the 2018 tests will likely have influenced test results leading to differences in fire behaviour. For all the thicknesses, the highest difference for the compared parameters between the two-test series was 13%, which was obtained for the peak HRR density of the 2-35 test series. For the 10 cm-35 kW/m^2 test series (4-35), a 3% difference between HRR density results is obtained between the 2018 tests and Robson's tests. These comparisons suggest that analysis carried out using a combination of the two-test series can be done to a good degree of confidence.

Table 2-6: Comparison of the Peak HRR Density for a 35 kW/m^2 Heat Flux (Robson, 2014)

Test Set	Peak HRR Density (kW/m^2)				
	Robson's Test Series		2018 Test Series		% Difference
	Average	σ	Average	σ	
2-35	472	19.5	544.1	37.1	13.3
3-35	504	20.6	520.4	43.7	3.2
4-35	420	19.5	406.4	35.0	3.4

Table 2-7: Comparison of the Mean HRR Density for a 35 kW/m^2 Heat Flux (Robson, 2014)

Test Set	Mean HRR Density (kW/m^2)				
	Robson's Test Series		2018 Test Series		% Difference
	Average	σ	Average	σ	
2-35	251	2.1	258.4	7.6	2.9
3-35	274	14.1	311.8	22.0	12.1
4-35	273	21.6	264.1	44.8	3.4

Table 2-8: Comparison of the Total Heat Released for a 35 kW/m^2 Heat Flux (Robson, 2014)

Test Set	Total Heat Released (MJ/m^2)				
	Robson's Test Series		2018 Test Series		% Difference
	Average	σ	Average	σ	
2-35	19.5	0.1	20.2	0.7	3.3
3-35	30.5	1.1	33.4	0.3	8.6
4-35	38	0.6	39.2	1.3	3.1

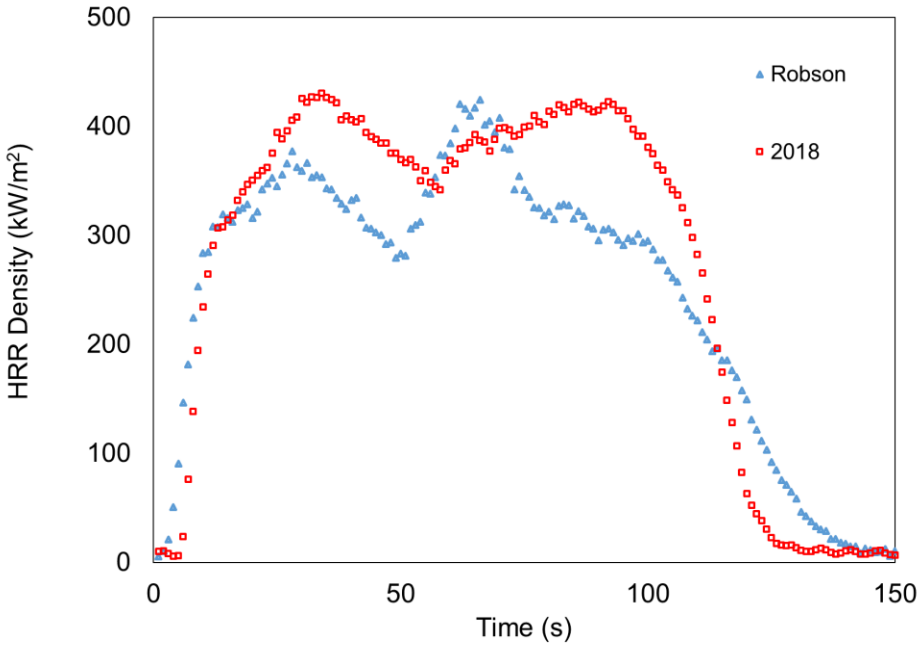

Figure 2-9: Comparison of Two HRR Density Curves Obtained for the 10 cm Thick Polyurethane Foam Specimens for a 35 kW/m^2 Heat Flux Exposure (Robson, 2014)

2.5.2 General Discussions on HRR Density Measurements

One of the most obvious observations from the results from the small-scale tests is the dependence of the peak HRR density on the heat flux. For the 5 cm (2 in) thick foam specimen, on average, values of peak HRR density measured at an incident heat flux of 50 kW/m^2 were 60% higher than the values of the peak HRR density measured at 5 kW/m^2 (Table 2-4). As discussed earlier, prior University of Saskatchewan research also indicated this dependence. An 80% to 135% increase in the values of the peak HRR density was reported to occur as the incident heat flux increased from 25 kW/m^2 to 75 kW/m^2 (Robson, 2014).

Two peaks are seen to occur in the general heat release rate density curve. The peaks represent significant events in the burning of the polyurethane foam. From video records, the first peak is observed to coincide with the breakdown of the foam structure from a solid to liquid polyol. The foam melts and forms a pool. This phase change results in the release of energy seen in the heat release rate density curve. The second peak is the actual burning of the liquid polyol. In the liquid phase, the pool has less thermal inertia and hence burns at a faster rate with higher temperatures. The combustion of the liquid polyol will, therefore, result in the release of more energy.

The two-stage burning behaviour was observed in previous University of Saskatchewan research (Robson, 2014), where small-scale polyurethane foam tests were conducted for heat flux exposures up to 75 kW/m^2. Pitts (Pitts, 2014) also observed this two-stage burning behaviour for cone calorimeter experiments at applied heat fluxes ranging from 8 kW/m^2 to 50 kW/m^2. Thermogravimetric (TGA) measurements carried out by Prasad, et al. (2009). also displayed the two distinct peak structures. Kramer et al. also observed the two-stage burning behaviour using a specialised sample holder to allow viewing of the foam collapse during cone calorimeter tests (Kramer, Zammarano, Linteris, Gedde, & Gilman, 2010).

It was also observed that for the 5 cm and 7.5 cm specimens, at lower incident heat fluxes, the two peaks are almost at the same height. With an increase in the incident heat flux, the second peak becomes steeper with a more inclined slope in the final decay phase (Figure 2-10). The peaks of the heat release rate curves for the 10 cm foam did not show as much variation for the heat flux levels included in this study (5 kW/m^2 – 35 kW/m^2). However, in previous University of Saskatchewan research (Robson, 2014), variations in peaks for 10 cm foams at a 75 kW/m^2 heat flux exposure are reported to occur. This suggests that the two peak burning behaviour is dependent on both the level of incident heat flux and the conduction of heat through the thickness of the foam.

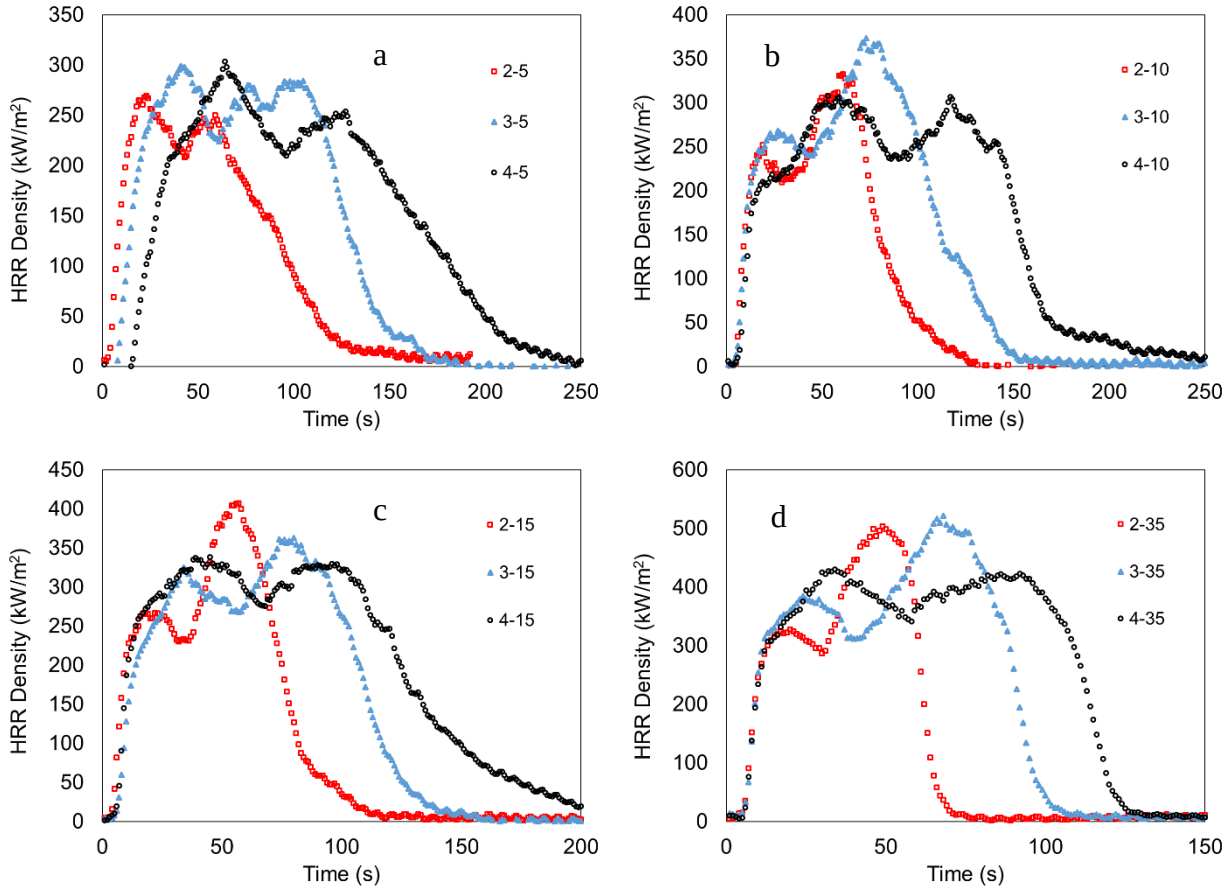

Figure 2-10: Comparison of the HRR Density Curves for Different Foam Thicknesses for Each Heat Flux (a – 5 kW/m^2, b – 10 kW/m^2, c – 15 kW/m2, d – 35 kW/m^2)

2.6 THERMOCOUPLE TEMPERATURE MEASUREMENTS

Temperatures of the foam measured during combustion are shown in Figure 2-11. The thermocouples labelled TC1 – TC5 (see Figure 2-5 for reference), represent the thermocouple locations starting from the top to the bottom of the foam sequentially. Representative plots of the measured temperatures are reported in Figure 2-11 for the different heat flux exposures. Other temperature graphs are reported in Appendix (A). Time zero values in the graphs have been adjusted to coincide with exposure of the foam to the incident heat flux. The data has also been truncated to limit fluctuations in readings caused by the thermocouples dislodging from the foam during the burn.

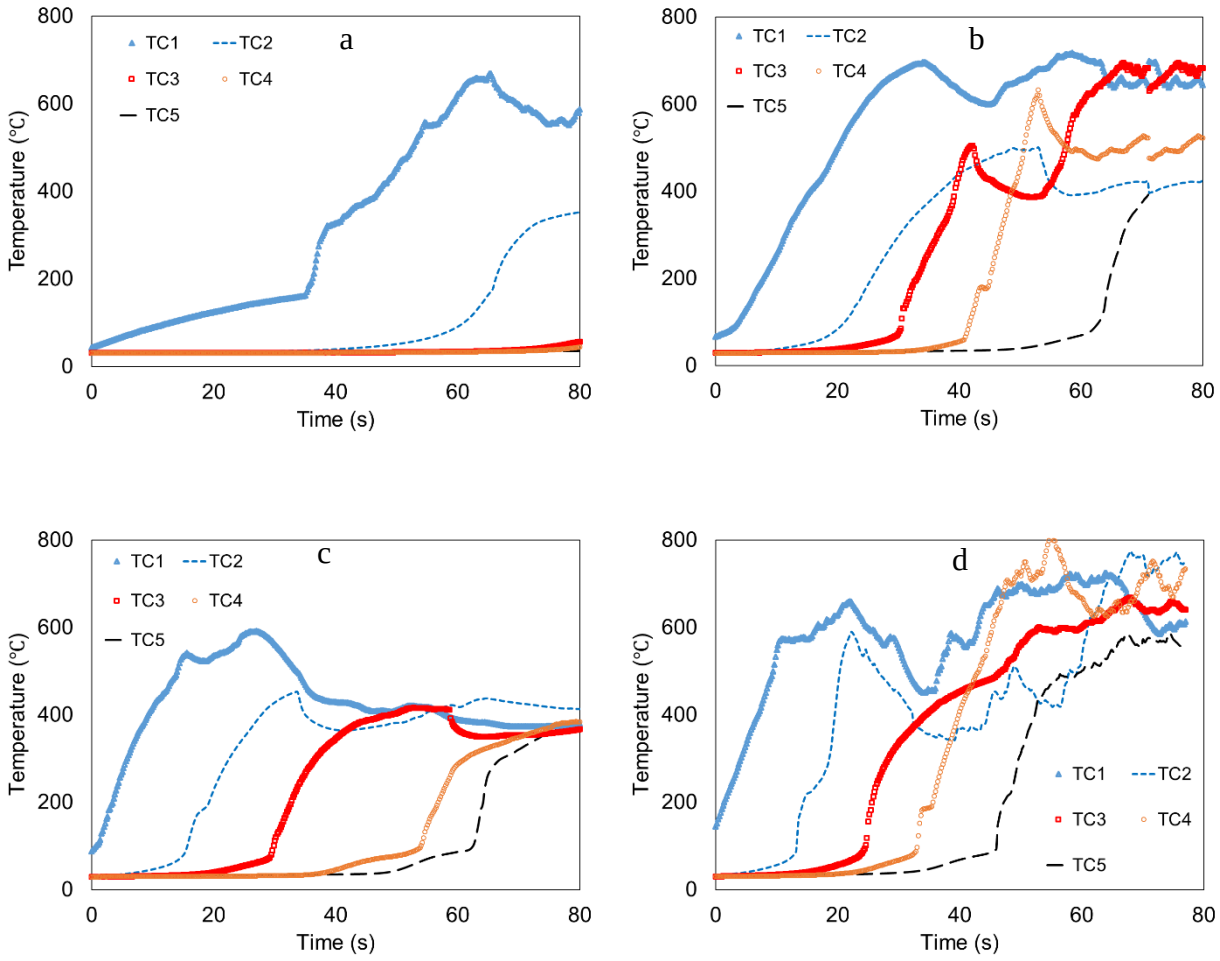

Figure 2-11: Representative Temperature Measurements During Combustion of 10 cm Polyurethane Specimens (a – 5 kW/m^2, b – 10 kW/m^2, c – 20 kW/m^2, d – 35 kW/m^2)

As expected, the initial temperature rise is observed first at TC1 as it is located on the top surface of the foam. The temperature data shows the highly insulative property of the foam. As the temperature of the foam around TC1 increases to 400°C, negligible temperature rise is measured around TC2 which is 2 cm below TC1. Consequently, almost no temperature rise is measured across TC3 to TC5. A transition point occurs between 100°C to 150°C where the general slope of the curve changes and a faster rate of temperature rise is observed. Video records indicate that the transition time period is consistent with the ignition time of the specimen. Before ignition of the foam can occur, moisture must be boiled off. The first slope corresponds with the heating of the material and removal of moisture prior to the more rapid temperature increase as the material breaks down and ignites while the second slope relates to the actual breakdown of the foam and subsequent ignition of the specimen. Maximum

temperatures recorded in this test were in the range of 600°C - 900°C. It is unclear if the maximum temperature measured was the temperature of the foam or the flame, however, previous research reports the degradation of the foam material at temperatures above 375°C (Ravey & Pierce, 1997).

Comparing the temperatures measured at different heat flux exposures, it is observed that the major difference occurs prior to ignition of the foam specimen. The time taken to raise the foam to ignition temperature is highly dependent on the level of heat flux exposure. For the 5 kW/m^2 tests, the length of the first slope which corresponds to moisture boil-off is the largest. This length shortens with an increase in heat flux and at the 35 kW/m^2, this slope is seen to be almost non-existent with instantaneous ignition of the foam occurring upon exposure to heat flux. Once the foam is ignited the rate of temperature rise is relatively consistent for all heat flux exposures. Figure 2-12 presents a comparison of representative temperatures of various incident heat fluxes for 30 s. Infrared temperature measurements were also recorded during the test. As seen in Figure 2-13, the infrared videos makes it easier to associate the temperatures measured to various physical events that occur during the experiment.

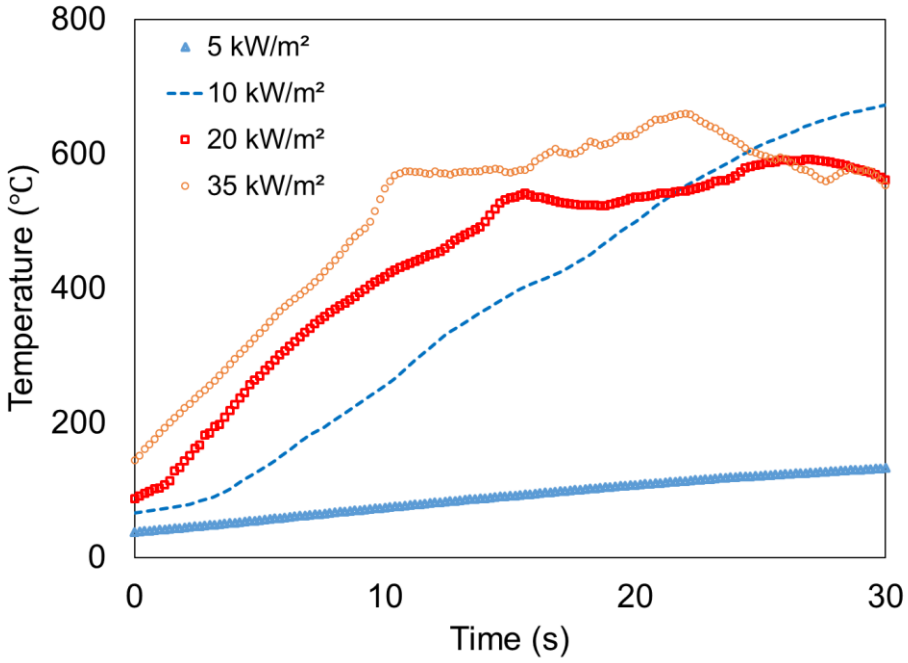

Figure 2-12: Comparison of Foam Surface Temperatures for Varying Heat Flux Exposures

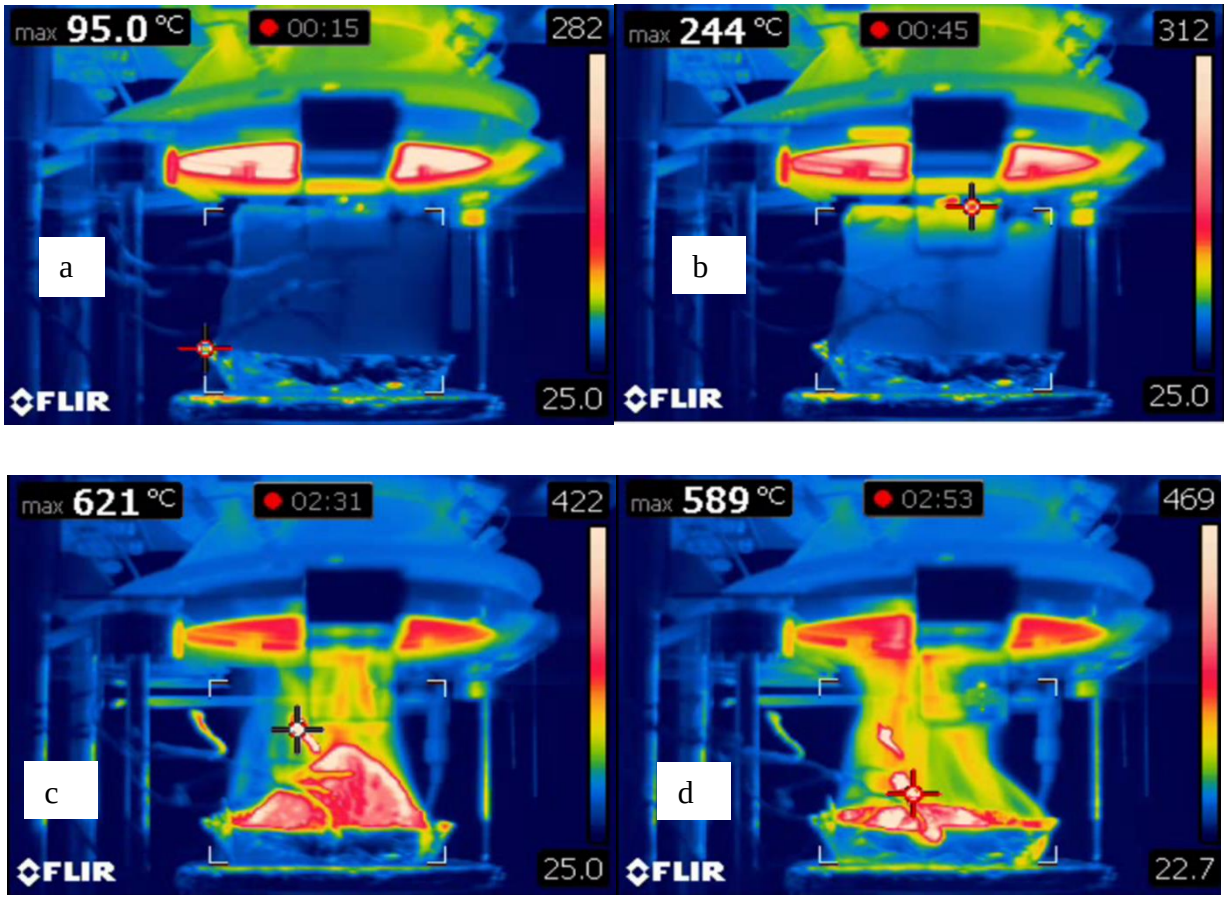

Figure 2-13: Infrared Temperature Measurements During Combustion of 10 cm Polyurethane Specimens Exposed to a 5 kW/m^2 Heat Flux Source

In Figure 2-13, photo-a shows the foam at initial exposure to the heat flux (test start). Photo-b shows the foam at the time of ignition after it has been exposed to the incident heat flux for 30 s. It is observed that the depth of thermal penetration is quite low for the foam. It is estimated that less than 2.0 cm of the foam experiences a temperature rise from radiation off the cone calorimeter. These photos confirm thermocouple measurements where minimal temperature rise was recorded for TC2 even when TC1 had reached surface temperatures of 400°C. Photo-c reveals the behaviour of the foam during burning. The foam burns from the outer surface and penetrates inwards. A conical shape is seen to develop from the burn pattern, indicating that internal foam temperatures may be significantly lower than outer surface temperatures. Photo-d shows the final stage of the burn where a total collapse of the solid foam has occurred. The molten material formed burns at a higher intensity than the solid foam and this is indicative of the second peak that is observed for heat release rate measurements.

A comparison of infrared temperatures at the top surface of the foam, and thermocouple measurements (TC1) was carried out for temperatures recorded prior to ignition of the foam specimen. Two methods were used to obtain temperature data from infrared videos. The first method involved manually recording temperatures at 5.0 s interval by matching the colour on the foam to the temperature colour scale and interpolating to obtain foam temperatures. This method presents various challenges as an interpretation of the colour is subjective and relies heavily on the accuracy of matching the temperature colour. A more sophisticated approach was employed using a Matlab code developed by an undergraduate research assistant at the University of Saskatchewan Fire Group. The code analyses the video frames and compares the colour at select points on the foam surface to that of the temperature colour scale to find the foam temperature. Figure 2-14 gives an example of the Matlab measurement points while Figure 2-15 shows the comparison of infrared and thermocouple measurements.

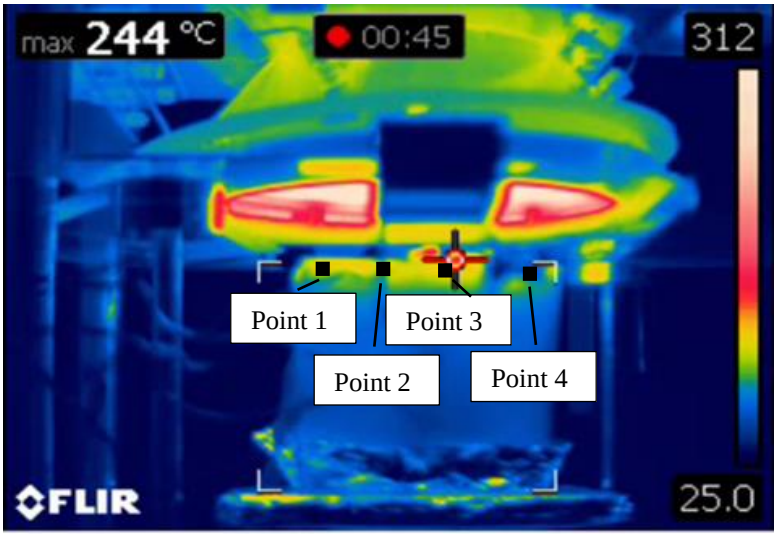

Figure 2-14: Location of Measurement Points for Matlab Temperature Interpolation

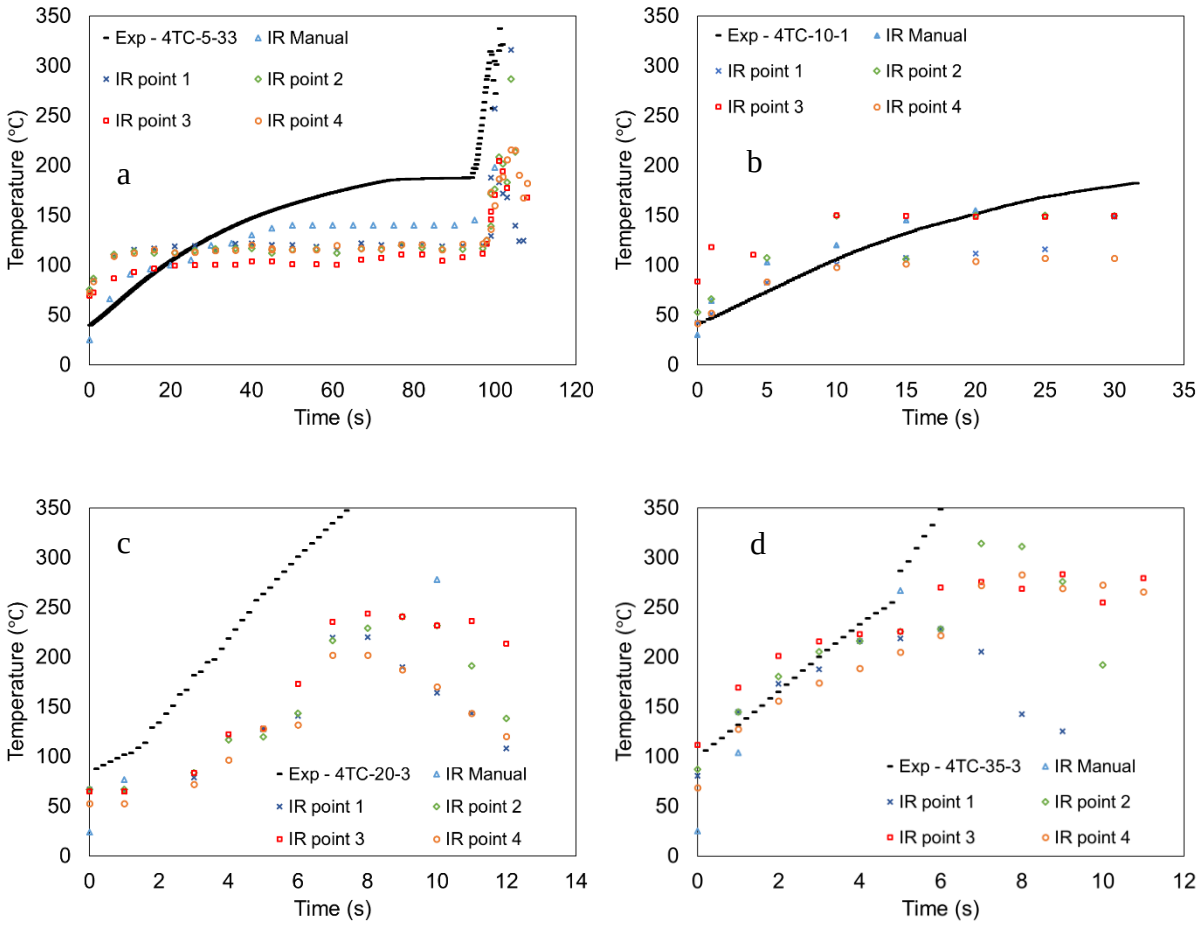

Figure 2-15: Comparison of Representative Infrared (Manual/4-Point Matlab Measurement) and Thermocouple Temperature Measurements During Combustion of 10 cm Polyurethane Specimens (a – 5 kW/m^2, b – 10 kW/m^2, c – 20 kW/m^2, d – 35 kW/m^2)

In general, the thermocouple measurements show reasonable agreement with infrared measurements. It is important to note that there are some uncertainties with infrared and thermocouple temperature measurements that may explain some of the differences in temperatures measured. As mentioned earlier, for infrared measurements, temperatures at areas of interest are read off a linear colour scale and errors exist in interpreting exact temperatures. Measurements are also impacted by gas and humidity. Given the nature of the polyurethane foam burn, the gaseous products released affect the ability of the infrared device to record accurate temperatures. On the other hand, thermocouple measurements were not corrected for errors due to radiation feedback and may explain why in some cases thermocouple measurements were higher than infrared measurements. The temperatures measured by the infrared camera were over an area of the foam as opposed to spot measurement recorded by the thermocouple. The location

of measurement was also different as the thermocouple measured temperatures at the top-centre of the foam while the infrared camera measured temperatures from the side-view.

The temperature data may be used to carry out a semi-infinite analysis of the foam. The semi-infinite idealisation is an approximation of the one-dimensional transient heat transfer process occurring in the foam. The approximation assumes that a solid material extends infinitely and hence the bottom surface conditions are not influenced by the top surface conditions (Incropera, Dewitt, Bergman, & Lavine, 2007). The temperatures measured in this experiment were used to study the depth of thermal penetration of the foam. The time taken for the foam at various depths to reach 150°C, 200°C, 300°C, 400°C and 500°C are reported in Table 2-9 to Table 2-12.

Table 2-9: Temperature Rise at Various Foam Depths (5 kW/m²)

Temperature °C	Time (s)				
	0 cm	2.0 cm	4.0 cm	6.0 cm	8.0 cm
150	9.8	42.8	57.0	68.4	79.2
200	11.2	45.6	58.8	70.2	80.0
300	14.0	48.6	64.4	72.0	83.6
400	15.6	98.6	80.6	75.2	91.6
500	17.0	120.0	92.4	80.6	101.0

Table 2-10: Temperature Rise at Various Foam Depths (10 kW/m²)

Temperature °C	Time (s)				
	0 cm	2.0 cm	4.0 cm	6.0 cm	8.0 cm
150	11.2	33.0	61.2	65.8	74.4
200	12.8	33.8	64.0	67.6	76.6
300	16.0	36.6	68.0	71.8	78.8
400	21.8	42.0	79.4	81.2	82.6
500	23.2	58.2	89.8	89.8	86.4

Table 2-11: Temperature Rise at Various Foam Depths (20 kW/m²)

Temperature °C	Time (s)				
	0 cm	2.0 cm	4.0 cm	6.0 cm	8.0 cm
150	4.6	10.2	25.6	37.8	63.0
200	7.0	11.4	26.8	40.0	65.4
300	8.4	13.8	29.2	40.8	69.0
400	9.8	17.4	31.6	42.2	75.0
500	11.2	19.8	33.6	45.6	80.8

Table 2-12: Temperature Rise at Various Foam Depths (35 kW/m²)

Temperature °C	Time (s)				
	0 cm	2.0 cm	4.0 cm	6.0 cm	8.0 cm
150	0.0	13.4	24.8	33.2	46.2
200	1.2	14.2	25.6	35.4	47.2
300	4.0	18.6	28.2	37.4	49.6
400	6.8	19.4	34.2	39.8	52.2
500	9.4	59.2	46.8	43.0	59.8

Typically, ignition of the foam occurs at temperatures above 300°C (Kramer, Zammarano, Linteris, Gedde, & Gilman, 2010). It is observed from the experimental results that temperatures at subsequent depths do not reach 150°C until ignition at the previous depth occurs. The foam offers a high resistance to heat penetrating vertically downward. Upon exposure to heat fluxes only the top surface area directly exposed to the cone heater shows appreciable temperature rise. These results suggest that ignition of the foam specimen should be similar for the range of foam thicknesses included in this study. After ignition, temperature rise within the foam is observed to be influenced by the direct impingement of the flame on the area of the foam being measured.

2.7 IGNITION TIME

The ignition times for the polyurethane foams were investigated. The ignition time in the context of this research is defined as the time taken for the foam to produce enough combustible volatiles (pyrolysis) and for the combustible volatiles to ignite via piloted ignition of the specimen. During heat release rate density tests carried out with the cone calorimeter, the time for ignition of the specimens was manually noted by the operator. Video records of the experiment taken with the Canon Vixia HF R500 video camera (Canon, Vancouver, CA) were used to verify the recorded ignition times using frame-by-frame video analysis. The video frame

analysis was done using DaVinci Resolve 15, an open-source video editing software (Port Melbourne, Australia). The software was used to step forward in time analysing each of the 30 frames per second to identify when ignition of the foam specimen occurred. Cone calorimeter data and video records from previous University of Saskatchewan foam test were also analysed (Robson, 2014).

For each heat flux exposure, the average ignition time given in Table 2-13 was calculated over a minimum of three representative values per heat flux exposure using various foam thicknesses. The number of average values varied for each heat flux exposure up to a maximum of 15. Based on the analysis of the depth of thermal penetration of the foam (Section 2.6), ignition in the cone calorimeter is assumed to be independent of the thickness of the foam due to the high insulative property of the foam. Ignition times can, therefore, be studied neglecting foam thickness. The ignition times for each thickness and incident heat flux are given in Appendix (B). A simple random uncertainty was determined for the ignition times for each heat flux based on the standard deviation and degrees of freedom. The uncertainty is plotted with the ignition times in Figure 2-16.

Table 2-13: Average Ignition Times of the Polyurethane Foam Specimens

Heat Flux (kW/m^2)	**Ignition Time (s)**		**Ignition Time$^{-1/2}$ ($s^{-1/2}$)**		**Uncertainty ($\pm s^{-1/2}$)**
	Average	**σ**	**Average**	**σ**	
5	147.7	65.37	0.09	0.02	0.04
10	27.0	9.84	0.17	0.02	0.06
15	11.5	2.08	0.25	0.02	0.05
20	7.6	0.60	0.36	0.01	0.06
25	4.2	0.51	0.49	0.03	0.07
35	2.1	0.38	0.70	0.06	0.13

As the incident heat flux increased, the standard deviation in ignition time measurements decreased. Only a thin layer of the foam is heated for ignition and at lower heat flux exposures, the convective and radiative heat losses from the foam to surroundings play a large role in affecting the time taken to raise the foam to its ignition temperature. Differences in measured ignition times will occur due to variations in ambient conditions at different test times. However, at higher heat flux exposures, these deviations in measured ignition times for similar heat flux exposures are minimised due to an abundance of energy that rapidly raises the foam to ignition

temperatures. The foam conducts heat at a much faster rate than it would lose heat, leading to consistent ignition times.

The critical heat flux of the foam may be determined using these measured ignition times. The critical heat flux is a limiting point, where below this value, the material is not expected to be able to produce the right concentration of combustible volatiles due to a lack of sufficient energy available to raise the foam to ignition temperature. The critical heat flux of a material may be determined by linearly extrapolating a plot of the inverse of the root of the time of ignition ($1/\sqrt{t_{ig}}$) versus the incident heat flux (Drysdale, 2011). The relationship between the incident heat flux and the ignition time was derived from the simplification of the semi-infinite heat transfer model (Section 4.2.2) where the heat flux is assumed constant and heat losses are ignored (Mikkola & Wichman, 1989). Figure 2-16 shows the plot of $1/\sqrt{t_{ig}}$ and the trend is used to determine the critical heat flux of the foam specimen. The critical heat flux of the foam specimen was calculated to be 1.9 kW/m^2. Below this critical heat flux, ignition of the foam is adjudged not to be possible. Research examining the interpretation of the ignition time data indicates that this method may provide a critical heat flux value that is only 70% accurate (Delichatsios, Panagiotou, & Kiley, 1991).

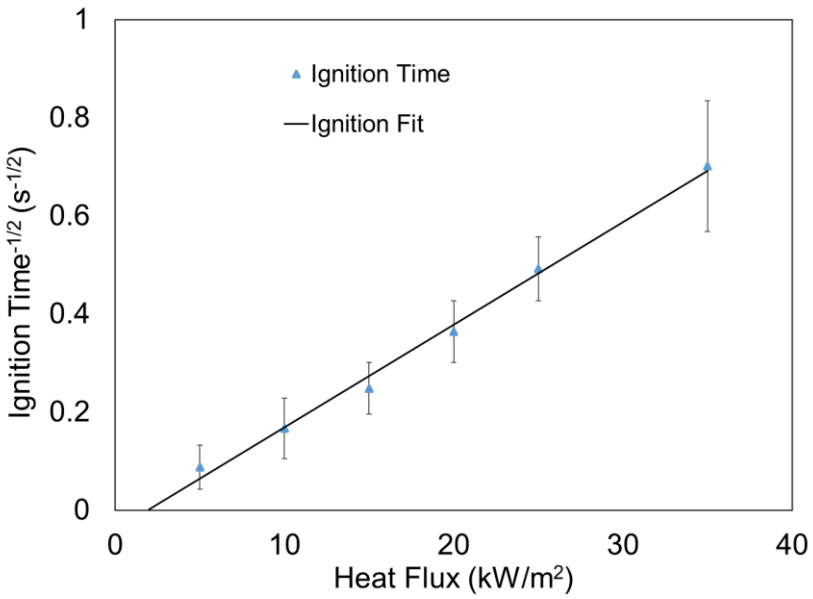

Figure 2-16: Time to Ignition for Polyurethane Foam Specimen

2.8 SUMMARY OF CHAPTER

This chapter focused on the experimental methodology and results obtained from small-scale cone calorimeter tests. The experiments conducted for various thicknesses showed good repeatability for heat release rate density measured at similar heat flux exposure levels. As observed in previous research, the peak heat release rate density measured showed a strong dependence on the incident heat flux levels (Ezinwa J. , 2009) (Robson, 2014). The general curve of the heat release rate density was also observed to be influenced by the level of heat flux exposure. Combustion of the foam was seen to occur in two stages corresponding to the breakdown of the solid foam structure and burning of the resultant liquid polyol. Consistency in heat release rate density measurements was also obtained when comparing the results of this research to previous University of Saskatchewan small-scale foam tests.

Another aspect described in this chapter was measurements of foam surface temperatures during combustion of the small-scale specimen. Peak surface temperatures were relatively similar for all heat flux exposure levels, but the time to attain peak temperatures was observed to be dependent on the level of incident heat flux. The rapid rate of temperature rise relates to the ignition time of the foam. An increase in incident heat flux causes the foam surface to reach ignition temperatures quickly, resulting in shorter ignition times. In this study, the measured ignition times at higher heat flux levels showed more repeatability than ignition times at lower heat flux levels. This is because, at higher heat flux levels, the magnitude of the energy transfer is much higher than at the lower heat flux levels. Hence, the foam is less influenced by heat losses to the surroundings.

Finally, the results from the study on ignition time were used to estimate the critical heat flux necessary to achieve foam ignition. Based on the data in this research a critical heat flux value of approximately 2 kW/m^2 is estimated. Given that the lowest heat flux level tested in this research (5 kW/m^2) was close to the calculated critical heat flux, it explains the large variations in the measured ignition time, since slight changes in ambient condition may further delay the ignition of the foam.

3 FULL-SCALE EXPERIMENTS

In this chapter, details on the full-scale experimental procedure, apparatus and materials are highlighted. The University of Saskatchewan Fire Research group has been involved in various full-scale tests and field fire experiments. While the full-scale tests described in this chapter were not conducted directly by the author, data sets from the University of Waterloo's shipping container test facility and furniture calorimeter, and the University of Saskatchewan public fire demonstration (dorm burn) were used in this research. Analysis of full-scale fire behaviour is critical to addressing the challenges associated with fire scaling. In this chapter, the author will provide an overview of the full-scale experiments and report results from the tests.

3.1 UNIVERSITY OF WATERLOO COMPARTMENT FOAM TEST

The University of Waterloo fire research group modified a shipping container for room fire testing at their Live Fire Facility. The test room measures 2.4 m wide by 3.5 m deep by 2.4 m high with a door opening measuring 0.91 m wide by 1.75 m high. The outside wall of the compartment was insulated with 25.4 mm thick Fiberfrax Durablanket S high-temperature insulation covered with a sheet of aluminium. The roof was also insulated with 50.8 mm thick insulation similar to the walls. The floor was lined with fireclay brick over square concrete blocks. More details on room construction can be found in Obach, 2011.

Inconel-sheathed ceramic wrapped type K-Type thermocouples were used to obtain compartment and external air temperatures. Ten thermocouple rakes consisting of eight individual thermocouples were instrumented to acquire the interior hot gas temperatures. Six of the rakes were placed vertically with thermocouples located at heights of 0.0 m, 0.5 m, 0.8 m, 1.1 m, 1.4 m, 1.7 m, 2.0 m, and 2.3 m off the floor. Six thermocouple rakes were placed in the compartment with three on opposite sides, while another three thermocouple rakes were placed horizontally 2.15 m from the floor. The final thermocouple rake was placed horizontally running from the centreline of the compartment, 2.05 m off the floor. Of importance to this research are the temperature measurements made using the six-thermocouple rakes located on either side of

the compartment as shown in Figure 3-1 (Fulton, Torvi, & Weckman, 2016). The figure also shows the position of the three different foam samples tested (C4, E4 and EE4). The compartment was further instrumented with water-cooled Gardon gauges, bi-directional probes and gas analyzers. Temperature data was collected using the Labview program, sampling from the National Instruments cFP – 2000 data logger (NI – St. Laurent, Quebec) at a frequency of 0.8 Hz (Obach, 2011).

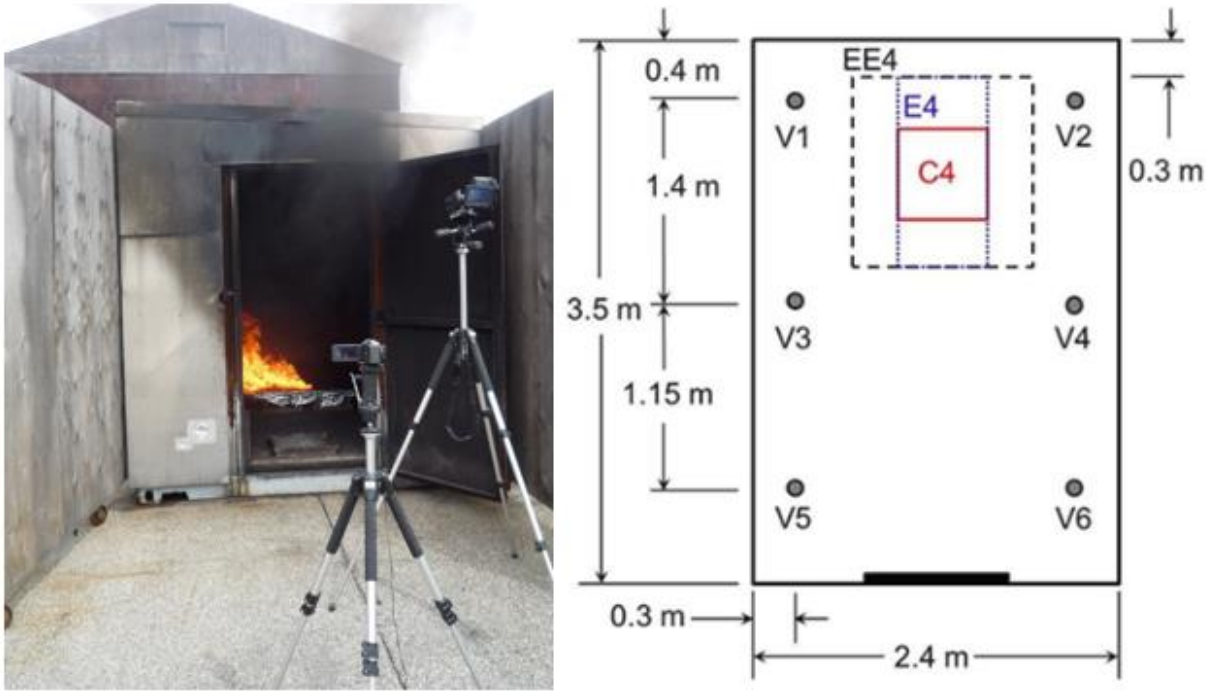

Figure 3-1: University of Waterloo Fire Compartment Foam Test and Thermocouple Locations (Fulton, Torvi, & Weckman, 2016)

3.1.1 Compartment Test Specimens

Three different polyurethane foam configurations were tested. The test configuration was selected to be similar to Robson who conducted a free burn test of the foams in a full-scale furniture calorimeter (Robson, 2014). The selection of the test configurations allowed the heat release rate measurements from the furniture calorimeter to be used to compare heat release rates predicted for the compartment foam test. While the foams were made from the same polyurethane material which allows for relative consistency in general fire behaviour, they varied in both size and ignition location. Material information given in Table 3-1 shows the nominal

dimensions for the test samples. Also, the foams used in the compartment tests were nominally the same foam as the specimens used in the cone calorimeter tests discussed in Chapter 2.

Table 3-1: Compartment Test Sample Details

Test Sample	Length (cm)		Width (cm)		Thickness (cm)		Nominal Mass (g)
	Avg.	σ	Avg.	σ	Avg.	σ	
C4	61.5	0.6	62.5	0.6	9.3	0.1	580
E4	62.3	0.9	126.9	0.8	9.7	0.1	1250
EE4	126.2	1.1	122.3	0.6	9.6	0.1	2500

The foams, which were leftover samples from Robson's furniture calorimeter tests (Section 2.4), were less dense than typical mattress foams. The foams were purchased from retail locations across Canada. The specimens were easily ignited using small hand-held ignition devices and did not show any indication of fire retardant (Fulton, Torvi, & Weckman, 2016). Prior to testing, specimen conditioning was carried out using a similar procedure to previous University of Waterloo furniture calorimeter tests (Robson, 2014). The foams were left in the conditioning chamber for at least a week at 50% relative humidity (±5%) and 21℃ (±2℃).

3.1.2 Experimental Procedure

The experiment was designed to study foam fire behaviour in a compartment. Four individual tests were carried out for the C4 and E4 samples while three tests were carried out for the EE4 sample. C4 refers to centre ignition of the foam while E4 and EE4 refer to ignition at the middle of the farthest edge of the foam sample from the door (Fulton, Torvi, & Weckman, 2016). The 4 refers to the nominal thickness of the foam in inches. The foam samples shown in Figure 3-2 were marked up with 10 cm by 10 cm gridlines to assist with manual measurements of flame spread rates.

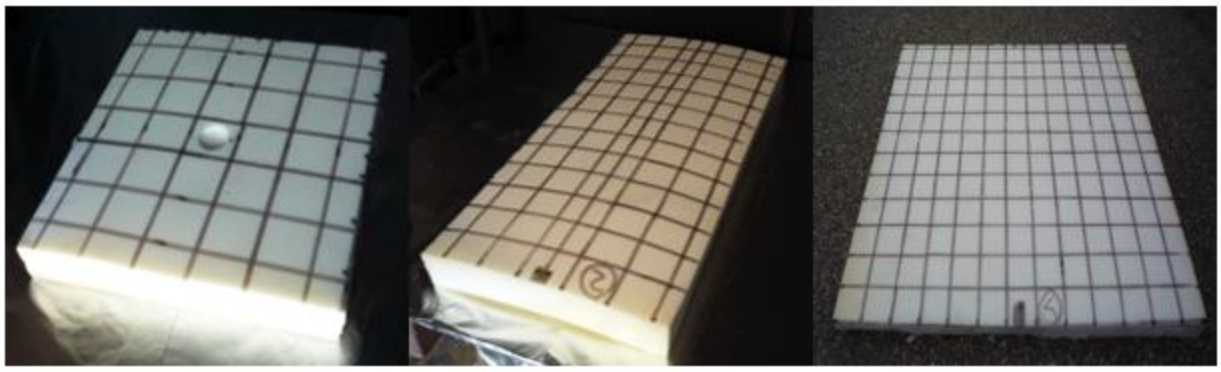

Figure 3-2: From Left to Right, Foam Sample C4, E4 and EE4 Showing Gridlines

The foam tests were conducted in May 2014 with ambient temperatures ranging from 10℃ to 13℃ and relative humidity values between 50 to 60% (Fulton, Torvi, & Weckman, 2016). Ambient wind also influenced test conditions as sometimes during testing, wind gusts caused the smoke to move out of the room or collect at some point in the room. For testing, the foams were placed on a 21 cm high brick and Durock platform with an aluminium foil coating. Ignition of the samples was done using a piloted ignition source at the centre or edge of the foam as previously discussed. For centre ignition, a small hole was cut in the centre of the specimen to help increase repeatability of ignition. The foam fire tests were conducted with the door fully open to achieve similarity with the ISO 9705 test room (ISO, 2016b).

As shown in Figure 3-3, infrared temperature measurements were taken using a FLIR T650sc IR camera (FLIR Systems, Burlington, ON). This assisted with determining flame spread rates. Video records of the tests were also taken using a Panasonic HC-V700M camcorder (Panasonic Canada Inc., Mississauga, ON) while photographs were taken at various times during the test with a Panasonic DMC-LZ10 digital camera (Panasonic Canada Inc., Mississauga, ON) to document significant events. A fan was used to cool down the test room in between tests to ensure similar initial conditions.

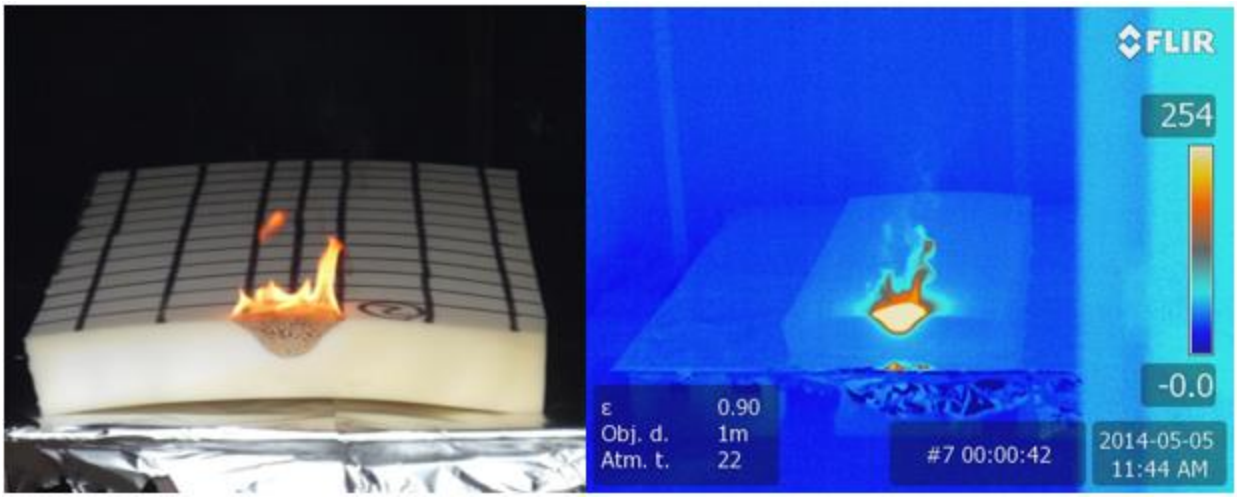

Figure 3-3: Still and Infrared Photographs of Test EE4-1 Taken Approximately 14 s after Ignition

3.2 TEMPERATURE MEASUREMENTS

This section reports temperature measurements taken during the shipping container tests. Results of space temperature measurements taken by thermocouples and foam surfaces temperature measured using infrared cameras are discussed. Subsequent chapters in this thesis will explore predicting the space temperatures measured during this test using various engineering correlations

3.2.1 Ceiling Temperature Measurements

The thermocouple rakes measured the internal compartment temperatures during the foam burn. The temperature measurements of the topmost thermocouples on the rakes (labelled V1-V6), are reported for the first 400 s of the test and will be compared to ceiling jet temperature predictions carried out using Alpert's correlation (Alpert, 1972) discussed in Section 1.5. The average temperatures measured for the various foam tests are reported in Figure 3-4, Figure 3-5 and Figure 3-6.

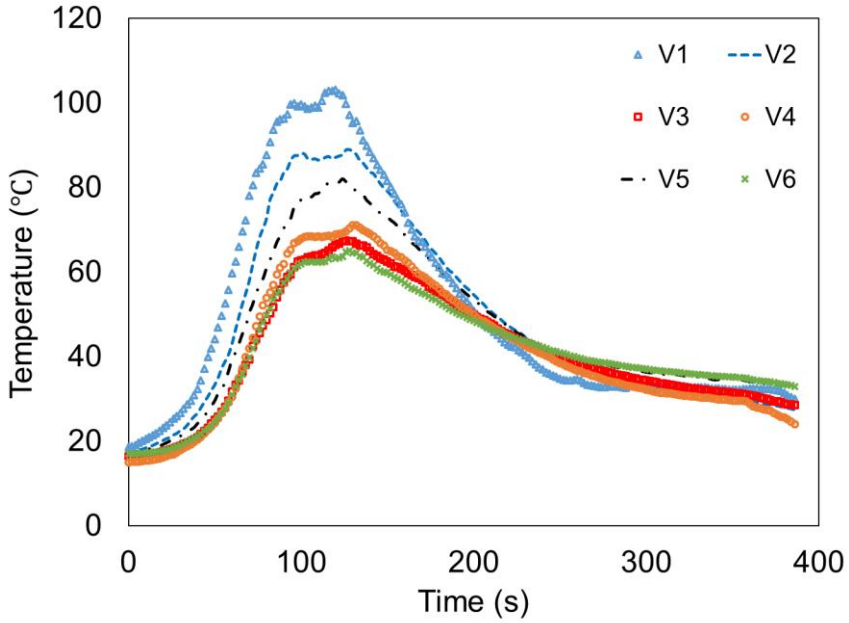

Figure 3-4: Average Ceiling Temperature Measurements for C4 Foam Tests

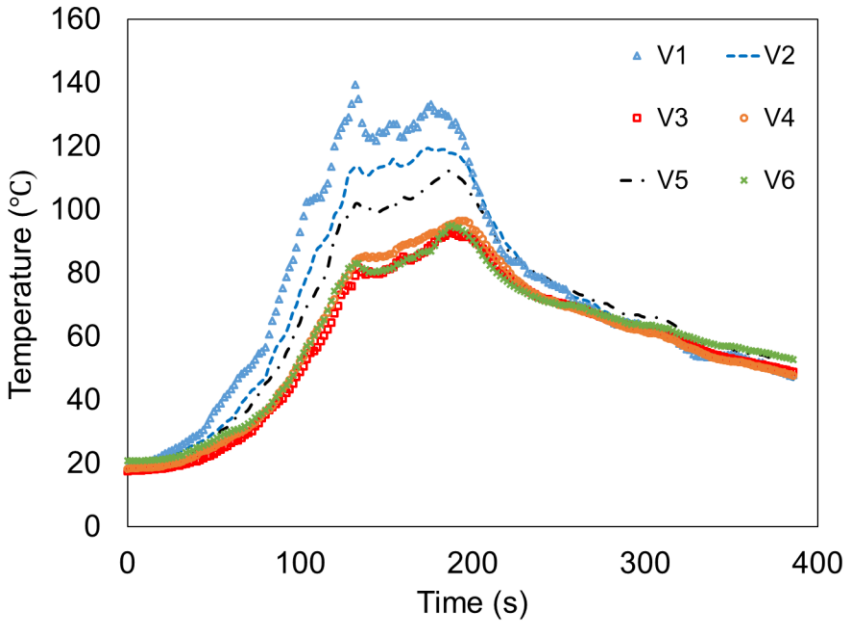

Figure 3-5: Average Ceiling Temperature Measurements for E4 Foam Tests

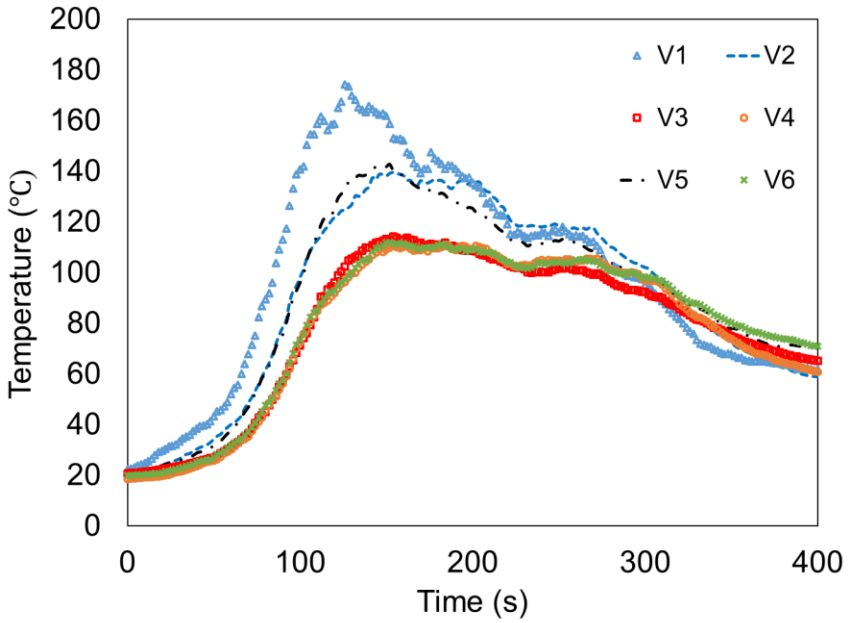

Figure 3-6: Average Ceiling Temperature Measurements for EE4 Foam Tests

The temperature measurements obtained are as a result of the smoke plume which builds up on the ceiling during the foam tests, as well as the radiative fluxes from the fire. The maximum temperatures obtained for the three different foam tests (C4, E4 and EE4) were in the range of 100℃ to 180℃, with higher temperatures obtained for the larger foam samples. Thermocouples V1 and V2 showed the highest temperature values as they were in close proximity to the burning samples. For the three different tests, temperatures measured by thermocouple V5 were higher than thermocouples V3 and V4 even though it was located further away from the fire origin. This may be explained by an uneven distribution of the smoke layer across the ceiling due to wind movement. Ceiling areas with preferential smoke movement will result in higher temperature readings when compared to surrounding areas. The temperature measurements across thermocouples V3, V4 and V6 showed similar values throughout the foam tests.

3.2.2 Vertical Temperature Measurements

The temperatures at heights of 0.0 m, 0.5 m, 0.8 m, 1.1 m, 1.4 m, 1.7 m, 2.0 m, and 2.3 m off the floor were measured by thermocouples arranged vertically on the thermocouple rake. Figure 3-7 to Figure 3-9 report the average temperatures measured at a particular height across all six thermocouples in the space for the C4, E4 and EE4 test series.

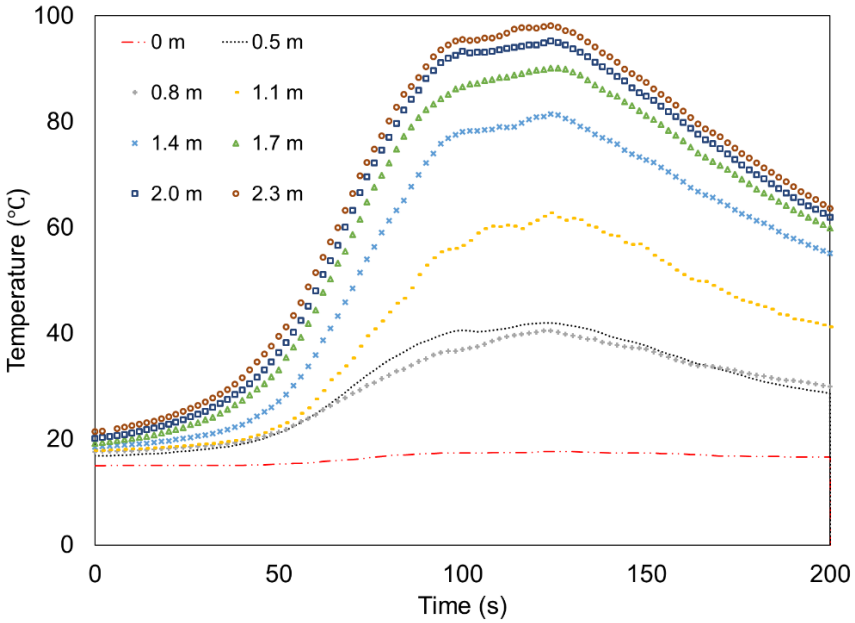

Figure 3-7: Average Vertical Temperature Distribution for C4 Foam Tests

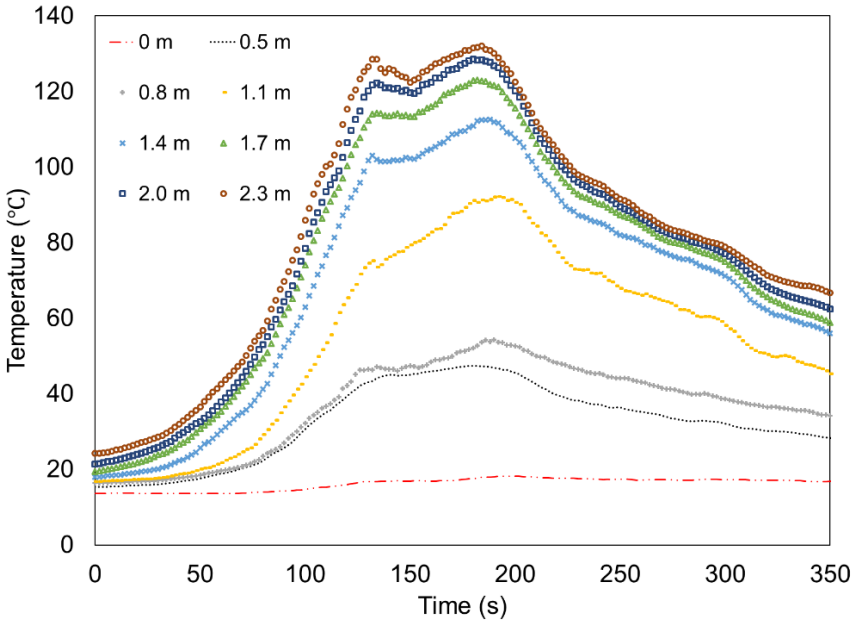

Figure 3-8: Average Vertical Temperature Distribution for E4 Foam Tests

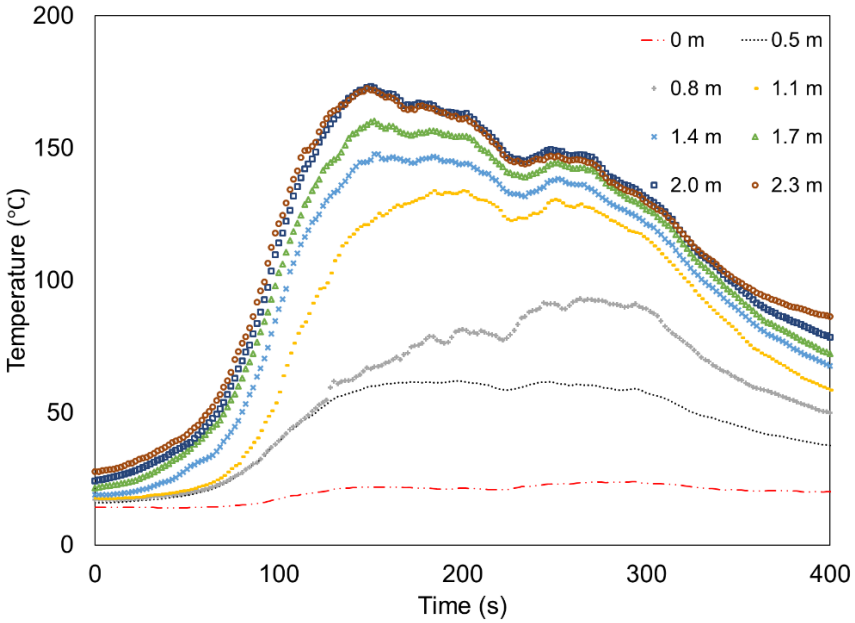

Figure 3-9: Average Vertical Temperature Distribution for EE4 Foam Tests

Thermocouple measurements indicate that during the fire, the temperature within the compartment increased with increase in height with hotter temperatures measured within the top 0.4 m of the ceiling. As the fire grows, the temperature distribution in the space is observed to stratify. Temperatures measured above 1.1 m are seen to generally be over 200% higher than temperatures below 0.8 m. Hot gases from combustion displace the cooler air within the space leading to elevated temperatures in the upper region of the room. The cool air is entrained in the lower region and provides oxygen necessary for continued combustion. Compartment fires are sometimes modelled by evaluating the temperature distribution within the space as control zones (William, Douglas, & Christopher, 2016). The data provided by the experimental vertical temperature distribution will aid research on compartment fire modelling.

3.2.3 Foam Surface Temperatures

To further investigate the foam fire behaviour, it was important to study the foam surface temperatures during combustion of the foam. The FLIR T650sc IR camera was set-up at one meter away from the test room to measure infrared temperatures within the space. The infrared camera was set to obtain images at either seven second (7 s) or fourteen second (14 s) intervals. A constant emissivity of 0.9 and an ambient temperature of 22°C was assumed and used as camera input parameters. The infrared camera has a spectral range of 7.5 to 13 µm (FLIR

System, 2016). The infrared camera measured temperatures across the entire foam surface and the maximum temperature obtained at any time is reported here.

A relatively linear surface temperature rise was seen for the various foam samples. The IR camera had an upper-temperature limit of 660°C and hence the maximum surface temperature recorded for the experiment was 660°C. As mentioned in Section 2.5.2, above temperatures of 375°C breakdown of the foam occurs and pyrolysis gases are evolved (Ravey & Pierce, 1997). Infrared measurements recorded after this temperature will be impacted by the hot gases and subsequent flames from the fire. Foam surface temperature measurements aid in understanding the rate of temperature rise across the foam surface for modelling applications. Figure 3-10 to Figure 3-12 reports the temperatures obtained for the different foam configurations. A good level of repeatability is attained for the temperatures in each test series.

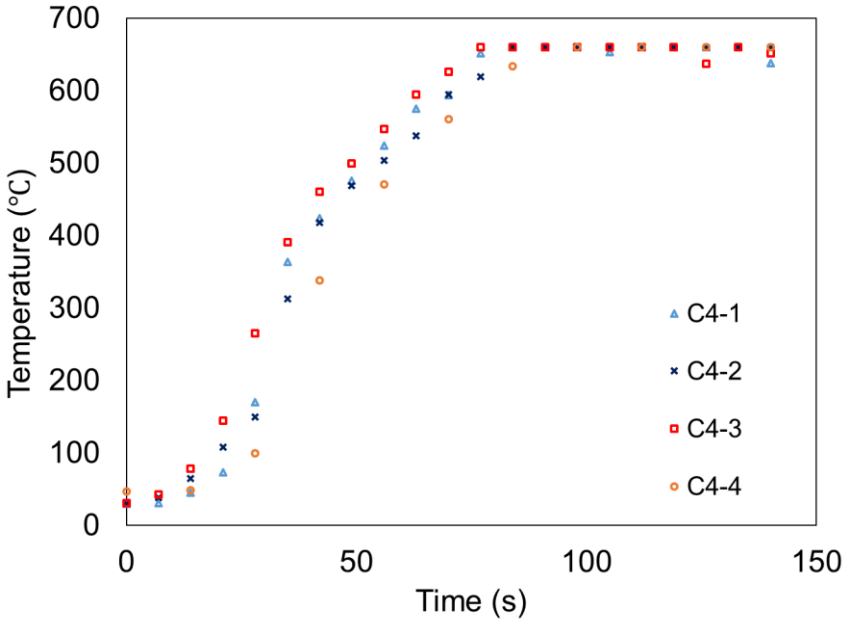

Figure 3-10: Infrared Camera Maximum Foam Surface Temperature Measurements (C4)

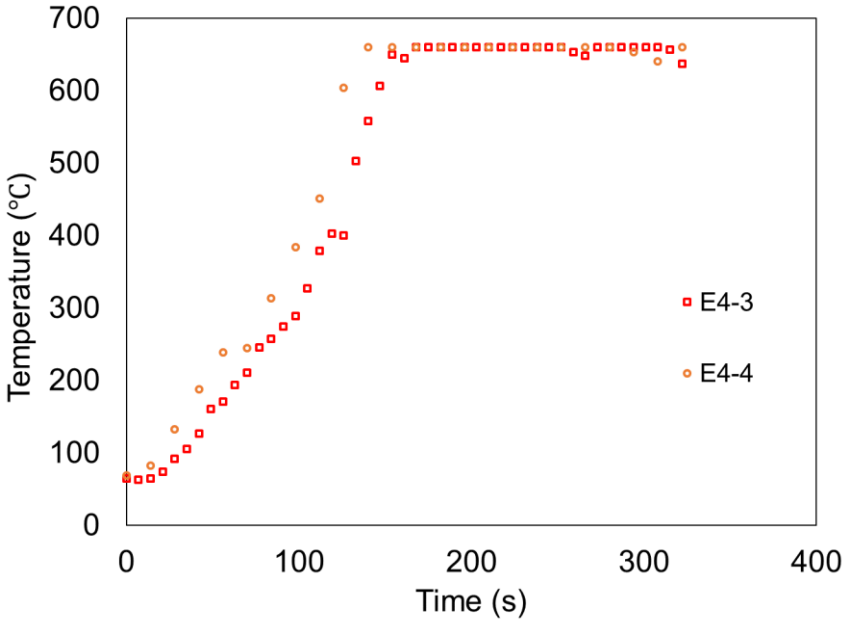

Figure 3-11: Infrared Camera Maximum Foam Surface Temperature Measurements (E4)

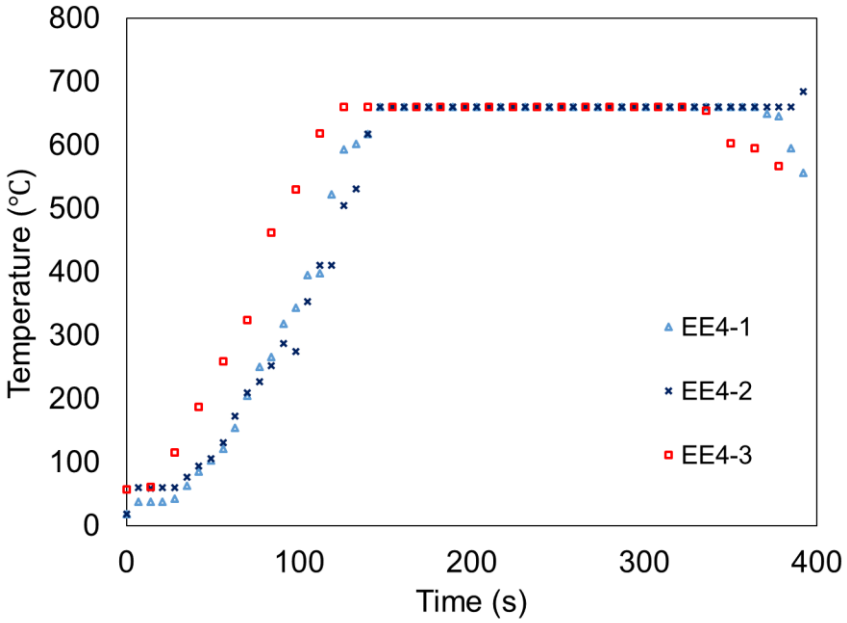

Figure 3-12: Infrared Camera Maximum Foam Surface Temperature Measurements (EE4)

3.2.4 Comparison of Temperature Measurements

Average ceiling temperatures measured by thermocouple V1 are compared in Figure 3-13 for the three different foams tested. A similar comparison was carried out in Figure 3-14 for the

foam surface temperature recorded in each test. The magnitude of ceiling temperature is seen to influenced by the size of the foam tested. Higher peak ceiling temperature was recorded for the larger foam specimen. The higher peak temperatures are due to increased fuel load for the larger specimen. The rate of ceiling temperature rise is consistent for all test types until after 50 s where a faster rate of temperature rise is observed for the C4 foam specimen.

The rate of temperature rise on the foam surface indicates a dependence on ignition location. A similar rate of foam surface temperature rise is observed for both edge ignition test (E4-3 and EE4-2) while a faster rate of temperature rise is recorded for the centre ignition test (C4). The faster rate of foam surface temperature rise obtained for the centre ignition tests is due to the pool fire formed at the centre of the foam during the burn. Air is also entrained from all side of the foam during the test causing the foam to burn out faster at elevated temperatures. The relationship of temperature with the rate of heat release could not be investigated since the heat release rate was not measured in the shipping container experiment. It is expected that the rate of temperature rise, peak temperatures and the rate of temperature decay will coincide with the behaviour of the full-scale heat release rate curve.

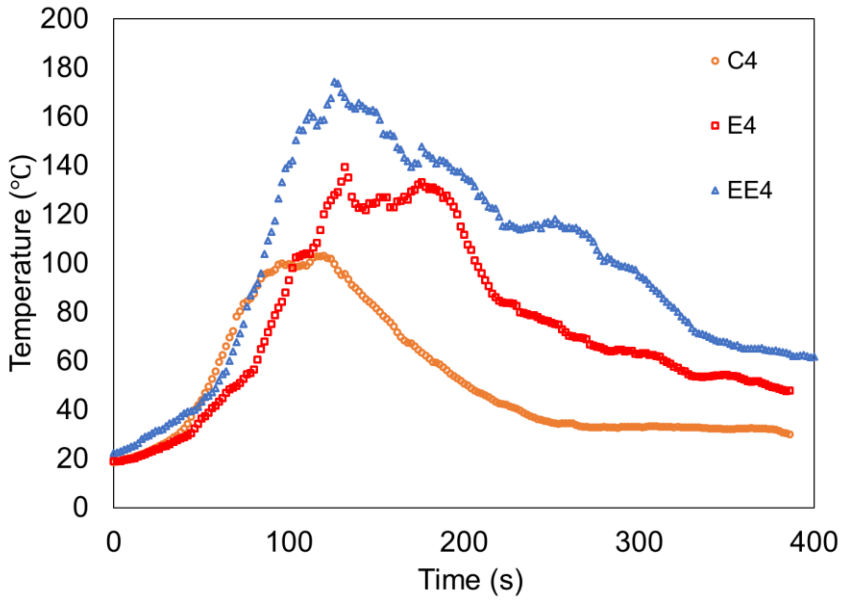

Figure 3-13: Comparison of Ceiling Temperature Measurements (V1) During Foam Tests

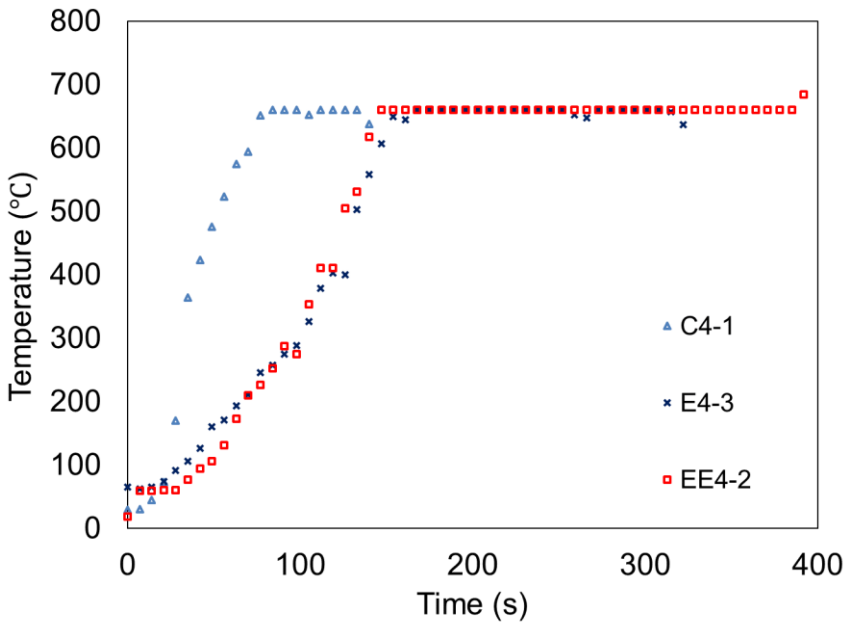

Figure 3-14: Comparison of Foam Surface Temperature Measurements During Foam Tests

3.3 MANUAL FLAME SPREAD RESULTS

Since the foam samples were marked with 10 cm by 10 cm gridlines, the rate of flame spread of the foam may be estimated by counting the number of squares ignited at any given time. Analyses of video records taken during testing were used to obtain flame areas. For the centre ignition tests, the numbers of ignited squares were counted at 10 s intervals while for the edge ignition, intervals of 30 s were used to determine the flame area. At each burn interval, partially burning squares were estimated as fractions and added to the total area of the flame. Plots of the flame spread rates for C4, E4 and EE4 test series are given in Figure 3-15, Figure 3-16 and Figure 3-17 respectively. The flame was assumed to grow symmetrically in all directions. For centre ignition tests, the one-dimensional flame can be said to grow radially as a circle until it reaches the outer limits of the foam. For the edge ignition tests, the one-dimensional flame area takes the shape of a semi-circle until the fire reaches the edge boundary, upon which the flame assumes an elliptical growth pattern till complete burnout of the foam specimen. The depth of flame penetration was not considered in determining the area spread rates. An assessment of the accuracy of the flame spread assumptions is provided in Chapter 5.

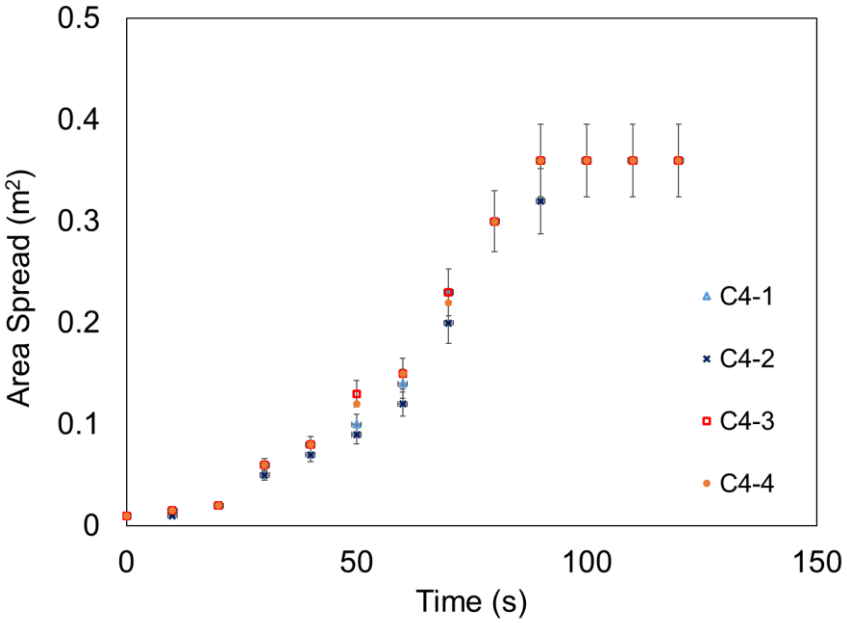

Figure 3-15: Manual Flame Area Measurements for Test C4

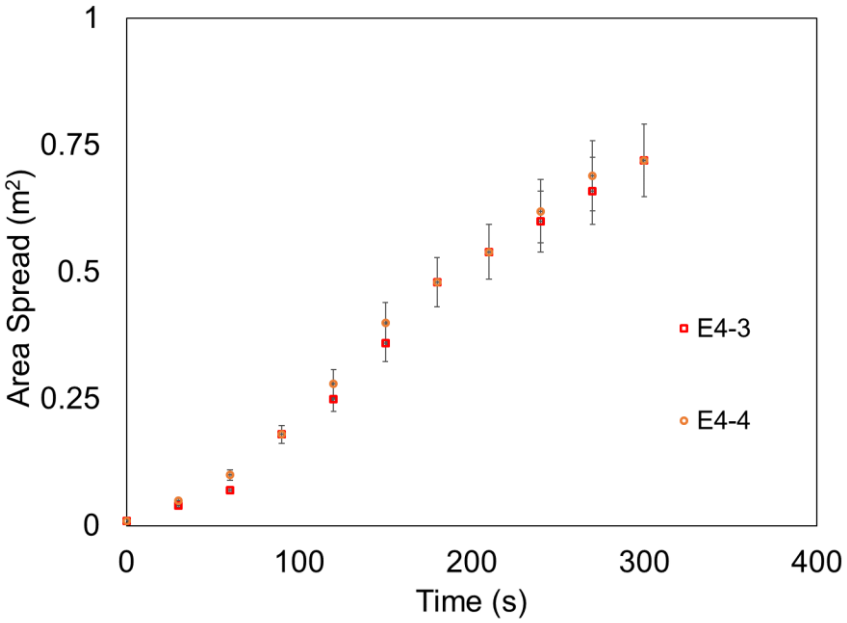

Figure 3-16: Manual Flame Area Measurements for Test E4

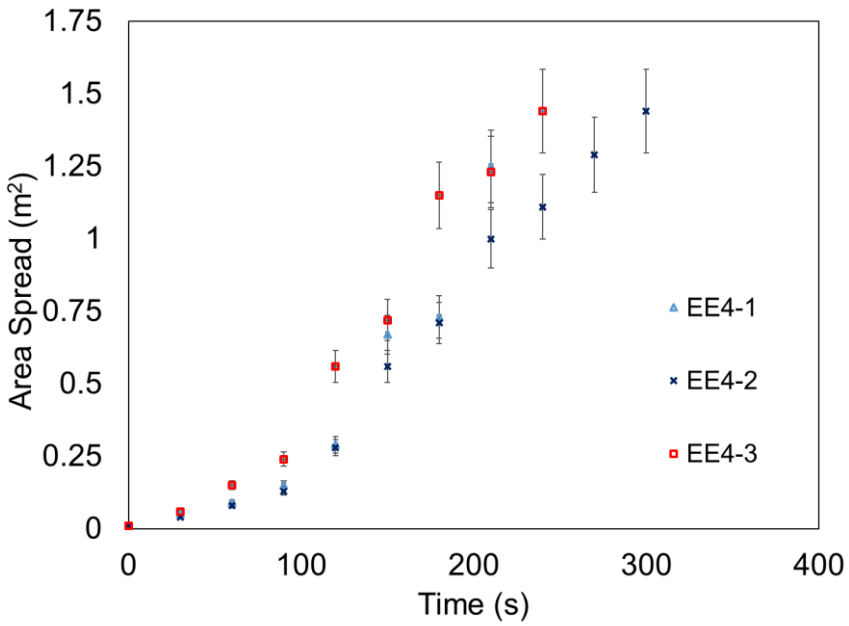

Figure 3-17: Manual Flame Area Measurements for Test EE4

For test series E4, only the flame areas for test three and four were determined. During the tests, burning molten material spread along the bottom sides of the foam and ignited other areas of the solid foam. This did not allow accurate determination of the flame areas since the fire burned at multiple locations on the foam. Precise determination of the area spread rates was also hindered by some other factors. Only one camera was used to take video records during testing and hence, the flame obscured visibility on the opposite side of the burn (this was especially true for centre ignition). The camera was set on a tripod at a height above the foam which led to some errors in counting the number of ignited squares due to the viewing angle. These errors, however, were not as pronounced in the earlier stages of the experiment when compared to the latter stages of the experiment. Once the fire becomes fully developed, larger deviations are seen to exist in measured values for each test series. A previous study estimates that errors in the manual flame spread measurement are approximately 10% of the actual area (Robson, 2014).

In foam furniture calorimeter tests, Robson determined the spread of flame on polyurethane foams based on IR images and an assumption that the flame front location was at any point on the foam with a temperature of 300°C (Robson, 2014). A MATLAB script converted IR images to binary images where a final determination of the area spread rate was obtained. Robson applied this process to foams with similar geometry to the compartment test

samples. The flame spread rates obtained from Robson's measurements were used as a comparison to the manually determined area spread rates. A comparison of the area spread rates for the E4 test sample is shown in Figure 3-18.

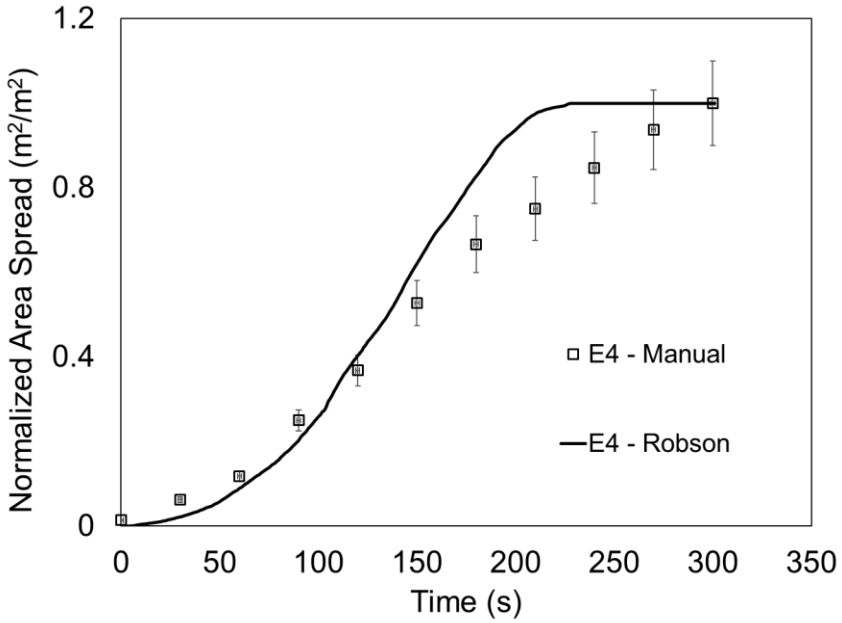

Figure 3-18: Comparison of Manual Area Spread Measurements to Robson's Automated Measurements for Test E4 (Robson, 2014)

From the data reasonable agreement exists between the manually determined flame spread rates in the compartment test and automated measurements in the furniture calorimeter test. For all tests, the maximum difference in the flame spread results obtained was generally about 25%. Differences in the results found using the two methods occur especially at the later stages of the experiment. It is not expected that flame spread rates are equal for both tests as experiments were carried out in different conditions. The rate of smoke build-up and air entrainment are different in both test conditions and will influence spread rates. Apart from the differences in test conditions, for both measurements there were also errors associated with the measurement technique applied. Robson identified inherent challenges associated with the accurate determination of flame spread using the automated method. Flickering of the flame front causes over-prediction of flame areas (Robson, 2014) which may explain why higher spread rates are recorded for the furniture calorimeter measurements at the later stages of the experiment. Manually, the errors in determining exactly when the foam is ignited and area of the

foam on fire results in differences in area spread results. Based on this comparison it is believed that the manual flame spread measurements could be used with a reasonable level of confidence.

3.4 FURNITURE CALORIMETER HEAT RELEASE RATE RESULTS

To conduct an analysis on the compartment test, information on how much heat is released is required. Heat release rates were not directly measured in the compartment foam test. However, in previous research, Robson made furniture calorimeter heat release rate (HRR) measurements on the same type of polyurethane foam used in the compartment foam test (Robson, 2014). For this research, it is assumed that for similar foam configurations, the HRR measurements in the compartment foam tests will be similar to the HRR obtained in the furniture calorimeter. This assumption allows for the comparison of HRR predictions made for the compartment fire tests.

To ascertain the validity of this assumption, a literature review was carried out for comparative tests in a furniture calorimeter burn (fuel controlled – surplus oxygen) to a compartment burn where oxygen may be limited for the fire (ventilation controlled). Obach conducted tests to compare the burning characteristics of these different test environments. The HRR for a set of uniformly constructed wooden cribs weighing around 15 kg was measured in the same compartment used in this research (shipping container) and compared to the HRR measured in a furniture calorimeter (Obach, 2011). A comparison of the HRR data shown in

Figure 3-19 indicates reasonable agreement in the growth phase of the fire for both test environments, with both tests reaching peak HRR at approximately 3% of each other (225 s after ignition). The peak HRR measurements were within 15% for both test environments. The furniture calorimeter results are denoted as free burn referring to the unrestricted supply of oxygen to the foam.

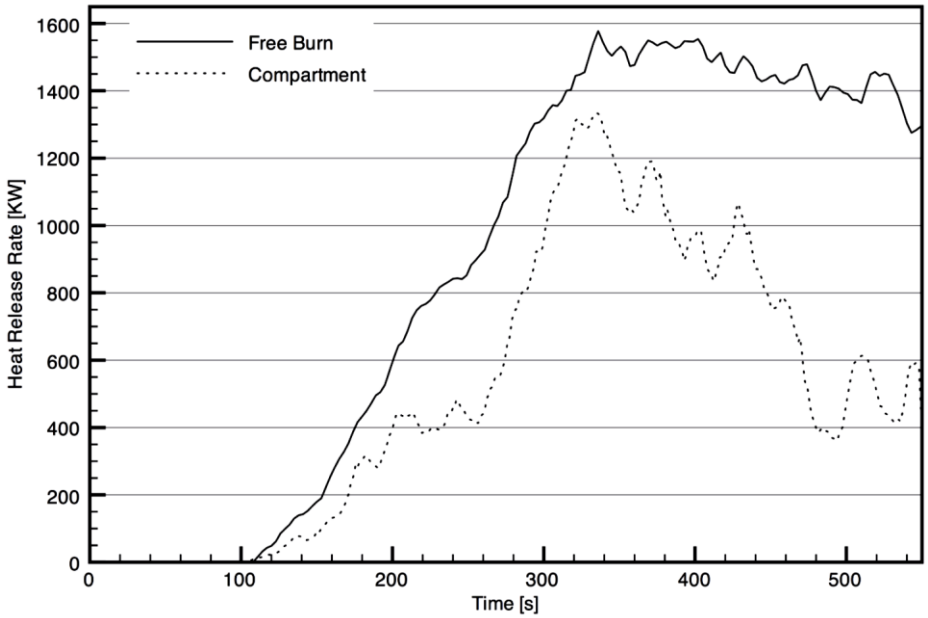

Figure 3-19: Heat Release Rate Comparison for a Wooden Crib Fire (Used with Permission, Obach, 2011)

As expected, the HRR measured for the compartment test was less than the values measured for the free burn. The variations in measurements are explained by the differences in ventilation conditions as the fire in the free burn easily entrains oxygen for combustion leading to higher HRR. Due to oxygen limitations, greater deviations in HRR measurements occurred in the decay phase of the fire. As discussed in Section 3.3, a similar trend was observed for flame spread measurements in both test conditions. HRR and flame spread are directly related and thus, impacted similarly by test environments. The HRR comparison suggests that it is satisfactory to use the HRR data for the free burn to represent the compartment fire provided that the fire remains fuel controlled. The maximum HRR recorded for each foam specimen in the furniture calorimeter test is less than 500 kW which means that the fire will remain fuel controlled and hence adequately represented using a furniture calorimeter HRR curve. McCaffery's correlation suggests that a 1.0 MW fire will be required to transition the burn to a ventilation-controlled fire (Drysdale, 2011).

The foams in the furniture calorimeter tests were cut to sizes similar to the compartment test therefore, the same naming nomenclature used previously to represent test samples is continued. The HRR measurements from Robson's furniture calorimeter tests for C4, E4 and EE4 are shown in Figure 3-20. The HRR data was refined to ensure that the start time (t = 0 s)

for the tests corresponds to when the fire was already established. This removed the time period where the fire is unpredictable and may be subject to the influence of ambient conditions such as wind drafts.

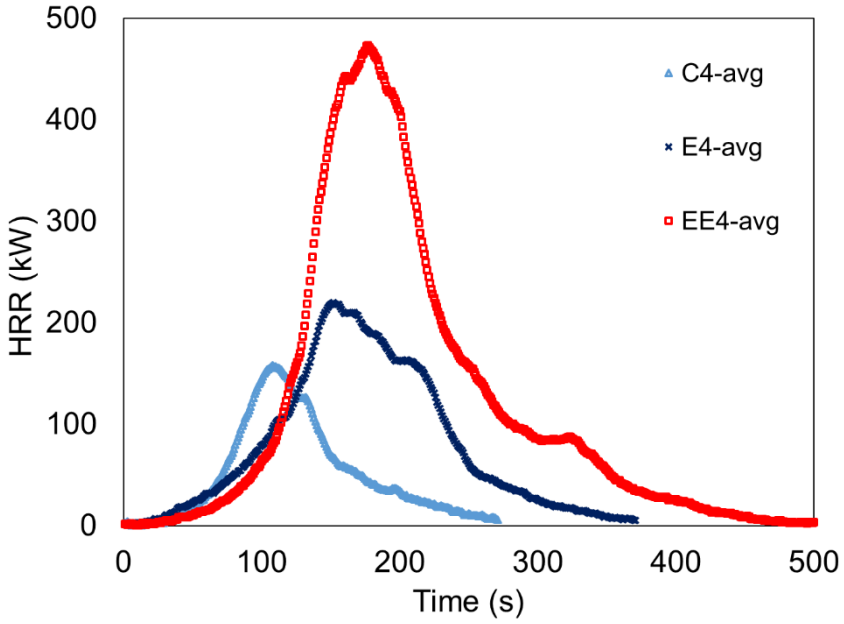

Figure 3-20: Average Furniture Calorimeter Heat Release Rate Measurements (Robson, 2014)

The average HRR was calculated for the three tests in each series of furniture calorimeter tests. The HRR results were generally repeatable for each test in the series with measured values within 14% of the average value (Robson, 2014). Robson reported variations in the peak heat release rate as well as the time to peak heat release rate. These variations were attributed to environmental conditions and changes in the exact composition of the specimens (Robson, 2014). Regardless, the trend of the growth and decay phase of the full-scale experiments showed reasonable agreement. Table 3-2 gives a summary of the full-scale HRR data.

Table 3-2: Summary of Full-Scale Furniture Calorimeter Test Results (Robson, 2014)

Test Series	Peak HRR (kW)		Time to Peak (s)		Total Heat Release (MJ)	
	Average	σ	Average	σ	Average	σ
C4	159.7	21.6	104.7	3.8	13.9	1.0
E4	237.0	24.8	161.7	11.0	28.9	3.9
EE4	485.9	34.8	182.0	11.3	58.0	3.7

3.5 SUMMARY OF CHAPTER

Chapter 3 focuses on full-scale testing of mattress (foam) specimen carried out at the University of Waterloo shipping container facility. Temperatures measured in the shipping container during the combustion of the foam specimen were reported for the two types of ignition locations investigated (centre and edge ignition). All foams tested in full-scale were of equal thickness (10 cm). The peak ceiling temperature obtained was observed to be a function of the size of the foam specimen and the distance of the thermocouple away from the burning foam. Vertical temperature distribution measurements indicate a hot gas stratification layer occurring between 0.8 to 1.1 m above the ground.

Foam surface temperatures were also studied. The rate of temperature rise across the foam is observed to be related to the ignition location. A higher rate of temperature rise is recorded for centre ignition when compared to edge ignition. This is explained by the formation of a faster propagating pool fire at the centre of the foam and air entrainment from all sides of the resulting fire. Flame areas were manually measured to investigate the behaviour of the fire based on ignition location. For the centre ignition tests, the flame was seen to spread generally in a circular pattern. The edge ignition tests showed flame spread in a semi-circular pattern until the flame reaches the foam boundaries where a transition to an elliptical burn pattern occurs.

4 SMALL-SCALE NUMERICAL MODEL

To study the heat transfer through the foam specimen, a model was developed to approximate the heat transfer process. A one-dimensional finite-difference model was used to simulate the transient temperature rise of the small-scale polyurethane specimen prior to ignition. The model, which was developed using Microsoft Excel ™, enabled the estimation of the time to ignition as well as the temperature required for ignition. The validity of the model was tested by comparing its results to related closed-form solutions for classical boundary problems. Temperatures predicted by the model were compared to experimental thermocouple measurements discussed in Chapter 2 and used to predict ignition times of the foam tests.

4.1 THE FINITE DIFFERENCE MODEL

The transient heat transfer in a foam specimen can be modelled using conservation principles and the resulting differential equation for heat transfer in a control volume. The solution of the governing equation determines the temperature field within the medium. The three-dimensional heat diffusion equation for Cartesian coordinates is given as (Incropera, Dewitt, Bergman, & Lavine, 2007);

$$\rho c_p(T)\frac{\partial T}{\partial t} = \frac{\partial}{\partial x}\left(k(T)\frac{\partial T}{\partial x}\right) + \frac{\partial}{\partial y}\left(k(T)\frac{\partial T}{\partial y}\right) + \frac{\partial}{\partial z}\left(k(T)\frac{\partial T}{\partial z}\right) + G \qquad (4.1)$$

Where

ρ is the density (kg/m^3)

c_p is the specific heat (J/kg°C)

T is the temperature (°C)

t is the time (s)

k(T) is the thermal conductivity as a function of the local temperature (W/m°C)

x, y, z are the distances in the various coordinates (m) and

G is the thermal energy generation rate per unit volume (W/m^3).

To appropriately model the heat transfer in the small-scale foam tests, three major assumptions were applied to solve the heat diffusion equation. The heat transfer in the foam specimen was assumed to be one-dimensional since the entire top surface of the foam is exposed to the incident heat flux from the cone calorimeter and the heat flows vertically downwards. The uniformity of the cone calorimeter heat flux exposures is discussed in Section 2.2. One-dimensional treatment of small-scale heat exposures has been used extensively in prior research. Aire (2014) applied the one-dimensional modelling approach in his study of wall assemblies exposed to varying cone calorimeter heat fluxes and obtained temperatures that were generally within 10% of experimental data. Enninful (2006) applied the same methodology for determining soil temperature profiles while Torvi (1992) applied the assumption to modelling skin exposed to flash fires. In general, for the configuration of interest, the one-dimensional assumption is thought to sufficiently capture the heat transfer processes within the control volume.

The second assumption in this model is that moisture in the foam is minimal and does not significantly affect the heat transfer process. Additionally, the effect of heat losses from the exposed sides of the foam was considered negligible. The internal energies associated with reactions and phase change are not directly accounted for in governing equation. Phase change was accounted for by varying the foam density during simulations. These assumptions allowed for simplification of the differential equation and ignoring the source term (G). Further analysis of the validity of the assumptions and impact on the accuracy of predictions are carried out in Section 4.5.

The foam was also assumed to behave as a semi-infinite solid which allowed for the constant temperature treatment of the bottom boundary condition. The temperature at the base of the foam was assumed to be equal to ambient temperature throughout the duration of the simulation.

The simplified one-dimensional governing equation becomes;

$$\rho c_p(T)\frac{\partial T}{\partial t} = \frac{\partial}{\partial x}\left(k(T)\frac{\partial T}{\partial x}\right) \tag{4.2}$$

4.2 INITIAL AND BOUNDARY CONDITIONS

The initial and boundary conditions used in the model were based on the cone calorimeter test conditions. The initial temperature of the foam specimen was assumed to be uniform and equal to the room ambient temperature at the beginning of the test. Upon testing, a heat flux boundary condition was applied to the exposed surface of the foam while the bottom boundary condition was assumed to be equal to the ambient temperature throughout the duration of the simulation.

4.2.1 Heat Flux Boundary Condition (x = 0)

The cone calorimeter provides a uniform heat flux ($\acute{q}$) to the surface of the exposed foam. The amount of heat flux incident on the foam is set using a calibration curve that relates the temperature of the cone element to the heat flux. At the top boundary (x = 0), the foam experiences radiative and convective heat transfer as shown in Figure 4-1. The mathematical treatment of the various modes of heat transfer on the surface of the specimen is presented below.

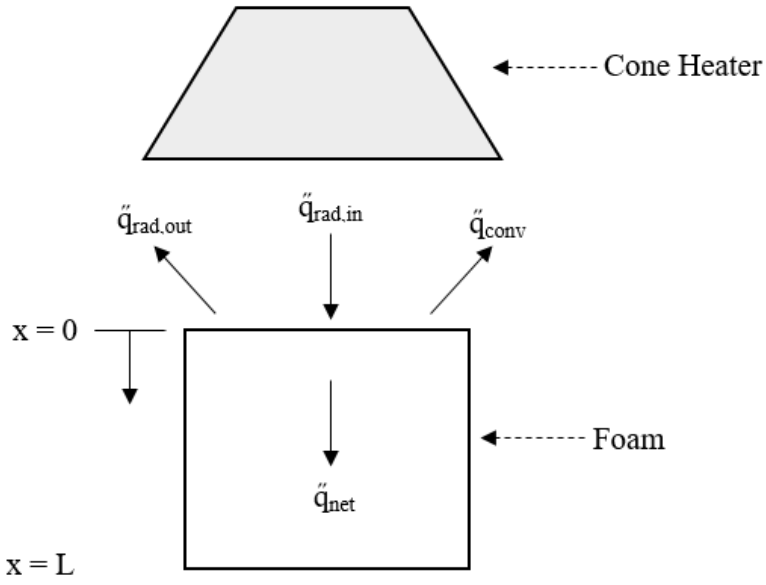

Figure 4-1: Schematic of the Foam Heat Transfer Exposed to the Cone Heater

a) Radiative Heat Flux ($\ddot{q}_{rad,in}$ and $\ddot{q}_{rad,out}$):

The radiative energy exchange between the cone and the foam as well as the foam and the environment are given respectively as;

$$\ddot{q}_{rad,in} = f_{1-3}\varepsilon\sigma(T^4{}_c - T^4{}_{x=0}) \quad (4.3)$$

$$\ddot{q}_{rad,out} = f_{1-surroundings}\varepsilon\sigma(T^4{}_{x=0} - T^4{}_a) \quad (4.4)$$

Where;

$\ddot{q}_{rad,in}$ is the incident heat flux from the cone calorimeter

$\ddot{q}_{rad,out}$ is the radiant heat loss from the foam

f is the view factor

ε is the emissivity

σ is Stephan-Boltzmann constant (W/m^2K^4)

T_c is the temperature of cone element (K)

$T_{x=0}$ is the temperature of the exposed foam surface (K) and

T_a is the temperature of the surroundings (K).

The view factor, $f_{1\text{-}3}$, (Figure 4-2) of the radiant heat transfer between the internal surface of the cone heater and the foam surface was modelled similarly to Aire's research (Aire, 2014). The model was based on work presented in Yuen et al (2007), and Wilson et al (2003) which determined the view factor between an elemental area dA1 and Area 2 and Area 4 as shown in Figure 4-2.

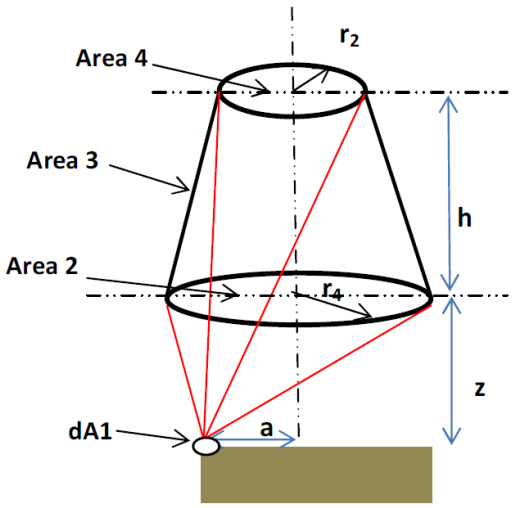

Figure 4-2: View Factor for the Radiative Exchange between the Internal Surface of a Cone Frustum to an elemental Surface dA1 (Aire, 2014)

Based on the view factor model, it was determined that the view factor between the elemental area dA1 and the internal surface of the cone heater is 0.711. The overall view factor for the exposed surface of the foam specimen was obtained by numerically integrating the elemental view factor over the entire surface of the specimen (0.1 m by 0.1 m). The final view factor $f_{1\text{-}3}$ was found to be 0.78. This value is in line with the value of this view factor reported in other studies (Janssens, 2016).

The view factor from the foam to the surroundings is determined assuming that the foam only interacts with the cone heater and the surroundings. Thus;

$$f_{1-surroundings} = 1 - f_{1-3} \tag{4.5}$$

b) Convective Heat Flux ($\ddot{q}_{conv}$)

As the temperature at the top surface of the foam increases, heat losses occur as a result of the convective air current flowing along the top boundary condition. The convective heat flux is given as;

$$\ddot{q}_{conv} = h(T_{x=0} - T_a) \tag{4.6}$$

Where h is the convective heat transfer coefficient (W/m^{2}K) and can be determined using an empirical correlation for natural convection for horizontal plates reported in Incropera et. al. The convective heat transfer coefficient is calculated using the Nusselt number which is the ratio

of convection to conduction heat transfer. The Nusselt number is given as (Incropera, Dewitt, Bergman, & Lavine, 2007);

$$Nu = \frac{hL}{k} \tag{4.7}$$

$$Nu = 0.54Ra_L^{\frac{1}{4}} \left(10^4 \leq Ra_L \leq 10^7\right) \tag{4.8}$$

$$Nu = 0.15Ra_L^{\frac{1}{3}} \left(10^7 \leq Ra_L \leq 10^{11}\right) \tag{4.9}$$

$$Ra_L = \frac{g\beta(T_s - T_\infty)L^3}{v\alpha} \tag{4.10}$$

Where;

Nu is the Nusselt number

Ra_L is the Rayleigh number

h is the convective heat transfer coefficient (W/m^2K)

L is the characteristic length (m)

k is the thermal conductivity (W/mK)

g is the acceleration due to gravity (m/s^2)

β is the thermal expansion coefficient of air (K^{-1})

T_s is the surface temperature (K)

T_∞ is the ambient temperature (K)

v is the kinematic viscosity of air (m^2/s) and

α is the thermal diffusivity of air (m^2/s).

The convective heat transfer coefficient was evaluated using three surface temperatures of 130℃, 230℃, 330℃ with an ambient temperature of 24℃. A film temperature ($T_f = (T_s + T_\infty)/2$) was calculated for the various surface temperatures and used to evaluate the properties of air. Using equation 4.7 – 4.10, the Rayleigh number was calculated to be in the range of $4.4 \times 10^6 – 4.9 \times 10^6$ and the Nusselt number was found to be between 25.2 – 25.6 for

the temperatures considered. A convective heat transfer coefficient in the range of 7.6 – 9.2 W/m^{2}K was calculated. For application into the model, a value of 8.5 W/m^{2}K was used as the convective heat transfer coefficient which is an average of the coefficients calculated. For a similar test configuration, Enninful used a value of 10 W/m^{2}K which was applied for heat fluxes of approximately 50 kW/m^2 (Enninful, 2006).

c) Net Heat Flux ($\ddot{q}_{net}$)

An energy balance on the top boundary (x = 0) of the foam was used to determine the net heat flux which is actually conducted into the foam specimen. From Figure 4-2, the net flux may be obtained as;

$$\ddot{q}_{net} = \ddot{q}_{rad,in} - \ddot{q}_{rad,out} - \ddot{q}_{conv} \tag{4.11}$$

$$\ddot{q}_{net} = f_{1-3}\varepsilon\sigma({T^4}_c - {T^4}_{x=0}) - [(1 - f_{1-3})\varepsilon\sigma({T^4}_{x=0} - {T^4}_a)] - h(T_{x=0} - T_a) \tag{4.12}$$

In order to use the finite volume method, the mass of the top boundary node (x = 0) must be considered. An energy balance, which accounts for energy storage and conduction to the rest of the foam yields the following equation;

$$\rho c_p(T)\frac{\Delta x}{2}\frac{\partial T}{\partial t} =$$
$$k(T)\frac{\partial T}{\partial x} + f_{1-3}\varepsilon\sigma({T^4}_c - {T^4}_{x=0}) - [(1 - f_{1-3})\varepsilon\sigma({T^4}_{x=0} - {T^4}_a)] - h(T_{x=0} - T_a) \tag{4.13}$$

4.2.2 Semi-Infinite Boundary Condition (x = L)

The semi-infinite assumption was applied to the bottom boundary where the temperature at the bottom of the foam is equal to ambient temperature ($T_{x=L} = T_a$). The assumption implies that for the duration of the simulation, the temperature at the base of the foam is unaffected by the heat flux exposure at the top boundary. The validity of the assumption is governed by the relationship between the depth of the foam (L), thermal diffusivity of the foam (α) and exposure time (t). The relationship is given as;

$$\frac{L}{2\sqrt{\alpha t}} \geq 2 \tag{4.14}$$

From equation 4.14 the maximum time of exposure (t_{max}) for which the semi-infinite boundary condition is valid may be calculated as;

$$t_{max} = \frac{\left(L/4\right)^2}{\alpha} \tag{4.15}$$

$$\alpha = \frac{k}{\rho c} \tag{4.16}$$

The thermophysical properties of the polyurethane foam at room temperature are taken as, k = 0.05 W/mK, c = 1324 J/kgK and ρ = 17 kg/m^3 (Prasad, et al., 2009) (Scott, Dodd, Larsen, Suo-Anttila, & Erickson, 2016). Equation 4.15 yields a maximum time of exposure as 287 s. Since the model is to be applied prior to ignition, the semi-infinite assumption is valid for when the ignition time of the foam specimen is less than 4 minutes and 45 seconds. This time is much longer than typical ignition time of the foam specimen considered in this research, hence, the simulations in this model were limited to 200 s.

4.3 DISCRETIZATION OF THE HEAT DIFFUSION EQUATION

The explicit method for discretizing partial differential equations was applied to transform the heat diffusion equation (equation 4.2) to a set of finite difference equations and to treat the top boundary condition (equation 4.13). The discretization process allows for the solution of the heat transfer problem. In the explicit method, the field variables are replaced by approximations based on the nodal values. The temperature at any node at a current time step (i) is determined from the knowledge of temperatures in the same node and surrounding nodes at the previous time step (i – 1). To discretize the spatial derivatives, the central differencing scheme was employed.

The finite difference equations are given below where *x* and *i* represent the nodal position and time of interest respectively;

a) For the top boundary node (x = 0)

$$\frac{(\rho_i c_p)^{i-1}\Delta x\left(T^{i}{}_{x=0} - T^{i-1}{}_{x=0}\right)}{2\Delta t} = k_x{}^{i-1}\frac{\left(T^{i-1}{}_{x+1} - T^{i-1}{}_{x=0}\right)}{\Delta x} + f_{1-3}\varepsilon\sigma\left(T^{4}{}_{c} - (T^{i-1}{}_{x=0})^{4}\right) - \left[(1 - f_{1-3})\varepsilon\sigma\left((T^{i-1}{}_{x=0})^{4} - T^{4}{}_{a}\right)\right] - h\left(T^{i-1}{}_{x=0} - T_a\right) \quad (4.17)$$

$$T^{i}{}_{x=0} = \left[2Fo\left(T^{i-1}{}_{x+1} - T^{i-1}{}_{x=0}\right) + \left[\frac{\Delta x}{k_x{}^{i-1}}\left(f_{1-3}\varepsilon\sigma\left(T^{4}{}_{c} - (T^{i-1}{}_{x=0})^{4}\right)\right)\right] - \left[\frac{\Delta x}{k_x{}^{i-1}}(1 - f_{1-3})\varepsilon\sigma\left((T^{i-1}{}_{x=0})^{4} - T^{4}{}_{a}\right)\right] - \left[\frac{\Delta x}{k_x{}^{i-1}}h\left(T^{i-1}{}_{x=0} - T_a\right)\right]\right] + T^{i-1}{}_{x=0} \quad (4.18)$$

Where;

$$Fo = \frac{\alpha\Delta t}{\Delta x^2} \quad (4.19)$$

The challenge with applying the explicit finite difference method is the instabilities that may arise as from the choice of Δx or Δt. For large values of Δx or Δt, unrealistic oscillations may occur leading to a solution that diverges from the true value. To ensure the stability of the solution, a criterion which is based on the Fourier number (Fo) is given as (Aire, 2014);

$$Fo \leq 0.5\left[1 + \frac{h\Delta x}{k_x{}^{i-1}} + \frac{\varepsilon\sigma\Delta x}{k_x{}^{i-1}} \times \frac{(T^{i-1}{}_{x})^{4}}{T^{i-1}}\right]^{-1} \quad (4.20)$$

b) For the interior nodes (0 < x < L)

$$\frac{(\rho_i c_p)^{i-1}\left(T^{i}{}_{x} - T^{i-1}{}_{x}\right)}{\Delta t} = \frac{k_x{}^{i-1}\left(T^{i-1}{}_{x+1} - T^{i-1}{}_{x} + T^{i-1}{}_{x-1}\right)}{\Delta x^2} \quad (4.21)$$

$$T^{i}{}_{x} = Fo\left(T^{i-1}{}_{x+1} - T^{i-1}{}_{x} + T^{i-1}{}_{x-1}\right) \quad (4.22)$$

For the interior nodes, the stability criterion is given as;

$$Fo \leq 0.5 \tag{4.23}$$

c) For the bottom boundary node

$$T^{i}_{x} = T_a \tag{4.24}$$

A close observation of the discretized solution may imply that the material thermal properties are treated independent of temperature. To simplify the solution of the finite difference equation, the author has decoupled the solutions relating the thermal properties with temperature. This is similar to Aire's evaluation of thermal properties for modelling heat transfer in gypsum board (Aire, 2014) and Torvi's treatment of thermal properties in modelling heat transfer in protective fabrics (Torvi, 1997). These properties are evaluated based on the nodal temperatures at the previous time step. This approach allows for quick convergence of the solution and easier identification of errors in the solution. The treatment of thermal properties is covered in section 4.5.

4.4 VALIDATION OF THE FINITE DIFFERENCE MODEL

To confirm the accuracy of the finite difference model, validations of the numerical solution was carried out using analytical solutions (closed form) for heat flux and convection boundary conditions. Properties of the foam used for validation were assumed constant and independent of temperature, to allow direct comparisons with the closed-form solutions. The constant properties of polyurethane foam used are presented in Table 4-1.

Table 4-1: Properties of Polyurethane Foam used for Validation Exercise (Prasad, et al., 2009) (Scott, Dodd, Larsen, Suo-Anttila, & Erickson, 2016).

Property	Value
Thickness, L (m)	0.1
Thermal Conductivity, k (W/m.°C)	0.05
Specific Heat, c_p (J/kg°C)	1324
Density, ρ (kg/m^3)	17

4.4.1 Constant Heat Flux Boundary Condition

An analytical solution reported by (Incropera, Dewitt, Bergman, & Lavine, 2007) was used to solve the temperature distribution within the foam specimen for a constant heat flux exposure using foam properties given in Table 4-1. Validation was carried out for heat fluxes of 5 kW/m^2, 10 kW/m^2, 20 kW/m^2 and 35 kW/m^2 at a time step of 1.0 s and grid sized with 15 nodes. A total exposure time of 200 s was simulated.

The closed-form solution is given as;

$$T(x,t) - T_i = \frac{2\ddot{q_o}\left(\frac{\alpha t}{\pi}\right)^{0.5}}{k}\exp\left(\frac{-x^2}{4\alpha t}\right) - \frac{\ddot{q_o}x}{k}erfc\left(\frac{x}{2\sqrt{\alpha t}}\right) \quad (4.25)$$

Where:

$\ddot{q_o}$ is the incident heat flux (kW/m^2)

α is the thermal diffusivity (m^2/s)

k is the thermal conductivity (W/mK)

x is the distance from the exposed surface (m)

Figure 4-3 reports the comparison between the analytical and numerical solution at the exposed surface of the foam for the 5 kW/m^2 heat flux exposure. Only one graph is presented as results were similar across all heat flux exposures.

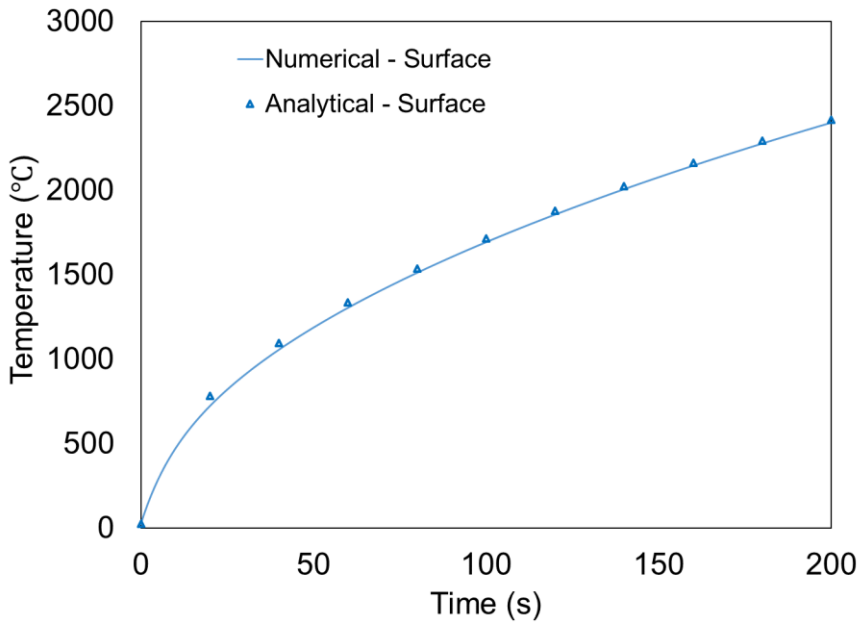

Figure 4-3: Comparison of Numerical and Analytical Results at Surface for 5 kW/m^2 Exposure

From Figure 4-3, it is observed that the numerical simulation predicts the temperatures obtained using the analytical solution to a good degree of accuracy. A maximum temperature difference of 7% was obtained at the surface when comparing the numerical model to the closed-form solution. The larger temperature differences were obtained at the beginning of the simulation after which the model converges with the analytical solution with a difference of less than 0.5%. Figure 4-4 presents the comparison of the numerical and analytical solution at a depth of 0.05 m from the exposed surface. An exposure time of 200 s was simulated.

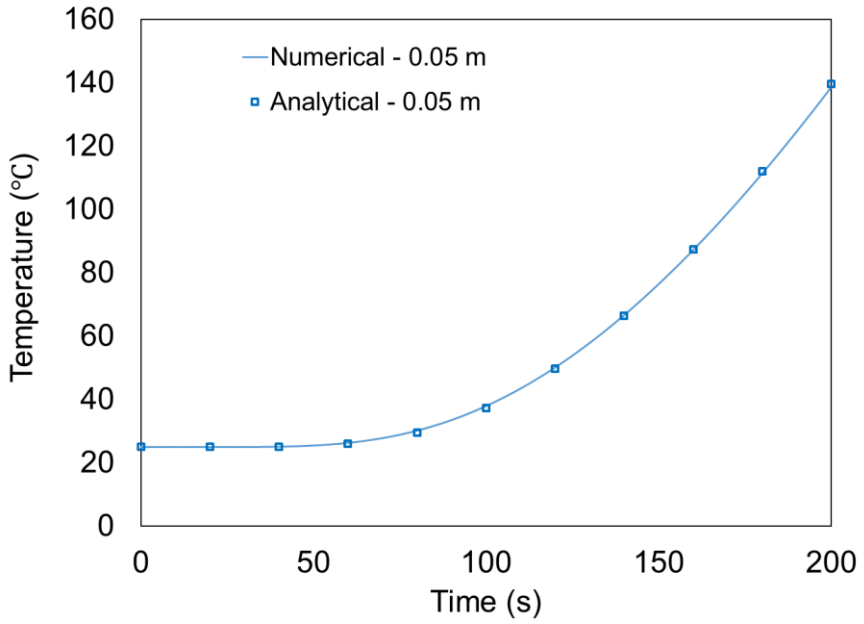

Figure 4-4: Comparison of Numerical and Analytical Results at 0.05 m for 5 kW/m^2 Exposure

Similar to the surface temperatures, at a depth of 0.05 m, a maximum temperature difference of 7% is obtained when comparing the numerical to the analytical solution. After 60 s, the temperature difference drops below 2%. These results show that the formulated differential equations, the discretization of the differential equations and the coding for the numerical solution were done appropriately. Further investigation of the time step selection and grid sizing will lead to improved accuracy in modelling the heat transfer problem.

4.4.2 Convection Boundary Condition

As seen in section 4.4.1, the temperatures predicted by the constant heat flux boundary condition are unrealistically high as the assumption does not account for equilibrium that may occur as the surface temperature of the foam reaches the cone element temperature, or account for heat losses. Applying a convection boundary condition is in some ways more realistic as the solution is limited by the temperature of the cone heater. The difficulty with this approach is that the heat transfer process from the cone element to the foam is primarily radiative. In order to apply a convection boundary condition, the radiation heat transfer equation is required to be transformed into an equivalent convective heat transfer equation to determine an effective convective heat coefficient. This effective convective heat coefficient may be determined by

transforming the equation for radiative heat transfer using the process of the difference of two squares. This treatment is presented below;

$$\ddot{q}_{rad,in} = f\varepsilon\sigma({T^4}_c - {T^4}_{x=0}) \tag{4.26}$$

$$\ddot{q}_{rad,in} = f\varepsilon\sigma({T^2}_c + {T^2}_{x=0})({T^2}_c - {T^2}_{x=0})$$

$$\ddot{q}_{rad,in} = f\varepsilon\sigma({T^2}_c + {T^2}_{x=0})(T_c + T_{x=0})(T_c - T_{x=0})$$

$$h_{eff} = f\varepsilon\sigma({T^2}_c + {T^2}_{x=0})(T_c + T_{x=0})$$

$$\ddot{q}_{rad,in} = h_{eff}(T_c - T_{x=0}) \tag{4.27}$$

The radiation heat transfer equation 4.27 closely mirrors the convective heat transfer equation, hence the closed-form solution for convective heat transfer may be applied. The closed-form solution is given in (Incropera, Dewitt, Bergman, & Lavine, 2007) as;

$$\frac{T(x,t) - T_i}{T_\infty - T_i} = erfc\left(\frac{x}{2\sqrt{\alpha t}}\right) - \left[\exp\left(\frac{hx}{k} + \frac{h^2\alpha t}{k^2}\right)\right]\left[erfc\left(\frac{x}{2\sqrt{\alpha t}} + \frac{h\sqrt{\alpha t}}{k}\right)\right] \tag{4.28}$$

Where;

$$h = h_{eff}$$

For the 5 kW/m^2, 10 kW/m^2, 20 kW/m^2 and 35 kW/m^2 heat flux exposure, the cone temperature was recorded as 350℃, 440℃, 547℃ and 665℃ respectively. From equation 4.28, the effective convective heat coefficient is calculated as 20.5 W/m^{2}K, 28.4 W/m^{2}K, 40.3 W/m^{2}K and 57.1 W/m^{2}K respectively using a view factor (*f*) of 0.9 and an emissivity (ε) of 0.9 (this view factor was assumed prior to evaluating the cone calorimeter view factor). The effective convective heat coefficient and the properties of polyurethane foam given in Table 4-1 were used in the closed-form solution. Figure 4-5 presents a comparison of the numerical and analytical solution obtained for surface temperatures and temperatures at a depth of 0.01 m for the 5 kW/m^2 heat flux exposure. Like the constant heat flux boundary condition, a similar trend was observed for other heat flux exposures. The numerical solution was calculated by setting the emissivity of the fire to zero and applying the effective convective heat coefficient values for the various heat fluxes.

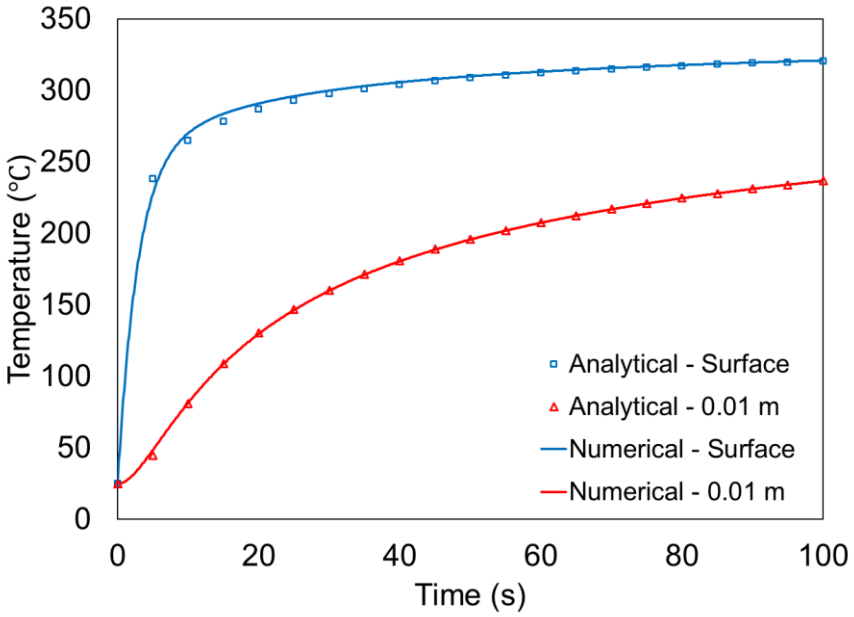

Figure 4-5: Comparison of Numerical and Analytical Results at Surface and Depth (5 kW/m^2)

The comparison of the numerical and analytical solutions for the convection boundary condition was generally within 5%. Similar to the heat flux boundary condition, the largest deviation occurred at the earlier stages of the simulation. This behaviour is typical for numerical solutions and is solved by refining the grid spacing and time step. Section 4.4.3 discusses grid refinement and time step selection.

4.4.3 Grid Size and Time Step Selection

As mentioned earlier, the selection of the grid size and time step influences the accuracy of predictions. The stability of the model is also impacted by the choice of these parameters. Thus, it is essential to investigate the optimal grid size and time step to be used in the heat transfer model. For analysis, the temperature at the surface of the 10 cm thick foam was modelled while exposed to a 5 kW/m^2 radiative heat source. The results obtained using 20, 30, 55 and 100 nodes are compared in Figure 4-6.

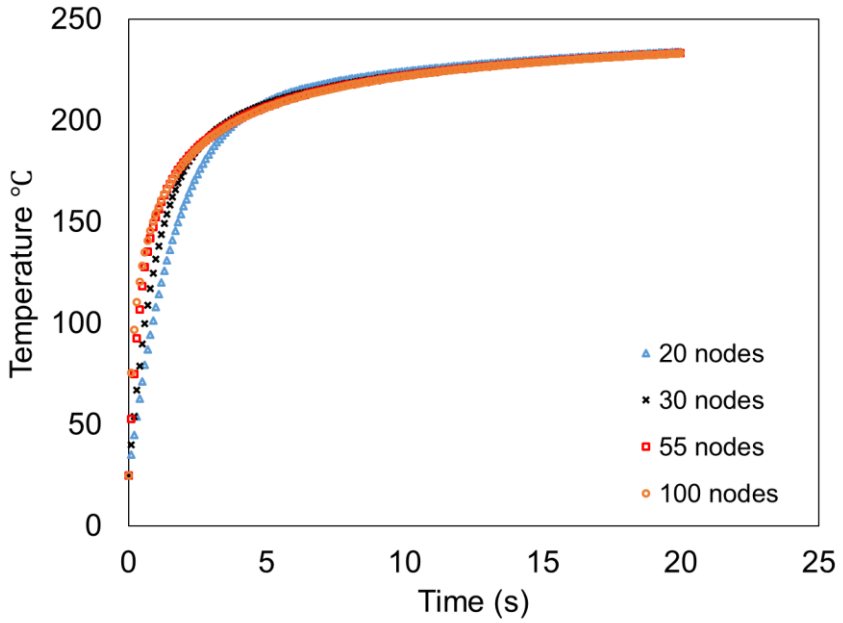

Figure 4-6: Effect of Grid Size on Foam Surface Temperature Predictions (5 kW/m^2)

From observations in Figure 4-6, the effect of grid size selection is noticed more during the earlier stages of the simulation. Comparing the 30 and 55 node simulation, the solution converges to less than 1% temperature difference within 2.4 s while convergence between the 55 nodes and 100 nodes simulation occurs within 1.3 s. Based on these results, the numerical simulations in this chapter were carried out using 100 nodes.

A comparison of temperature prediction for different timesteps is shown in Figure 4-7. The variations in temperatures predicted using time steps of 0.05 s, 0.1 s and 0.15 s are almost negligible. It was adjudged that the timestep has a less significant impact on predicted temperatures. Therefore, for the numerical simulations in this chapter, a time step of 0.1 s and a grid size using 100 nodes were chosen.

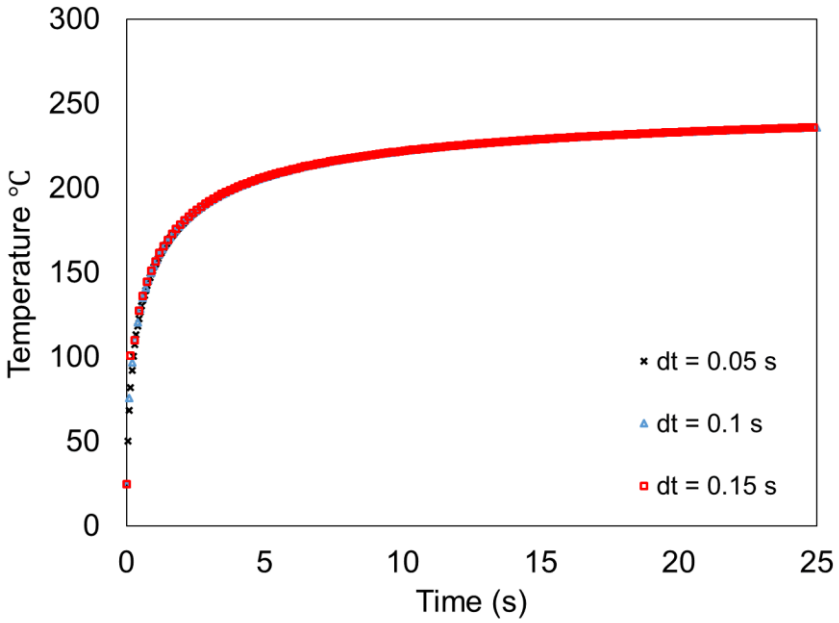

Figure 4-7: Effect of Timestep on Foam Surface Temperature Predictions (5 kW/m^2)

4.5 THERMAL PROPERTIES USED IN THE MODEL

It can be difficult to define the thermal properties of polyurethane foam. The thermal properties vary from foam to foam due to the presence of moisture, ageing of the foam and differences in the manufacturing process which affect the foam microstructure. The thermal properties of polyurethane also exhibit a large dependence on temperature (Pau, Fleischmann, Spearpoint, & Li, 2014). From the time of exposure of the foam to heat flux to the time of ignition and degradation of the foam, the specimen experiences wide variations in temperature and hence properties. To adequately model heat transfer in the foam, the variations in thermal properties must be accounted for. Various authors have reported a range of values for thermal properties and this research will attempt to quantify the effects of these variations.

As mentioned in section 4.3, the thermal properties were uncoupled from the finite difference solution and solved independently at each time step. The final thermal properties used in the model are derived using a combination of values from the literature and experimentally determined data. The values used for specific thermal properties are discussed below.

4.5.1 Thermal Conductivity of Polyurethane Foam

The thermal conductivity of the polyurethane foam was measured using the FOX 314 Heat Flow Meter (LaserComp. Saugus, MA). The apparatus measures the thermal conductivity of the foam by creating a temperature difference across the foam. The general principle behind the thermal conductivity measurement is Fourier's law. Constant top and bottom surface temperatures are maintained using thermostatic elements in the upper and lower plates. A square heat flux meter is embedded in the upper and lower plate to measure the heat conducted through the test specimen. The thermal conductivity of the specimen is then calculated using the average measured upper and lower heat flux along with the temperature difference and the thickness of the specimen (ASTM, 2017h).

To study the variation of thermal conductivity with temperature, three test series consisting of three individual tests were conducted. A polyurethane foam specimen with dimension 10 cm x 10 cm x10 cm was placed in a polystyrene holder to prevent compression of the foam. The upper and lower temperatures for the test series were 10℃ and 35℃, 20℃ and 45℃, and 25℃ and 50℃ respectively. Due to limitations in the upper-temperature limit of the FOX Heat Flow Meter, tests were not conducted at higher temperatures. The Fox Heat Flow Meter samples the temperature and heat transfer every 0.5 seconds and organizes the data in sets consisting of 514 samples. Steady-state conditions are determined when temperatures are within ±0.2℃ of the set temperature and the heat flow is within 2% of the previously measured data set. The average thermal conductivity at steady-state conditions is measured. The instrument calculates thermal conductivities to within 1% accuracy (LaserComp, 2004). Table 4-2 reports the results of the foam thermal conductivity tests.

Table 4-2: Results of Polyurethane Foam Thermal Conductivity Tests

Upper Temp (℃)	Lower Temp (℃)	Mean Temp (℃)	Upper Cond (W/m℃)	Lower Cond (W/m℃)	Average Cond (W/m℃)
10.01	35.02	22.52	0.05641	0.04645	0.05143
10.01	35.02	22.52	0.05586	0.04685	0.05135
10.01	35.02	22.52	0.05587	0.04641	0.05114
20.02	45.02	32.52	0.05471	0.04799	0.05135
20.02	45.02	32.52	0.05486	0.04783	0.05135
20.02	45.02	32.52	0.05491	0.04782	0.05137
25.02	50.02	37.52	0.05563	0.04938	0.05251
25.02	50.02	37.52	0.05570	0.04926	0.05248
25.02	50.02	37.52	0.05588	0.04917	0.05252

From Table 4-2, it is observed that the thermal conductivity of the foam increases with temperature. Correlating the measured thermal conductivity with temperature, a linear relationship was established. The linear relationship is given as;

$$k(T) = k_{amb} + 0.00007(T - T_{amb}) \tag{4.29}$$

where;

k is the thermal conductivity (W/m.℃)

T is the temperature (℃).

From the literature, reported values of the thermal conductivity of polyurethane foams at room temperature are within the range measured by the FOX meter. Prasad et al. (2009) reports the thermal conductivity as 0.05 W/m.°C while Valencia et al. (2009) reports this value as 0.045 W/m.°C.

The model is expected to predict foam temperatures up to ignition, as such, a further literature search was conducted to determine if the linear approximation is adequate for temperatures closer to ignition. The thermal conductivity of polyurethane polyol (melt) is approximately 0.1 W/m.°C (Prasad, et al., 2009) (Valencia, Rogaume, & Guillaume, 2009). Scott et al.(2016) reports the thermal conductivity of the foam at 250℃ as 0.071 W/m.°C. At 250°C, polyurethane is reported to undergo a breakdown in its structure and ignition ensues (Kramer, Zammarano, Linteris, Gedde, & Gilman, 2010), hence the thermal conductivity given by

Scott et al. (2016) will be used as a basis to verify the linear model. The linear model and data from Scott et al. are plotted in Figure 4-8. From the graph, it is observed that the linear model predicts the thermal conductivity at 250℃ to within 5% of the measured data.

The structure of polyurethane foam allows for air pockets in its pores. The air contained therein will have an influence on the overall thermal conductivity of the foam and it is expected that some similarities between the thermal conductivity of air and polyurethane exist. The thermal conductivity of air (Incropera, Dewitt, Bergman, & Lavine, 2007) is plotted in Figure 4-8. It is seen that the slope of the thermal conductivity of polyurethane mimics the slope of the curve for the thermal conductivity of air. Given these reasons, it is concluded that the linear model (Equation 4.29) sufficiently approximates the increase in thermal conductivity within the temperature range of interest of this research (20°C to 300°C). The thermal conductivity of the foam is solved using the linear equation with temperatures calculated at the previous time step by the finite-difference model.

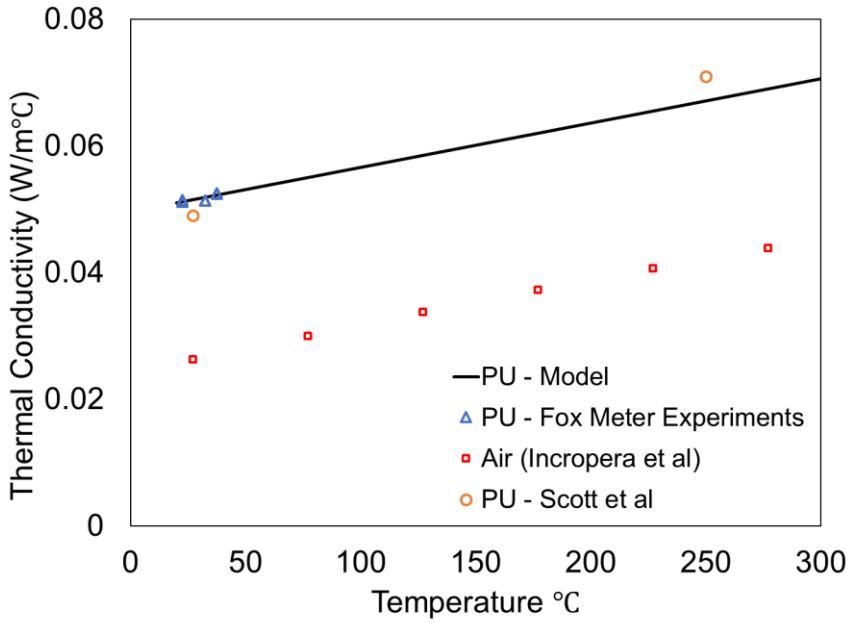

Figure 4-8: Variation of Thermal Conductivity with Temperature

4.5.2 Specific Heat of Polyurethane Foam

Dao et al. (2016) and Valencia (2009) reported the specific heat of polyurethane foam at room temperature as 1320 J/kg.°C and 1300 J/kg.°C respectively. However, both authors do not

specify exactly at what temperature these measurements were taken. The temperature-dependent specific heat of polyurethane foam reported by Taylor et al.(1998) is shown in Figure 4-9. The specific heat was given for temperatures ranging from 23℃ to 250℃. A linear correlation was established from this data and is given as;

$$C_p(T) = C_{amb} + 4.08\,(T - Tamb)$$

where;

$C_p(T)$ is the specific heat (J/kg℃)

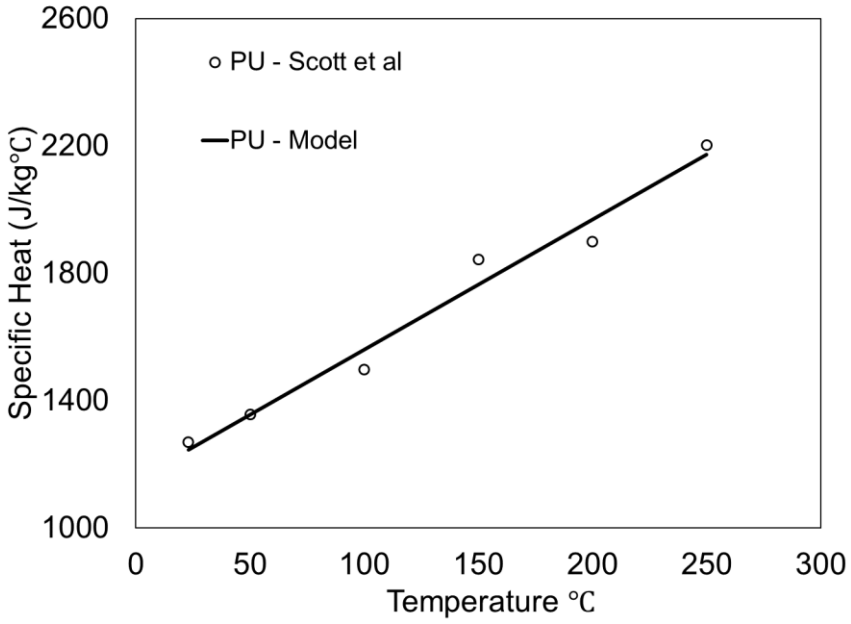

Figure 4-9: Specific Heat of Polyurethane Foam

4.5.3 Density of Polyurethane foam

During combustion, polyurethane foam experiences a phase change from solid to liquid (polyol) and the density of the foam changes during this process. Due to the highly insulative property of the foam, on exposure to a heat flux, significant temperature rise will occur only within a thin layer exposed directly to the cone calorimeter and the change in density is only seen in this layer. (Kramer, Zammarano, Linteris, Gedde, & Gilman, 2010). There is limited information in the literature on the relationship between foam density with temperature. In general, the solid phase density of polyurethane is low and may vary depending on the

manufacturing process. The liquid phase density (polyol) is reported to be in the range of 800kg/m^3 to 1035kg/m^3 (Pau, Fleischmann, Spearpoint, & Li, 2014), (Prasad, et al., 2009), (Valencia, Rogaume, & Guillaume, 2009). Kramer et al. notes that the ratio of solid foam to liquid foam density is approximately 1:40 (Kramer, Zammarano, Linteris, Gedde, & Gilman, 2010).

Based on the liquid and solid phase density measurements by Prasad et al. (2009), a linear relationship of density with temperature was assumed and is shown in Figure 4-10. It is expected that this approximation will introduce some uncertainties in the temperature predictions, especially for predictions of density at lower temperatures. However, this approach attempts to capture the density change due to phase change. A sensitivity analysis of the impact of density is presented in Section 4.7.3. The linear equation is given as;

$$\rho(T) = \rho_{amb} + 3.09\ (T - T_{amb})$$

Where;

$\rho(T)$ is the temperature-dependent density (kg/m^3).

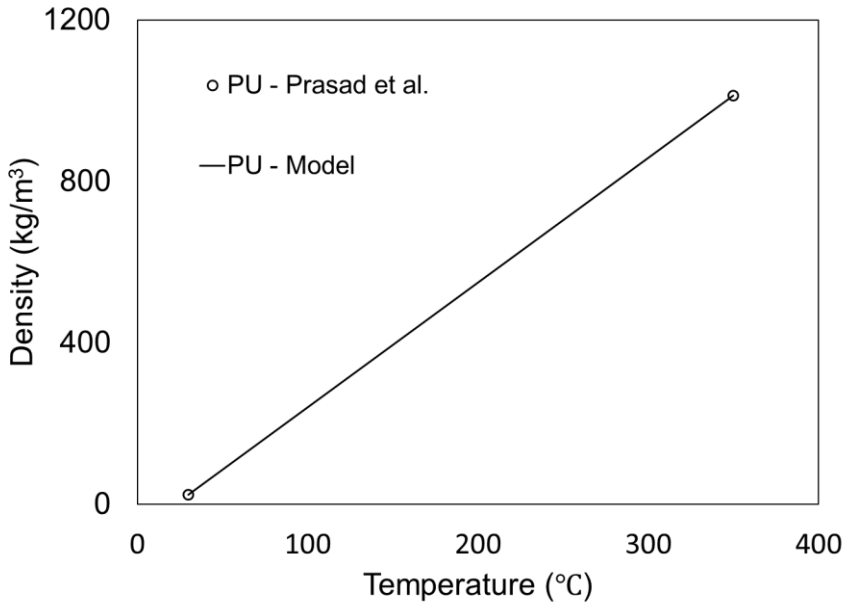

Figure 4-10: Density of Polyurethane Foam

4.6 NUMERICAL RESULTS

Foam temperatures were predicted at 0.1 cm increments from the top surface of the foam (0 cm) to the bottom of the foam specimen (10 cm) at each time step. The temperature at the bottom of the foam was assumed to be constant and equal to ambient temperature throughout the simulation. The input parameters to the model are given in Table 4-3 below;

Table 4-3: Model Inputs

Input Parameters	Value
Cone Temperature (K)	Varies with Heat Flux
Ambient Temperature (K)	303
Foam Height (m)	0.1
Nodes	100
View Factor	0.78
Emissivity (Babrauskas, 2016b)	0.9

Figure 4-11 to Figure 4-14 present the temperatures predicted for the 10 cm thick polyurethane foam specimens at the surface (0 cm), 0.1 cm, 2 cm, 4 cm and 6 cm in depth. The depths were selected to allow for comparison with the cone calorimeter thermocouple tests discussed in Section 2.7. The variable thermal properties discussed in Section 4.5 were employed in this model. The simulation was done for heat fluxes of 5 kW/m^2, 10 kW/m^2, 20 kW/m^2 and 35 kW/m^2.

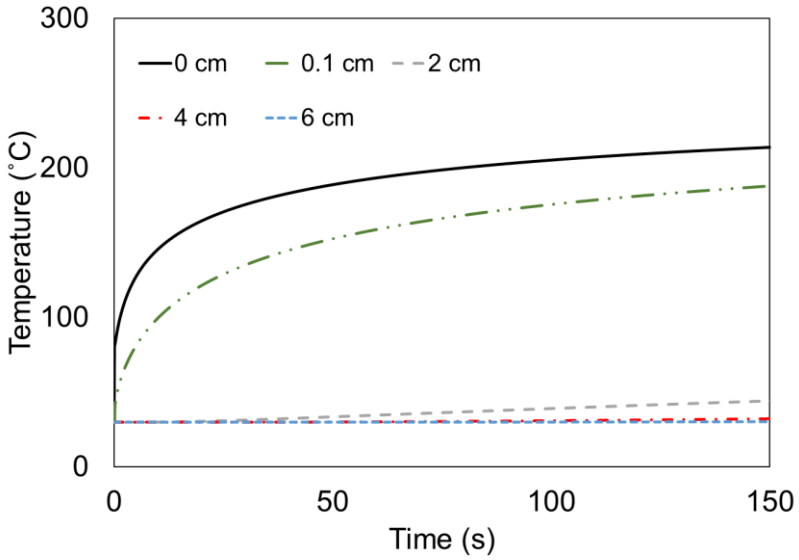

Figure 4-11: Temperature Predictions for 10 cm Thick Polyurethane Foam Exposed to 5 kW/m^2 Heat Flux

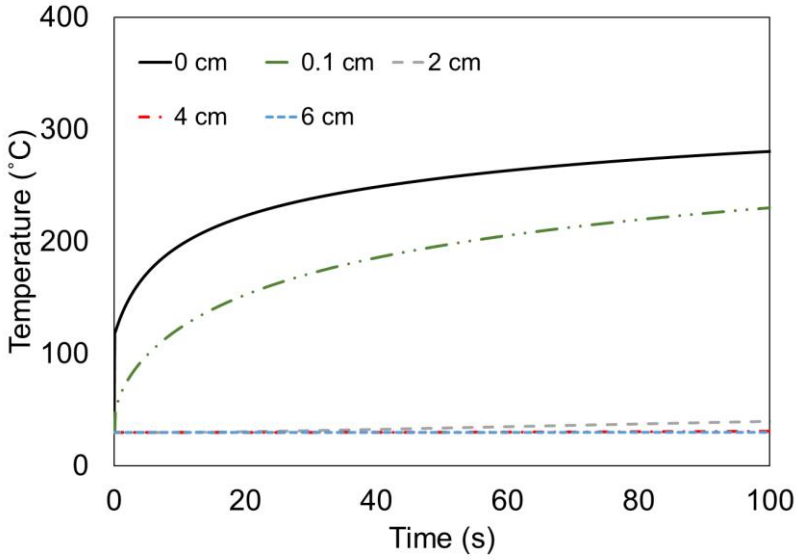

Figure 4-12: Temperature Predictions for 10 cm Thick Polyurethane Foam Exposed to 10 kW/m^2 Heat Flux

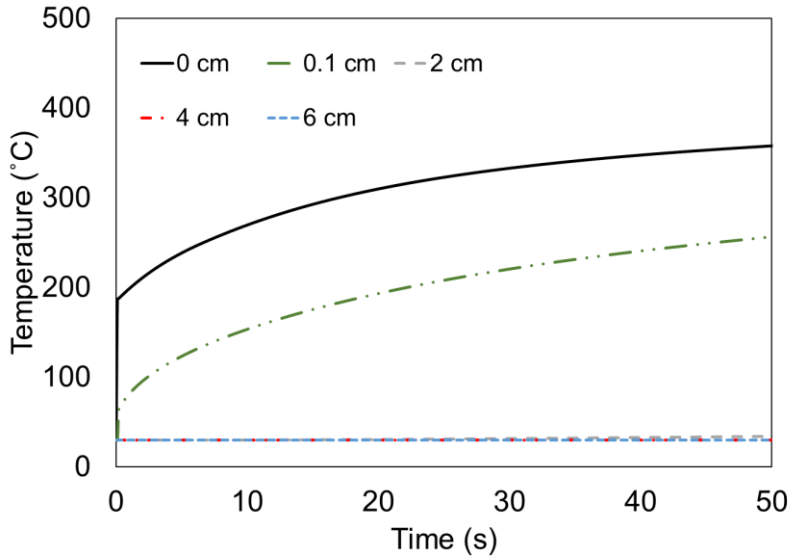

Figure 4-13: Temperature Predictions for 10 cm Thick Polyurethane Foam Exposed to 20 kW/m^2 Heat Flux

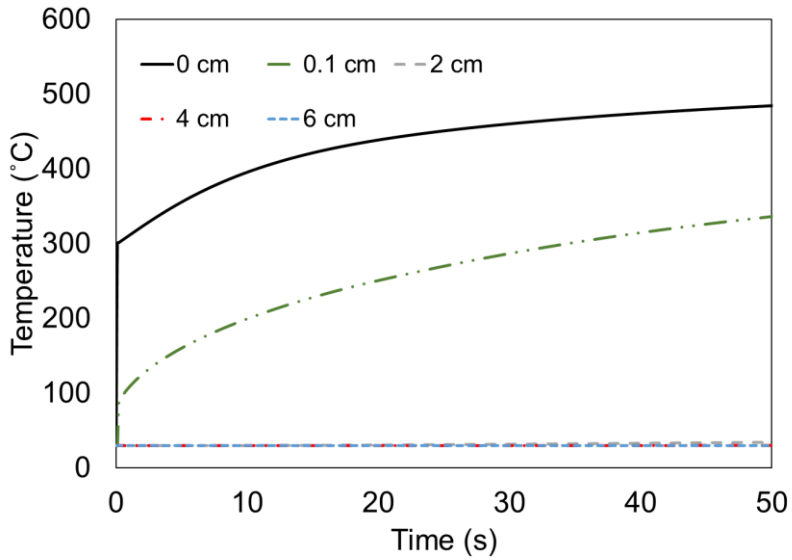

Figure 4-14: Temperature Predictions for 10 cm Thick Polyurethane Foam Exposed to 35 kW/m^2 Heat Flux

The temperature predictions at a depth of 0.1 cm for the various heat fluxes are presented in Figure 4-15. As expected, the rate of temperature rise increases with higher incident heat flux exposures. Also, the maximum temperatures recorded on the foam prior to ignition are also

influenced by the level of heat flux exposure with higher heat fluxes leading to higher foam surface temperatures.

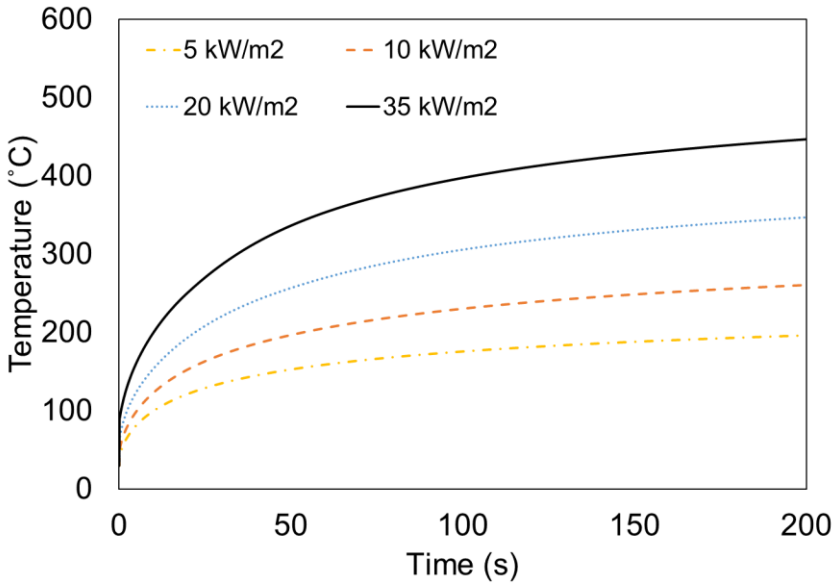

Figure 4-15: Temperature Predictions at 0.1 cm from foam surface for Various Heat Flux Exposures

4.7 SENSITIVITY STUDIES

The impact of foam properties in predicting temperatures was studied by carrying out a sensitivity analysis. The study gives insight on which property has the most influence on temperature predictions and enables the quantification of numerical uncertainties. The thermal properties discussed in subsequent sections were varied by ±20% and used to predict foam temperatures for the 10 kW/m^2 heat flux exposure. The temperatures were compared at a depth of 0.1 cm where significant temperature rise occurs. Surface temperatures of the foam may be used as markers to identify physical/chemical events that occur during foam combustion. Since the goal of the model is to predict the time to ignition of the foam, the effect of the thermal properties on the time to predict 100°C, 150°C and 200°C was studied.

4.7.1 Variation in Foam Thermal Conductivity

Figure 4-16 shows the ±20% changes in thermal conductivity of polyurethane foam. The difference in temperature predictions at a depth of 0.1 cm due to the ±20% change in thermal conductivity is given in Figure 4-17.

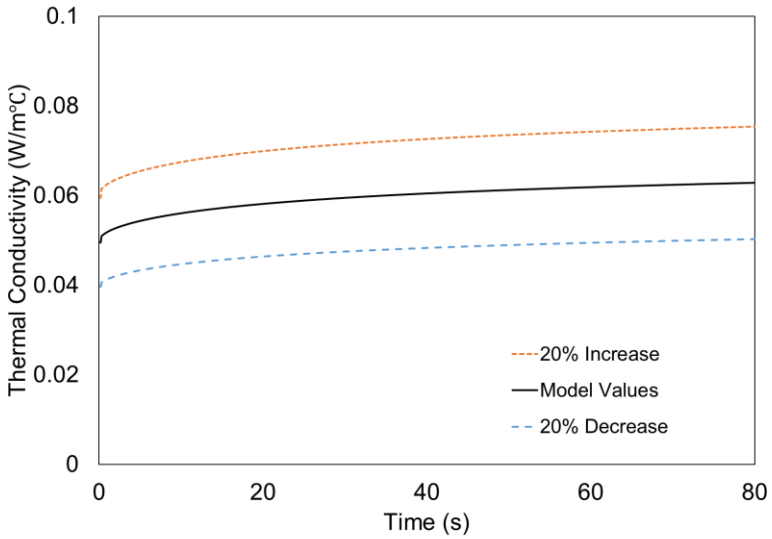

Figure 4-16: Variation in Thermal Conductivity of Polyurethane Foam

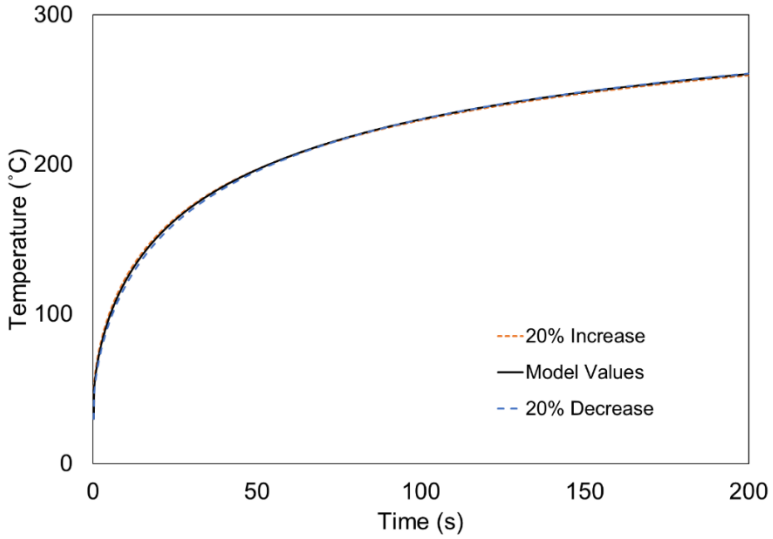

Figure 4-17: Sensitivity of Polyurethane Foam Temperature (0.1 cm in depth) to ±20% Variations in Thermal Conductivity

From Figure 4-17, it is observed that the variation in thermal conductivity of the foam has little impact on temperature rise. This is explained by the magnitude of change in the other thermal properties. The slope of the specific heat and density curves are over 90% greater than the slope of thermal conductivity. This means that temperature predictions will be more affected by these properties. Table 4-4 presents the effect of the ±20% change in thermal conductivity on the time to reach various temperatures. The greatest difference occurs in the time predicted for the foam to reach 100°C (11.3% from the base model) after which the model converges at higher temperatures.

Table 4-4: Effect of Thermal Conductivity Variations on Time to Reach 100°C, 150°C and 200°C

Temperature (°C)	20% Decrease		Model Values	20% Increase	
	Time (s)	% Difference	Time (s)	Time (s)	% Difference
100	5.9	11.3	5.3	4.8	9.4
150	20	5.8	18.9	18.3	3.2
200	54.6	1.9	53.6	53.5	0.2

4.7.2 Variation in Foam Specific Heat

The specific heat of the foam was also varied by ±20%. Figure 4-18 shows the changes in specific heat while Figure 4-19 compares the difference in temperature predictions at a depth of 0.1 cm due to the ±20% change in specific heat.

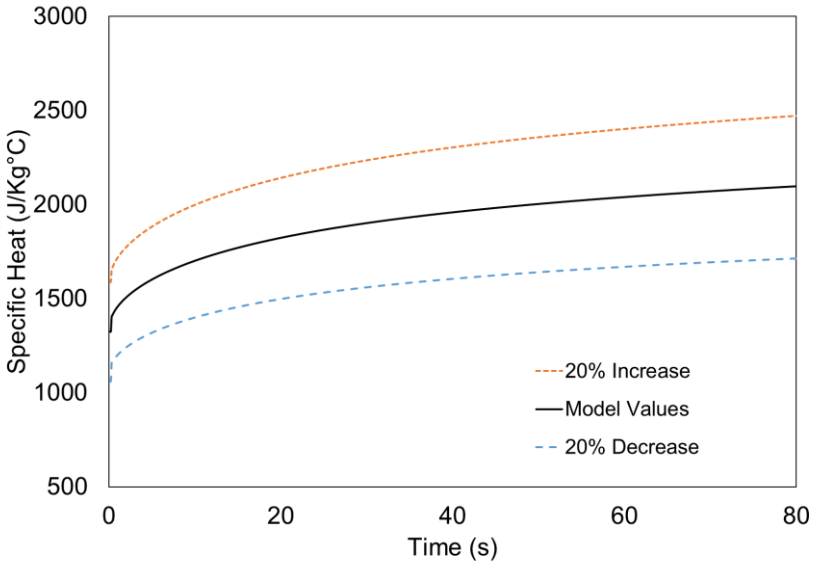

Figure 4-18: Variation in Specific Heat of Polyurethane Foam

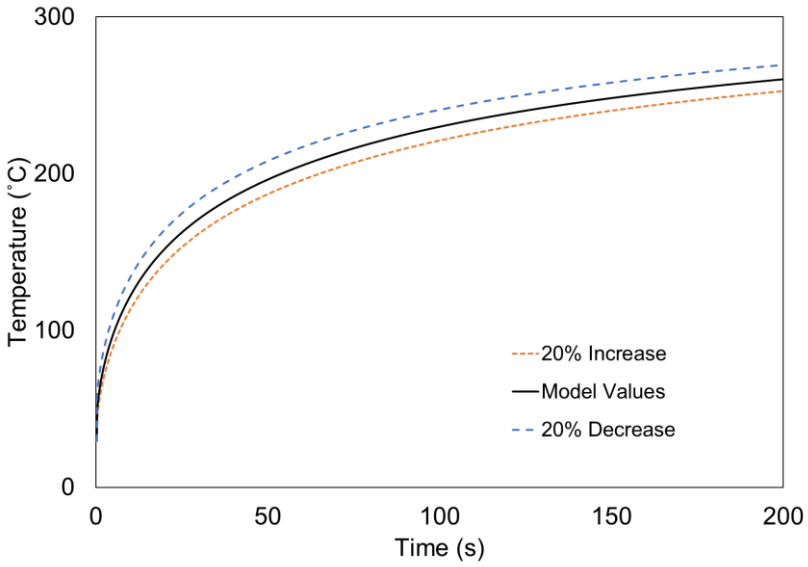

Figure 4-19: Sensitivity of Polyurethane Foam Temperature (0.1 cm in depth) to ±20% Variations in Specific Heat

The specific heat is seen to have a greater impact on temperature predictions. Comparing the time predicted for the foam to reach 100°C, 150°C and 200°C (Table 4-5), up to about a 30%

difference in predicted times to reach temperature levels are observed when the specific heat is changed by 20%.

Table 4-5: Effect of Specific Heat Variation on Time to 100°C, 150°C and 200°C

Temperature (°C)	20% Decrease		Model Values	20% Increase	
	Time (s)	% Difference	Time (s)	Time (s)	% Difference
100	3.6	32.1	5.3	6.8	28.3
150	14.5	23.3	18.9	23.2	22.8
200	42.2	21.3	53.6	64.8	20.9

4.7.3 Variation in Foam Density

As discussed in Section 4.5.3, there are uncertainties in estimating the effect of change in density with temperature. It is, therefore, necessary to understand how accurately the density of the foam must be known. A sensitivity study was carried out similar to other thermal properties by varying the density by ±20% (Figure 4-20). The effect of the variation in density on temperature predictions at a depth of 0.1 cm is given in Figure 4-21.

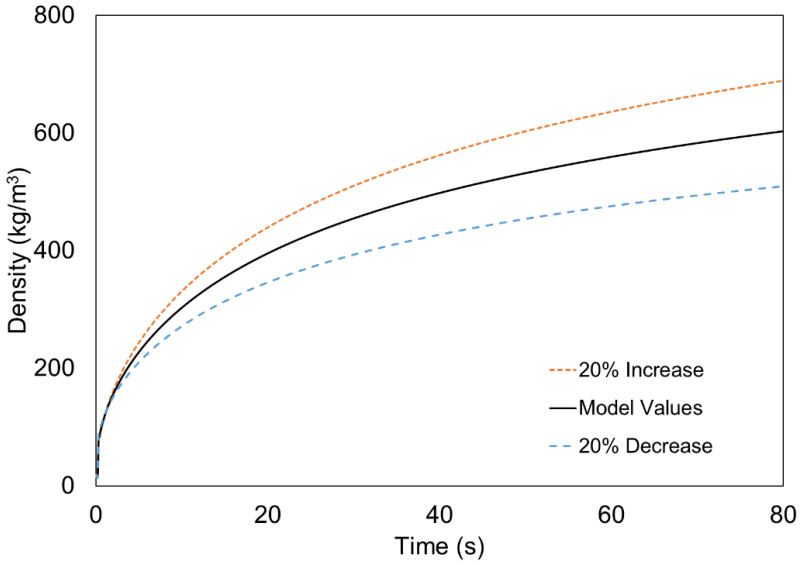

Figure 4-20: Variation in the Density of Polyurethane Foam

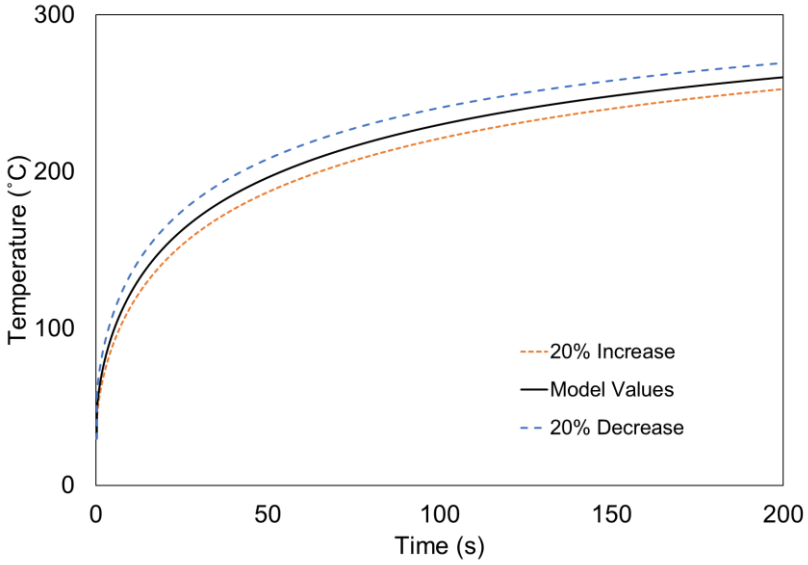

Figure 4-21: Sensitivity of Polyurethane Foam Temperature (0.1 cm in depth) to ±20% Variations in Density

Table 4-6 presents a comparison of the time to attain certain benchmark temperatures due to density variations. Up to 30% difference is obtained by decreasing the density by 20%. The behaviour is similar to the effect of specific heat on temperature predictions.

Table 4-6: Effect of Density Variation on Time to 100°C, 150°C and 200°C

Temperature (°C)	20% Decrease		Model Values	20% Increase	
	Time (s)	% Difference	Time (s)	Time (s)	% Difference
100	3.6	32.1	5.3	6.8	28.3
150	14.5	23.3	18.9	23.2	22.8
200	42.2	21.3	53.6	64.8	20.9

4.7.4 Variation in Heat Loss

The heat loss from the foam was calculated based on a convection and radiation boundary condition. The resulting energy balance determines how much heat is conducted through the foam. The sensitivity of temperature to ±20% variation in radiative and convective losses is presented in Table 4-7. The variation was obtained by multiplying the heat loss component of the discretized heat diffusion equation (Equation 4.17) by 0.8 and 1.2. This approach allowed for an investigation of the combined effect of radiative and convective heat losses.

Table 4-7 compares the difference in the time predicted to reach 100°C, 150°C and 200°C. Heat loss is driven by the temperature of the foam at any given time step and thus heat losses are more impactful at higher temperatures. From Table 4-7, the greatest difference is obtained in time predicted to reach 200°C. Approximately 10% difference is obtained by increasing the heat losses by 20%.

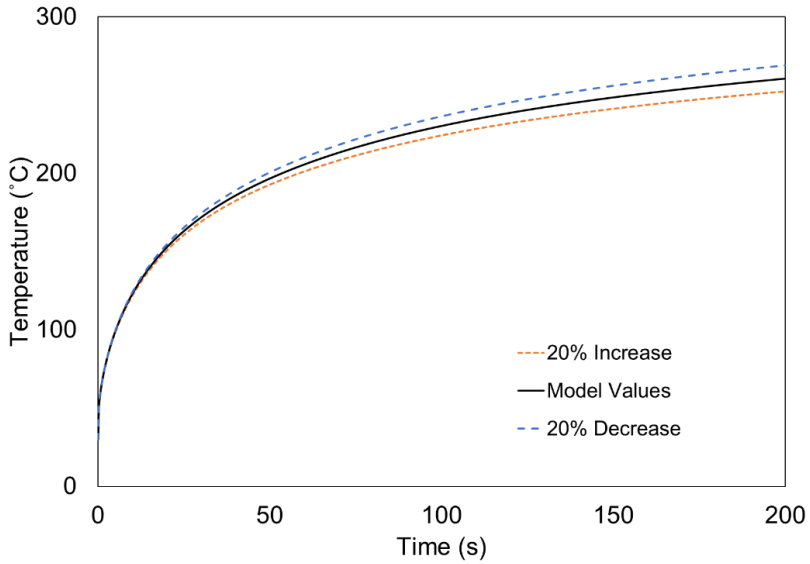

Figure 4-22: Sensitivity of Polyurethane Foam Temperature (0.1 cm in depth) to ±20% Variations in Heat Loss

Table 4-7: Effect of Heat Loss Variation on Time to 100°C, 150°C and 200°C

Temperature (°C)	20% Decrease		Model Values	20% Increase	
	Time (s)	% Difference	Time (s)	Time (s)	% Difference
100	5.1	1.9	5.2	5.3	1.9
150	18.1	3.7	18.8	19.6	4.3
200	49.4	7.7	53.5	58.3	9.0

4.7.5 Summary of Sensitivity Study

The results of the sensitivity study on the time predicted for the foam to reach 100°C, 150°C and 200°C indicate that the specific heat and density have the most impact on temperature predictions. A 30% decrease in time for the foam to reach 100°C is obtained for a 20% decrease in the specific heat and density respectively. Both properties affect the temperature in a similar

manner as they combine to form the volumetric heat capacity of the foam. This Fourier Field equation solves the temperature field as a function of the volumetric heating rate. Thus, both properties have an equivalent impact on the temperatures predicted by the model.

The foam thermal conductivity is seen to have minimal effect on temperature predictions. Polyurethane foam has a low thermal diffusivity (approximately 2 mm/s calculated at room temperature) as the ratio of conduction to the volumetric heat capacity is small. Only a thin layer of the foam directly exposed to radiative heat from the cone calorimeter will experience significant temperature rise. Heat conduction through the depth of the foam will happen at a much slower rate while the top layer of the foam reaches ignition temperature. An 11% difference in time to reach 100°C is obtained for a 20% decrease in thermal conductivity. The sensitivity of the model to heat losses is also considered minimal when compared to the effect of specific heat and density. Less than 10% difference in the time to reach 200°C is obtained by increasing the heat losses by 20%. Based on this sensitivity study, the specific heat and density are the properties which must be known most accurately in order to improve the accuracy of the model.

4.8 COMPARISON OF EXPERIMENTAL AND NUMERICAL RESULTS

The comparison of the experimental temperatures measured in Section 2.6 and numerical temperature predictions for the various heat flux exposures was carried out for the foam surface temperature and the temperature at a depth of 0.1 cm. From the temperature profiles predicted by the model at various heat fluxes, it is observed that the foam is highly insulative with negligible temperature rise observed at depths greater than 2 cm from the surface of the foam. For example, results of the 35 kW/m^2 temperature predictions show that after 20 s, foam surface temperatures exceed 400°C while temperatures at depths greater than 2 cm show minimal temperature rise. This behaviour is also observed in experimental thermocouple and infrared temperature measurements. While variations are expected for infrared images as videos are captured from the side of the foam as opposed to the centre (Section 2.6), the infrared image in Figure 4-23 also shows almost no heat transfer through the foam depth during the period prior to ignition of the foam. The temperature rise was seen to occur in the polyol layer formed on the top surface of the foam.

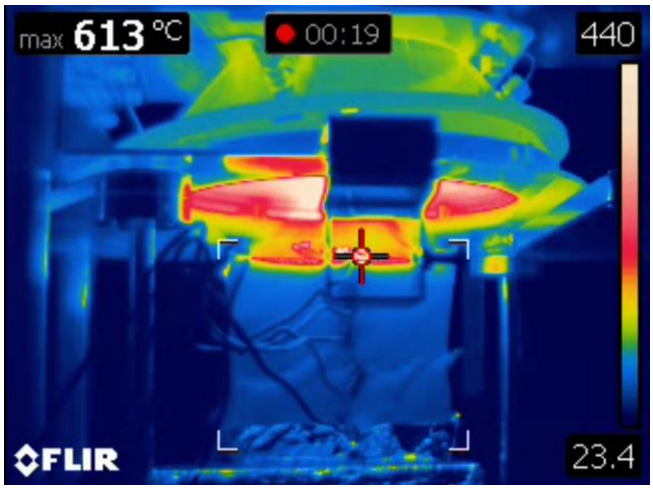

Figure 4-23: Infrared Temperature Measurements for 10 cm Thick Polyurethane Foam Exposed to 10 kW/m^2 Heat Flux (12 s exposure time)

Temperature rise in the foam at depth is observed to be mainly a function of the flame front position. Upon ignition of the foam, the flame spreads and causes the material to recede as it burns out. The model will begin to fail at this point due to a change in the boundary conditions (moving boundary problem). The moving boundary problem is not considered in the scope of this research as the emphasis is on predicting the onset of ignition of the foam. Phase change also becomes more rapid after ignition due to flame spread and a simple approximation of a linear relationship of density with temperature does not sufficiently capture this process. The comparisons of the experimental temperatures measured in Section 2.6 and numerical temperature predictions for the various heat flux exposures are done for the surface temperature and the temperature of the first internal node (depth of 0.1 cm from the surface). From literature, it is expected that ignition of the foam will be governed by the heat transfer taking place within a few millimetres from the top surface of the foam (Kramer, Zammarano, Linteris, Gedde, & Gilman, 2010).

4.8.1 Heat Transfer for 5 kW/m^2 Heat Flux Exposure

Temperature measurements from cone calorimeter tests were compared to the results of the numerical model at the foam surface and at a depth of 0.1 cm for the 5 kW/m^2 heat flux exposure in Figure 4-24. Ignition of the foam specimen is indicated by the rapid spike in

experimentally measured temperatures. Temperatures measured using infrared imagery at five-second intervals are also presented for comparison.

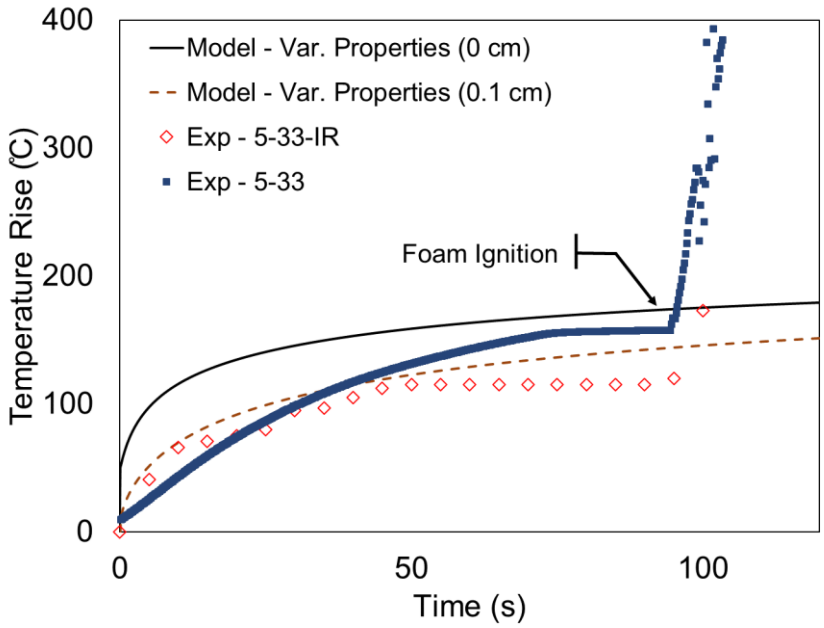

Figure 4-24: Comparison of Experimental and Numerical Temperature Predictions for 5 kW/m^2 Heat Flux Exposure

One of the first observations from the temperature comparisons is that experimental temperatures are more closely predicted by the numerical model at a depth of 0.1 cm (first internal node) rather than at the surface (0 cm). This may be attributed to the experimental set-up and is discussed in more detail in Section 4.8.5. As expected, the model is unable to predict the rapid temperature rise at ignition as this would involve accounting for the exothermic reactions which occur during ignition of the foam.

A comparison of measured times and the times predicted by the model to reach 70°C, 100°C, 120°C and 150°C is given in Table 4-8.

Table 4-8: Comparison of Experimental and Numerical Results for 5 kW/m^2 Heat Flux Exposure

Temperature Rise (°C)	Exp - 5-1	Exp - 5-3	Exp - 5-33	Average	Std. Dv.	Model
	Time (s)	Time (s)	Time (s)	Time (s)	Time (s)	Time (s)
70	18.2	13.4	18.4	16.7	2.3	10.1
100	29.4	22.4	30.8	27.5	3.7	25.8
120	39.8	30	41.6	37.1	5.1	46.2
150	58.8	36	67.4	54.1	13.2	115.1

4.8.2 Heat Transfer for 10 kW/m^2 Heat Flux Exposure

Temperature measurements from cone calorimeter tests were compared to the numerical model for the 10 kW/m^2 heat flux exposure in Figure 4-25. Similar to the 5 kW/m^2 heat flux exposure, experimentally measured temperatures are more closely predicted by the model at a depth of 0.1 cm (first internal node) prior to ignition of the foam. A comparison of measured times and the times predicted by the model to reach 70°C, 100°C, 120°C, 150°C and 200°C is given in Table 4-9.

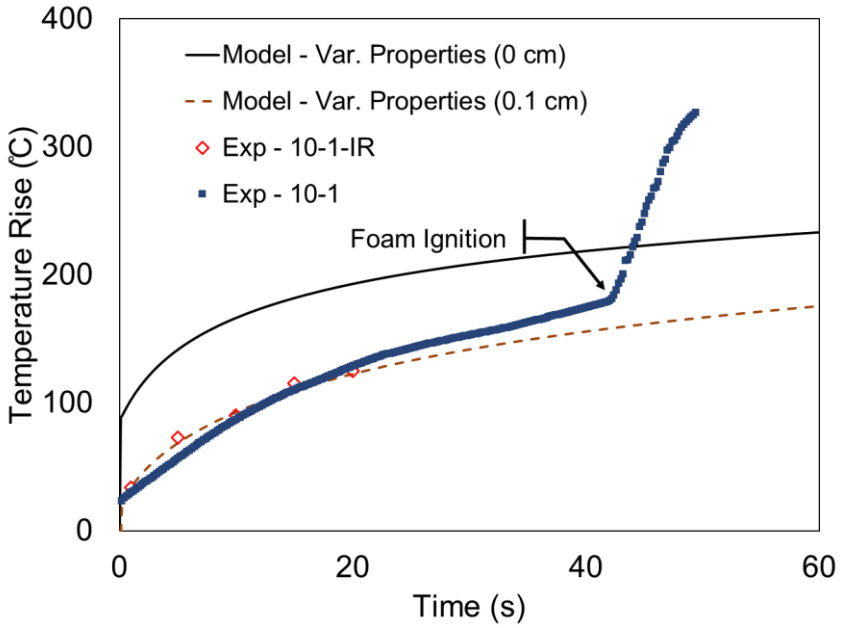

Figure 4-25: Comparison of Experimental and Numerical Temperature Predictions for 10 kW/m^2 Heat Flux Exposure

Table 4-9: Comparison of Experimental and Numerical Results for 10 kW/m^2 Heat Flux Exposure

Temperature Rise (°C)	Exp - 10-1	Exp - 10-2	Exp - 10-3	Average	Std. Dv.	Model
	Time (s)	Time (s)	Time (s)	Time (s)	Time (s)	Time (s)
70	7	6.8	6.4	6.7	0.2	5.2
100	12.6	11	7.6	10.4	2.1	11.9
120	17.6	13.2	8.6	13.1	3.7	18.8
150	28.2	13.8	9.6	17.2	8.0	35.5
200	43	68.8	11.6	41.1	23.4	99.4

4.8.3 Heat Transfer for 20 kW/m^2 Heat Flux Exposure

Temperature measurements from cone calorimeter tests were compared to the numerical model for the 20 kW/m^2 heat flux exposure in Figure 4-26. Experimentally measured temperatures are reasonably predicted by the model at a depth of 0.1 cm (first internal node) prior to ignition of the foam. The model breaks down rapidly as the ignition of the foam specimen occurs in a short duration (~4 – 8 s) due to higher incident heat fluxes. A comparison of measured times and the times predicted by the model to 70°C, 100°C, 120°C, 150°C and 200°C is given in Table 4-10.

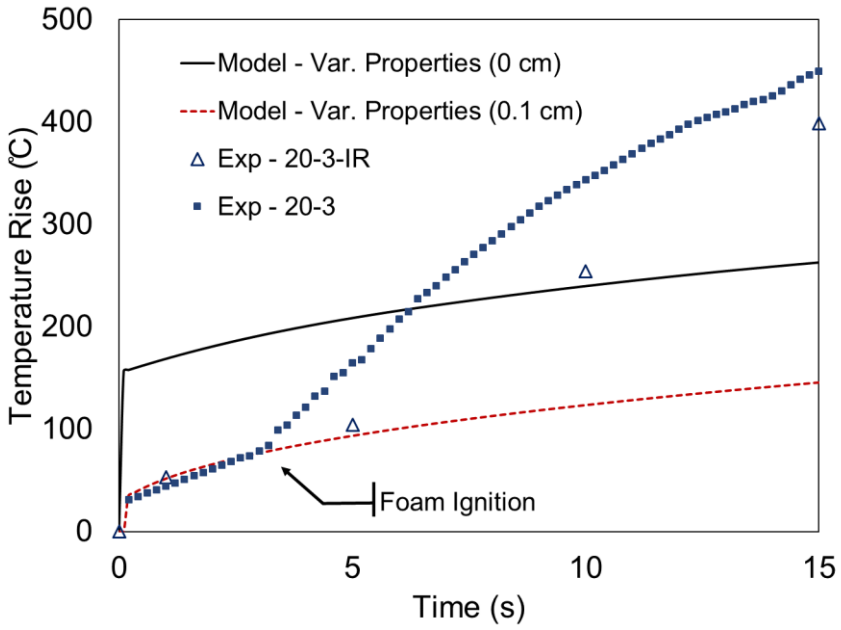

Figure 4-26: Comparison of Experimental and Numerical Temperature Predictions for 20 kW/m^2 Heat Flux Exposure

Table 4-10: Comparison of Experimental and Numerical Results for 20 kW/m^2 Heat Flux Exposure

Temperature Rise (°C)	Exp - 20-1	Exp - 20-2	Exp - 20-3	Average	Std. Dv.	Model
	Time (s)	Time (s)	Time (s)	Time (s)	Time (s)	Time (s)
70	5.8	4	2.4	4.1	1.4	2.3
100	8	6.4	3.4	5.9	1.9	5.9
120	9	7.4	3.8	6.7	2.2	9.3
150	10.4	8.2	4.4	7.7	2.5	16.1
200	12	10.2	5.8	9.3	2.6	34.2

4.8.4 Heat Transfer for 35 kW/m^2 Heat Flux Exposure

Temperature measurements from cone calorimeter tests were compared to the numerical model for the 35 kW/m^2 heat flux exposure in Figure 4-27. Experimentally measured temperatures prior to ignition of the foam are reasonably predicted by the model at a depth of 0.1 cm (first internal node). The model breaks down in a short duration due to the ignition of the foam specimen. A comparison of measured times and the times predicted by the model to reach 70°C, 100°C, 120°C, 150°C and 200°C is given in Table 4-11.

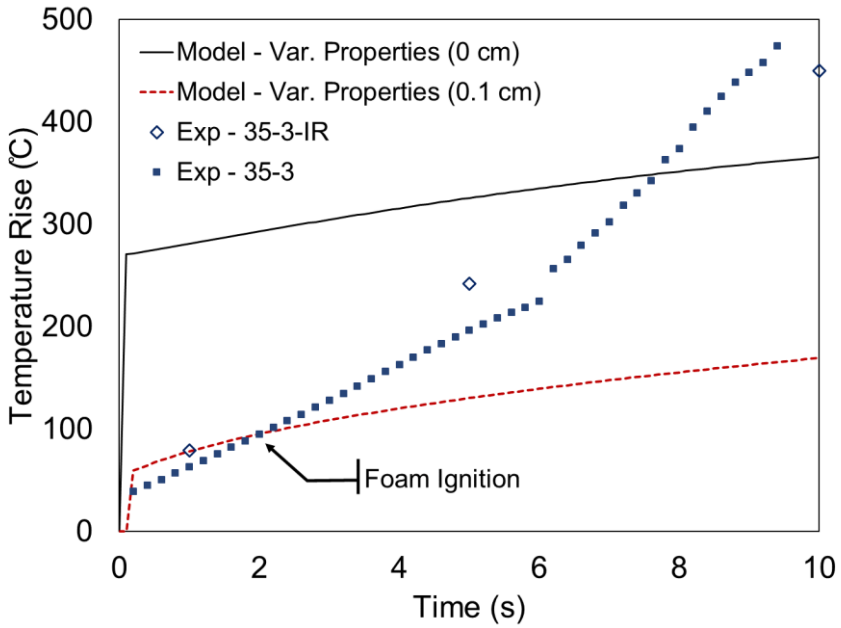

Figure 4-27: Comparison of Experimental and Numerical Temperature Predictions for 35 kW/m^2 Heat Flux Exposure

Table 4-11: Comparison of Experimental and Numerical Results for 35 kW/m^2 Heat Flux Exposure

Temperature Rise (°C)	Exp - 35-1	Exp - 35-2	Exp - 35-3	Average	Std. Dv.	Model
	Time (s)	Time (s)	Time (s)	Time (s)	Time (s)	Time (s)
70	2.6	1.8	1.2	1.9	0.6	0.6
100	3.6	3.0	2.0	2.9	0.7	2.3
120	4.2	3.4	2.6	3.4	0.7	3.9
150	5	3.8	3.6	4.1	0.6	7.2
200	6.4	4.6	5.0	5.3	0.8	15.3

4.8.5 Discussion of Results

From the results presented in Figure 4-24 to Figure 4-27, the surface temperature predicted by the model (0 cm) overpredicts experimental temperatures measured by the surface thermocouple. However, the model is reasonably successful in predicting temperature measurements at a depth of 0.1 cm (first internal node) until ignition of the foam. To explain why experimental surface temperatures were better predicted by the model at the first internal node, the experimental set-up was investigated to determine the point of temperature measurement by the thermocouple.

In Figure 4-28, grooves are seen to be formed after installation of the "surface" mounted thermocouples. As the foam is left for conditioning, the weight of the thermocouples causes the foam to collapse causing the thermocouples to descend into the foam. The temperatures measured by the "surface" mounted thermocouples are in actual sense temperatures measured at some depth into the foam. The comparison of experimental and numerical results suggests that temperatures measured by the thermocouple may nominally be at some depth just below the surface of the foam. In this thesis, this depth was approximated as the first internal node from the top surface (0.1 cm). Infrared temperature measurements also confirm the temperatures measured within the top 0.1 cm surface of the foam are in line with thermocouple readings. Again, it should also be noted that infrared temperatures were measured from the side of the foam and thus, measurements are not expected to read top surface temperatures.

Figure 4-28: Location of Surface Mounted Thermocouples

In general, prior to ignition of the foam specimen, a reasonable agreement exists between the experimental and numerical temperature profiles considering the simplifying assumptions that were used to develop the model. Table 4-8 to Table 4-11 compares the time predicted by the model to reach certain temperatures which correspond to reaction stages for polyurethane foam combustion. For all heat flux exposures, a percentage difference in the range of 0.5 – 43% was obtained for times predicted for a temperature rise of 70°C, 100° and 120°C. As the foam temperature rises above 150°C, the model breaks down and is unable to predict temperatures with reasonable accuracy.

Comparing the performance of the model by heat flux exposure, the model does a better job of predicting temperatures at lower heat fluxes (5 kW/m^2 and 10 kW/m^2). This is expected as at lower heating rates reactions occur much more slowly and the model will do a better job of accounting for the changes in thermal properties. The short duration of the high heat flux exposure tests also raises questions on the response time of thermocouple. For rapid temperature rise, there will be a time delay for the thermocouple to respond to temperature increase which leads to uncertainties in the temperatures measured.

The thermal properties used in the model play a major role in the accuracy of the temperature predictions. As discussed earlier, there are uncertainties in estimating thermal properties as the values used were from literature and not specific to the foam tested. From the sensitivity study carried out, the specific heat and density accounted for most uncertainties in the thermal properties. A 20% change in density and specific heat will cause a 30% change in temperature. Another factor that was not considered in the model was the effect of preheating by the pilot ignition. For the low heat flux exposures, due to extended periods before ignition, the experimental temperatures measured may be influenced by heating from the spark ignitor. An alternative to the current experimental set-up is proposed for future research. The test may be conducted without the spark ignitor which will eliminate the effect of pre-heating on the foam and in some cases (lower heat flux levels) prevent flaming ignition from occurring. This set-up will allow temperature data to be collected over a longer duration to reduce the uncertainties associated with measurements.

The effect of evaporation and pyrolysis and their impact on thermal decomposition was not primarily considered as part of this model. It is noted that endothermic energy will be

required to remove moisture in the foam. For this research, the moisture in the conditioned foam specimen was measured to be approximately 2.0%. The boil-off of moisture may affect temperature predictions at the earlier stages of the fire. In situations where there are concerns about increased moisture content, application of the apparent heat capacity method implemented by Torvi (1997) should be explored. The energy required to evaporate moisture can be accounted for in the specific heat of the foam and used to calculate foam temperatures.

Energy will be evolved as a result of the combustion reactions occurring in the foam. The assumption in this model is that the pyrolysis reactions are more pronounced right at the onset of ignition of the foam. Since interest is in predicting the time required to heat the foam to the point of ignition, the effect of pyrolysis was neglected. In reality, pyrolysis begins to occur right after evaporation of moisture in the foam albeit in small quantities as the foam surface reaches ignition temperatures. Some researchers have attempted to quantify the rate of the pyrolysis reaction using the Arrhenius equation (Prasad, et al., 2009) or solved the pyrolysis reaction as a function of the mass-loss rate (Weng & Hasemi, 2008). The heat evolved from pyrolysis may be added as a source term in the finite-difference model.

4.9 PREDICTION OF IGNITION TIME OF POLYURETHANE FOAM

The ignition time of polyurethane foam can be predicted based on the temperature rise. Thermal degradation occurs as the surface of the foam reaches ignition temperatures. Various researchers have conducted an experimental investigation on the reactions occurring in polyurethane foams prior to ignition. The degradation of the foam is characterised by the decomposition of its constituent compounds (urea bonds and TDI compounds).

Mass loss rate curves obtained from thermogravimetric (TGA) testing of polyurethane foam are shown in Figure 4-29 (Kramer, Zammarano, Linteris, Gedde, & Gilman, 2010). The tests were conducted at low and high heating rates in nitrogen (solid line) and air (dotted line). As seen in the results, the mass loss occurred in two stages. The first stage was initiated by the breakdown of urethane and urea groups at approximately 200°C while the second stage corresponds to the production of volatiles above 300°C.

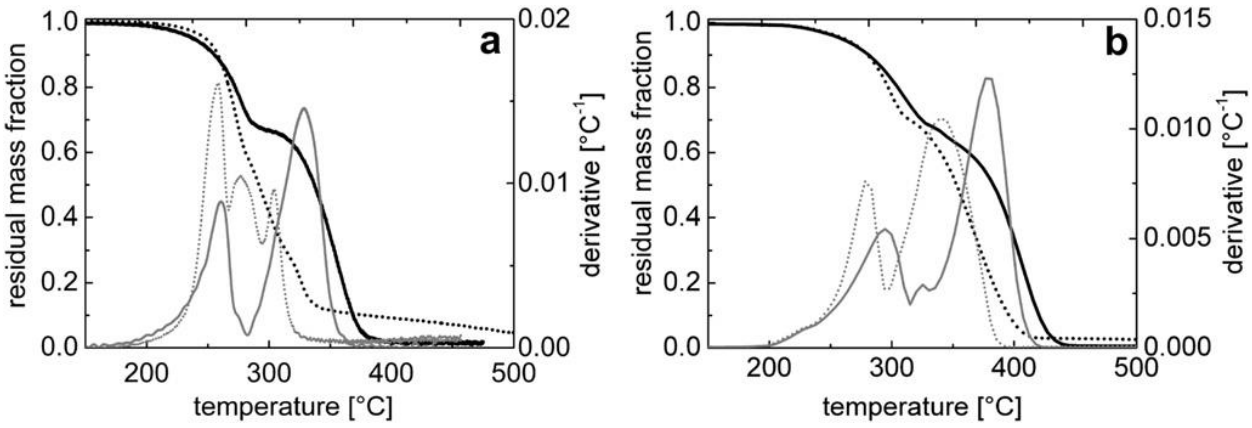

Figure 4-29: Thermogravimetric and Differential Signal Tests of Pure Polyurethane Foam at 5°C/min (a) and 176°C/min (b) (Nitrogen – Solid Line, Air – Dotted Line) (Used with Permission, Kramer, Zammarano, Linteris, Gedde, & Gilman, 2010)

The results from the TGA tests indicate that significant mass loss of the foam occurs above 200°C, which could be interpreted as the ignition temperature. However, it must be noted that the TGA tests are carried out in nitrogen for sample sizes smaller than the cone calorimeter test specimen and at lower heating rates. For TGA tests carried out in air, the curve shifts, and the mass loss is seen to occur at lower temperatures. In real-life testing conditions, it is expected that ignition temperatures will be lower than reported by TGA tests. This point was highlighted by Kramer et. al. (2010) where he asserted that the oxidative process must be considered when studying the degradation process of the foam due to the low-density open-cell structure of the foam.

A comparison of experimental and numerical ignition times is given in Table 4-12. The experimental ignition time is compared to the time taken by the model to predict a 100°C, 120°C and 150°C temperature rise.

Table 4-12: Comparison of Experimental and Numerical Model Ignition Times

Heat Flux (kW/m^2)	**Experimental Ignition Time (s)**		**Model Ignition Time (s)**		
	Average	**σ**	**100°C**	**120°C**	**150°C**
5	147.7	65.37	25.8	46.2	115.1
10	27.0	9.84	11.9	18.8	35.5
20	7.6	0.60	5.9	9.3	16.1
35	2.1	0.38	2.3	2.9	7.6

From Table 4-12, ignition times predicted by the model as a 120°C rise in temperature most closely matched experimental data. The difference between the model (120°C) and experiment for the 35 kW/m^2 was 38%. The 20 kW/m^2 model predicted ignition time to within 22% of experimental data while the ignition time predicted for the 10 kW/m^2 heat flux exposure was within 30% of experimental ignition time. The model was unable to successfully predict ignition time for the 5 kW/m^2 exposure. A 70% difference was observed between the model and experimental results. However, there was a large variance in experimental measurements for the 5 kW/m^2 heat flux exposure. At lower heating rates, the decomposition of the foam is influenced more by environmental conditions causing inconsistencies in fire behaviour. This will, in turn, affect the ability of the model to predict ignition temperatures accurately.

As noted earlier, ignition of the foam specimen can be correlated to the temperature spikes seen on the graphs (Figure 4-24 to Figure 4-27). The temperature spikes are a result of the decomposition of the foam upon ignition. When comparing the experimental temperatures measured at the beginning of the spikes across all heat fluxes, it is observed that for all tests, the foam temperature rise at the onset of the spike falls within the range of 90°C to 150°C. This results in a mean temperature rise of 120°C ±30°C. This large temperature variance (±25%) points to the difficulty in using a single temperature criterion in predicting the ignition time of the polyurethane foam specimen. Upon ignition, the decomposition of the foam is rapid, and the resulting temperature rise also happens at a rapid rate. Once moisture completely boils-off and the surface of the foam has been exposed to enough energy, ignition of the foam may occur at any time within this temperature range. This inherent variability in the ignition temperature explains why the model may not perform well in predicting ignition time as a single temperature may not be sufficient criteria to determine ignition time.

In conclusion, the simple model developed to predict ignition shows promise in predicting the foam heat transfer prior to ignition of the specimen. Upon ignition, a more complex chemical process occurs, and the model is unable to capture the exothermic and endothermic reactions that take place. This is why other models such as constant property models or semi-infinite models typically applied for other materials (wood, gypsum board) do not have sufficient capacity to model the reactions occurring during polyurethane foam

combustion. This model forms a foundation upon which to build, as processes such as pyrolysis, smouldering and charring may be added to improve the predictive capability of the model.

4.10 SUMMARY OF CHAPTER

This chapter presented a numerical model of the heat transfer process prior to ignition of the polyurethane foam specimen developed using a number of simplifying assumptions. The numerical solution modelled the radiative, convective and conductive heat transfer occurring during cone calorimeter testing for various heat flux exposures (5 kW/m^2, 10 kW/m^2, 20 kW/m^2 and 35 kW/m^2). Thermal properties were treated as a function of temperature but were solved uncoupled from the general one-dimensional heat transfer equation.

The combustion process of polyurethane foam is complex involving various reactions. The author isolated the solid phase heat transfer process and argues that modelling the reaction occurring in this phase (ignoring gas/liquid phase reactions) shows potential in predicting the ignition time of the specimen when quick and approximate solutions are required. Knowledge of the temperature at which the combustion of the foam specimen occurs is required. The solid phase heat transfer process is sufficient for predicting approximate ignition times since reactions occurring upon onset of the liquid/gas phase reactions are rapid and ignition of the foam once the foam transitions to a liquid polyol is almost instantaneous. However, when more accurate prediction of ignition time is required such as in applications for fire scaling and flame spread predictions, this model serves as a building block for the development of more complex models.

5 FULL-SCALE FIRE MODELLING

As mentioned in previous chapters, it is of interest in this research to study the scalability of mattress fires using information from cone calorimeter tests. This chapter will cover the methodology used to predict full-scale polyurethane foam flame spread, heat release rates as well as compartment temperatures. The results of the prediction are compared to full-scale experimental results measured during the University of Waterloo furniture calorimeter and shipping container tests reported in Chapter 3.

5.1 FLAME SPREAD

The rate at which flame spreads across a combustible material affects the overall fire behaviour of the material. Materials with greater resistance to flame spread exhibit slower fire development while rapidly propagating fires are usually characterised by high flame spread rates. In order to study fire scaling, the rate of flame spread must be considered. In previous University of Saskatchewan research on fire scaling, the treatment of flame spread has been based solely on experimental data from video and infrared measurements (Robson, 2014). This poses a challenge for full-scale fire predictions as experimental tests are still required to predict full-scale fire behaviour. The work on flame spread presented in this thesis presents the first step to obtaining a fully independent mattress flame spread correlation.

The t^2 fire growth model discussed in equation (1.9) formed the basis for flame spread prediction. basic assumption is that fire grows as the square of time and coefficients which describe the rate of propagation of the fire (slow, medium, fast and ultra-fast) are used to characterise various materials (Drysdale, 2011). The t^2-fire growth model is given as

$$\dot{Q} = \alpha(t - t_0)^2 \tag{5.1}$$

Where;

Q is the heat release rate (kW)

α is the fuel-dependent fire growth coefficient (kW/s^2)

t_0 is the incubation time for the fire (s)

In the t^2 model, the rate of fire growth is influenced by the rate of flame spread which is accounted for in the fuel-dependent growth coefficient (α). By mirroring the t^2 fire growth model an attempt was made to decouple the rate of flame spread from the overall rate of heat release. As discussed in Section 3.3, Robson used an automated method to measured flame spread rates for similar size specimens in a furniture calorimeter test (Robson, 2014). The spread of flame measured during the furniture calorimeter tests was assumed to approximate the parabolic t^2 fire curve. Flame areas obtained from experimental infrared measurements were analysed and used to determine area spread rates for the centre and edge ignition test series based on a curve fit of the experimental data.

The general equation representing flame spread is given as;

$$A(t)/A_{total} = \beta(t)^2 \quad (5.2)$$

Where;

$A(t)$ is the area of the flame at the time of interest (m^2)

A_{total} is the total area of the foam slab (m^2)

β is the coefficient describing the rate of propagation of the flame (s^{-2})

The flame/area spread rate curve obtained using this model predicts the overall area of the specimen for which the flame front has passed. This spread rate, A(t), serves as an input for full-scale heat release rate predictions. The coefficient of flame propagation (β) was evaluated based on the average flame areas measured for each test series. At every time step, the beta value was calculated by dividing the measured non-dimensional flame area by the square of the time. The final coefficient of flame propagation was calculated as an average over the test duration.

For the C4 test, the coefficient of flame propagation was calculated as 1.1 x 10^{-4} (s^{-2}). Flame areas predicted using this coefficient of propagation were generally within 9.7% of the measured flame area. The most deviation occurred within the first 15 s of the test (50%), where the model under-predicted the average experimental flame areas. The magnitude of the

deviations measured for the first 20 s are in fact smaller than the percentage may suggest since the flame areas measured at this time are relatively small. Excluding the first 15 s, predicted flame areas are within 5% of the average experimental areas. The area model and experimental flame areas measured for the three tests in the C4 test series are compared in Figure 5-1.

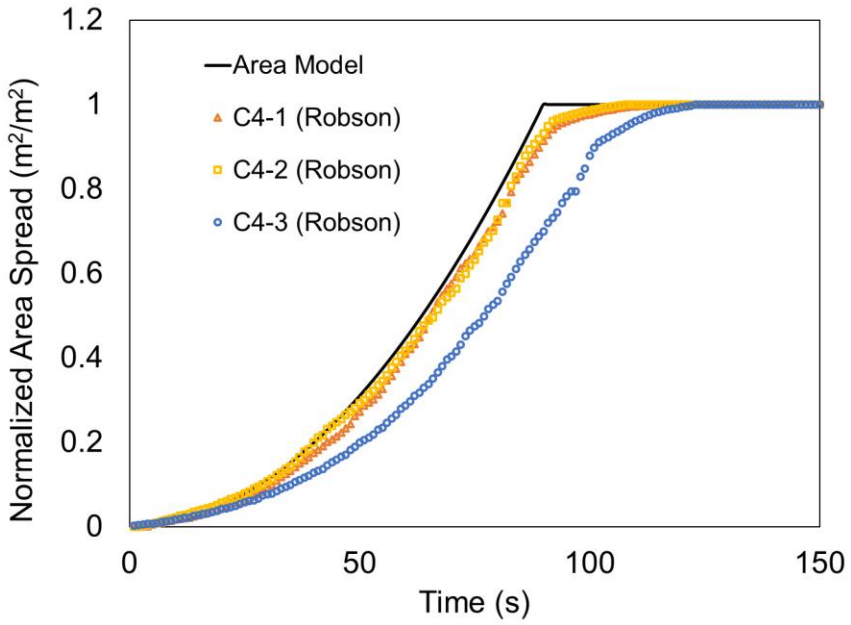

Figure 5-1: C4 Flame Spread Model

For the E4 test, the coefficient of flame propagation was calculated as 3.7×10^{-5} (s^{-2}). The graph of the area model compared to the experimentally measured flame areas for the E4 test series is presented in Figure 5-2. Flame areas predicted by the E4 area model are generally within 20% of the average experimental flame areas with most deviations occurring after 100 s. For the EE4 test series, the coefficient of propagation was calculated as 4.1×10^{-5} (s^{-2}). When comparing the predictions for the EE4 area model to average experimental flame areas, predicted flame areas are usually within 20% of the average experimental flame areas. The area model and experimental flame areas measured for the three tests in the EE4 test series are compared in Figure 5-3.

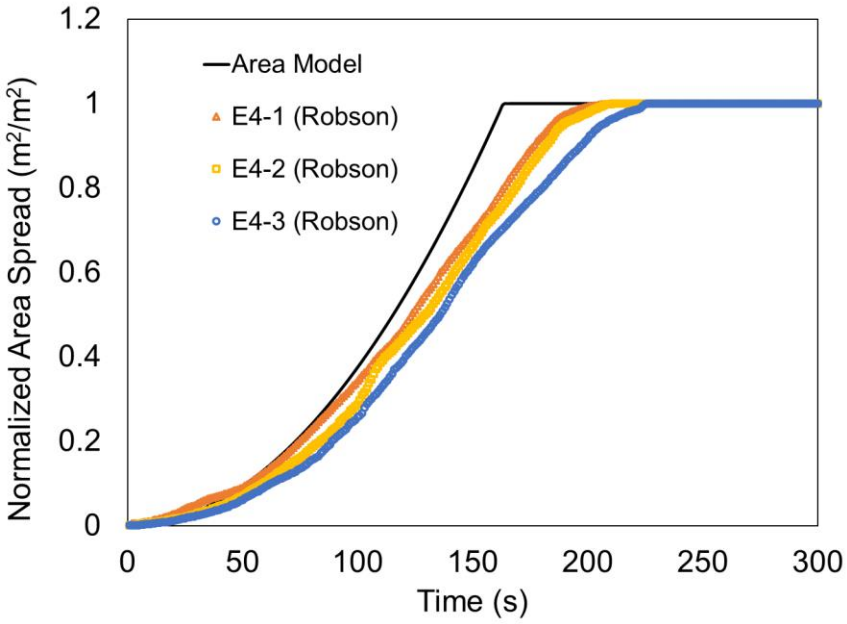

Figure 5-2: E4 Flame Spread Model

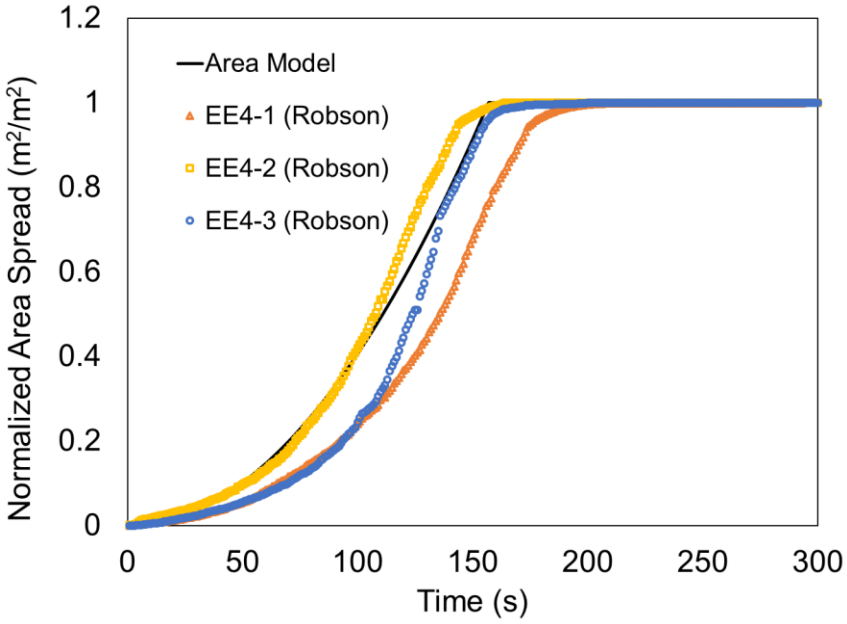

Figure 5-3: EE4 Flame Spread Model

5.1.1 Discussion of Flame Spread Rates

As seen in the proposed flame spread models (Figure 5-1 to Figure 5-3), the model is conservative as it predicts larger areas than experimental measurements. The coefficient of flame propagation (β) is calculated as an average over the measured data. This means that at earlier

stages of the fire when the rate of flame spread is much slower, predicted areas will be higher than experimental data. The model for centre ignition does the best job of predicting experimental flame area measurements. This is in part due to a more consistent burn pattern observed for centre ignition tests as compared to the edge ignition test. In the centre ignition test, a pool fire is formed at the centre of the foam and burns at a relatively steady rate as air is entrained from all sides around the circular flame boundary. The consistency in the burn pattern allows the fire to grow parabolically as the square of time. The model for edge ignition did a good job of predicting flame areas but not to the degree of accuracy of the centre ignition model since changes to the fire growth pattern influenced predictions.

Observing Figure 5-2, it is noticed that for the E4 test series, the model begins to deviate at approximately 100 s. Further investigation of experimental data indicated that a transition point occurs as the flame reaches the boundaries of the specimen. Before the flame reaches the foam boundaries, the fire follows the parabolic fire growth curve. After the transition point, a discontinuity in flame spread behaviour occurs with the flame spread rate slowing down. Before the transition point, the coefficient of flame propagation was calculated to be 5.1×10^{-5} (s^{-2}). After the transition point, the flame spread slows down and the coefficient of fire propagation was calculated to be 2.7×10^{-5} (s^{-2}). Ezinwa observed similar behaviour in edge ignition tests and pointed out a change from a radial burn pattern to the elliptical burn pattern as the flame approaches the foam boundaries (Ezinwa, 2009). The transition may be attributed to the dynamics of air entrainment during burning.

5.1.2 Comparison of Flame Spread Rates

One of the goals of this research is to investigate correlations for predicting room temperatures. The rate at which flame spreads in the compartment should be considered. The developed area spread model which will serve as input data for temperature predictions is based on furniture calorimeter data. As discussed in Section 3.4, the test conditions for the furniture calorimeter and shipping container differ which is expected to influence flame spread. In order to ensure that the flame spread model reasonably represents the flame spread in the shipping container test environment, the model is compared to area spread data measured from the shipping container tests (Section 3.3). It is important to highlight that the specimen in both test

environments were of similar size and geometry Figure 5-4 to Figure 5-10 presents the comparison of the area spread rates.

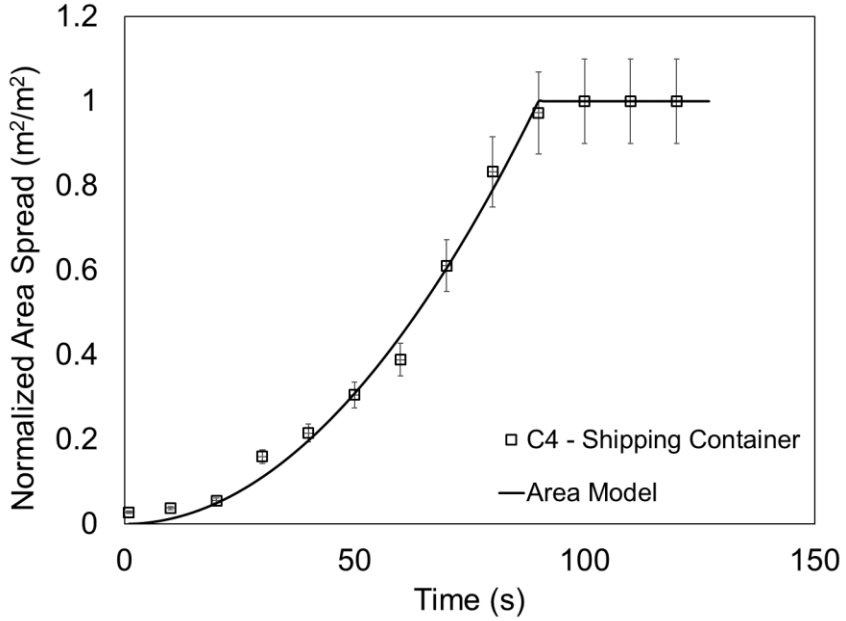

Figure 5-4: Comparison of Flame Area Model and Shipping Container Area Spread Rates for C4 tests

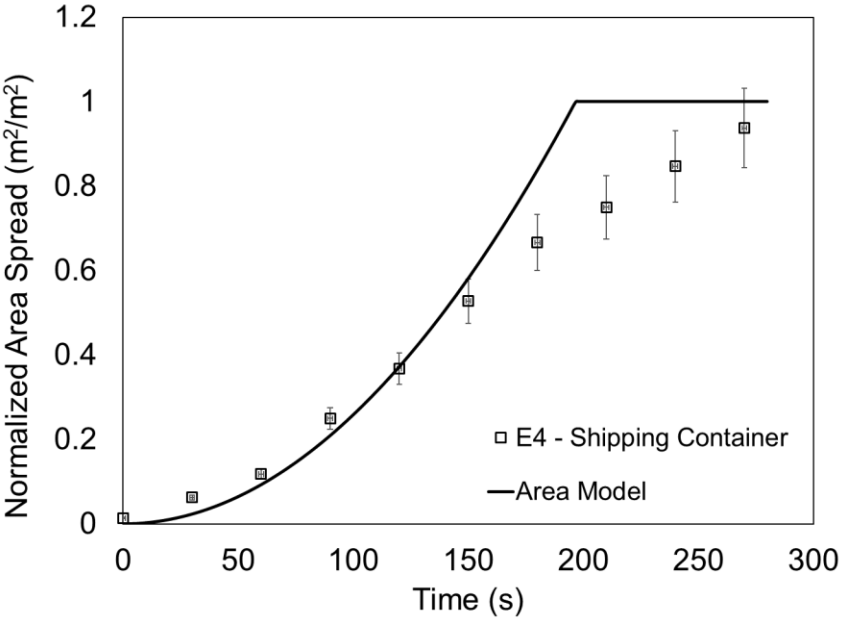

Figure 5-5: Comparison of Flame Area Model and Shipping Container Area Spread Rates for E4 tests

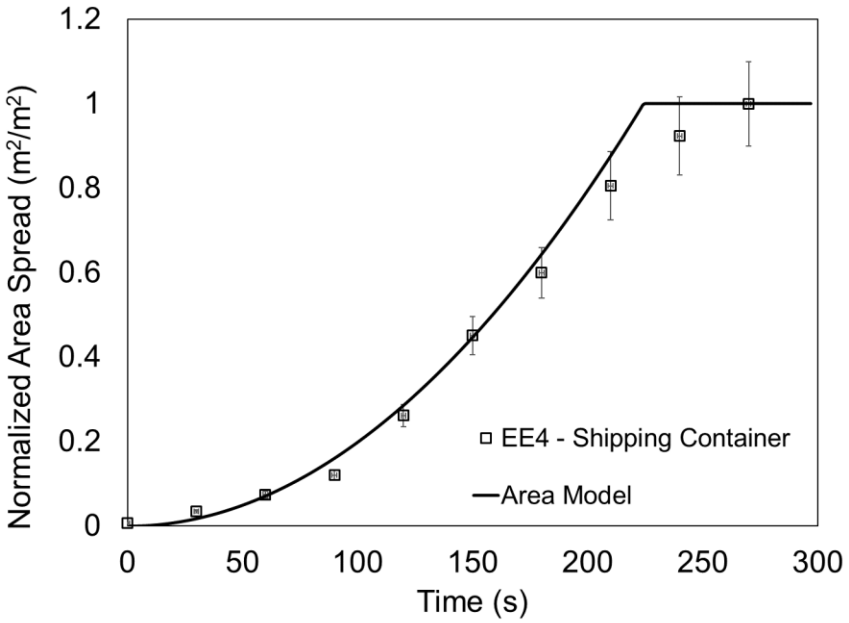

Figure 5-6: Comparison of Flame Area Model and Shipping Container Area Spread Rates for EE4 tests

The area spread model shows good agreement with the measured area spread rates in the shipping container for the first 150 s for all test configurations. For the edge ignition tests, deviations in spread rates start to occur as the fire burns along the foam boundaries (approximately 150 s). As discussed in the previous section, air entrainment plays a role in the deviations observed. Another factor that may affect flame spread rates is the interaction of the fire with its surroundings. This effect becomes more apparent in a compartment test as the radiative feedback and pre-heating of the foam by the hot gases building up in the space becomes significant. The pre-heating of the foam will cause the flame to spread faster. However, a competing factor also affecting flame spread is the reduced availability of oxygen in the shipping container test room. This hinders fast propagation of flames. It is not entirely clear which of these factors dominates in affecting flame spread rate. A simple comparison (Figure 5-7) of the flame areas measured in the shipping container to the furniture calorimeter (where there is ample supply of oxygen and radiative feedback from hot gases is negligible) suggests that the availability of oxygen may pose a more significant effect than the radiative feedback, since the spread of flame was faster in the furniture calorimeter. This information relates to the work of Obach, 2011 where HRR for wood cribs measured in free burn showed a faster rate of heat

released than in the compartment tests (Figure 3-19). Future work on the effect of radiative feedback as well as oxygen limitation in compartment tests is proposed.

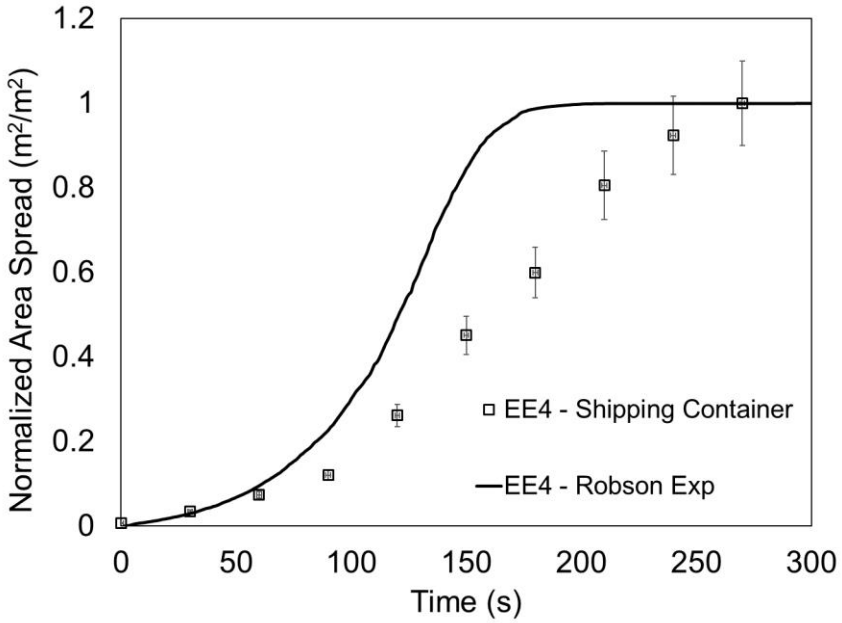

Figure 5-7: Comparison of Flame Spread Rate for the EE4 Test Series

5.1.3 Application of Flame Spread Rates

In order to analyse the flame spread rates for heat release rate and temperature predictions for the shipping container experiment, some idealisations involving the fire growth patterns are required to be made. For an infinitely large piece of foam with negligible thickness, a constant radial flame spread over the area of the foam is assumed. The flame can be assumed to spread in a circular pattern for the centre ignition tests (C4 test series) while the edge ignition tests (E4 and EE4 test series) can be assumed to grow as a semi-circle. The spread of flame along the depth of the foam may also be ignored. For a foam specimen with a finite area, it is important to note some of the limitations of these assumptions. A schematic of the flame growth pattern is provided in Figure 5-8.

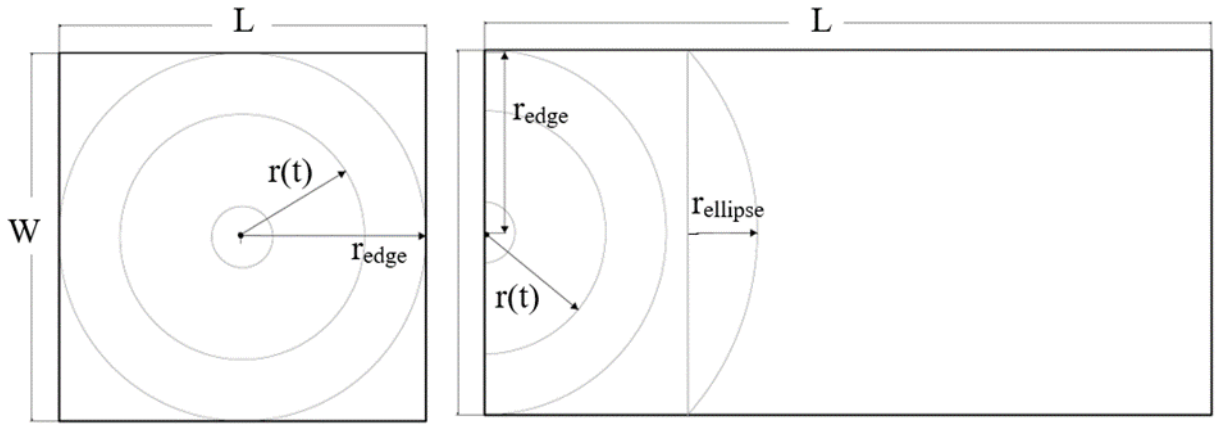

Figure 5-8: Schematic of Centre and Edge Ignition Flame Spread Patterns

As seen in Figure 5-8, these assumptions of a circular and semi-circular flame spread pattern begin to breakdown as the flame approaches the foam boundaries. For the centre ignition, the breakdown occurs as r(t) reaches r_{edge}. Due to the geometry of the foams burned in the shipping container tests, results show that deviation from a circular burn pattern does not occur till later stages of the test (approximately 90 s) when over 90% of the foam is burnt out. This means that in this research, the assumption of a circular burn pattern will remain valid for most of the test duration. For the edge ignition tests, the assumption of a semi-circular burn pattern breaks down as r(t) reaches r_{edge}. The flame is estimated to reach the foam boundary at approximately 60 s after ignition with less than 20% of the foam burned. The flame transitions from a semi-circular burn pattern to more of an elliptical pattern. There is an inherent difficulty with modelling the elliptical flame spread pattern. To accomplish this, a knowledge of the change in the radial distance must be known.

In this thesis, the CBUF model applied for predicting heat release rates only required the change in area as an input parameter. However, it may be of interest for further modelling applications to determine the flame front locations based on the geometry of the foam fire. A simple method is proposed for flame front determination with knowledge of the radial spread rates. As mentioned earlier, area spread for centre ignition may be sufficiently represented as a circle, hence, the area of the circle based on the time-dependent diameter of the flame can be calculated to determine the flame front location. For the edge ignition, the area of a semi-circle will adequately model the flame front until the flame reaches the foam boundary where the area

may then be evaluated as an ellipse by multiplying the radial distance by a factor (*x*) to account for the change in the radial spread rate due to an elliptical burn pattern. Once r(t) becomes greater than the width of the foam (W), the flame area may be calculated as the area of the ellipse plus the rectangular area traversing the length of the foam. The factor (*x*) which accounts for the change in the radial spread rate was not evaluated in this thesis but is proposed for future work. For clarity, the equations for flame area are summarised below (refer to Figure 5-8):

For centre ignition,

$$A(t) = \pi\big(r(t)\big)^2 \tag{5.3}$$

For edge ignition,

$$A(t) = \frac{\pi\big(r(t)\big)^2}{2}\ for\ [r(t) < \frac{W}{2}] \tag{5.4}$$

$$A(t) = \frac{\pi(r(t))\left(\frac{W}{2}\right)}{2}\ for\ [r(t) = \frac{W}{2} = r_{edge}] \tag{5.5}$$

$$A(t) = \frac{\pi(r_{ellipse})\left(\frac{W}{2}\right)}{2} + \big((r(t) - r_{ellipse}) \times W\big)\ for\ [r(t) > \frac{W}{2}\ and\ r_{ellipse} = xr_{edge}] \tag{5.5}$$

Investigation of the effect of foam thickness was outside the scope of this research as full-scale test specimen were limited to 10 cm thick foams. The area spread model was correlated from experimental data and thus the effect of the thickness will be accounted for within the model. In modelling applications for thinner or thicker foam specimens, variations will occur due to changes in foam thickness. In Robson (2014) study on the effect of foam thickness, the thicker specimens (10 cm) were observed to produce more rapidly growing area spread curves than the thinner foams (2.5 cm).

5.2 FULL-SCALE HRR PREDICTIONS

As discussed in Section 1.3, the European Commission Measurements and Testing Report EUR 16477 (Sundstrom, 1996) presented models from their research on the Combustion Behaviour of Upholstered Furniture (CBUF Models). These models were used to predict full-scale fire behaviour of upholstered furniture from small-scale tests. Model II which is of interest

to this thesis is based on the model of Wickstrom and Goransson for predicting heat release rate (HRR) of fires due to upward flame spread in ceiling and wall linings (Wickstrom, 1992).

CBUF model II enables the prediction of fire growth in a mattress using cone calorimeter test data. The model applies the convolution theorem with the assumption that an elemental area burning in the full-scale mattress test will contribute the same amount of heat release as a representative sample burned in the cone calorimeter. The model can be expressed mathematically as;

$$Q(t) = \int_0^t q''(t-\tau) A_f(\tau) d\tau \tag{5.6}$$

Where;

$Q(t)$	is the predicted full-scale heat release rate of the mattress (kW)
$q''(t-\tau)$	is the heat release rate density measured in the cone calorimeter (kW/m^2),
$A_f(\tau)$	is the area burning rate (m^2/s),
τ	is a dummy variable (s).

The convolution integral requires knowledge of the small-scale heat release rate density (measured in the cone calorimeter) and the area burning rate of the mattress. The CBUF convolution model for full-scale mattress fire heat release rate predictions has been used extensively in previous University of Saskatchewan research. Ezinwa utilised the CBUF model to predict furniture calorimeter tests based on manually measured area burning rates and a Gaussian curve fitted to cone calorimeter data (Ezinwa, 2009). A reasonable degree of agreement existed for the earlier stages of the fire, but the model overpredicted the peak heat release rate and did not perform as well in predicting the decay stage of the fire. Ezinwa indicated that the incident heat flux for the cone calorimeter tests, the thickness of the mattress sample as well as the subsequent pool fire obtained influenced the accuracy of predictions of the convolution model.

The CBUF model was applied to predict the full-scale heat release rates (HRR) obtainable in the University of Waterloo shipping container tests for the centre (C4) and edge ignition (E4, EE4). The major challenge encountered in this work was that only space

temperatures were measured in the shipping container tests hence no direct comparison of HRR predictions could be made for the shipping container test. The results of HRR predictions in the shipping container test will be compared to previous data collected in full-scale furniture calorimeter test of representative specimen (Robson, 2014).

The development of the model entailed using averages of experimentally determined heat release rate densities measured by the cone calorimeter for incident heat flux exposures of 25 kW/m^2, 35 kW/m^2, 50 kW/m^2, and 75 kW/m^2 (Section 2.5). Only the small-scale HRR density for the 10 cm thick specimen was considered since full-scale tests were only carried out to this foam thickness. The HRR density averages were taken as a combination of the current cone calorimeter test and previous small-scale data collected by Robson for similar test specimens (Robson, 2014). The CBUF model also required information of the area spread rates in a full-scale mattress fire. As discussed in Section 5.1, the t^2-flame spread model developed for the centre and edge ignition was used.

5.2.1 Coding of the CBUF Model

The CBUF model was coded using Microsoft Excel. The framework of the code was based on the model previously developed by Robson, 2014 and adjusted to suit this specific application. Equation 5.3 was solved by applying the discrete convolution technique and is given as (Robson, 2014);

$$Q^N = \sum_{i=0}^{N} \Delta A^i q''^{N-i} \tag{5.7}$$

Where;

Q^N is the predicted full-scale heat release rate at increment N (kW)

ΔA^i is the differential burning area at increment i (m^2)

$q''(t-\tau)$ is the HRR density at increment $N - i$ (kW/m^2)

For simplicity, the differential burning area and HRR were evaluated separately. The time steps were set to correspond with the sampling rate of the cone calorimeter data (1 s). At each time step, the differential area is calculated and inputted into equation 5.7. This is then solved

with information from the cone calorimeter test. The syntax in Microsoft Excel is written as (Robson, 2014);

"SUMPRODUCT ("*differential area*", SUBTOTAL (9, OFFSET ("*HRR density*", LARGE (ROW (("*differential area*",)-ROW ("*Initial HRR density*"), ROW(INDIRECT("1:"&ROWS("*HRR density*")))),0,1)))".

The HRR calculated by the code at any time is the convolved product of the HRR density and the differential flame area summed with the total HRR to the time of interest. The inputs "*differential area*" and "*HRR density*" correspond to the summation of the columns for ΔA and $\dot{q}''$ up to the time of interest on the spreadsheet. The "*Initial HRR density*" is $\dot{q}''$ at the first time evaluated by the code. A screenshot of the spreadsheet is provided in Figure 5-9

	A	H	K	L	M
10	Time	q"	Flame Area	ΔA	Q
11	(s)	(kW/m²)	(m)	(m)	(kW)
18	5	381.67	0.0011	0.0004	0.0038
19	6	437.23	0.0015	0.0005	0.0059
20	7	477.44	0.0021	0.0006	0.0081
21	8	510.73	0.0027	0.0006	0.0104
22	9	510.46	0.0035	0.0007	0.0129
23	10	505.15	0.0043	0.0008	0.0156
24	11	498.92	0.0052	0.0009	0.0187
25	12	504.87	0.0062	0.0010	0.0218
26	13	494.96	0.0072	0.0011	0.0248
27	14	502.54	0.0084	0.0012	0.0277
28	15	509.20	0.0096	0.0012	0.0305
29	16	518.86	0.0110	0.0013	0.0337
30	17	515.54	0.0124	0.0014	0.0375
31	18	519.53	0.0139	0.0015	0.0426
32	19	519.18	0.0155	0.0016	0.0500

Figure 5-9: Sample Spreadsheet used to Evaluate the CBUF Model

5.2.2 Model Validation and Sensitivity Study

The general framework of the model employed in this thesis is based on previous work carried out by Ezinwa (2009) and Robson (2014). Robson established that a time step of 1 s was sufficient for the numerical approach. Peak HRR predictions made using a time step of one second resulted in a percent error of 3.1% for the centre ignition test and 0.3% for the edge ignition test when compared to the closed-form solution (Robson, 2014). The closed-form solution employed by Robson for HRR validation combined the area spread relationship developed by Wickstrom and Goransson for room lining materials with a single Gaussian distribution curve for HRR density. The convolution of both expressions which was solved using Maple™ Computer Algebra system is given as (Robson, 2014);

$$Q = \frac{2\ddot{q}_{max} A_0 a}{t_{ig}} \int_0^t \exp(-b(c - t + \tau)^2)\, \tau d\tau \qquad (5.8)$$

Where;

$\ddot{q}_{max}$ is the heat release rate density (kW/m^2)

A_0 is the initial burning area due to ignition (m^2),

a is the peak heat release rate measured in the cone calorimeter, during a test of polyurethane foam (kW/m^2),

b is a value that determines the width of the peak value (s^{-2}) and

c controls the time to peak heat release rate density (s).

Ezinwa (2009) found that the HRR density and area spread inputs scaled linearly with the CBUF model. A ±10% change in HRR density resulted in a ±10% change in CBUF model predictions. Similarly, a ±10% change in area spread resulted in a ±10% change in CBUF model predictions. This indicates that both components of the CBUF model will have similar impacts on the accuracy of prediction. More details on sensitivity analysis can be found in Ezinwa (2009) and Robson (2014).

In order to check the coding of the model and assess the performance of the CBUF model, HRR predicted using Equation 5.7 for a 50 kW/m^2 incident heat flux HRR density is compared to predictions made by Robson's CBUF model, where the specific area burning rates from each furniture calorimeter tests were used to predict HRR results. Figure 5-10 to Figure 5-12 give a graphical comparison for the test series.

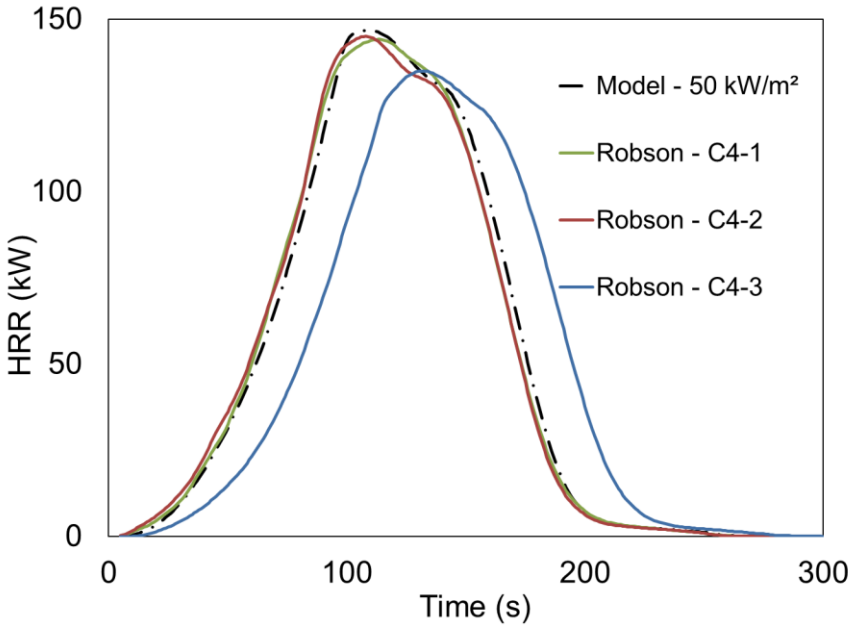

Figure 5-10: Comparison of Predicted Heat Release Rate to Robson CBUF Model (C4 Test Series)

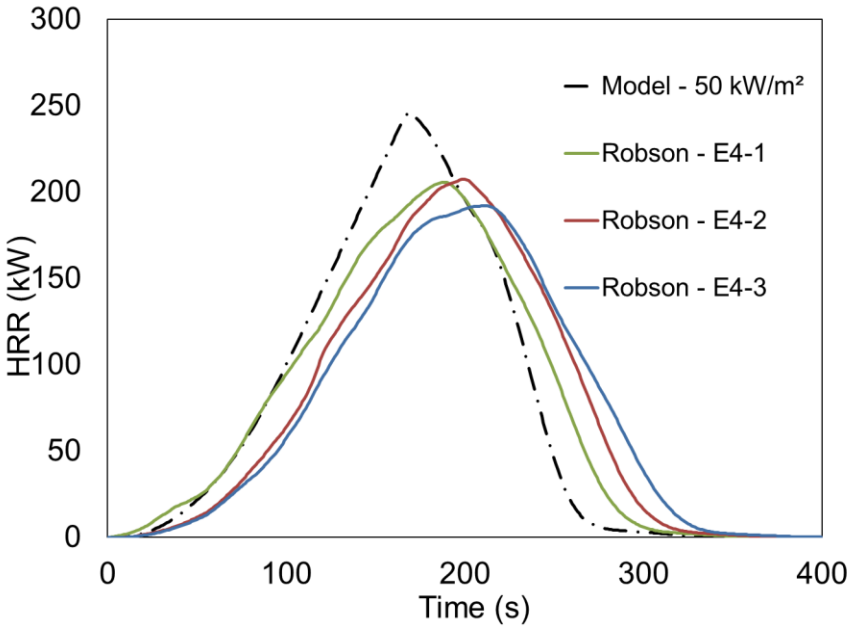

Figure 5-11: Comparison of Predicted Heat Release Rate to Robson CBUF Model (E4 Test Series)

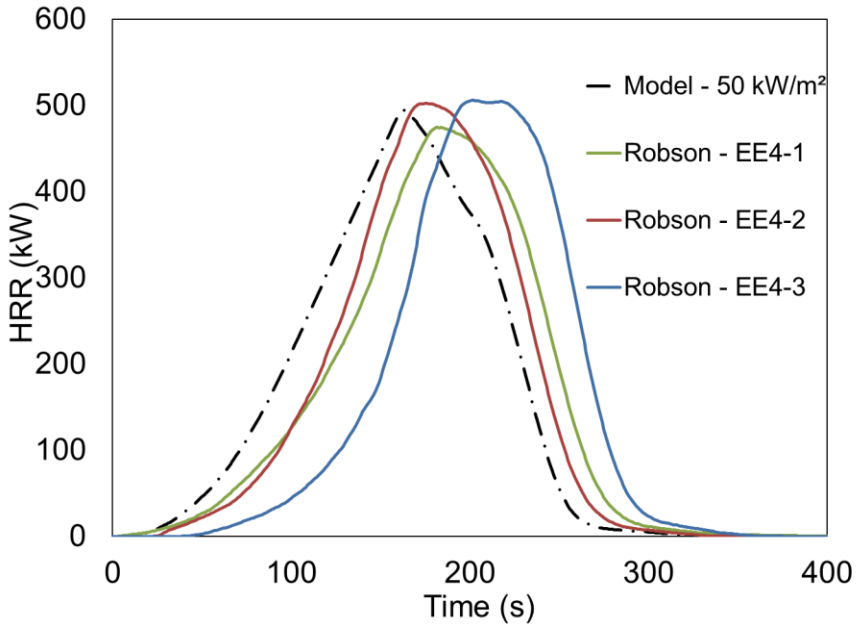

Figure 5-12: Comparison of Predicted Heat Release Rate to Robson CBUF Model (EE4 Test Series)

The comparisons of HRR predictions shown are for the 50 kW/m^2 heat flux. Robson's CBUF model was carried out for 10 cm nominally thick foams. The flame spread rate for each individual test served as inputs to the model. This approach accounted for the variations in fire behaviour for each test. From the HRR comparison, the C4 model showed a good level of agreement with Robson's model. The slope of the fire growth phase and the decay phase closely matches Robson's model. The similarity in HRR predictions for the C4 model is explained by the almost exact flame spread rate in both models (Figure 5-1).

The E4 and EE4 models did not show as good of an agreement as did the C4 model. The major reason behind this is the variation in the rate of flame spread predicted by the area model. As discussed in Section 5.1.1, the model does not capture deviations in area spread rates from a parabolic growth pattern. For the E4 and EE4 HRR predictions, the general shape of the HRR curve is similar to Robson's. The predictions made for the growth phase (up to 100 s) for the E4 test closely matches the predictions made by Robson. The growth phase of the EE4 test series is higher than the HRR determined by Robson's model, however, areas predicted for that phase of the fire are higher than measured values. The peak HRR predicted for the E4 test is also higher than Robson's model. Finally, a faster rate of decay is predicted by the current HRR model for the E4 and EE4 test series.

5.2.3 Results of the Convolution Model

As mentioned earlier, the HRR was not measured in the University of Waterloo shipping container test. To compare HRR predictions to experimental data, HRR averages from furniture calorimeter test results of 10 cm thick polyurethane samples were used for the various test series. It is important to reiterate that the shipping container and furniture calorimeter create two different fire conditions. It is not expected that heat release rates based solely on furniture calorimeter data will precisely represent heat release rates in the shipping container. As discussed in section 3.4, a study on the fire dynamics of both test environments indicates that the peak HRR measurements were within 15% for both test environments (Obach, 2011).

The shipping container is an enclosed compartment while the furniture calorimeter is open with minimal restriction to air movement. The enclosed nature of the shipping container causes a build-up of hot gases which radiates back to the foam propagating the fire even further. On the other hand, there is limited oxygen entrainment as the air can only be supplied from the door of the room. As discussed in Section 5.1.2, these two competing factors influence fire behaviour in the shipping container compartment. In the furniture calorimeter, hot gases are collected through the hood for analysis. A hot gas layer does not fully develop in this test environment, but oxygen is entrained from all sides of the foam leading to faster-developing fires.

A plot comparing experimental results from the furniture calorimeter and the CBUF model predictions for the centre ignition test series is given in Figure 5-13. A summary of the C4 model results is presented in Table 5-1.

Table 5-1: Summary of CBUF Model Results for the C4 Test Series

	25 kW/m^2	35 kW/m^2	50 kW/m^2	75 kW/m^2	Experiment
Peak HRR (kW)	124.7	134.5	146.8	183.5	157.9
Time to Peak (s)	113.0	109.0	103.0	95.0	101.0
THR (MJ)	15.0	14.5	14.4	15.2	13.7

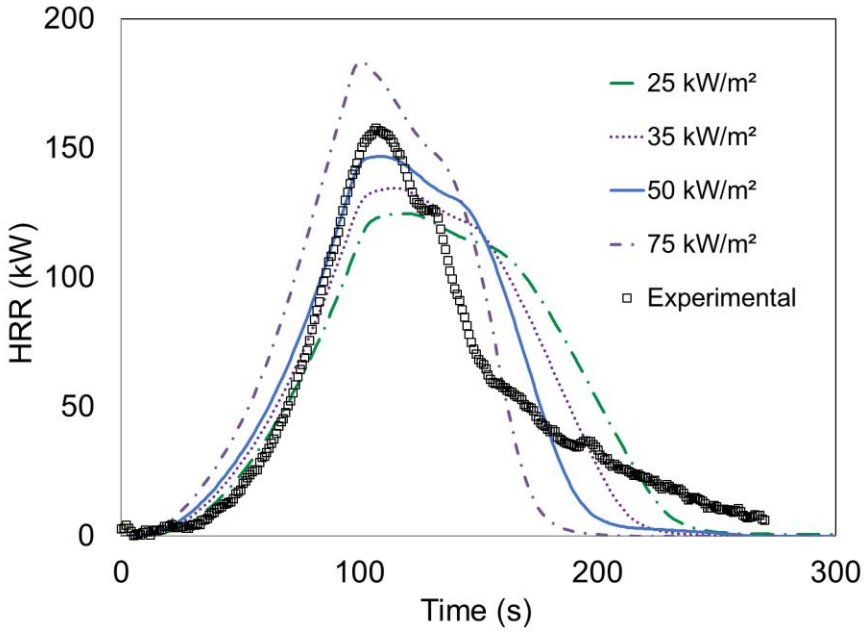

Figure 5-13: Comparison of Experimental and Predicted Heat Release Rate for Center Ignition (C4 Test Series)

As seen in Figure 5-13, the CBUF model does a good job of predicting the experimental HRR. One of the first observations from this result is the dependence of the CBUF model on the incident heat flux of the small scale HRR density. Higher incident heat fluxes will lead to higher peak HRR, faster time to peak HRR (faster growth phase) and shorter time to extinction (faster decay period). This behaviour is representative of an actual fire scenario as increased incident heat fluxes will lead to materials burning out at a faster rate. The 25 kW/m^2 model does the best job of predicting the HRR in the early part of the fire growth phase (before 80 s) while the 50 kW/m^2 model has the best agreement to later times in the growth phase, the peak HRR, time to peak HRR and the total heat released (THR). The HRR in the decay phase was better modelled by the 75 kW/m^2 heat flux exposure until approximately 60 kW where the rate of decay slowed down. The CBUF model was unable to capture the decrease in the decay rate observed.

Figure 5-14 presents the results of the CBUF model for the E4 test series compared to the furniture calorimeter experimental data. Overall, the CBUF model compares relatively well with experimental heat release rates. A summary of the E4 model results is presented in Table 5-2.

Table 5-2: Summary of CBUF Model Results for the E4 Test Series

	25 kW/m^2	35 kW/m^2	50 kW/m^2	75 kW/m^2	Experiment
Peak HRR (kW)	228.6	236.0	245.8	282.3	219.9
Time to Peak (s)	168.0	165.0	163.0	161.0	145.0
THR (MJ)	30.4	29.5	29.3	31.0	29.1

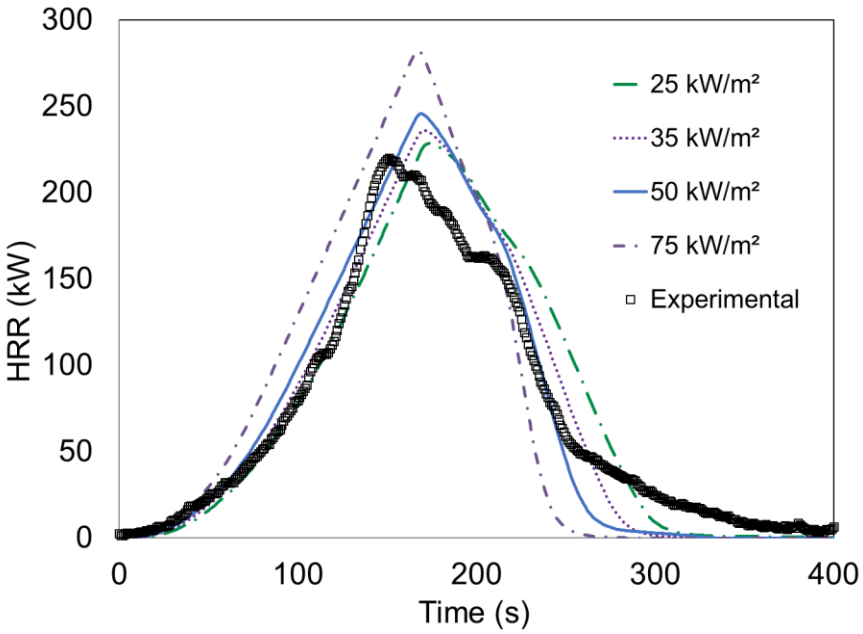

Figure 5-14: Comparison of Experimental and Predicted Heat Release Rate for Edge Ignition (E4 Test Series)

Similar to the C4 test series, the growth phase of the fire is better approximated by the 25 kW/m^2 model until after 120 s where the slope of the HRR curve deviates from the CBUF model and shows a more rapid rate of heat release. This time coincides with the period at which deviations in the flame area model occurs (Section 5.1.1) and may explain the deviation in HRR predictions. The 50 kW/m^2 model does a better job of predicting HRR in the later stages of the growth phase. The magnitude of the peak heat release rate was better predicted by the 25 kW/m^2 model, but the model did not show good agreement in the time to reach peak heat release rate. Finally, the 50 kW/m^2 CBUF model shows reasonable agreement in predicting the experimental data in the decay phase as well as the THR.

Figure 5-15 presents the results of the CBUF model compared to furniture calorimeter HRR measurements for the EE4 test series. Comparison done for this test series showed the least agreement with experimental data. The CBUF model overpredicts HRR measured in the growth phase of the EE4 experiments. The 35 kW/m^2 model was able to predict the magnitude of the peak heat release rate. The 50 kW/m^2 model sufficiently captured the decay phase of the fire and did a good job of predicting the THR.

Table 5-3: Summary of CBUF Model Results for EE4 Test Series

	25 kW/m^2	35 kW/m^2	50 kW/m^2	75 kW/m^2	Experiment
Peak HRR (kW)	456.9	473.4	494.3	570.7	473.3
Time to Peak (s)	162.0	159.0	157.0	155.0	170.0
THR (MJ)	59.9	58.1	57.7	60.9	57.7

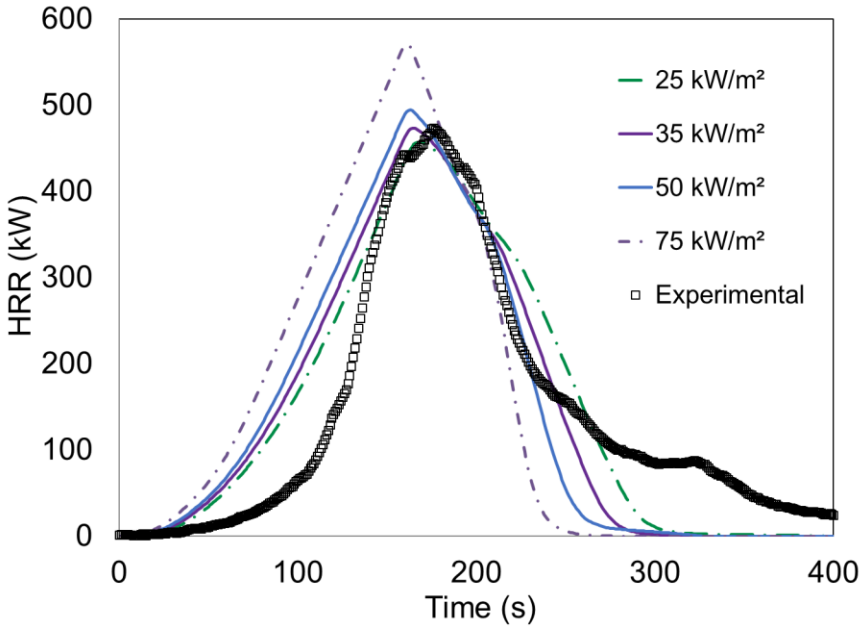

Figure 5-15: Comparison of Experimental and Predicted Heat Release Rate for Edge Ignition (EE4 Test Series)

From the results of the CBUF model, it is observed that deviations in predictions increased as the foam becomes larger. Results suggest that an incubation period occurs before the fire begins to fully propagate. This behaviour is more apparent in the EE4 test series. As shown in Figure 5-16, the CBUF model was modified to account for the incubation period. A

delay in the HRR curve was obtained assuming an incubation time of 20 s. The results summary given in Table 5-4 shows that the peak HRR, time to peak HRR as well as the THR was better predicted by the CBUF model. Future work is proposed to investigate the incubation times for the various test configurations and its impact on area spread and HRR predictions.

Table 5-4: Summary of Modified CBUF Model Results for EE4 Test Series

	25 kW/m^2	35 kW/m^2	50 kW/m^2	75 kW/m^2	Experiment
Peak HRR (kW)	456.9	473.4	494.3	570.7	473.3
Time to Peak (s)	182.0	179.0	177.0	175.0	170.0
THR (MJ)	59.9	58.1	57.7	60.9	57.7

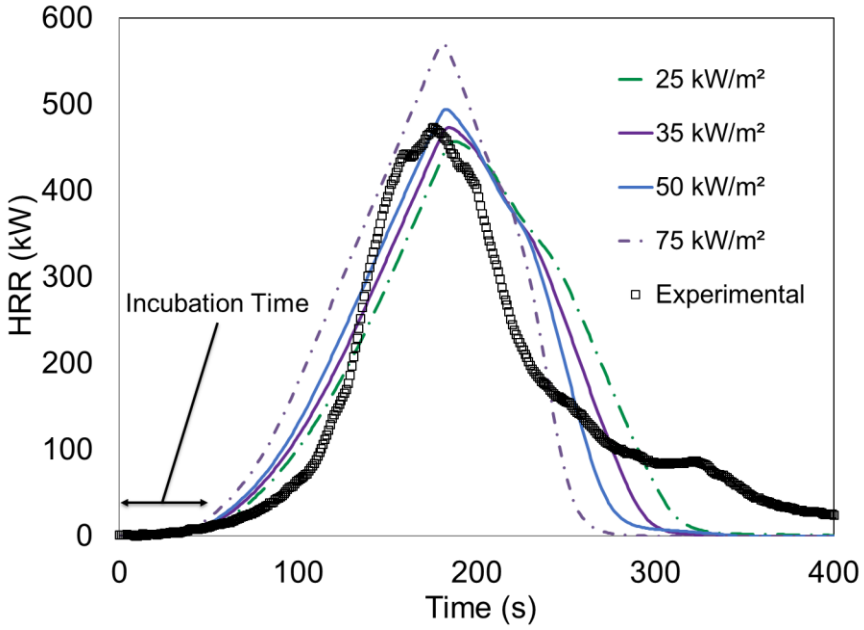

Figure 5-16: Comparison of Experimental and Predicted Heat Release Rate for Edge Ignition Accounting for a 20 s Incubation Period (EE4 Test Series)

Finally, results of the CBUF model highlight the impact of change in fire behaviour as the flame reaches the edge of the foam. Comparing the edge ignition series, EE4 tests were carried out on foams with a nominal area approximately 50% more than the E4 tests. It is expected that the flame will reach the edge of the foam when a substantial percentage of the foam is unburned. The edge effects become significantly more pronounced as a result which further explains deviations observed in the CBUF model results for the larger EE4 test specimen.

5.3 CEILING TEMPERATURE PREDICTIONS

The goal of this thesis was to explore a predictive methodology to evaluate compartment fire dynamics. Over the course of this chapter, flame spread, and heat release rates have been modelled. The remainder of this chapter will detail engineering methods applied to compartment temperature prediction in fire scenarios. These methods typically rely on information about the heat release and flame spread rates modelled in previous sections.

As discussed in Section 1.5, Alpert's correlation predicts the maximum smoke jet temperature across the ceiling of the compartment based on the convective heat release rate, the height of the compartment, the radial distance along the ceiling from the centre of the plume and a factor (k) that accounts for the location of the fire relative to its position with the walls of the room (Alpert, 1972). Alpert's two ceiling jet equations which are a function of the ratio of the radial distance to the height of the room are given as (Drysdale, 2011);

$$T_{max} - T_{amb} = 5.38 \frac{(\frac{k\mathrm{Q}}{r})^{\frac{2}{3}}}{H} \qquad [r > 0.18H] \tag{5.9}$$

$$T_{max} - T_{amb} = 16.9 \frac{(k\mathrm{Q})^{\frac{2}{3}}}{H^{\frac{5}{3}}} \qquad [r \leq 0.18H] \tag{5.10}$$

Where Q is the convective heat release rate (kW),

H is the height of the compartment (m),

r is the radial distance along the ceiling from the centre of the plume (m), and

k is a factor that accounts for the location of the fire.

Alpert's correlation was used to predict ceiling temperatures in the shipping container test. Ceiling temperatures measured by thermocouples and reported in Section 3.1 are compared to predictions made using Alpert's correlation. As identified in Section 1.5, the shortfall of Alpert's correlation is in the treatment of the radial distance (r) from the fire. Typically, this radial distance is assumed constant over the duration of the fire. This is not an entirely accurate representation given the physical behaviour of the fire. As the polyurethane foam burns, the centre of the fire plume will continually shift across the surface of the mattress until it is

completely burned. The subsequent section discusses the computation of Alpert's correlation for this thesis.

5.3.1 Implementation of Alpert's Correlation

Alpert's correlation was computed in Microsoft Excel for the three different test series (C4, E4 and EE4). Since the correlation is relatively simple to implement, it was more efficient to perform Excel sheet calculations as opposed to writing scripts. Information on the geometry of the shipping container, location of the thermocouples and positioning of the foam which are required for temperature comparisons are detailed in Section 3.1. For inputs into the calculation, the heat release rate of the foam was supplied from the predicted CBUF model heat release rates at 50 kW/m^2. This heat flux level was selected as it appeared to be the best choice of heat flux based on your comparison with the measured HRR values. Further investigation of the heat release rate input is discussed in Section 5.3.3. The height of the shipping container was 2.4 m and a k-factor of 1.0 was used for calculations since the fire was not in contact with the shipping container walls.

The radial distance of the fire to the various thermocouple locations was modified for this research. As already discussed, this value is typically assumed constant which introduces uncertainties, especially for transient fire modelling. To account for the changing distance, a simplified version of the area spread model discussed in Section 5.1 was used to determine the flame front position at any time of interest. The edge of the flame front was assumed to be the centreline of the smoke plume which changed over the course of the test. The heat release rate of the fire was still calculated for the entire area of the flame on fire at any given time. Figure 5-17 and Figure 5-18 illustrate the changing plume centre for the centre and edge ignition. The equation used to calculate the radial distance is given as;

$$r(t) = r_i - r_f(\mathrm{t}) \qquad \left[\mathrm{r}_f(\mathrm{t}) < \frac{\mathrm{W}}{2}\right] \tag{5.11}$$

$$r(t) = r_i - \frac{W}{2} \qquad \left[\mathrm{r}_f(\mathrm{t}) \geq \frac{\mathrm{W}}{2}\right] \tag{5.12}$$

$$r_{f_c}(t) = \sqrt{\frac{A(t)}{\pi}} \quad or \quad r_{f_e}(t) = \sqrt{\frac{2A(t)}{\pi}} \tag{5.13}$$

Where r(t) is the changing radial distance from the thermocouple, r_i is the initial radial distance at the start of the test, r_f is the changing radius of the flame (centre and edge ignition), W is the width of the foam and A(t) is the flame area calculated by Equation 5.2.

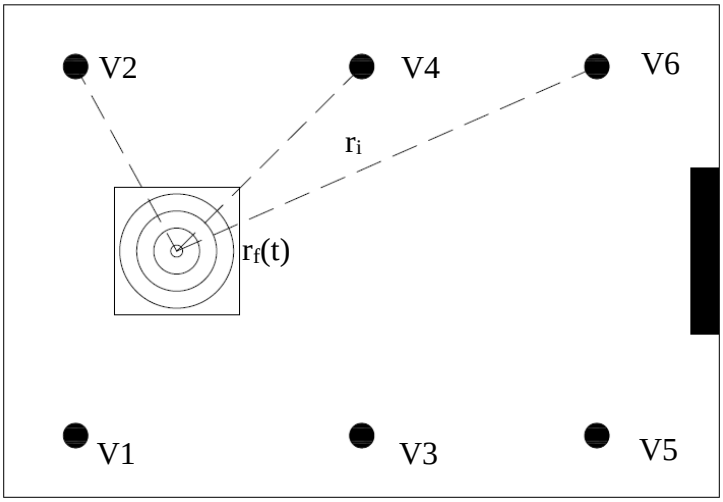

Figure 5-17: Modified Radial Distance Based on Changing Plume Centre (Centre Ignition)

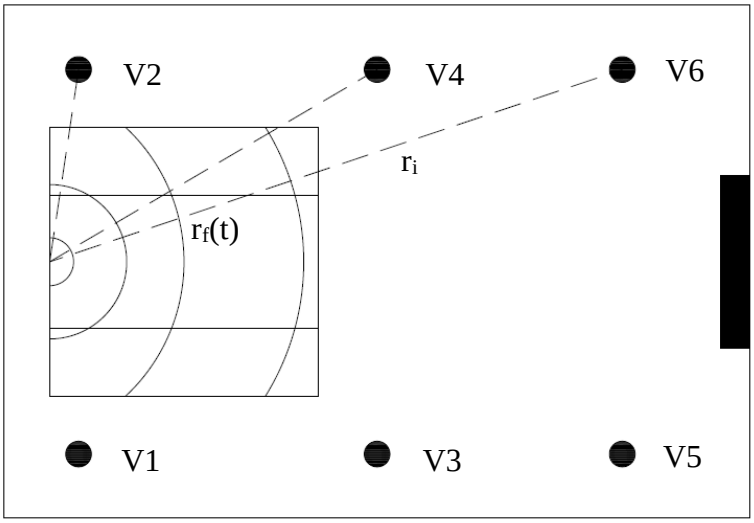

Figure 5-18: Modified Radial Distance Based on Changing Plume Centre (Edge Ignition)

For the centre ignition test, the flame was assumed to grow as circle up until the boundaries of the foam to prevent over predictions of the flame area. Once the flame reaches the boundaries, the radial distance is calculated as the straight-line distance from the edge of the foam to the thermocouple of interest. The flame was assumed to grow as a semi-circle for the edge ignition tests until the fire reaches the foam boundaries. After the flame reaches the width

of the foam, the area of the semi-circle formed begins to traverse the length axis of the foam maintaining the same radial growth pattern as the semi-circle while the width axis assumes a constant radial value determined by the width of the foam.

Alpert's correlation was also evaluated using a constant value of the radial distance which was based on the distance of the thermocouple from the ignition location. This distance was assumed constant throughout the duration of the test for the centre and edge ignition and allowed for comparison on the effect of flame spread on the predictive ability of Alpert's correlation.

5.3.2 Results of Temperature Predictions

Figure 5-19 to Figure 5-21 compare the temperatures predicted using Alpert's correlation for varying radial distance (V# - Alpert's) and constant radial distance (V# - Alpert's const R) to temperatures measured by six ceiling thermocouples indicated by V1 – V6 for the C4, E4 and EE4 test series. The experimental temperatures (ceiling jet temperature) were averaged over four tests for the C4 and E4 series while temperatures were averaged over three tests for the EE4 series. Thermocouples V1 and V2 were located closest to the fire origin and farthest from the door of the test room while V5 and V6 were located 0.55 m from the door. Refer to Figure 3-1 for more details on thermocouple locations.

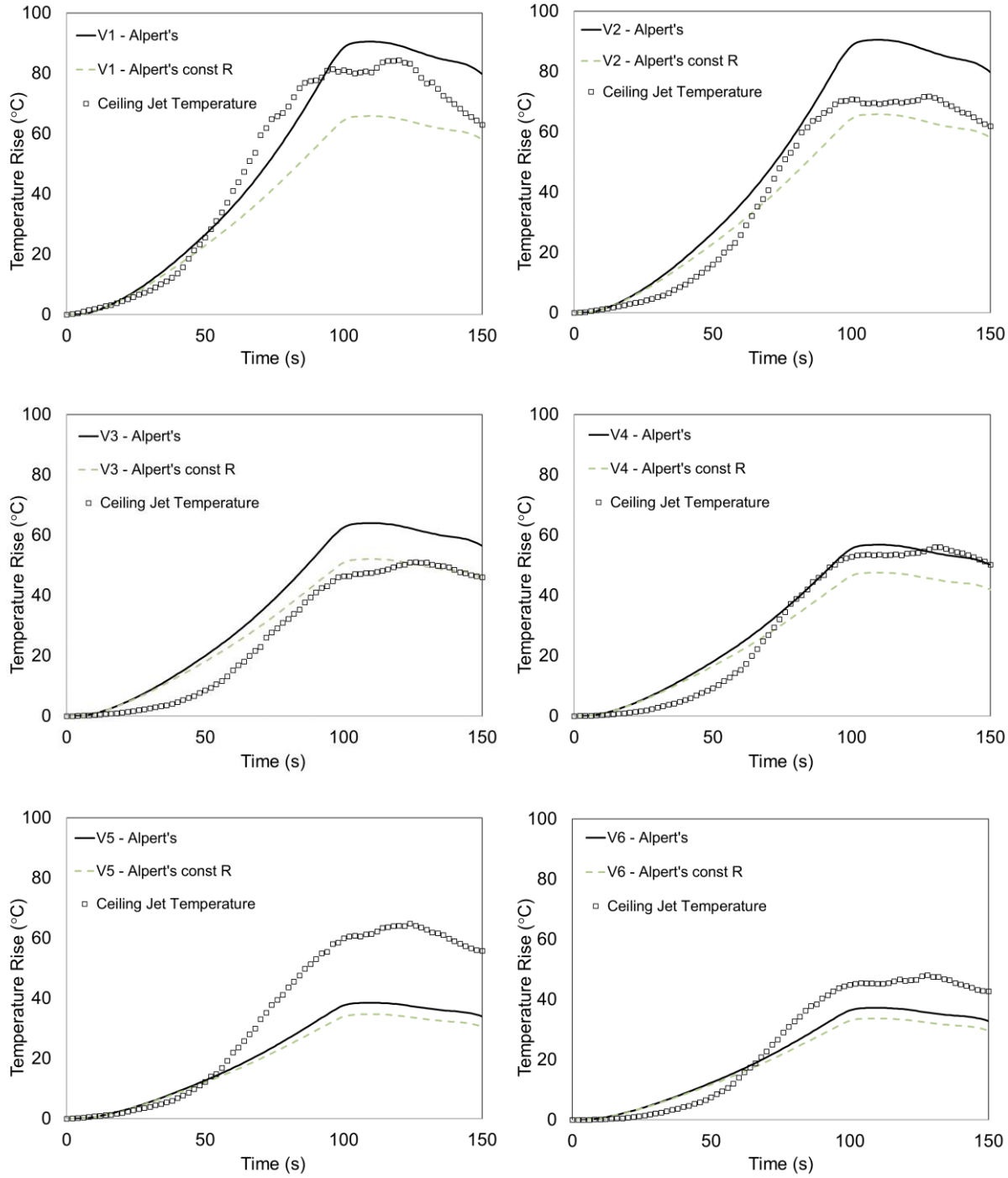

Figure 5-19: Comparison of Predicted and Measured Ceiling Temperatures (C4 Test Series)

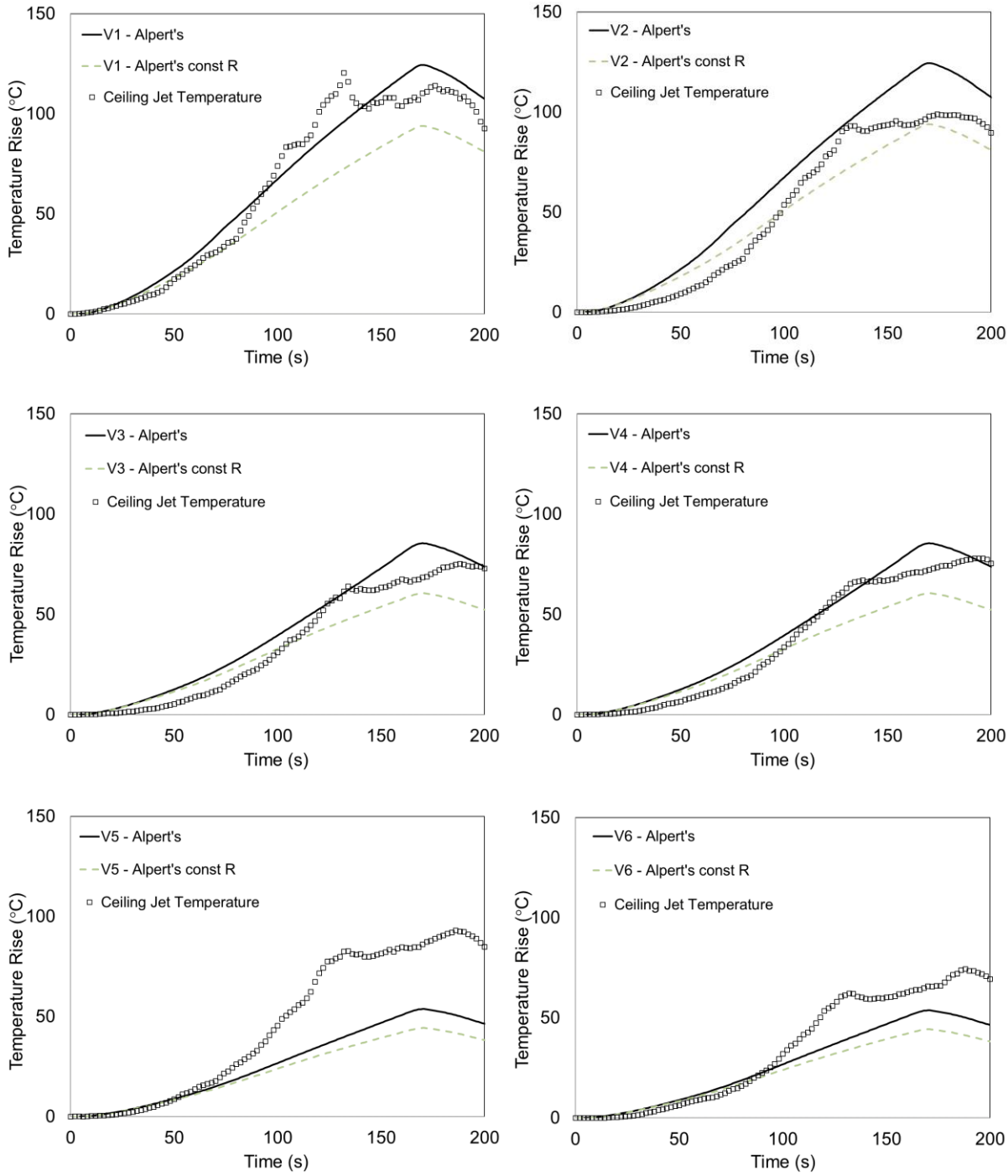

Figure 5-20: Comparison of Predicted and Measured Ceiling Temperatures (E4 Test Series)

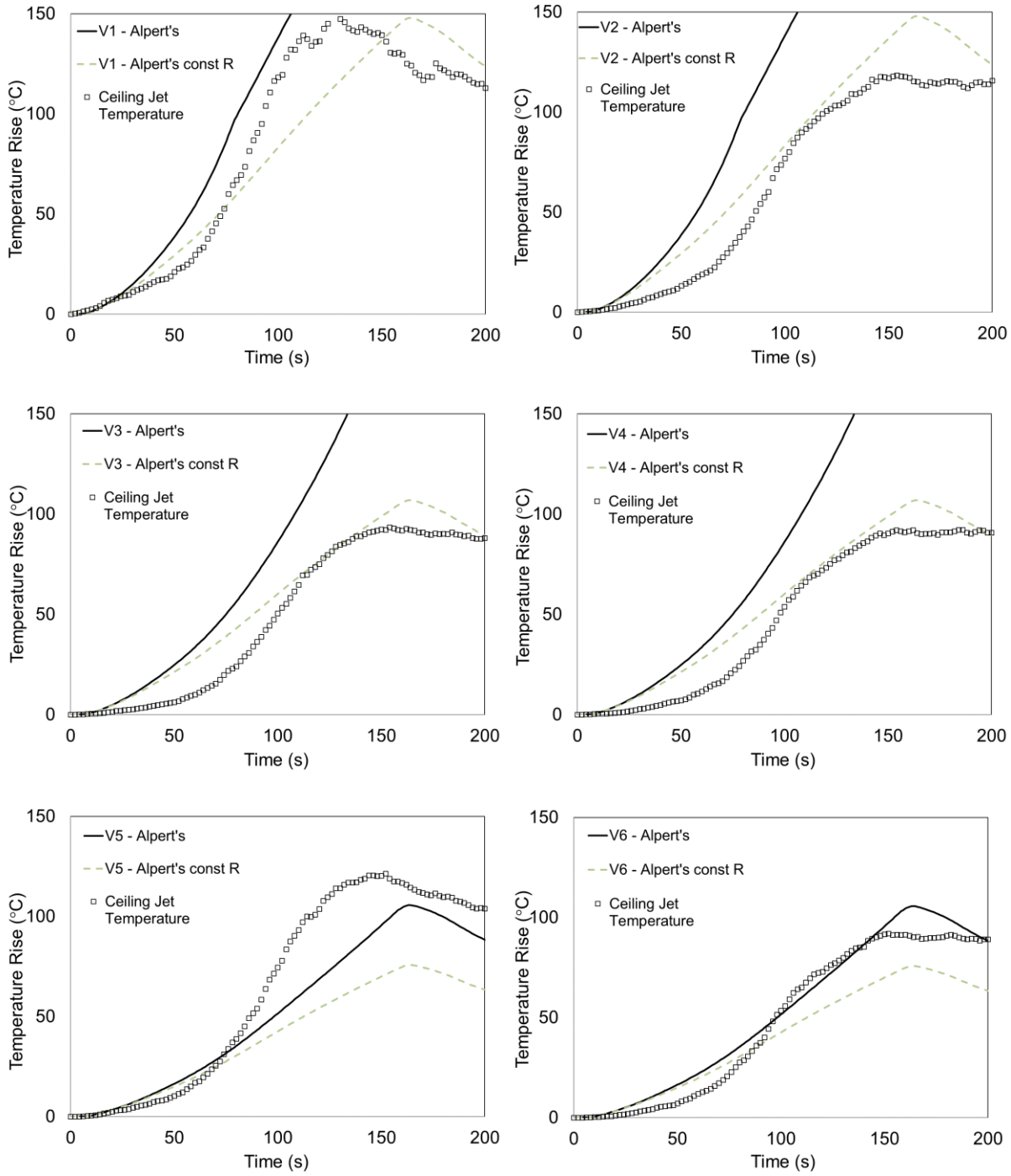

Figure 5-21: Comparison of Predicted and Measured Ceiling Temperatures (EE4 Test Series)

5.3.3 Discussion of Results

The comparison of predicted temperatures to measured room temperatures shows that Alpert's correlation satisfactorily predicts the temperature rise within the fire compartment for the various test series. An important factor to consider when using Alpert's correlation is its predictive limitations. Breakdown in Alpert's correlation starts upon sufficient build-up of a smoke layer along the ceiling. The correlation also fails once flame impinges on the ceiling surface (Drysdale, 2011). The flames in this test did not impinge on the ceiling of the shipping container so the use of flame height correlations to predict failure of Alpert's correlation was not applied. Investigation of experimental video records indicates that a sufficient build-up of a smoke layer occurred at approximately 50 s for all tests. This time was determined as when a visible layer of smoke can be seen from the test doorway. In general, for the first 50 s of the C4, E4 and EE4 test series, Alpert's correlation predicts temperature rises to ±5°C for most thermocouple measurements albeit some deviations occurring for some thermocouples in each series. It is unclear if Alpert's correlation is inherently conservative but considering its application for ceiling detector response time calculations, it is expected that temperatures predicted by Alpert's correlation are generally higher than measured temperatures.

As seen in the graphs (Figure 5-14 to Figure 5-17), temperature predictions were also made assuming a constant radial distance (R). At the beginning of the calculation, the temperatures for the constant radial distance were relatively close to predictions made for the varying radial distance. The temperatures start to deviate as the effect of flame spread becomes more pronounced. The varying radial distance enables the model to account for the fire getting closer to the thermocouple location leading to a more rapid temperature rise.

Observing the temperatures reported for each thermocouple in Figure 5-14 to Figure 5-17, it is seen that there were differences in the temperatures measured for thermocouples located at similar distances away from the foam. Given ideal conditions, it would be expected that both thermocouples (for example V1 and V2) would record similar temperature rise within the same fire compartment. This is not the case as shown in Figure 5-22, there was preferential movement of hot gases to certain corners of the room.

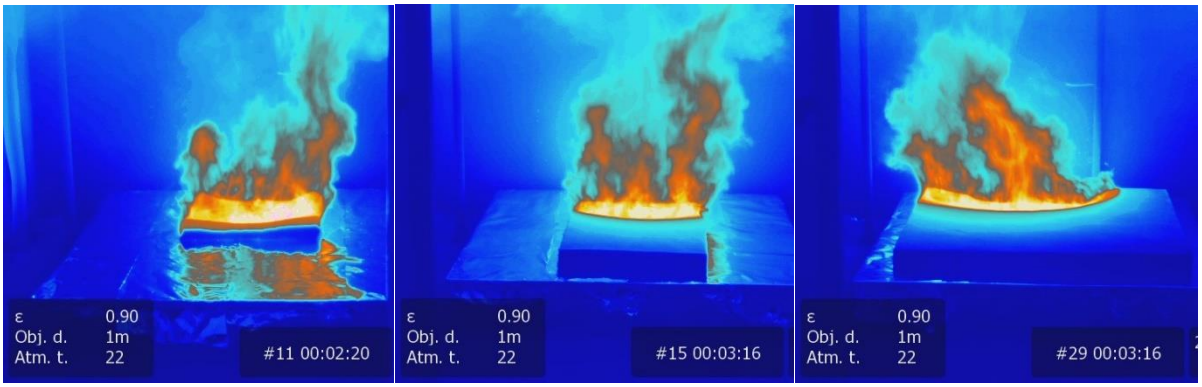

Figure 5-22: IR Images Showing Preferential Smoke Movement in Test Room for C4, E4 and EE4 Test Series (Left to Right)

The migration of combustion gases to these locations was influenced by wind movement and individual foam composition which affected flame spread characteristics. Thermocouples located in areas experiencing preferential smoke movement showed rapid temperature rise but also quickly deviated from temperatures predicted by Alpert's correlation. Also, over the duration of the test, the direction of smoke movement may change resulting in another thermocouple measuring higher temperatures. Alpert's correlation does not account for varying ceiling jet patterns which explains why some thermocouples did not show as good of an agreement as others in the same test series. For example, in the C4 and E4 tests, temperatures predicted by Alpert's correlation for thermocouple V1 closely modelled experimental temperatures while predictions made for thermocouple V2 were slightly overpredicted. It can be inferred that there was preferential migration of hot gases to the thermocouples located along the same axis as V1 for the C4 and E4 test series. This behaviour points to the influence of smoke movement on the predictive ability of Alpert's correlation and shows that consideration must be made to account for wind movement.

After 50 s, it is observed that for all tests, temperature measurements for thermocouples V5 and V6 located by the door showed the most deviation from temperatures predicted by Alpert's correlation. This behaviour is due to the hot gases leaving the test room. As the hot gases attempt to escape from the room, its movement is obstructed by the 0.65 m lip above the door. This forms a pocket where hot gases collect leading to elevated temperatures in that region. Again, this is outside the validity range of Alpert's correlation. Alpert's correlation was determined based on a series of fires that was allowed to flow unconfined in the horizontal

direction. The obstruction to the flow of hot gases by the lip will result in the faster breakdown of Alpert's correlation.

Another factor which impacts temperature predictions is the material heat release rate. Figure 5-23 shows the effect of heat release rate on the temperatures predicted for thermocouple V1 in the C4 tests. HRR predictions at 25 kW/m^2, 35 kW/m^2, 50 kW/m^2 and 75 kW/m^2 were used as inputs to Alpert's correlation. It is seen that the lower heat fluxes perform better at predicting ceiling temperatures at earlier stages of the fire. As the fire progresses, the higher heat fluxes start to perform better at predicting the ceiling temperatures. Typically, a k-factor accounts for the position of the flame and its resultant effect on the rate of heat released by the fire. This factor is taken as 1.0, 2.0 and 4.0 to describe flames away from the wall, by the wall and by the corner of the test room respectively. However, no description on the distance away from the wall is given for the correlation. In this research, this factor was selected as 1.0 since the foam was not by the wall. This lack of clarity may introduce errors in modelling since the interpretation is left to the user. An investigation of the variation in the k-factor with the distance away from the wall is proposed for future work.

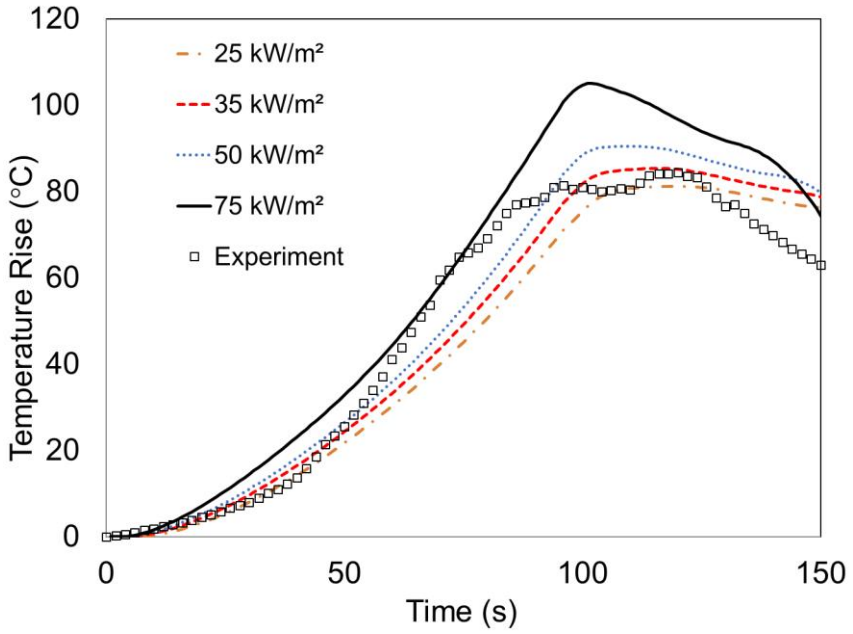

Figure 5-23: Effect of Heat Release Rate on Temperature Predictions (V1 – C4 Test Series)

Finally, when considering the application of Alpert's correlation for ceiling fire detector design, standard fixed temperature response devices are typically designed to approximately

30 – 40°C rise in temperature (NFPA, 2019). Alpert's correlation has shown to have sufficient predictive capabilities for this temperature range and failure due to flame impingement and hot gas build-up will occur at much higher temperatures. Also, the design is usually limited to a fixed location without accounting for flame spread. The application of a changing radial distance with accurate flame spread information possesses the potential to widen the scope of application of Alpert's correlation.

5.4 SUMMARY OF CHAPTER

This chapter focused on the prediction of full-scale experimental flame spread, heat release rate and compartment temperatures. The area spread model was developed by correlating experimental flame spread rates and determining a coefficient of flame propagation which was applied to a t^2 area growth model. The area growth model, while conservative, did a reasonable job in predicting area spread rates. The area spread rates were combined with the small-scale cone calorimeter HRR density measurements in the CBUF convolution model to predict full-scale heat release rates. This process performed reasonably well in scaling fire test results, but a better agreement was obtained when using data for the 50 kW/m^2 HRR density. Future work on HRR density selection is proposed as results indicate that a combination of various HRR densities may lead to better full-scale HRR predictions. Finally, Alpert's correlation was demonstrated to be valid in predicting ceiling jet temperatures for applications in ceiling detector response times. The radial distance of the flame to a point of interest was varied using information from the area spread models. Temperature predictions made considering the varying radial distance as opposed to a constant radial distance showed an ability to capture the effect of flame spread on temperature predictions.

6 CONCLUSIONS AND FUTURE WORK

This research has been focused on improving methods for scaling small-scale fire test data to predict full-scale fire behaviour. The emphasis of the study was on polyurethane foam fires. This goal was accomplished by experimentally and numerically analysing small-scale cone calorimeter tests, full-scale furniture calorimeter tests as well as room fire tests. Investigations of models and correlations for flame spread, heat release rate and temperature predictions have contributed to the fire scaling body of knowledge.

6.1 CONCLUSIONS

Conclusions will be presented in two parts corresponding to the small-scale analysis and full-scale analysis. Small-scale experiments were conducted to complement the previous cone calorimeter test. Numerically analysis of fire behaviour was also carried out. The following conclusions were drawn out from this section of the thesis;

1. As observed in previous studies (Robson, 2014), the level of incident heat flux during testing was seen to impact cone calorimeter test results. Higher peak heat release rate and shorter burn duration were observed for higher incident heat flux levels. Combustion of the foam was seen to occur in two stages corresponding to the breakdown of the solid foam structure and burning of the resultant liquid polyol.
2. Foam temperatures were also measured during cone calorimeter tests. It was found that the incident heat flux level affected the time to attain peak temperature. An increase in incident heat flux also caused the foam surface to reach ignition temperatures quickly, resulting in shorter ignition times. Using experimental data and theoretical approximations, the critical heat flux value for polyurethane foams was calculated as 2 kW/m^2. Additionally, it was observed that on exposure to heat flux significant temperature rise was recorded on a thin layer on the top of the foam surface. Temperatures at other depths of the foam remained relatively close

to ambient conditions until ignition of the foam occurred. This behaviour demonstrates the semi-infinite nature of polyurethane foam heat transfer and suggests that foam temperatures may be adequately modelled using a semi-infinite approximation in the early portions of heating.

3. The small-scale heat transfer model developed was reasonably successful in predicting the temperature rise of the foam for various incident heat flux exposures prior to ignition. It was found that for temperature rise above 150°C, the model breaks down and more significant deviations from temperature predictions occur. Ignition times of the foam were predicted based on the assumption that a 120°C rise in surface temperature is required for ignition. The model was able to estimate the ignition time of the 10 kW/m^2, 20 kW/m^2 and 35 kW/m^2 incident heat flux but was unable to adequately predict the ignition time for the 5 kW/m^2 heat flux level. Results from the modelling exercise suggest that one temperature may not be sufficient to accurately predict ignition time. Possibly incorporating a model of the gas phase reaction may improve the capability of the model to predict ignition time.

The conclusions drawn from the full-scale experiments analysis and fire scaling are presented below;

1. Flame areas were manually measured from video records of tests conducted in the University of Waterloo shipping container test. For the centre ignition tests, the flame was seen to generally spread in a circular pattern. The edge ignition tests showed flame spread in a semi-circular pattern until the flame reaches the foam boundaries where a transition to an elliptical burn pattern occurs. Similar observations were made in previous studies albeit for a different test environment. Results suggest that the transition from a semi-circular burn pattern to an elliptical burn pattern in the edge ignition test is fairly independent of the test environment and more related to the geometry of the burning material.
2. A time-dependent area model was developed to predict polyurethane flame spread rates. The centre ignition tests showed the closest agreement to the parabolic area curve while the edge ignition tests were reasonably modelled the parabolic curve

at the earlier times of the test. A transition point was seen to occur for the edge ignition tests where the rate of flame spread changes. The model was not able to account for the change in the flame spread pattern. Area model predicts flame spread to within 5% and 20% of experimental data for the centre and edge ignition tests respectively.

3. The CBUF model continued to demonstrate success in predicting full-scale heat release rates using small-scale cone calorimeter data. The growth phase of the heat release rate curve, the peak heat release rate and the total heat released were adequately modelled. The CBUF model did a better job of predicting the heat release rates measured for the centre ignition than the edge ignition test. This was attributed to the shortcomings of the flame spread model which served as an input to the CBUF model to capture transition points that occur as the flame reaches the foam boundaries. The model did not perform as well in predicting the decay phase of the fire. However, predictions of the total heat released were within 5% of experimental data.
4. Ceiling jet temperatures were predicted for the shipping container. Alpert's correlation was modified to account for varying radial distance due to flame spread. The modified correlation did better in predicting the ceiling jet temperatures when compared to the constant radial distance correlation. The performance of the correlation was restricted by the inherent limitations of the correlation. In determination of sprinkler and smoke detector activation times, the model sufficiently captured the temperature rise (30°C to 40°C) necessary for this application.

6.2 FUTURE WORK

Over the course of this research, various questions have been raised, which could lead to work to further improve on the work that has been done.

1. Investigation of surface temperatures during cone calorimeter testing should be continued. Information from such research will improve the ability to model small-scale heat transfer and provide data for verification purposes. In this research, foams were ignited using a spark ignition source. It would be beneficial

to conduct a test where heat transfer from a single radiative source (cone heater) is considered and errors due to the effect of the spark igniter may be isolated. Additionally, in cases (lower heat flux level) where flaming combustion does not occur, there will be a longer duration to collect data which may help reduce uncertainties associated with temperature measurements.

2. The small-scale numerical model developed in this research only explored the solid phase heat transfer process. A separate model on the liquid and gas phase should be developed. The phase changes may be coupled to provide an overall picture of the complete polyurethane combustion process. The more complex heat transfer model will improve the ability of the model to capture specific combustion phenomenon and enable better predictions of the time for breakdown of foam structure, ignition time, mass loss rate and the rate of foam regression which will tie into the prediction of flame spread.
3. One of the limitations of the numerical model was the availability of information on the thermal properties of polyurethane foam. Experimental studies should be conducted to improve this area and correlations relating the thermal properties of the foam to temperature should be developed.
4. Further studies are required for the flame spread model development. Analysis of the spread rates for thinner and thicker foam specimen should be carried out. Also, comparison of spread rates for the centre and edge ignition tests should be conducted for foams of similar geometry to reduce the uncertainties due to the difference in fuel loads. As mentioned, edge effects which cause a transition of the flame spread pattern from a semi-circular geometry to an elliptical geometry should be accounted for. Investigation of incubation times for the various test configurations and its impact of area spread and heat release rate predictions should be considered. Additionally, a more complex numerical flame spread model may be developed.
5. In this study, analysis of data obtained from the furniture calorimeter test was used to predict fire behaviour in compartment tests. Future work on the effect of radiative feedback as well as oxygen limitation in compartment tests is proposed. This will aid to improve understanding of the fire behaviour in both test

environments. For applications in Alpert's correlation, an investigation of the variation in the k-factor with the distance away from the wall is proposed for future work

REFERENCES

Aire, C. (2014). *MSc. Thesis: Experimental and Numerical Modeling of Heat Transfer in Wall Assemblies.* Saskatoon: University of Saskatchewan.

Alpert, R. L. (1972). Calculation of Response Time of Ceiling-Mounted Fire Detectors. *Fire Technology, 8*(3), 181-195.

ANSYS. (2013). *ANSYS CFX-Solver Theory Guide.* Canonsburg, PA: ANSYS Inc.

ASTM. (2017a). *ASTM D3675: Standard Test Method for Surface Flammability of Flexible Cellular Materials Using a Radiant Heat Energy Source.* West Conshohocken, PA: ASTM International.

ASTM. (2017b). *ASTM E1354: Standard Test Method for Heat and Visible Smoke Release Rates for Materials and Products Using an Oxygen Consumption Calorimeter.* West Conshohocken, PA: ASTM International.

ASTM. (2017c). *ASTM E1590: Standard Test Method for Fire Testing of Mattresses.* West Conshohocken, PA: ASTM International.

ASTM. (2017d). *ASTM E2257: Standard Test Method for Room Fire Test of Wall and Ceiling Materials and Assemblies.* West Conshohocken, PA: ASTM International.

ASTM. (2017f). *ASTM E906: Standard Test Method for Heat and Visible Smoke Release Rates for Materials and Products Using a Thermopile Method.* West Conshohocken, PA: ASTM International.

ASTM. (2017g). *ASTM E1474: Standard Test Method for Determining the Heat Release Rate of Upholstered Furniture and Mattress Components or Composites Using a Bench Scale Oxygen Consumption Calorimeter.* West Conshohocken, PA: ASTM International.

ASTM. (2017h). *ASTM C518: Standard Test Method for Steady-State Thermal Transmission Properties by Means of the Heat Flow Meter Apparatus.* West Conshohocken, PA: ASTM International.

Babrauskas, V. (2016a). Heat Release Rates. In M. Hurley, *SFPE Handbook of Fire Protection Engineering* (5 ed., pp. 779-896). Greenbelt, MD: Springer.

Babrauskas, V. (2016b). The Cone Calorimeter. In M. Hurley, *SFPE Handbook of Fire Protection Engineering* (5 ed., pp. 952-978). Greenbelt, MD: Springer.

Baroudi, D., & Kokkala. (1992). *Analysis of Upward Flame Spread.* Espoo: VTT Publications.

Butler, K. (2009). A Model of Melting and Dripping Thermoplastic Objects in Fire. *11th International Fire and Materials Conference*, (pp. 341-352). San Francisco, CA.

Chivas, C., Guillaume, E., Sainrat, A., & Barbosa, V. (2009). Assessment of Risks and Benefits in the Use of Flame Retardants in Upholstered Furniture in Continental Europe. *Fire Safety Journal, 44*(5), 801-807.

Cleary, T. G., Ohlemiller, T. J., & Villa, K. (1992). *The Influence of Ignition Source on the Flaming Fire Hazard of Upholstered Furniture.* Gaithersburg, MD: NIST.

Dao, D. Q., Luche, J., Rogaume, T., Richard, F., Bustamante-Valencia, L., & Ruban, S. (2016). Polyamide 6 and Polyurethane Used as Liner for Hydrogen Composite Cylinder: An Estimation of Fire Behaviours. *Fire Technology, 52*(2), 397-420.

Delichatsios, M. A., Panagiotou, T., & Kiley, F. (1991). The Use of Time to Ignition Data for Characterizing the Thermal Inertia and the Minimum (Critical) Heat Flux for Ignition or Pyrolysis. *Combustion and Flame, 84*(3-4), 323-332.

Drysdale, D. (2011). *An Introduction to Fire Dynamics.* West Sussex, UK: John Wiley and Sons.

Enninful, E. (2006). *MSc. Thesis: Predicting Temperature Profiles in Soil During Simulated Forest Fires.* Saskatoon: University of Saskatchewan.

Evarts, B. (2011). *Home Mattress and Bedding Fires.* Quincy, MA: National Fire Protection Association.

Ezinwa, J. (2009). *MSc. Thesis: Modelling Full-Scale Fire Test Behaviour of Polyurethane Foams Using Cone Calorimeter Data.* Saskatoon: University of Saskatchewan.

Ezinwa, J. U., Torvi, D. A., & Weckman, E. J. (2009). Full-Scale Fire Modelling of Polyurethane Foams Using Cone Calorimeter Data. *Proceedings of Combustion Institute-Canadian Section.* Montréal, QC: Combustion Institute-Canadian Section.

FLIR System. (2016). *FLIR T650sc - Portable Thermal Imaging Camera.* Burlington, ON: FLIR Systems, Inc.

Fulton, M., Torvi, D., & Weckman, E. (2016). Evaluation of Ceiling Temperatures Predicted Using Furniture Calorimeter Fire Test Data. *Proceedings of Combustion Institute-Canadian Section.* Waterloo, ON: Combustion Institute-Canadian Section.

Hadden, R., Alkatib, A., Rein, G., & Torero, J. L. (2014). Radiant Ignition of Polyurethane Foam: The Effect of Sample Size. *Fire Technology, 50*, 673-691.

Hilado, C. J. (1968). Flame Retardant Urethane Foams. *Journal of Cellular Plastics, 4*(9), 339-344.

Hurd, M., Torvi, D. A., Weckman, E. J., & Enninful, E. (2007). Small and Full-Scale Testing of Polyurethane Foams for Mattress. *Proceedings of Combustion Institute-Canadian Section.* Banff, AB: Combustion Institute-Canadian Section.

Incropera, F., Dewitt, D., Bergman, T., & Lavine, A. (2007). *Fundamentals of Heat and Mass Transfer* (6th ed.). Hoboken, NJ: John Wiley & Sons.

ISO. (2015a). *ISO 5660-1: Reaction-to-Fire Tests-Heat Release, Smoke Production and Mass Loss Rate.* Geneva: International Organization for Standardization.

ISO. (2016b). *ISO 9705: Full-scale Room Test for Surface Products.* Geneva: International Organization for Standardization.

Janssens, M. (2016). Calorimetry. In Hurley, *SFPE Handbook of Fire Protection Engineering* (5 ed., pp. 905-946). Greenbelt, MD: Springer.

Kashiwagi, T. (1994). Polymer Combustion and Flammability - Role of the Condensed Phase. *Twenty-Fifth Symposium (International) on Combustion/The Combustion Institute* (pp. 1423-1437). Pittsburgh, PA: The Combustion Institute.

Kashiwagi, T., & Ohlemiller, T. (1982). A Study of Oxygen Effects on Non Flaming Transient Gasification of PMMA and PE During Thermal Irradiation. *Nineteenth Symposium (International) on Combustion* (pp. 815-823). Pittsburgh, PA: The Combustion Institute.

Kerber, S. (2012). *Analysis of Changing Residential Fire Dynamics and Its Implications on Firefighter Operational Timeframes.* Northbrook, IL: Underwriters Laboratories (UL).

Kramer, R. H., Zammarano, M., Linteris, G. T., Gedde, U. W., & Gilman, J. W. (2010). Heat Release and Structural Collapse of Flexible Polyurethane Foam. *Polymer Degradation and Stability, 95*(6), 1115–1122.

LaserComp. (2004). *FOX200 and FOX300 Series Instrument Manual and Guide.* Saugis, MA: LaserComp.

Lawson, R. (2012). SFPE classic paper review: A review of classic work by Dr William J. Parker on heat release rate measurements by oxygen consumption. *Journal of Fire Protection Engineering, 22*(1), 5-9.

Levin, B. C., Paabo, M., Gurman, J. L., & Harris. (1987). Effects of Exposure to Single or Multiple Combinations of the predominant Toxic Gases and Low Oxygen Atmospheres Produced in Fires. *Toxicological Sciences, 9*, 236-250.

McGrattan, K., Hostikka, S., McDermott, R., Floyd, J., Weinschenk, C., & Overholt, K. (2013). *Fire Dynamics Simulator User Guide.* Maryland: NIST.

Mikkola, E., & Wichman, I. (1989). On the Thermal Ignition of Combustible Materials. *Fire and Materials*(14), 87-96.

National Fire Protection Association. (2004a). *NFPA 271: Standard Method of Test for Heat and Visible Smoke Release Rates for Materials and Products Using an Oxygen Consumption Calorimeter.* Quincy, MA: National Fire Protection Association.

National Fire Protection Association. (2005b). *NFPA 92B: Standard for Smoke Management Systems in Malls, Atria, and Large Spaces.* Quincy, MA: National Fire Protection Association.

NFPA. (2019). *NFPA 72 - National Fire Alarm and Signaling Code.* Quinc, MA: National Fire Protection Association.

Obach, M. (2011). *MSc. Thesis: Effects of Initial Fire Attack Suppression Tactics on the Firefighter and Compartment Environment.* Waterloo, ON: University of Waterloo.

Ohlemiller, T. (1985). Modeling of Smoldering Combustion Propagation. *Progress in Energy and Combustion Science* (pp. 277-310). Gaithersburg, MD: Elsevier Ltd.

Pau, D. S., Fleischmann, C. M., Spearpoint, M. J., & Li, K. Y. (2014). Thermophysical Properties of Polyurethane Foams and their Melts. *Fire and Materials*, 433-450.

Pitts, W. (2014). Role of Two Stage Pyrolysis in Fire Growth on Flexible Polyurethane Foam Slabs. *Fire and Materials, 38,* 323-338.

Polyurethane Foam Association. (2016a). *INTOUCH: Flexible Polyurethane Foam - A Primer.* London, TN: Polyurethane Foam Association.

Polyurethane Foam Association. (2016b). *INTOUCH: Information on Flexible Polyurethane Foam.* Wayne, NJ: Polyurethane Foam Association.

Prasad, K., Kramer, R., Marsh, N., Nyden, M., Ohlemiller, T., & Zammarano, M. (2009). Numerical Simulation of Fire Spread on Polyurethane Foam Slabs. *11th International Fire and Materials Conference,* (pp. 697-708). San Francisco, CA.

Purser, D. (2010). *Asphyxiant Components of the Fire Effluents.* Cambridge: Woodhead Publishing.

Putzeys, O., Fernandez-Pello, C., Rein, G., & Urban, D. (2008). The piloted transition to flaming in smoldering fire retarded and non-fire retarded polyurethane foam. *Fire and Materials, 32*, 485-499.

Ravey, M., & Pierce, E. (1997). Flexible Polyurethane Foam. 1. Thermal Decomposition of a Polyether-Based, Water-Blown Commercial Type of Flexible Polyurethane Foam. *Journal of Applied Polymer Science, 63,* 47.

Rezazadeh, M. (2014). *PhD Thesis: Evaluation of Performance of in-use Firefighters' Protective Clothing using Non-Destructive Tests.* Saskatoon, SK: University of Saskatchewan.

Robson, L. (2014). *MSc. Thesis: Scalability of Cone Calorimeter Test Results for The Prediction of Full Scale Fire Behavior of Polyurethane Form.* Saskatoon, SK: University of Saskatchewan.

Robson, L. D., Obach, M. R., Ezinwa, J. U., Torvi, D. A., & Weckman, E. J. (2010). Effects of Polyurethane Foam Thickness on Flame Spread and Heat Release Rates in Furniture Calorimeter Tests. *Proceedings of Combustion Institute - Canadian Section.* Ottawa, ON: Combustion Institute-Canadian Section.

Robson, L., Torvi, D., Obach, M., & Weckman, E. (2014). Effects of Variations in Incident Heat Flux when Using Cone Calorimeter Test Data for Prediction of Full-Scale Heat Release Rates of Polyurethane Foam. *Fire and Materials, 40*, 89-113.

Saber, H., Kashef, A., Bwalya, A., & Lougheed, G. (2010). *Numerical and Experimental Investigations of Fire Behaviour due to Polyurethane Foam and Wood Cribs in a Medium-Sized Residential Room.* Ottawa, ON: National Research Council of Canada.

Scott, S. N., Dodd, A. B., Larsen, M. E., Suo-Anttila, J. M., & Erickson, K. L. (2016). Validation of Heat Transfer, Thermal Decomposition, and Container Pressurization of Polyurethane Foam Using Mean Value and Latin Hypercube Sampling Approaches. *Fire Technology*, 121-147.

Standards Council of Canada. (2013). *CAN/CGSB-4.2 No/No 27.7-2013 Textile Test Methods Combustion Resistance of Mattresses - Cigarette Test.* Ottawa, ON: Standards Council of Canada.

Statistics Canada. (2017). *Fire Statistics in Canada, Selected Observations from the National Fire Information Database 2005 to 2014.* Canadian Centre for Justice Statistics. Ottawa: Statistics Canada.

Steckler, K. (2001). Estimation of Rate of Heat Release by Means of Oxygen Consumption Measurements. In D. Lide, *A Century of Excellence in Measurements, Standards, and Technology* (pp. 280-282). Gaithersburg, MD: National Institute of Standards and Technology.

Stephenson, D. G. (1959). *St. Lawrence Burns.* Ottawa, ON: National Research Council Canada.

Su, J. (2002). Fire Detection and Suppression Studies at Kemano Village. *Sixth Fire Suppression and Detection Research Application Symposium.* Tampa, FL: National Research Council.

Sundstrom, B. (1996). *CBUF: Fire Safety of Upholstered Furniture: The Final Report on the CBUF Research Programme.* London, UK: European Commission Measurements and Testing.

Taylor, R., Groot, H., & Ferrier, J. (1998). *Thermophysical Properties of Two Foams.* West Lafayette, IN: Thermophysical Properties Res. Lab.

Threlfall, T. G., & Torvi, D. A. (2005). Temperature Measurements in Full-Scale Fire Tests of Mattresses. *Proceedings of Combustion Institute - Canadian Section.* Saskatoon, SK: Combustion Institute Canadian Section.

Threlfall, T. G., & Torvi, D. A. (2006). Comparison of Predicted and Measured Temperatures in Fire Tests of Mattresses. *Proceedings of Combustion Institute - Canadian Section.* Waterloo, ON: Combustion Institute-Canadian Section.

Torvi, D. (1992). *MSc. Thesis: A Finite Element Model of Heat Transfer in Skin Subjected to a Flash Fire.* Edmonton: University of Alberta.

Torvi, D. (1997). *PhD Thesis: Heat Transfer in Thin Fibrous Materials Under High Heat Flux Conditions.* Edmonton: University of Alberta.

U.S. Consumer Product Safety Commission. (2011). *16 CFR Part 1633: Standard for the Flammability (Open Flame) of Mattress Sets.* Bethesda, MA: Code of Federal Regulations (CFR).

U.S. Consumer Product Safety Commission. (2014). *16 CFR Part 1632: Standard for the Flammability of Mattresses and Mattress Pads.* Bethesda, Maryland: Code of Federal Regulations.

Underwriters Laboratories of Canada. (2017). *CAN/ULC-S137: Standard Method of Test for Fire Growth in Mattresses (Open Flame Test).* Toronto, ON: Underwriters Laboratories of Canada.

Valencia, L. B. (2009). *PhD Thesis: Experimental and Numerical Investigation of the Thermal Decomposition of Materials at Three Scales: Application to Polyether Polyurethane Foam used in Upholstered Furniture.* Edinburgh: University of Edinburgh.

Valencia, L. B., Rogaume, T., & Guillaume, E. (2009). New Method for Simulating the Kinetic of Toxic Gases Production of Upholstered Furniture Fire. *Proceedings of the 11th International Conference on Fire and Materials* (pp. 685-695). San Francisco, CA: Interscience Communications Limited, London, England.

Weng, W. G., & Hasemi, Y. (2008). A numerical model for flame spread along combustible flat solid with charring material with experimental validation of ceiling flame spread and upward flame spread. *Fire and Materials*(32), 87-102.

Wickstrom, U. G. (1992). Full-Scale/Bench-Scale Correlations of Wall and Ceiling Linings. *Fire and Materials*(16), 15-22.

William, W., Douglas, C., & Christopher, W. (2016). Zone Computer Fire Models for Enclosures. In M. Hurley, *SFPE Handbook of Fire Protection Engineering* (pp. 1024 - 1032). Greenbelt, MD: Springer.

Wilson, M. T., Dlugogorski, B. Z., & Kenedy, E. Z. (2003). Uniformity of Radiant Heat Fluxes in Cone Calorimeter. *Proceedings Seventh International Symposium on Fire Safety Science*, (pp. 815-827).

Witkowski, A., Stec, A., & Hull, R. (2016). Thermal Decomposition of Polymeric Materials. In SFPE, & M. J. Hurley (Ed.), *SFPE Handbook of Fire Protection Engineering* (5 ed., pp. 167-254). Greenbelt, MD: Springer.

Yuen, R., Yeoh, G., de Vahl, D., & Leonardi, E. (2007). Modelling the Pyrolysis of Wet Wood – II. Three-dimensional Cone Calorimeter Simulation. *International Journal of Heat and Mass Transfer, 50*, 4387-4399.

APPENDIX A: SMALL-SCALE THERMOCOUPLE MEASUREMENTS

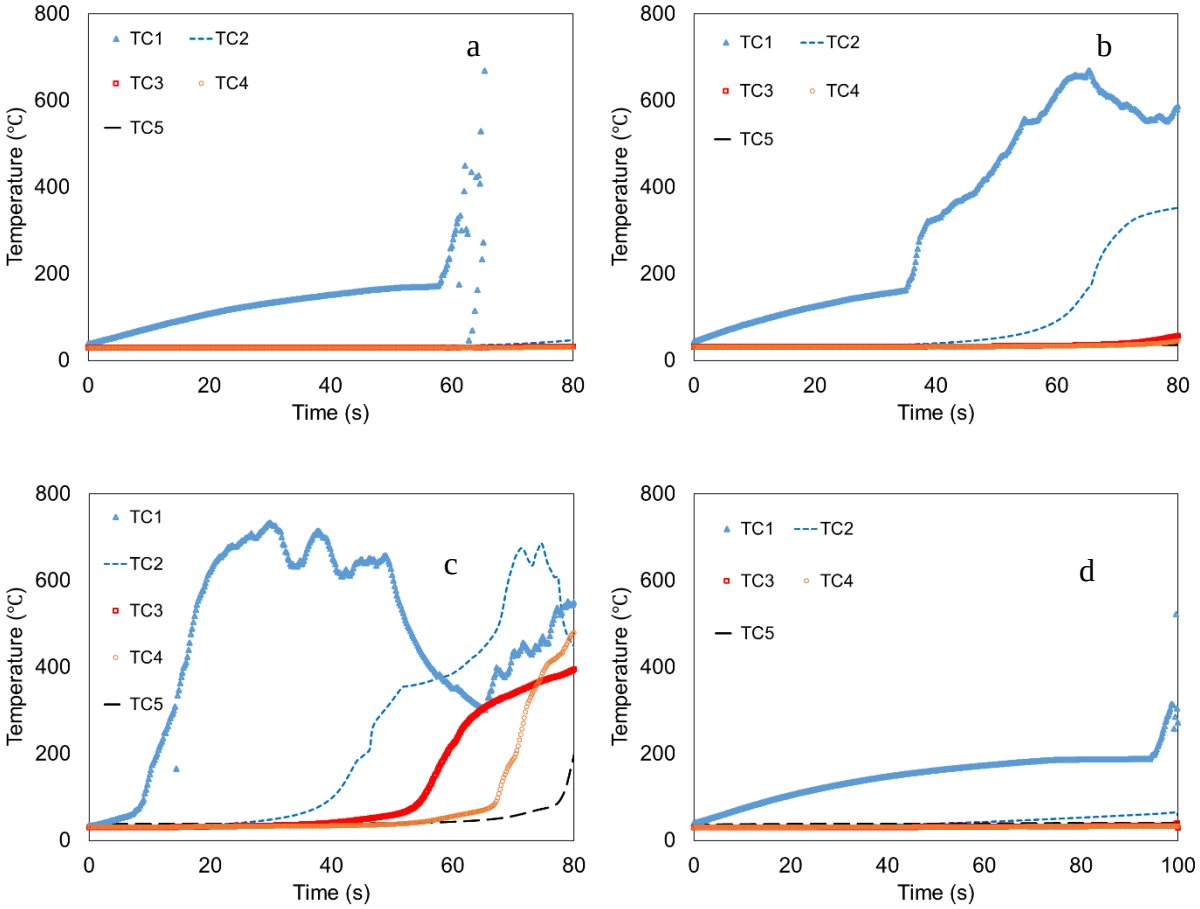

Figure A-1: Temperature Measurements During Combustion of 10 cm Polyurethane Specimens for 5 kW/m^2 Heat Flux Exposure
(a - Experiment 4-5-1, b - Experiment 4-5-3, c - Experiment 4-5-22, d - Experiment 4-5-33)

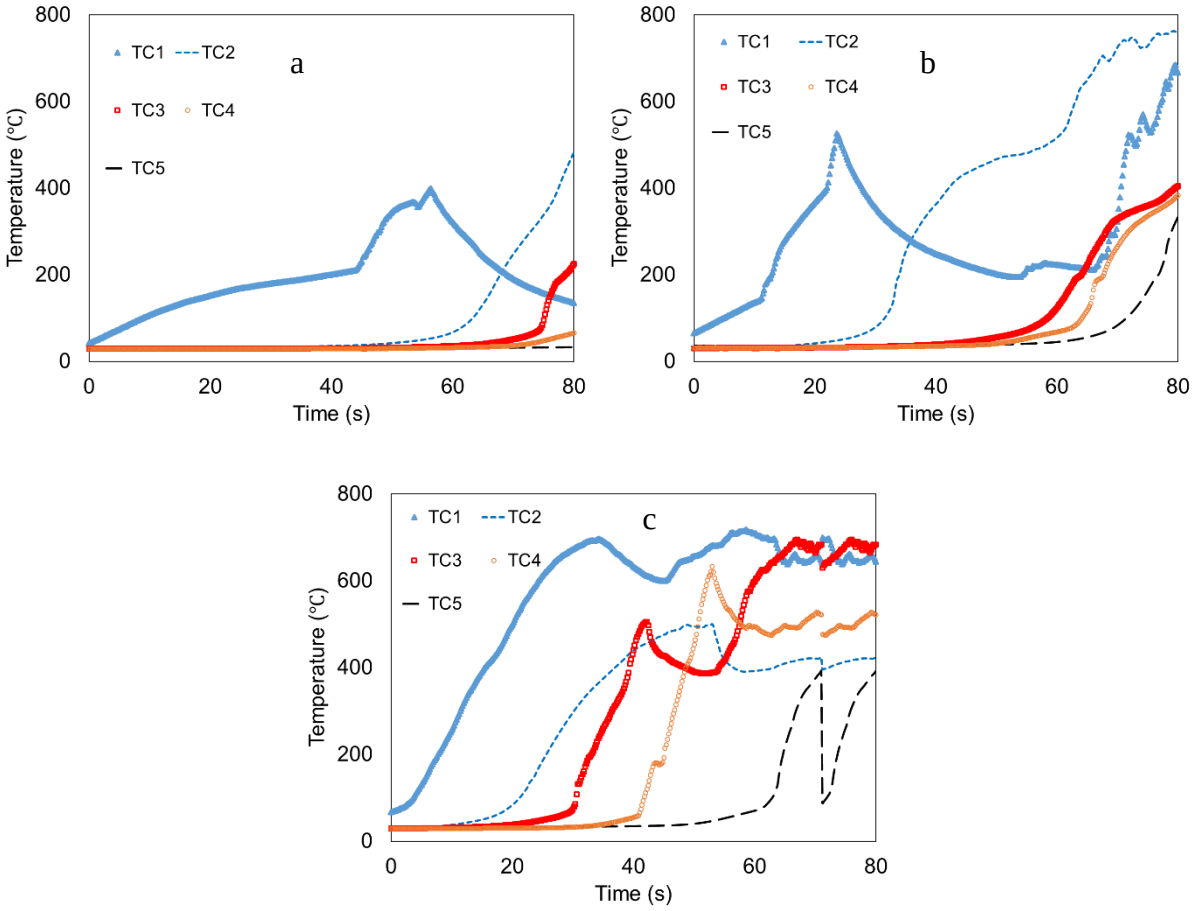

Figure A-2: Temperature Measurements During Combustion of 10 cm Polyurethane Specimens for 10 kW/m^2 Heat Flux Exposure
(a - Experiment 4-10-1, b - Experiment 4-10-2, c - Experiment 4-10-3)

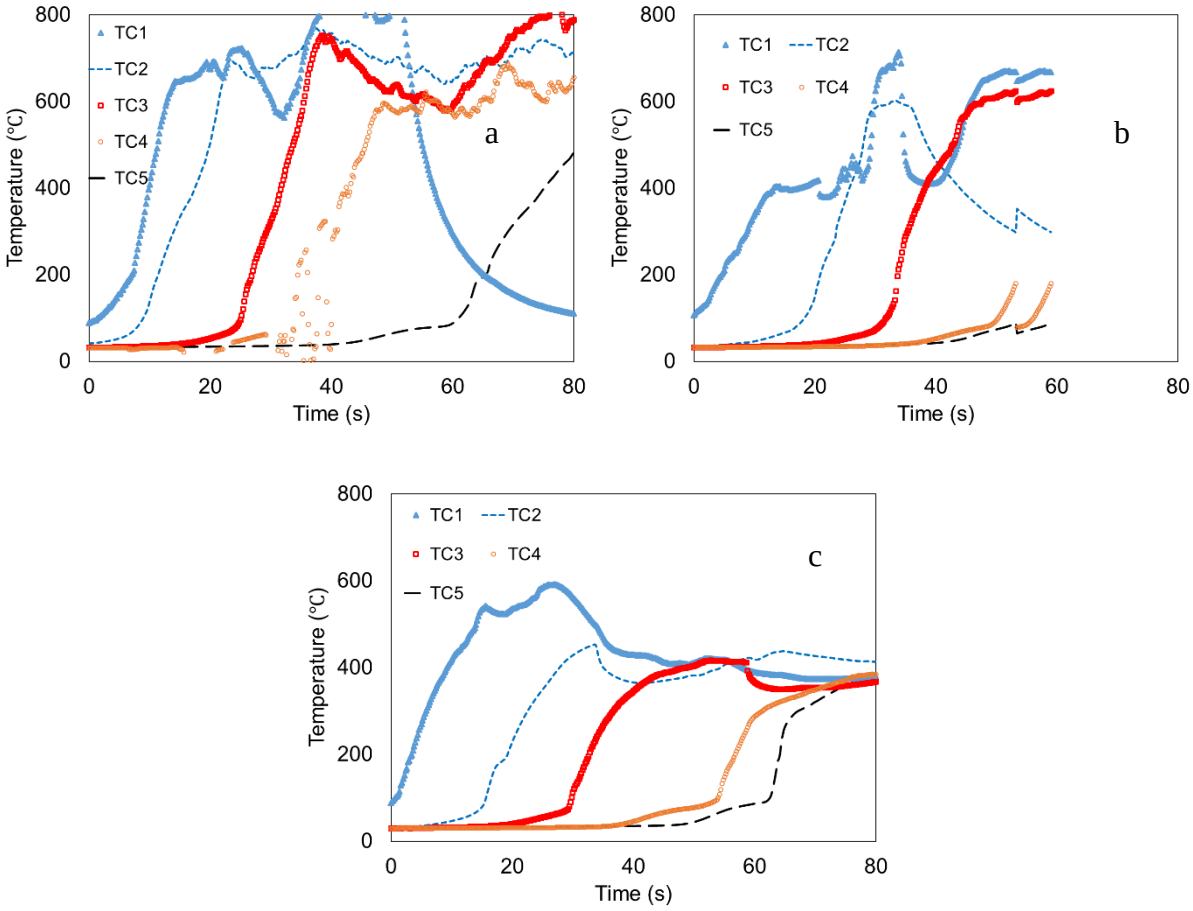

Figure A-3: Temperature Measurements During Combustion of 10 cm Polyurethane Specimens for 20 kW/m^2 Heat Flux Exposure
(a - Experiment 4-20-1, b - Experiment 4-20-2, c - Experiment 4-20-3)

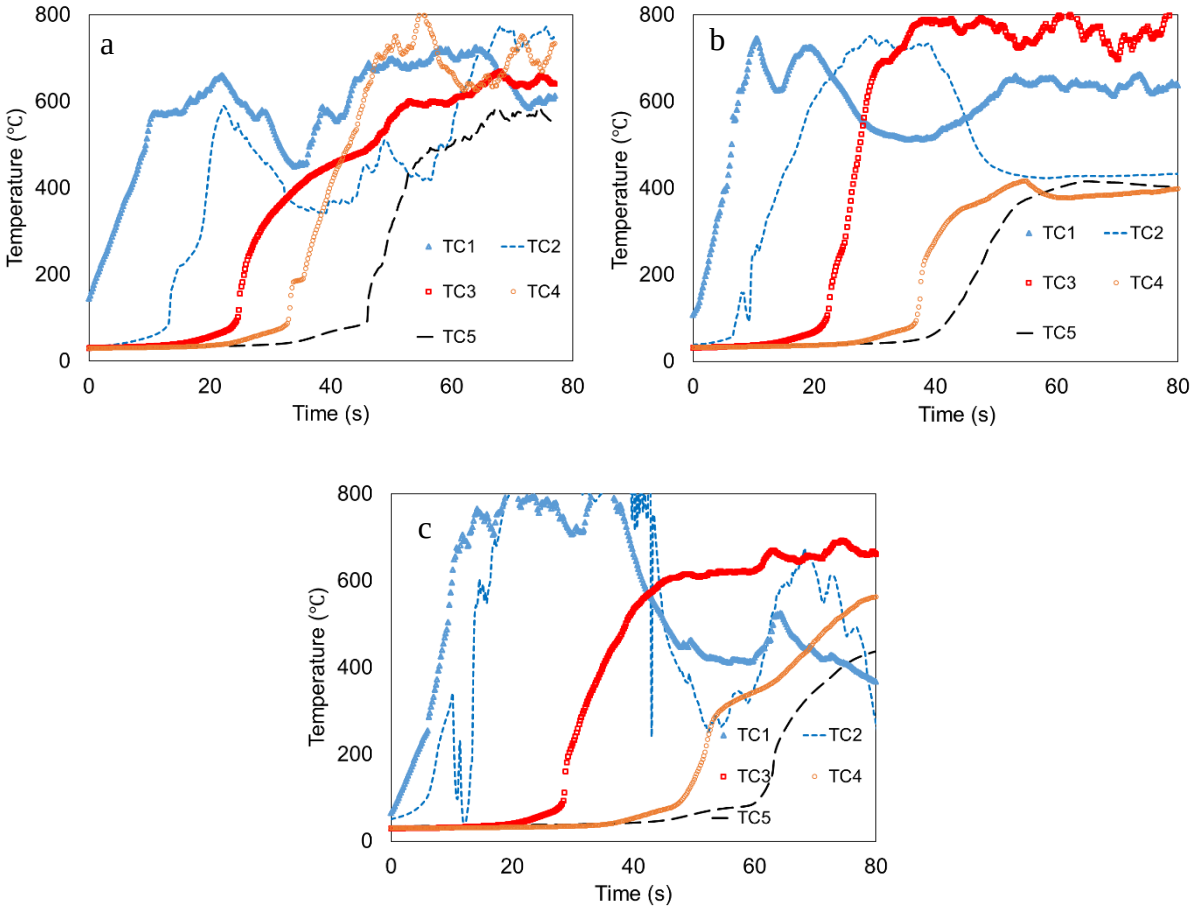

Figure A-4: Temperature Measurements During Combustion of 10 cm Polyurethane Specimens for 35 kW/m^2 Heat Flux Exposure
(a - Experiment 4-35-1, b - Experiment 4-35-2, c - Experiment 4-35-3)

APPENDIX B: IGNITION TIMES FOR CONE CALORIMETER POLYURETHANE FOAM TEST

Ignition times were reported for cone calorimeter tests conducted during this research and previous University of Saskatchewan cone calorimeter test (Robson, 2014). The methodology for determining ignition time is detailed in Section 2.7.

Table A-1: Ignition Times of the Polyurethane Foam Specimens at 5 kW/m^2 Heat Flux Exposure

Heat Flux (kW/m²)	Ignition Time (s)
5	116.0
5	97.0
5	180.0
5	287.0
5	147.0
5	135.0
5	72.0

Table A-2: Ignition Times of the Polyurethane Foam Specimens at 10 kW/m^2 Heat Flux Exposure

Heat Flux (kW/m²)	Ignition Time (s)
10	46.0
10	46.0
10	28.0
10	30.0

Table A-3: Ignition Times of the Polyurethane Foam Specimens at 15 kW/m^2 Heat Flux Exposure

Heat Flux (kW/m²)	Ignition Time (s)
15	17.0
15	18.0
15	14.0

Table A-4: Ignition Times of the Polyurethane Foam Specimens at 20 kW/m^2 Heat Flux Exposure

Heat Flux (kW/m²)	Ignition Time (s)
20	8.0
20	7.1
20	4.2

Table A-5: Ignition Times of the Polyurethane Foam Specimens at 25 kW/m^2 Heat Flux Exposure

Heat Flux (kW/m²)	Ignition Time (s)
25 (Robson)	3.9
25 (Robson)	4.0
25 (Robson)	4.1
25 (Robson)	5.0
25 (Robson)	3.7
25 (Robson)	4.7
25 (Robson)	3.7
25 (Robson)	3.7
25 (Robson)	4.7

Table A-6: Ignition Times of the Polyurethane Foam Specimens at 35 kW/m^2 Heat Flux Exposure

Heat Flux (kW/m²)	Ignition Time (s)
35	2.0
35	2.0
35	2.0
35	2.0
35	2.0
35 (Robson)	1.8
35 (Robson)	1.6
35 (Robson)	2.1
35 (Robson)	2.1
35 (Robson)	2.4
35 (Robson)	2.6
35 (Robson)	1.4
35 (Robson)	2.9
35 (Robson)	2.4
35 (Robson)	1.7

Table A-7: Ignition Times of the Polyurethane Foam Specimens at 50 kW/m^2 Heat Flux Exposure

Heat Flux (kW/m²)	Ignition Time (s)
50	1.0
50 (Robson)	1.3
50 (Robson)	0.8
50 (Robson)	1.1
50 (Robson)	1.0
50 (Robson)	1.3
50 (Robson)	1.2
50 (Robson)	1.4
50 (Robson)	1.4
50 (Robson)	1.1
50 (Robson)	1.0

Table A-8: Ignition Times of the Polyurethane Foam Specimens at 75 kW/m^2 Heat Flux Exposure

Heat Flux (kW/m²)	Ignition Time (s)
75 (Robson)	0.4
75 (Robson)	0.5
75 (Robson)	0.7
75 (Robson)	0.7
75 (Robson)	0.7
75 (Robson)	0.6
75 (Robson)	0.8
75 (Robson)	0.6
75 (Robson)	0.6
75 (Robson)	0.6
75 (Robson)	0.5

APPENDIX C: SMALL-SCALE HEAT TRANSFER MODEL EXCEL CODE

```
Module1 - 1

Sub Button8_Click()

'INPUT PARAMETERS AND VARIABLES

    Dim TempC As Double
        TempC = Sheets("Semi").Range("B3").Value    'Cone Temperature

    Dim TempA As Double
        TempA = Sheets("Semi").Range("B4").Value    'Ambient Temperature


    Dim Rhoi As Double
        Rhoi = Sheets("Semi").Range("B11").Value    'Initial Density

    Dim Rhop As Double
        Rhop = Sheets("Semi").Range("E11").Value    'Density at previous timestep

    Dim Rho As Double
        Rho = Rhoi                                  'Density at current timestep

    Dim L As Double
        L = Sheets("Semi").Range("B12").Value       'Foam Thickness

    Dim TC As Integer
        TC = Sheets("Semi").Range("B14").Value      'Grid number


    Dim pi As Double
        pi = Sheets("Semi").Range("B17").Value       'Pi

    Dim dt As Double
        dt = Sheets("Semi").Range("B18").Value       'Time Step

    Dim sig As Double
        sig = Sheets("Semi").Range("B19").Value      'Stephan-Boltzmann constant

    Dim VF As Double
        VF = Sheets("Semi").Range("B20").Value       'View Factor

    Dim E As Double
        E = Sheets("Semi").Range("B21").Value        'Emissivity


    Dim cpRT As Double
        cpRT = Sheets("Semi").Range("B24").Value     'Specific Heat

    Dim cpRTp As Double
        cpRTp = Sheets("Semi").Range("E24").Value    'Specific Heat at Room Temperature

    Dim cpSlope As Double
        cpSlope = Sheets("Semi").Range("B25").Value  'Slope of Specific Heat

    Dim rhoSlope As Double
        rhoSlope = Sheets("Semi").Range("B27").Value 'Slope of Density

    Dim ki As Double
        ki = Sheets("Semi").Range("B28").Value       'Thermal Conductivity at Room Temperature

    Dim kp As Double
        kp = Sheets("Semi").Range("E28").Value       'Thermal Conductivity at previous timestep

    Dim h As Double
        h = Sheets("Semi").Range("B30").Value        'Convective Heat Coefficient

    Dim tg As Double
        tg = Sheets("Semi").Range("B32").Value       'Simulation Runtime
```

```
'DEFINITIONS

    Dim k As Double
        k = ki

    Dim xl As Double
        xl = L / (TC)

    Dim t As Double
        t = 0

    Dim x As Double

    Dim cp As Double
        cp = cpRT

    Dim Temp As Double
        Temp = TempA

    Dim TempP As Double
        TempP = TempA

    Dim alpha As Double

    Dim n As Integer
        n = 2

    Dim b As Integer
        b = 2

    Dim m As Double

    Dim stab As Double

    Dim Fo As Double

    Dim kf As Double
        kf = k

    Dim kb As Double
        kb = k

    Dim TempPb As Double
        TempPb = TempA

    Dim TempPf As Double
        TempPf = TempA


'VARIABLE PROPERTIES CALCULATION

Do Until t > tg

        x = 0
        b = 2
        m = TC + 4

        Sheets("FDM").Cells(n, 1).Value = t
        Sheets("FDMR").Cells(n, 1).Value = t
        Sheets("CP").Cells(n, 1).Value = t
        Sheets("K").Cells(n, 1).Value = t
        Sheets("Rho").Cells(n, 1).Value = t

    Do Until x > L

        Sheets("FDM").Cells(1, b).Value = x
        Sheets("FDMR").Cells(1, b).Value = x
```

```
            If t = 0 Then

                Temp = TempA
                Sheets("FDM").Cells(n, b).Value = (Temp - 273)
                Sheets("FDMR").Cells(n, b).Value = (Temp - TempA)
                Sheets("CP").Cells(n, b).Value = cp
                Sheets("CP").Cells(n, m).Value = (TempP - 273)
                Sheets("K").Cells(n, b).Value = k
                Sheets("K").Cells(n, m).Value = (TempP - 273)
                Sheets("Rho").Cells(n, b).Value = Rho
                Sheets("Rho").Cells(n, m).Value = (TempP - 273)

            ElseIf t > 0 Then

                TempP = (Sheets("FDM").Cells(n - 1, b).Value) + 273

                If TempP > Trecl Then

                Rho = (Rhop)
                cp = (cpRTp)
                k = (kp)
                Sheets("Rho").Cells(n, b).Value = Rho
                Sheets("Rho").Cells(n, m).Value = (TempP - 273)
                Sheets("CP").Cells(n, b).Value = cp
                Sheets("CP").Cells(n, m).Value = (TempP - 273)
                Sheets("K").Cells(n, b).Value = k
                Sheets("K").Cells(n, m).Value = (TempP - 273)

                Else

                'Density

                    Rho = (rhoSlope * (TempP - TempA) + Rhoi)

                    Sheets("Rho").Cells(n, b).Value = Rho
                    Sheets("Rho").Cells(n, m).Value = (TempP - 273)

                'Specific Heat equation

                    cp = (cpRT + cpSlope * (TempP - TempA))

                    Sheets("CP").Cells(n, b).Value = cp
                    Sheets("CP").Cells(n, m).Value = (TempP - 273)

                'Thermal Conductiity equation

                    k = ((0.00007 * (TempP - TempA)) + ki)

                    Sheets("K").Cells(n, b).Value = k
                    Sheets("K").Cells(n, m).Value = (TempP - 273)

               End If

'HEAT TRANSFER CALCULATION

If x = 0 Then

    TempPf = (Sheets("FDM").Cells(n - 1, b + 1).Value) + 273

    Fo = (k * dt) / (Rho * cp * (xl ^ 2))

    stab = Fo * (1 + ((h * xl) / k) + ((E * sig * xl) / k) * ((TempP ^ 4) / TempP))

    Sheets("Semi").Range("B38").Value = stab

    If stab > 0.5 Then

    Sheets("Semi").Range("B39").Value = stab

    End If

    Temp = ((2 * Fo) * ((TempPf - TempP) + ((xl / k) * (VF * E * sig * (TempC ^ 4 - TempP ^ 4)))
    - ((xl / k) * (1 - VF) * E * sig * (TempP ^ 4 - TempA ^ 4))
    - ((xl / k) * (h * (TempP - TempA))))) + TempP

    Sheets("FDM").Cells(n, b).Value = (Temp - 273)
    Sheets("FDMR").Cells(n, b).Value = (Temp - TempA)
```

```
ElseIf x >= L - xl Then

        Temp = TempA

        Sheets("FDM").Cells(n, b).Value = (Temp - 273)
        Sheets("FDMR").Cells(n, b).Value = (Temp - TempA)

ElseIf x <= L Then

    TempPb = (Sheets("FDM").Cells(n - 1, b - 1).Value) + 273

    TempPf = (Sheets("FDM").Cells(n - 1, b + 1).Value) + 273

    Temp = TempP + (((k * dt) / (Rho * cp * xl * xl)) * (TempPf - (2 * TempP) + TempPb))

        Sheets("FDM").Cells(n, b).Value = (Temp - 273)
        Sheets("FDMR").Cells(n, b).Value = (Temp - TempA)

 End If

End If

    b = b + 1

    x = x + xl

    m = m + 1

    Loop

        t = t + dt

        n = n + 1

    Loop
End Sub
```

APPENDIX D: PERMISIONS TO REPRODUCE

Permission for Figure 1 1: Structure of Polyurethane

SPRINGER NATURE LICENSE TERMS AND CONDITIONS

Oct 27, 2019

This Agreement between Department of Mechanical Engineering ("You") and Springer Nature ("Springer Nature") consists of your license details and the terms and conditions provided by Springer Nature and Copyright Clearance Center.

License Number	4435150011625
License date	Sep 24, 2018
Licensed Content Publisher	Springer Nature
Licensed Content Publication	Springer eBook
Licensed Content Title	Thermal Decomposition of Polymeric Materials
Licensed Content Author	Artur Witkowski, Anna A. Stec, T. Richard Hull
Licensed Content Date	Jan 1, 2016
Type of Use	Thesis/Dissertation
Requestor type	academic/university or research institute
Format	print and electronic
Portion	figures/tables/illustrations
Number of figures/tables/illustrations	1
Will you be translating?	no
Circulation/distribution	<501
Author of this Springer Nature content	no
Title	Modelling Flame Spread For Polyurethane Foam
Instructor name	Prof. David Torvi
Institution name	University of Saskatchewan
Expected presentation date	Dec 2018
Portions	Table 7.1
Requestor Location	Department of Mechanical Engineering University of Saskatchewan 105 Administration Place Saskatoon, SK S7N 5A2 Canada Attn: Department of Mechanical Engineering
Billing Type	Invoice
Billing Address	Department of Mechanical Engineering University of Saskatchewan 105 Administration Place Saskatoon, SK S7N 5A2 Canada Attn: Department of Mechanical Engineering
Total	**0.00 USD**
Terms and Conditions	

Springer Nature Terms and Conditions for RightsLink Permissions

Springer Nature Customer Service Centre GmbH (the Licensor) hereby grants you a non-exclusive, world-wide licence to reproduce the material and for the purpose and requirements specified in the attached copy of your order form, and for no other use, subject to the conditions below:

1. The Licensor warrants that it has, to the best of its knowledge, the rights to license reuse of this material. However, you should ensure that the material you are requesting is original to the Licensor and does not carry the copyright of another entity (as credited in the published version).

   If the credit line on any part of the material you have requested indicates that it was reprinted or adapted with permission from another source, then you should also seek permission from that source to reuse the material.

2. Where **print only** permission has been granted for a fee, separate permission must be obtained for any additional electronic re-use.

3. Permission granted **free of charge** for material in print is also usually granted for any electronic version of that work, provided that the material is incidental to your work as a whole and that the electronic version is essentially equivalent to, or substitutes for, the print version.

4. A licence for 'post on a website' is valid for 12 months from the licence date. This licence does not cover use of full text articles on websites.

5. Where **'reuse in a dissertation/thesis'** has been selected the following terms apply: Print rights of the final author's accepted manuscript (for clarity, NOT the published version) for up to 100 copies, electronic rights for use only on a personal website or institutional repository as defined by the Sherpa guideline (www.sherpa.ac.uk/romeo/).

6. Permission granted for books and journals is granted for the lifetime of the first edition and does not apply to second and subsequent editions (except where the first edition permission was granted free of charge or for signatories to the STM Permissions Guidelines http://www.stm-assoc.org/copyright-legal-affairs/permissions/permissions-guidelines/), and does not apply for editions in other languages unless additional translation rights have been granted separately in the licence.

7. Rights for additional components such as custom editions and derivatives require additional permission and may be subject to an additional fee. Please apply to Journalpermissions@springernature.com/bookpermissions@springernature.com for these rights.

8. The Licensor's permission must be acknowledged next to the licensed material in print. In electronic form, this acknowledgement must be visible at the same time as the figures/tables/illustrations or abstract, and must be hyperlinked to the journal/book's homepage. Our required acknowledgement format is in the Appendix below.

9. Use of the material for incidental promotional use, minor editing privileges (this does not include cropping, adapting, omitting material or any other changes that affect the meaning, intention or moral rights of the author) and copies for the disabled are permitted under this licence.

10. Minor adaptations of single figures (changes of format, colour and style) do not require the Licensor's approval. However, the adaptation should be credited as shown in Appendix below.

Appendix — Acknowledgements:

For Journal Content:
Reprinted by permission from [**the Licensor**]: [**Journal Publisher** (e.g. Nature/Springer/Palgrave)] [**JOURNAL NAME**] [**REFERENCE CITATION** (Article name, Author(s) Name), [**COPYRIGHT**] (year of publication)

For **Advance Online Publication papers:**
Reprinted by permission from [**the Licensor**]: [**Journal Publisher** (e.g. Nature/Springer/Palgrave)] [**JOURNAL NAME**] [**REFERENCE CITATION** (Article name, Author(s) Name), [**COPYRIGHT**] (year of publication), advance online publication, day month year (doi: 10.1038/sj.[JOURNAL ACRONYM].)

For Adaptations/Translations:
Adapted/Translated by permission from [**the Licensor**]: [**Journal Publisher** (e.g. Nature/Springer/Palgrave)] [**JOURNAL NAME**] [**REFERENCE CITATION** (Article name, Author(s) Name), [**COPYRIGHT**] (year of publication)

Note: For any republication from the British Journal of Cancer, the following credit line style applies:

Reprinted/adapted/translated by permission from [**the Licensor**]: on behalf of Cancer Research UK: : [**Journal Publisher** (e.g. Nature/Springer/Palgrave)] [**JOURNAL NAME**] [**REFERENCE CITATION** (Article name, Author(s) Name),

Permission for Figure 1 2: Thermal Decomposition of Polyurethane Foam

JOHN WILEY AND SONS LICENSE TERMS AND CONDITIONS

Oct 27, 2019

This Agreement between Department of Mechanical Engineering ("You") and John Wiley and Sons ("John Wiley and Sons") consists of your license details and the terms and conditions provided by John Wiley and Sons and Copyright Clearance Center.

License Number	4435420697633
License date	Sep 24, 2018
Licensed Content Publisher	John Wiley and Sons
Licensed Content Publication	Wiley Books
Licensed Content Title	Fire Science and Combustion
Licensed Content Date	Jul 11, 2011
Licensed Content Pages	34
Type of Use	Dissertation/Thesis
Requestor type	University/Academic
Format	Print and electronic
Portion	Figure/table
Number of figures/tables	1
Original Wiley figure/table number(s)	Fig 1.3
Will you be translating?	No
Title of your thesis / dissertation	Modelling Flame Spread For Polyurethane Foam
Expected completion date	Dec 2018
Expected size (number of pages)	1
Requestor Location	Department of Mechanical Engineering University of Saskatchewan 105 Administration Place Saskatoon, SK S7N 5A2 Canada Attn: Department of Mechanical Engineering
Publisher Tax ID	EU826007151
Total	**0.00 USD**
Terms and Conditions	

TERMS AND CONDITIONS

This copyrighted material is owned by or exclusively licensed to John Wiley & Sons, Inc. or one of its group companies (each a"Wiley Company") or handled on behalf of a society with which a Wiley Company has exclusive publishing rights in relation to a particular work (collectively "WILEY"). By clicking "accept" in connection with completing this licensing transaction, you agree that the following terms and conditions apply to this transaction (along with the billing and payment terms and conditions established by the Copyright Clearance Center Inc., ("CCC's Billing and Payment terms and conditions"), at the time that you opened your RightsLink account (these are available at any time at http://myaccount.copyright.com).

Terms and Conditions

- The materials you have requested permission to reproduce or reuse (the "Wiley Materials") are protected by copyright.

- You are hereby granted a personal, non-exclusive, non-sub licensable (on a stand-alone basis), non-transferable, worldwide, limited license to reproduce the Wiley Materials for the purpose specified in the licensing process. This license, **and any CONTENT (PDF or image file) purchased as part of your order,** is for a one-time use only and limited to any maximum distribution number specified in the license. The first instance of republication or reuse granted by this license must be completed within two years of the date of the grant of this license (although copies prepared before the end date may be distributed thereafter). The Wiley Materials shall not be used in any other manner or for any other purpose, beyond what is granted in the license. Permission is granted subject to an appropriate acknowledgement given to the author, title of the material/book/journal and the publisher. You shall also duplicate the copyright notice that appears in the Wiley publication in your use of the Wiley Material. Permission is also granted on the understanding that nowhere in the text is a previously published source acknowledged for all or part of this Wiley Material. Any third party content is expressly excluded from this permission.

- With respect to the Wiley Materials, all rights are reserved. Except as expressly granted by the terms of the license, no part of the Wiley Materials may be copied, modified, adapted (except for minor reformatting required by the new Publication), translated, reproduced, transferred or distributed, in any form or by any means, and no derivative works may be made based on the Wiley Materials without the prior permission of the respective copyright owner.**For STM Signatory Publishers clearing permission under the terms of the STM Permissions Guidelines only, the terms of the license are extended to include subsequent editions and for editions in other languages, provided such editions are for the work as a whole in situ and does not involve the separate exploitation of the permitted figures or extracts,** You may not alter, remove or suppress in any manner any copyright, trademark or other notices displayed by the Wiley Materials. You may not license, rent, sell, loan, lease, pledge, offer as security, transfer or assign the Wiley Materials on a stand-alone basis, or any of the rights granted to you hereunder to any other person.

- The Wiley Materials and all of the intellectual property rights therein shall at all times remain the exclusive property of John Wiley & Sons Inc, the Wiley Companies, or their respective licensors, and your interest therein is only that of having possession of and the right to reproduce the Wiley Materials pursuant to Section 2 herein during the continuance of this Agreement. You agree that you own no right, title or interest in or to the Wiley Materials or any of the intellectual property rights therein. You shall have no rights hereunder other than the license as provided for above in Section 2. No right, license or interest to any trademark, trade name, service mark or other branding ("Marks") of WILEY or its licensors is granted hereunder, and you agree that you shall not assert any such right, license or interest with respect thereto

- NEITHER WILEY NOR ITS LICENSORS MAKES ANY WARRANTY OR REPRESENTATION OF ANY KIND TO YOU OR ANY THIRD PARTY, EXPRESS, IMPLIED OR STATUTORY, WITH RESPECT TO THE MATERIALS OR THE ACCURACY OF ANY INFORMATION CONTAINED IN THE MATERIALS, INCLUDING, WITHOUT LIMITATION, ANY IMPLIED WARRANTY OF MERCHANTABILITY, ACCURACY, SATISFACTORY QUALITY, FITNESS FOR A PARTICULAR PURPOSE, USABILITY, INTEGRATION OR NON-INFRINGEMENT AND ALL SUCH WARRANTIES ARE HEREBY EXCLUDED BY WILEY AND ITS LICENSORS AND WAIVED BY YOU.

- WILEY shall have the right to terminate this Agreement immediately upon breach of this Agreement by you.

- You shall indemnify, defend and hold harmless WILEY, its Licensors and their respective directors, officers, agents and employees, from and against any actual or threatened claims, demands, causes of action or proceedings arising from any breach of this Agreement by you.

- IN NO EVENT SHALL WILEY OR ITS LICENSORS BE LIABLE TO YOU OR ANY OTHER PARTY OR ANY OTHER PERSON OR ENTITY FOR ANY SPECIAL, CONSEQUENTIAL, INCIDENTAL, INDIRECT, EXEMPLARY OR PUNITIVE DAMAGES, HOWEVER CAUSED, ARISING OUT OF OR IN CONNECTION WITH THE DOWNLOADING, PROVISIONING, VIEWING OR USE OF THE MATERIALS REGARDLESS OF THE FORM OF ACTION, WHETHER FOR BREACH OF CONTRACT, BREACH OF WARRANTY, TORT, NEGLIGENCE, INFRINGEMENT OR OTHERWISE (INCLUDING, WITHOUT LIMITATION, DAMAGES BASED ON LOSS OF PROFITS, DATA, FILES, USE, BUSINESS OPPORTUNITY OR CLAIMS OF THIRD PARTIES), AND WHETHER OR NOT THE PARTY HAS BEEN ADVISED OF THE POSSIBILITY OF SUCH DAMAGES. THIS LIMITATION SHALL APPLY NOTWITHSTANDING ANY FAILURE OF ESSENTIAL PURPOSE OF ANY LIMITED REMEDY PROVIDED HEREIN.

- Should any provision of this Agreement be held by a court of competent jurisdiction to be illegal, invalid, or unenforceable, that provision shall be deemed amended to achieve as nearly as possible the same economic effect as the original provision, and the legality, validity and enforceability of the remaining provisions of this Agreement shall not be affected or impaired thereby.

- The failure of either party to enforce any term or condition of this Agreement shall not constitute a waiver of either party's right to enforce each and every term and condition of this Agreement. No breach under this agreement shall be deemed waived or

excused by either party unless such waiver or consent is in writing signed by the party granting such waiver or consent. The waiver by or consent of a party to a breach of any provision of this Agreement shall not operate or be construed as a waiver of or consent to any other or subsequent breach by such other party.

- This Agreement may not be assigned (including by operation of law or otherwise) by you without WILEY's prior written consent.
- Any fee required for this permission shall be non-refundable after thirty (30) days from receipt by the CCC.
- These terms and conditions together with CCC's Billing and Payment terms and conditions (which are incorporated herein) form the entire agreement between you and WILEY concerning this licensing transaction and (in the absence of fraud) supersedes all prior agreements and representations of the parties, oral or written. This Agreement may not be amended except in writing signed by both parties. This Agreement shall be binding upon and inure to the benefit of the parties' successors, legal representatives, and authorized assigns.
- In the event of any conflict between your obligations established by these terms and conditions and those established by CCC's Billing and Payment terms and conditions, these terms and conditions shall prevail.
- WILEY expressly reserves all rights not specifically granted in the combination of (i) the license details provided by you and accepted in the course of this licensing transaction, (ii) these terms and conditions and (iii) CCC's Billing and Payment terms and conditions.
- This Agreement will be void if the Type of Use, Format, Circulation, or Requestor Type was misrepresented during the licensing process.
- This Agreement shall be governed by and construed in accordance with the laws of the State of New York, USA, without regards to such state's conflict of law rules. Any legal action, suit or proceeding arising out of or relating to these Terms and Conditions or the breach thereof shall be instituted in a court of competent jurisdiction in New York County in the State of New York in the United States of America and each party hereby consents and submits to the personal jurisdiction of such court, waives any objection to venue in such court and consents to service of process by registered or certified mail, return receipt requested, at the last known address of such party.

WILEY OPEN ACCESS TERMS AND CONDITIONS

Wiley Publishes Open Access Articles in fully Open Access Journals and in Subscription journals offering Online Open. Although most of the fully Open Access journals publish open access articles under the terms of the Creative Commons Attribution (CC BY) License only, the subscription journals and a few of the Open Access Journals offer a choice of Creative Commons Licenses. The license type is clearly identified on the article.

The Creative Commons Attribution License

The Creative Commons Attribution License (CC-BY) allows users to copy, distribute and transmit an article, adapt the article and make commercial use of the article. The CC-BY license permits commercial and non-

Creative Commons Attribution Non-Commercial License

The Creative Commons Attribution Non-Commercial (CC-BY-NC)License permits use, distribution and reproduction in any medium, provided the original work is properly cited and is not used for commercial purposes.(see below)

Creative Commons Attribution-Non-Commercial-NoDerivs License

The Creative Commons Attribution Non-Commercial-NoDerivs License (CC-BY-NC-ND) permits use, distribution and reproduction in any medium, provided the original work is properly cited, is not used for commercial purposes and no modifications or adaptations are made. (see below)

Use by commercial "for-profit" organizations

Use of Wiley Open Access articles for commercial, promotional, or marketing purposes requires further explicit permission from Wiley and will be subject to a fee.

Further details can be found on Wiley Online Library http://olabout.wiley.com/WileyCDA/Section/id-410895.html

Other Terms and Conditions:

v1.10 Last updated September 2015

Questions? customercare@copyright.com or +1-855-239-3415 (toll free in the US) or +1-978-646-2777.

Permission for Figure 1 5: Schematic View of the Furniture Calorimeter

SPRINGER NATURE LICENSE TERMS AND CONDITIONS

Oct 27, 2019

This Agreement between Department of Mechanical Engineering ("You") and Springer Nature ("Springer Nature") consists of your license details and the terms and conditions provided by Springer Nature and Copyright Clearance Center.

License Number	4697410721860
License date	Oct 27, 2019
Licensed Content Publisher	Springer Nature
Licensed Content Publication	Springer eBook
Licensed Content Title	Calorimetry
Licensed Content Author	Marc Janssens
Licensed Content Date	Jan 1, 2016
Type of Use	Thesis/Dissertation
Requestor type	academic/university or research institute
Format	print and electronic
Portion	figures/tables/illustrations
Number of figures/tables/illustrations	1
Will you be translating?	no
Circulation/distribution	1 - 29
Author of this Springer Nature content	no
Title	Experimental and Numerical Investigation of Fire Behaviour in Polyurethane Foams
Institution name	University of Saskatchewan
Expected presentation date	Nov 2019
Portions	Fig 27.17
Requestor Location	Department of Mechanical Engineering University of Saskatchewan 105 Administration Place Saskatoon, SK S7N 5A2 Canada Attn: Department of Mechanical Engineering
Total	0.00 CAD
Terms and Conditions	

Springer Nature Customer Service Centre GmbH
Terms and Conditions

This agreement sets out the terms and conditions of the licence (the **Licence**) between you and **Springer Nature Customer Service Centre GmbH** (the **Licensor**). By clicking 'accept' and completing the transaction for the material (**Licensed Material**), you also confirm your acceptance of these terms and conditions.

1. Grant of License

1. 1. The Licensor grants you a personal, non-exclusive, non-transferable, world-wide licence to reproduce the Licensed Material for the purpose specified in your order only. Licences are granted for the specific use requested in the order and for no other use, subject to the conditions below.

1. 2. The Licensor warrants that it has, to the best of its knowledge, the rights to license reuse of the Licensed Material. However, you should ensure that the material you are requesting is original to the Licensor and does not carry the copyright of another entity (as credited in the published version).

1. 3. If the credit line on any part of the material you have requested indicates that it was reprinted or adapted with permission from another source, then you should also seek permission from that source to reuse the material.

2. Scope of Licence

2. 1. You may only use the Licensed Content in the manner and to the extent permitted by these Ts&Cs and any applicable laws.

2. 2. A separate licence may be required for any additional use of the Licensed Material, e.g. where a licence has been purchased for print only use, separate permission must be obtained for electronic re-use. Similarly, a licence is only valid in the language selected and does not apply for editions in other languages unless additional translation rights have been granted separately in the licence. Any content owned by third parties are expressly excluded from the licence.

2. 3. Similarly, rights for additional components such as custom editions and derivatives require additional permission and may be subject to an additional fee. Please apply to Journalpermissions@springernature.com/bookpermissions@springernature.com for these rights.

2. 4. Where permission has been granted **free of charge** for material in print, permission may also be granted for any electronic version of that work, provided that the material is incidental to your work as a whole and that the electronic version is essentially equivalent to, or substitutes for, the print version.

2. 5. An alternative scope of licence may apply to signatories of the STM Permissions Guidelines, as amended from time to time.

3. Duration of Licence

3. 1. A licence for is valid from the date of purchase ('Licence Date') at the end of the relevant period in the below table:

Scope of Licence	Duration of Licence
Post on a website	12 months
Presentations	12 months
Books and journals	Lifetime of the edition in the language purchased

4. Acknowledgement

4. 1. The Licensor's permission must be acknowledged next to the Licenced Material in print. In electronic form, this acknowledgement must be visible at the same time as the figures/tables/illustrations or abstract, and must be hyperlinked to the journal/book's

homepage. Our required acknowledgement format is in the Appendix below.

5. Restrictions on use

5. 1. Use of the Licensed Material may be permitted for incidental promotional use and minor editing privileges e.g. minor adaptations of single figures, changes of format, colour and/or style where the adaptation is credited as set out in Appendix 1 below. Any other changes including but not limited to, cropping, adapting, omitting material that affect the meaning, intention or moral rights of the author are strictly prohibited.

5. 2. You must not use any Licensed Material as part of any design or trademark.

5. 3. Licensed Material may be used in Open Access Publications (OAP) before publication by Springer Nature, but any Licensed Material must be removed from OAP sites prior to final publication.

6. Ownership of Rights

6. 1. Licensed Material remains the property of either Licensor or the relevant third party and any rights not explicitly granted herein are expressly reserved.

7. Warranty

IN NO EVENT SHALL LICENSOR BE LIABLE TO YOU OR ANY OTHER PARTY OR ANY OTHER PERSON OR FOR ANY SPECIAL, CONSEQUENTIAL, INCIDENTAL OR INDIRECT DAMAGES, HOWEVER CAUSED, ARISING OUT OF OR IN CONNECTION WITH THE DOWNLOADING, VIEWING OR USE OF THE MATERIALS REGARDLESS OF THE FORM OF ACTION, WHETHER FOR BREACH OF CONTRACT, BREACH OF WARRANTY, TORT, NEGLIGENCE, INFRINGEMENT OR OTHERWISE (INCLUDING, WITHOUT LIMITATION, DAMAGES BASED ON LOSS OF PROFITS, DATA, FILES, USE, BUSINESS OPPORTUNITY OR CLAIMS OF THIRD PARTIES), AND
WHETHER OR NOT THE PARTY HAS BEEN ADVISED OF THE POSSIBILITY OF SUCH DAMAGES. THIS LIMITATION SHALL APPLY NOTWITHSTANDING ANY FAILURE OF ESSENTIAL PURPOSE OF ANY LIMITED REMEDY PROVIDED HEREIN.

8. Limitations

8. 1. ***BOOKS ONLY:*** Where **'reuse in a dissertation/thesis'** has been selected the following terms apply: Print rights of the final author's accepted manuscript (for clarity, NOT the published version) for up to 100 copies, electronic rights for use only on a personal website or institutional repository as defined by the Sherpa guideline (www.sherpa.ac.uk/romeo/).

9. Termination and Cancellation

9. 1. Licences will expire after the period shown in Clause 3 (above).

9. 2. Licensee reserves the right to terminate the Licence in the event that payment is not received in full or if there has been a breach of this agreement by you.

Appendix 1 — Acknowledgements:

For Journal Content:
Reprinted by permission from **[the Licensor]**: **[Journal Publisher** (e.g. Nature/Springer/Palgrave)] **[JOURNAL NAME] [REFERENCE CITATION** (Article name, Author(s) Name), **[COPYRIGHT]** (year of publication)

For **Advance Online Publication papers:**
Reprinted by permission from **[the Licensor]**: **[Journal Publisher** (e.g. Nature/Springer/Palgrave)] **[JOURNAL NAME] [REFERENCE CITATION** (Article name, Author(s) Name), **[COPYRIGHT]** (year of publication), advance online publication, day month year (doi: 10.1038/sj.[JOURNAL ACRONYM].)

For Adaptations/Translations:
Adapted/Translated by permission from **[the Licensor]**: **[Journal Publisher** (e.g. Nature/Springer/Palgrave)] **[JOURNAL NAME] [REFERENCE CITATION** (Article name, Author(s) Name), **[COPYRIGHT]** (year of publication)

Note: For any republication from the British Journal of Cancer, the following credit line style applies:

Reprinted/adapted/translated by permission from **[the Licensor]**: on behalf of Cancer Research UK: : **[Journal Publisher** (e.g. Nature/Springer/Palgrave)] **[JOURNAL NAME] [REFERENCE CITATION** (Article name, Author(s) Name), **[COPYRIGHT]** (year of publication)

For **Advance Online Publication** papers:
Reprinted by permission from The **[the Licensor]**: on behalf of Cancer Research UK: **[Journal Publisher** (e.g. Nature/Springer/Palgrave)] **[JOURNAL NAME] [REFERENCE CITATION** (Article name, Author(s) Name), **[COPYRIGHT]** (year of publication), advance online publication, day month year (doi: 10.1038/sj.[JOURNAL ACRONYM])

For Book content:
Reprinted/adapted by permission from **[the Licensor]**: **[Book Publisher** (e.g. Palgrave Macmillan, Springer etc) **[Book Title]** by **[Book author**(s)] **[COPYRIGHT]** (year of publication)

Other Conditions:

Version 1.2

Permission for Figure 1 6: The ISO 9705 Room Fire Test

JOHN WILEY AND SONS LICENSE TERMS AND CONDITIONS

Oct 27, 2019

This Agreement between Department of Mechanical Engineering ("You") and John Wiley and Sons ("John Wiley and Sons") consists of your license details and the terms and conditions provided by John Wiley and Sons and Copyright Clearance Center.

License Number	4435420566855
License date	Sep 24, 2018
Licensed Content Publisher	John Wiley and Sons
Licensed Content Publication	Wiley Books
Licensed Content Title	The Pre-Flashover Compartment Fire
Licensed Content Date	Jul 11, 2011
Licensed Content Pages	38
Type of Use	Dissertation/Thesis
Requestor type	University/Academic
Format	Print and electronic
Portion	Figure/table
Number of figures/tables	1
Original Wiley figure/table number(s)	Fig 9.15 (b)
Will you be translating?	No
Title of your thesis / dissertation	Modelling Flame Spread For Polyurethane Foam
Expected completion date	Dec 2018
Expected size (number of pages)	1
Requestor Location	Department of Mechanical Engineering University of Saskatchewan 105 Administration Place Saskatoon, SK S7N 5A2 Canada Attn: Department of Mechanical Engineering
Publisher Tax ID	EU826007151
Total	**0.00 USD**
Terms and Conditions	

TERMS AND CONDITIONS

This copyrighted material is owned by or exclusively licensed to John Wiley & Sons, Inc. or one of its group companies (each a"Wiley Company") or handled on behalf of a society with which a Wiley Company has exclusive publishing rights in relation to a particular work (collectively "WILEY"). By clicking "accept" in connection with completing this licensing transaction, you agree that the following terms and conditions apply to this transaction (along with the billing and payment terms and conditions established by the Copyright Clearance Center Inc., ("CCC's Billing and Payment terms and conditions"), at the time that you opened your RightsLink account (these are available at any time at http://myaccount.copyright.com).

Terms and Conditions

- The materials you have requested permission to reproduce or reuse (the "Wiley Materials") are protected by copyright.

- You are hereby granted a personal, non-exclusive, non-sub licensable (on a stand-alone basis), non-transferable, worldwide, limited license to reproduce the Wiley Materials for the purpose specified in the licensing process. This license, **and any CONTENT (PDF or image file) purchased as part of your order,** is for a one-time use only and limited to any maximum distribution number specified in the license. The first instance of republication or reuse granted by this license must be completed within two years of the date of the grant of this license (although copies prepared before the end date may be distributed thereafter). The Wiley Materials shall not be used in any other manner or for any other purpose, beyond what is granted in the license. Permission is granted subject to an appropriate acknowledgement given to the author, title of the material/book/journal and the publisher. You shall also duplicate the copyright notice that appears in the Wiley publication in your use of the Wiley Material. Permission is also granted on the understanding that nowhere in the text is a previously published source acknowledged for all or part of this Wiley Material. Any third party content is expressly excluded from this permission.

- With respect to the Wiley Materials, all rights are reserved. Except as expressly granted by the terms of the license, no part of the Wiley Materials may be copied, modified, adapted (except for minor reformatting required by the new Publication), translated, reproduced, transferred or distributed, in any form or by any means, and no derivative works may be made based on the Wiley Materials without the prior permission of the respective copyright owner.**For STM Signatory Publishers clearing permission under the terms of the STM Permissions Guidelines only, the terms of the license are extended to include subsequent editions and for editions in other languages, provided such editions are for the work as a whole in situ and does not involve the separate exploitation of the permitted figures or extracts,** You may not alter, remove or suppress in any manner any copyright, trademark or other notices displayed by the Wiley Materials. You may not license, rent, sell, loan, lease, pledge, offer as security, transfer or assign the Wiley Materials on a stand-alone basis, or any of the rights granted to you hereunder to any other person.

- The Wiley Materials and all of the intellectual property rights therein shall at all times remain the exclusive property of John Wiley & Sons Inc, the Wiley Companies, or their respective licensors, and your interest therein is only that of having possession of and the right to reproduce the Wiley Materials pursuant to Section 2 herein during the continuance of this Agreement. You agree that you own no right, title or interest in or to the Wiley Materials or any of the intellectual property rights therein. You shall have no rights hereunder other than the license as provided for above in Section 2. No right, license or interest to any trademark, trade name, service mark or other branding ("Marks") of WILEY or its licensors is granted hereunder, and you agree that you shall not assert any such right, license or interest with respect thereto

- NEITHER WILEY NOR ITS LICENSORS MAKES ANY WARRANTY OR REPRESENTATION OF ANY KIND TO YOU OR ANY THIRD PARTY, EXPRESS, IMPLIED OR STATUTORY, WITH RESPECT TO THE MATERIALS OR THE ACCURACY OF ANY INFORMATION CONTAINED IN THE MATERIALS, INCLUDING, WITHOUT LIMITATION, ANY IMPLIED WARRANTY OF MERCHANTABILITY, ACCURACY, SATISFACTORY QUALITY, FITNESS FOR A PARTICULAR PURPOSE, USABILITY, INTEGRATION OR NON-INFRINGEMENT AND ALL SUCH WARRANTIES ARE HEREBY EXCLUDED BY WILEY AND ITS LICENSORS AND WAIVED BY YOU.

- WILEY shall have the right to terminate this Agreement immediately upon breach of this Agreement by you.

- You shall indemnify, defend and hold harmless WILEY, its Licensors and their respective directors, officers, agents and employees, from and against any actual or threatened claims, demands, causes of action or proceedings arising from any breach of this Agreement by you.

- IN NO EVENT SHALL WILEY OR ITS LICENSORS BE LIABLE TO YOU OR ANY OTHER PARTY OR ANY OTHER PERSON OR ENTITY FOR ANY SPECIAL, CONSEQUENTIAL, INCIDENTAL, INDIRECT, EXEMPLARY OR PUNITIVE DAMAGES, HOWEVER CAUSED, ARISING OUT OF OR IN CONNECTION WITH THE DOWNLOADING, PROVISIONING, VIEWING OR USE OF THE MATERIALS REGARDLESS OF THE FORM OF ACTION, WHETHER FOR BREACH OF CONTRACT, BREACH OF WARRANTY, TORT, NEGLIGENCE, INFRINGEMENT OR OTHERWISE (INCLUDING, WITHOUT LIMITATION, DAMAGES BASED ON LOSS OF PROFITS, DATA, FILES, USE, BUSINESS OPPORTUNITY OR CLAIMS OF THIRD PARTIES), AND WHETHER OR NOT THE PARTY HAS BEEN ADVISED OF THE POSSIBILITY OF SUCH DAMAGES. THIS LIMITATION SHALL APPLY NOTWITHSTANDING ANY FAILURE OF ESSENTIAL PURPOSE OF ANY LIMITED REMEDY PROVIDED HEREIN.

- Should any provision of this Agreement be held by a court of competent jurisdiction to be illegal, invalid, or unenforceable, that provision shall be deemed amended to achieve as nearly as possible the same economic effect as the original provision, and the legality, validity and enforceability of the remaining provisions of this Agreement shall not be affected or impaired thereby.

- The failure of either party to enforce any term or condition of this Agreement shall not constitute a waiver of either party's right to enforce each and every term and condition of this Agreement. No breach under this agreement shall be deemed waived or

excused by either party unless such waiver or consent is in writing signed by the party granting such waiver or consent. The waiver by or consent of a party to a breach of any provision of this Agreement shall not operate or be construed as a waiver of or consent to any other or subsequent breach by such other party.

- This Agreement may not be assigned (including by operation of law or otherwise) by you without WILEY's prior written consent.
- Any fee required for this permission shall be non-refundable after thirty (30) days from receipt by the CCC.
- These terms and conditions together with CCC's Billing and Payment terms and conditions (which are incorporated herein) form the entire agreement between you and WILEY concerning this licensing transaction and (in the absence of fraud) supersedes all prior agreements and representations of the parties, oral or written. This Agreement may not be amended except in writing signed by both parties. This Agreement shall be binding upon and inure to the benefit of the parties' successors, legal representatives, and authorized assigns.
- In the event of any conflict between your obligations established by these terms and conditions and those established by CCC's Billing and Payment terms and conditions, these terms and conditions shall prevail.
- WILEY expressly reserves all rights not specifically granted in the combination of (i) the license details provided by you and accepted in the course of this licensing transaction, (ii) these terms and conditions and (iii) CCC's Billing and Payment terms and conditions.
- This Agreement will be void if the Type of Use, Format, Circulation, or Requestor Type was misrepresented during the licensing process.
- This Agreement shall be governed by and construed in accordance with the laws of the State of New York, USA, without regards to such state's conflict of law rules. Any legal action, suit or proceeding arising out of or relating to these Terms and Conditions or the breach thereof shall be instituted in a court of competent jurisdiction in New York County in the State of New York in the United States of America and each party hereby consents and submits to the personal jurisdiction of such court, waives any objection to venue in such court and consents to service of process by registered or certified mail, return receipt requested, at the last known address of such party.

WILEY OPEN ACCESS TERMS AND CONDITIONS

Wiley Publishes Open Access Articles in fully Open Access Journals and in Subscription journals offering Online Open. Although most of the fully Open Access journals publish open access articles under the terms of the Creative Commons Attribution (CC BY) License only, the subscription journals and a few of the Open Access Journals offer a choice of Creative Commons Licenses. The license type is clearly identified on the article.

The Creative Commons Attribution License

The Creative Commons Attribution License (CC-BY) allows users to copy, distribute and transmit an article, adapt the article and make commercial use of the article. The CC-BY license permits commercial and non-

Creative Commons Attribution Non-Commercial License

The Creative Commons Attribution Non-Commercial (CC-BY-NC)License permits use, distribution and reproduction in any medium, provided the original work is properly cited and is not used for commercial purposes.(see below)

Creative Commons Attribution-Non-Commercial-NoDerivs License

The Creative Commons Attribution Non-Commercial-NoDerivs License (CC-BY-NC-ND) permits use, distribution and reproduction in any medium, provided the original work is properly cited, is not used for commercial purposes and no modifications or adaptations are made. (see below)

Use by commercial "for-profit" organizations

Use of Wiley Open Access articles for commercial, promotional, or marketing purposes requires further explicit permission from Wiley and will be subject to a fee.

Further details can be found on Wiley Online Library http://olabout.wiley.com/WileyCDA/Section/id-410895.html

Other Terms and Conditions:

v1.10 Last updated September 2015

Questions? customercare@copyright.com or +1-855-239-3415 (toll free in the US) or +1-978-646-2777.

Permission for Figure 1 7: Schematic View of the Cone Calorimeter

SPRINGER NATURE LICENSE TERMS AND CONDITIONS

Oct 27, 2019

This Agreement between Department of Mechanical Engineering ("You") and Springer Nature ("Springer Nature") consists of your license details and the terms and conditions provided by Springer Nature and Copyright Clearance Center.

License Number	4435141282629
License date	Sep 24, 2018
Licensed Content Publisher	Springer Nature
Licensed Content Publication	Springer eBook
Licensed Content Title	Calorimetry
Licensed Content Author	Marc Janssens
Licensed Content Date	Jan 1, 2016
Type of Use	Thesis/Dissertation
Requestor type	academic/university or research institute
Format	print and electronic
Portion	figures/tables/illustrations
Number of figures/tables/illustrations	3
Will you be translating?	no
Circulation/distribution	<501
Author of this Springer Nature content	no
Title	Modelling Flame Spread For Polyurethane Foam
Instructor name	Prof. David Torvi
Institution name	University of Saskatchewan
Expected presentation date	Dec 2018
Portions	Fig. 27.11 Table 27.3
Requestor Location	Department of Mechanical Engineering University of Saskatchewan 105 Administration Place Saskatoon, SK S7N 5A2 Canada Attn: Department of Mechanical Engineering
Billing Type	Invoice
Billing Address	Department of Mechanical Engineering University of Saskatchewan 105 Administration Place Saskatoon, SK S7N 5A2 Canada Attn: Department of Mechanical Engineering
Total	0.00 CAD
Terms and Conditions	

Springer Nature Terms and Conditions for RightsLink Permissions

Springer Nature Customer Service Centre GmbH (the Licensor) hereby grants you a non-exclusive, world-wide licence to reproduce the material and for the purpose and requirements specified in the attached copy of your order form, and for no other use, subject to the conditions below:

1. The Licensor warrants that it has, to the best of its knowledge, the rights to license reuse of this material. However, you should ensure that the material you are requesting is original to the Licensor and does not carry the copyright of another entity (as credited in the published version).

   If the credit line on any part of the material you have requested indicates that it was reprinted or adapted with permission from another source, then you should also seek permission from that source to reuse the material.

2. Where **print only** permission has been granted for a fee, separate permission must be obtained for any additional electronic re-use.

3. Permission granted **free of charge** for material in print is also usually granted for any electronic version of that work, provided that the material is incidental to your work as a whole and that the electronic version is essentially equivalent to, or substitutes for, the print version.

4. A licence for 'post on a website' is valid for 12 months from the licence date. This licence does not cover use of full text articles on websites.

5. Where **'reuse in a dissertation/thesis'** has been selected the following terms apply: Print rights of the final author's accepted manuscript (for clarity, NOT the published version) for up to 100 copies, electronic rights for use only on a personal website or institutional repository as defined by the Sherpa guideline (www.sherpa.ac.uk/romeo/).

6. Permission granted for books and journals is granted for the lifetime of the first edition and does not apply to second and subsequent editions (except where the first edition permission was granted free of charge or for signatories to the STM Permissions Guidelines http://www.stm-assoc.org/copyright-legal-affairs/permissions/permissions-guidelines/), and does not apply for editions in other languages unless additional translation rights have been granted separately in the licence.

7. Rights for additional components such as custom editions and derivatives require additional permission and may be subject to an additional fee. Please apply to Journalpermissions@springernature.com/bookpermissions@springernature.com for these rights.

8. The Licensor's permission must be acknowledged next to the licensed material in print. In electronic form, this acknowledgement must be visible at the same time as the figures/tables/illustrations or abstract, and must be hyperlinked to the journal/book's homepage. Our required acknowledgement format is in the Appendix below.

9. Use of the material for incidental promotional use, minor editing privileges (this does not include cropping, adapting, omitting material or any other changes that affect the meaning, intention or moral rights of the author) and copies for the disabled are permitted under this licence.

10. Minor adaptations of single figures (changes of format, colour and style) do not require the Licensor's approval. However, the adaptation should be credited as shown in Appendix below.

Appendix — Acknowledgements:

For Journal Content:
Reprinted by permission from [**the Licensor**]: [**Journal Publisher** (e.g. Nature/Springer/Palgrave)] [**JOURNAL NAME**] [**REFERENCE CITATION** (Article name, Author(s) Name), [**COPYRIGHT**] (year of publication)

For **Advance Online Publication papers:**
Reprinted by permission from [**the Licensor**]: [**Journal Publisher** (e.g. Nature/Springer/Palgrave)] [**JOURNAL NAME**] [**REFERENCE CITATION** (Article name, Author(s) Name), [**COPYRIGHT**] (year of publication), advance online publication, day month year (doi: 10.1038/sj.[JOURNAL ACRONYM].)

For Adaptations/Translations:
Adapted/Translated by permission from [**the Licensor**]: [**Journal Publisher** (e.g. Nature/Springer/Palgrave)] [**JOURNAL NAME**] [**REFERENCE CITATION** (Article name, Author(s) Name), [**COPYRIGHT**] (year of publication)

Note: For any republication from the British Journal of Cancer, the following credit line style applies:

Reprinted/adapted/translated by permission from [**the Licensor**]: on behalf of Cancer Research UK: : [**Journal Publisher** (e.g. Nature/Springer/Palgrave)] [**JOURNAL NAME**] [**REFERENCE CITATION** (Article name, Author(s) Name),

Permission for Figure 3 19: Heat Release Rate Comparison for a Wooden Crib Fire

Re: Permission to Use Figure 3.16 in Obach 2011

Beth Weckman <beth.weckman@uwaterloo.ca>

Mon 10/28/2019 5:04 AM

To: Ugo-Okeke, Obi <obiora.okeke@usask.ca>

Obi

We grant you permission to use the Figure 3.16 of Obach 2011 - Effects of Initial Fire Attack Suppression Tactics on the Firefighter and Compartment Environment in your MSc. research titled *Experimental and Numerical Investigation of Fire Behaviour in Polyurethane Foams*. Best wishes with completion of your thesis!

Sincerely
Beth Weckman

Professor
Fire Research Lab
University of Waterloo
Waterloo, ON N2L 3G1

519-888-4567 x 43345
ejweckman@uwaterloo.ca

From: Ugo-Okeke, Obi <obiora.okeke@usask.ca>
Sent: Sunday, October 27, 2019 11:55 PM
To: Beth Weckman
Subject: Permission to Use Figure 3.16 in Obach 2011

Good day Prof. Weckman,

On behalf of the Department of Mechanical Engineering, University of Saskatchewan, Saskatoon, Saskatchewan, Canada. I would like to request permission to include figure 3.16 of Obach 2011 - Effects of Initial Fire Attack Suppression Tactics on the Firefighter and Compartment Environment in my MSc. research titled *Experimental and Numerical Investigation of Fire Behaviour in Polyurethane Foams*. As my work is solely for educational purposes, it will not be sold and will be available to all members of the Fire research community upon request. Proper acknowledgement of your publication will be included with the reproduction.

If you agree to grant us permission, please provide us with an email to signify acceptance.

We appreciate your consideration of our permissions request.

Sincerely,

Obi Ugo-Okeke
MSc. Candidate. Department of Mechanical Engineering,
University of Saskatchewan.

Permission for Figure 4 29: Thermogravimetric and Differential Signal Tests of Pure Polyurethane Foam at 5°C/min (a) and 176°C/min (b) (Nitrogen – Solid Line, Air – Dotted Line)

ELSEVIER LICENSE
TERMS AND CONDITIONS

Oct 28, 2019

This Agreement between Department of Mechanical Engineering ("You") and Elsevier ("Elsevier") consists of your license details and the terms and conditions provided by Elsevier and Copyright Clearance Center.

License Number	4697430231761
License date	Oct 28, 2019
Licensed Content Publisher	Elsevier
Licensed Content Publication	Polymer Degradation and Stability
Licensed Content Title	Heat release and structural collapse of flexible polyurethane foam
Licensed Content Author	R.H. Krämer,M. Zammarano,G.T. Linteris,U.W. Gedde,J.W. Gilman
Licensed Content Date	Jun 1, 2010
Licensed Content Volume	95
Licensed Content Issue	6
Licensed Content Pages	8
Start Page	1115
End Page	1122
Type of Use	reuse in a thesis/dissertation
Intended publisher of new work	other
Portion	figures/tables/illustrations
Number of figures/tables/illustrations	1
Format	both print and electronic
Are you the author of this Elsevier article?	No
Will you be translating?	No
Original figure numbers	Fig 2
Title of your thesis/dissertation	Experimental and Numerical Investigation of Fire Behaviour in Polyurethane Foams
Publisher of new work	University of Saskatchewan
Expected completion date	Nov 2019
Estimated size (number of pages)	1
Requestor Location	Department of Mechanical Engineering University of Saskatchewan 105 Administration Place Saskatoon, SK S7N 5A2 Canada Attn: Department of Mechanical Engineering
Publisher Tax ID	GB 494 6272 12

Total 0.00 CAD

Terms and Conditions

INTRODUCTION

1. The publisher for this copyrighted material is Elsevier. By clicking "accept" in connection with completing this licensing transaction, you agree that the following terms and conditions apply to this transaction (along with the Billing and Payment terms and conditions established by Copyright Clearance Center, Inc. ("CCC"), at the time that you opened your Rightslink account and that are available at any time at http://myaccount.copyright.com).

GENERAL TERMS

2. Elsevier hereby grants you permission to reproduce the aforementioned material subject to the terms and conditions indicated.
3. Acknowledgement: If any part of the material to be used (for example, figures) has appeared in our publication with credit or acknowledgement to another source, permission must also be sought from that source. If such permission is not obtained then that material may not be included in your publication/copies. Suitable acknowledgement to the source must be made, either as a footnote or in a reference list at the end of your publication, as follows:
"Reprinted from Publication title, Vol /edition number, Author(s), Title of article / title of chapter, Pages No., Copyright (Year), with permission from Elsevier [OR APPLICABLE SOCIETY COPYRIGHT OWNER]." Also Lancet special credit - "Reprinted from The Lancet, Vol. number, Author(s), Title of article, Pages No., Copyright (Year), with permission from Elsevier."
4. Reproduction of this material is confined to the purpose and/or media for which permission is hereby given.
5. Altering/Modifying Material: Not Permitted. However figures and illustrations may be altered/adapted minimally to serve your work. Any other abbreviations, additions, deletions and/or any other alterations shall be made only with prior written authorization of Elsevier Ltd. (Please contact Elsevier at permissions@elsevier.com). No modifications can be made to any Lancet figures/tables and they must be reproduced in full.
6. If the permission fee for the requested use of our material is waived in this instance, please be advised that your future requests for Elsevier materials may attract a fee.
7. Reservation of Rights: Publisher reserves all rights not specifically granted in the combination of (i) the license details provided by you and accepted in the course of this licensing transaction, (ii) these terms and conditions and (iii) CCC's Billing and Payment terms and conditions.
8. License Contingent Upon Payment: While you may exercise the rights licensed immediately upon issuance of the license at the end of the licensing process for the transaction, provided that you have disclosed complete and accurate details of your proposed use, no license is finally effective unless and until full payment is received from you (either by publisher or by CCC) as provided in CCC's Billing and Payment terms and conditions. If full payment is not received on a timely basis, then any license preliminarily granted shall be deemed automatically revoked and shall be void as if never granted. Further, in the event that you breach any of these terms and conditions or any of CCC's Billing and Payment terms and conditions, the license is automatically revoked and shall be void as if never granted. Use of materials as described in a revoked license, as well as any use of the materials beyond the scope of an unrevoked license, may constitute copyright infringement and publisher reserves the right to take any and all action to protect its copyright in the materials.
9. Warranties: Publisher makes no representations or warranties with respect to the licensed material.
10. Indemnity: You hereby indemnify and agree to hold harmless publisher and CCC, and their respective officers, directors, employees and agents, from and against any and all

claims arising out of your use of the licensed material other than as specifically authorized pursuant to this license.
11. No Transfer of License: This license is personal to you and may not be sublicensed, assigned, or transferred by you to any other person without publisher's written permission.
12. No Amendment Except in Writing: This license may not be amended except in a writing signed by both parties (or, in the case of publisher, by CCC on publisher's behalf).
13. Objection to Contrary Terms: Publisher hereby objects to any terms contained in any purchase order, acknowledgment, check endorsement or other writing prepared by you, which terms are inconsistent with these terms and conditions or CCC's Billing and Payment terms and conditions. These terms and conditions, together with CCC's Billing and Payment terms and conditions (which are incorporated herein), comprise the entire agreement between you and publisher (and CCC) concerning this licensing transaction. In the event of any conflict between your obligations established by these terms and conditions and those established by CCC's Billing and Payment terms and conditions, these terms and conditions shall control.
14. Revocation: Elsevier or Copyright Clearance Center may deny the permissions described in this License at their sole discretion, for any reason or no reason, with a full refund payable to you. Notice of such denial will be made using the contact information provided by you. Failure to receive such notice will not alter or invalidate the denial. In no event will Elsevier or Copyright Clearance Center be responsible or liable for any costs, expenses or damage incurred by you as a result of a denial of your permission request, other than a refund of the amount(s) paid by you to Elsevier and/or Copyright Clearance Center for denied permissions.

LIMITED LICENSE

The following terms and conditions apply only to specific license types:
15. **Translation**: This permission is granted for non-exclusive world **English** rights only unless your license was granted for translation rights. If you licensed translation rights you may only translate this content into the languages you requested. A professional translator must perform all translations and reproduce the content word for word preserving the integrity of the article.
16. **Posting licensed content on any Website**: The following terms and conditions apply as follows: Licensing material from an Elsevier journal: All content posted to the web site must maintain the copyright information line on the bottom of each image; A hyper-text must be included to the Homepage of the journal from which you are licensing at http://www.sciencedirect.com/science/journal/xxxxx or the Elsevier homepage for books at http://www.elsevier.com; Central Storage: This license does not include permission for a scanned version of the material to be stored in a central repository such as that provided by Heron/XanEdu.
Licensing material from an Elsevier book: A hyper-text link must be included to the Elsevier homepage at http://www.elsevier.com . All content posted to the web site must maintain the copyright information line on the bottom of each image.

Posting licensed content on Electronic reserve: In addition to the above the following clauses are applicable: The web site must be password-protected and made available only to bona fide students registered on a relevant course. This permission is granted for 1 year only. You may obtain a new license for future website posting.
17. **For journal authors:** the following clauses are applicable in addition to the above:
Preprints:
A preprint is an author's own write-up of research results and analysis, it has not been peer-reviewed, nor has it had any other value added to it by a publisher (such as formatting, copyright, technical enhancement etc.).
Authors can share their preprints anywhere at any time. Preprints should not be added to or enhanced in any way in order to appear more like, or to substitute for, the final versions of

articles however authors can update their preprints on arXiv or RePEc with their Accepted Author Manuscript (see below).
If accepted for publication, we encourage authors to link from the preprint to their formal publication via its DOI. Millions of researchers have access to the formal publications on ScienceDirect, and so links will help users to find, access, cite and use the best available version. Please note that Cell Press, The Lancet and some society-owned have different preprint policies. Information on these policies is available on the journal homepage.
Accepted Author Manuscripts: An accepted author manuscript is the manuscript of an article that has been accepted for publication and which typically includes author-incorporated changes suggested during submission, peer review and editor-author communications.
Authors can share their accepted author manuscript:

- immediately
  - via their non-commercial person homepage or blog
  - by updating a preprint in arXiv or RePEc with the accepted manuscript
  - via their research institute or institutional repository for internal institutional uses or as part of an invitation-only research collaboration work-group
  - directly by providing copies to their students or to research collaborators for their personal use
  - for private scholarly sharing as part of an invitation-only work group on commercial sites with which Elsevier has an agreement
- After the embargo period
  - via non-commercial hosting platforms such as their institutional repository
  - via commercial sites with which Elsevier has an agreement

In all cases accepted manuscripts should:

- link to the formal publication via its DOI
- bear a CC-BY-NC-ND license - this is easy to do
- if aggregated with other manuscripts, for example in a repository or other site, be shared in alignment with our hosting policy not be added to or enhanced in any way to appear more like, or to substitute for, the published journal article.

Published journal article (JPA): A published journal article (PJA) is the definitive final record of published research that appears or will appear in the journal and embodies all value-adding publishing activities including peer review co-ordination, copy-editing, formatting, (if relevant) pagination and online enrichment.
Policies for sharing publishing journal articles differ for subscription and gold open access articles:
Subscription Articles: If you are an author, please share a link to your article rather than the full-text. Millions of researchers have access to the formal publications on ScienceDirect, and so links will help your users to find, access, cite, and use the best available version.
Theses and dissertations which contain embedded PJAs as part of the formal submission can be posted publicly by the awarding institution with DOI links back to the formal publications on ScienceDirect.
If you are affiliated with a library that subscribes to ScienceDirect you have additional private sharing rights for others' research accessed under that agreement. This includes use for classroom teaching and internal training at the institution (including use in course packs and courseware programs), and inclusion of the article for grant funding purposes.
Gold Open Access Articles: May be shared according to the author-selected end-user license and should contain a CrossMark logo, the end user license, and a DOI link to the formal publication on ScienceDirect.
Please refer to Elsevier's posting policy for further information.

18. **For book authors** the following clauses are applicable in addition to the above: Authors are permitted to place a brief summary of their work online only. You are not allowed to download and post the published electronic version of your chapter, nor may you scan the printed edition to create an electronic version. **Posting to a repository:** Authors are permitted to post a summary of their chapter only in their institution's repository.
19. **Thesis/Dissertation**: If your license is for use in a thesis/dissertation your thesis may be submitted to your institution in either print or electronic form. Should your thesis be published commercially, please reapply for permission. These requirements include permission for the Library and Archives of Canada to supply single copies, on demand, of the complete thesis and include permission for Proquest/UMI to supply single copies, on demand, of the complete thesis. Should your thesis be published commercially, please reapply for permission. Theses and dissertations which contain embedded PJAs as part of the formal submission can be posted publicly by the awarding institution with DOI links back to the formal publications on ScienceDirect.

Elsevier Open Access Terms and Conditions
You can publish open access with Elsevier in hundreds of open access journals or in nearly 2000 established subscription journals that support open access publishing. Permitted third party re-use of these open access articles is defined by the author's choice of Creative Commons user license. See our open access license policy for more information.
Terms & Conditions applicable to all Open Access articles published with Elsevier:
Any reuse of the article must not represent the author as endorsing the adaptation of the article nor should the article be modified in such a way as to damage the author's honour or reputation. If any changes have been made, such changes must be clearly indicated.
The author(s) must be appropriately credited and we ask that you include the end user license and a DOI link to the formal publication on ScienceDirect.
If any part of the material to be used (for example, figures) has appeared in our publication with credit or acknowledgement to another source it is the responsibility of the user to ensure their reuse complies with the terms and conditions determined by the rights holder.
Additional Terms & Conditions applicable to each Creative Commons user license:
CC BY: The CC-BY license allows users to copy, to create extracts, abstracts and new works from the Article, to alter and revise the Article and to make commercial use of the Article (including reuse and/or resale of the Article by commercial entities), provided the user gives appropriate credit (with a link to the formal publication through the relevant DOI), provides a link to the license, indicates if changes were made and the licensor is not represented as endorsing the use made of the work. The full details of the license are available at http://creativecommons.org/licenses/by/4.0.
CC BY NC SA: The CC BY-NC-SA license allows users to copy, to create extracts, abstracts and new works from the Article, to alter and revise the Article, provided this is not done for commercial purposes, and that the user gives appropriate credit (with a link to the formal publication through the relevant DOI), provides a link to the license, indicates if changes were made and the licensor is not represented as endorsing the use made of the work. Further, any new works must be made available on the same conditions. The full details of the license are available at http://creativecommons.org/licenses/by-nc-sa/4.0.
CC BY NC ND: The CC BY-NC-ND license allows users to copy and distribute the Article, provided this is not done for commercial purposes and further does not permit distribution of the Article if it is changed or edited in any way, and provided the user gives appropriate credit (with a link to the formal publication through the relevant DOI), provides a link to the license, and that the licensor is not represented as endorsing the use made of the work. The full details of the license are available at http://creativecommons.org/licenses/by-nc-nd/4.0.
Any commercial reuse of Open Access articles published with a CC BY NC SA or CC BY NC ND license requires permission from Elsevier and will be subject to a fee.
Commercial reuse includes:

- Associating advertising with the full text of the Article
- Charging fees for document delivery or access
- Article aggregation
- Systematic distribution via e-mail lists or share buttons

Posting or linking by commercial companies for use by customers of those companies.

20. **Other Conditions**:

v1.9